universität wien

DISSERTATION / DOCTORAL THESIS

Titel der Dissertation /Title of the Doctoral Thesis

„ Identification and characterization of point mutations that rescue loss of CPC function in budding yeast”

verfasst von / submitted by

Matthew Norman Clarke BSc., MSc.

angestrebter akademischer Grad / in partial fulfilment of the requirements for the degree of

Doctor of Philosophy (PhD)

Wien, 2023 / Vienna 2023

Studienkennzahl lt. Studienblatt / degree programme code as it appears on the student record sheet:	UA 794 685 490
Dissertationsgebiet lt. Studienblatt / field of study as it appears on the student record sheet:	Molekulare Biologie

Betreut von / Supervisor: Assoc. Prof. Christopher S. Campbell, PhD

Table of Contents

Acknowledgements

First and foremost, I would like to express my immense thanks to my PhD supervisor, Dr. Christopher Campbell. Chris has not only been a very patient mentor but has also helped me improve my work ethic and organizational skills hugely. I'm very grateful that Chris allowed me the opportunity to work on this project. At the beginning of the project we were both unsure where it would lead, but I'd say it was quite successful in the end even though it was sometimes tough work. I have always relished a challenge and enjoyed getting the work for this project done. I am also very thankful Chris was always available to give me support, as well as a push, when I required motivation. Chris also helped me improve my presentation and poster design skills very much and I will always be grateful for what he has taught me.

It would be amiss if I did not express my thanks to the entire Campbell lab including but not limited to Manuel, Sophie, and Tamara for all the advice and help they gave me over the years. I would not have been able to fully function without their assistance (especially Sophie's help with making overnights) and I am very grateful I got to know such friendly and endearing people. I will miss our lunchtime chats.

A special thanks should be given to Maddy and Sarah who patiently helped me figure out where everything was when I was first starting out. I would also like to thank Alex, as well as the entire Dammermann lab for their advice and support during our joint lab meetings. I will never forget the invaluable information I learned about *C. elegans* and the centrosome.

I also need to thank the members of my PhD committee Christa Bücker and Anna Obenauf; their advice during my committee meetings has been very helpful. A special thanks must be given to Tesi and Gerlinde for all the help they gave me regarding the administrative maze that is academic science. I'd still be totally lost without them.

This acknowledgement would not be complete without mentioning Theo, Nacho and Kathi. Their companionship and support have helped shape who I am as a scientist and friend, and they have aided me through some very challenging moments during my PhD. I cannot express enough the respect and appreciation I have for them. Theo must be given an extra thanks not only for helping me with my project, but also for providing significant assistance in the writing of this thesis.

Many thanks must be given to my sister, Joanna, and my parents who have helped me immensely by providing a variety of support and comforting advice when I was feeling down about my project. I'd like to express my unending gratitude toward them.

Last but certainly not least, I need to thank my girlfriend, Sarah. Her kindness and warmth have helped me cope with the pressures of my PhD. She also pushes me when I get complacent, which is an invaluable asset in a partner and friend.

Cheers and thanks for all the fish.

Abstract

The presence of both aneuploidy and high rates of missegregation (chromosomal instability, CIN) are hallmarks of cancer. However, such genetic defects are highly detrimental to the growth of healthy cells, which begs the question: how exactly can cells adapt to persistent CIN, and the subsequent aneuploidy, to become the highly proliferative cells associated with cancer?

To understand how cells are able to adapt, we induced persistent CIN and aneuploidy in budding yeast by deleting a component of the chromosomal passenger complex (CPC), Bir1. Previous work in our lab found that the initial adaptation to high rates of CIN and aneuploidy (*bir1Δ-ad*) was achieved by the selection of specific beneficial aneuploidies. These allowed for reduced CIN and improved growth of the *bir1Δ-ad* cells.

However, we wished to investigate how these CPC deficient cells continue to adapt to persistent CIN over even longer durations of time (*bir1Δ-ad2*). In this project we discovered multiple point mutations, in at least two distinct pathways, that suppress loss of CPC function. The suppressor mutations discovered fall into roughly four categories: members of the outer kinetochore, the SCF^{Cdc4} ubiquitin ligase complex, a master regulator of the spindle assembly checkpoint (SAC): MPS1, and the CPC itself. The suppressor mutations reduced CIN rather than ameliorating the detrimental effects caused by aneuploidy, and the beneficial aneuploidies from the partially adapted (*bir1Δ-ad*) cells were reduced.

Together these data demonstrate a timeline of adaptation to loss of CPC function; at first cells with deficient CPC activity select for beneficial aneuploidies, but as time goes on they eventually accumulate suppressor mutations that specifically target the source of CIN and can therefore reduce the need for such aneuploidies. These experiments give us a better understanding of how healthy cells potentially adapt to CIN and aneuploidy, as they evolve into cancer cells.

Zusammenfassung

Das Vorhandensein von Aneuploidie und hoher Missegregationsraten (chromosomale Instabilität, CIN) sind Hauptmerkmale von Krebs. Solche genetischen Defekte sind jedoch sehr schädlich für das Wachstum gesunder Zellen, was die Frage aufwirft: Wie genau können sich Zellen an persistierende CIN und die anschließende Aneuploidie anpassen, um die hochproliferativen Zellen zu werden, die mit Krebs assoziiert sind? Um zu verstehen, wie sich Zellen anpassen können, induzierten wir persistierende CIN und Aneuploidie in sporulierter Hefe, indem wir eine Komponente des „chromosomal passenger complex“ (CPC), BIR1, delitierten. Frühere Arbeiten in unserem Labor ergaben, dass die anfängliche Anpassung an hohe Raten von CIN und Aneuploidie (bir1Δ-ad) durch die Auswahl spezifischer nützlicher Aneuploidien erreicht wurde. Diese ermöglichten eine reduzierte CIN und ein verbessertes Wachstum der bir1Δ-ad Zellen. Wir wollten jedoch untersuchen, wie sich diese CPC-defizienten Zellen über noch längere Zeiträume an persistierende CIN anpassen (bir1Δ-ad2).In diesem Projekt entdeckten wir mehrere Punktmutationen in mindestens zwei verschiedenen Pathways, die den Verlust der CPC-Funktion kompensieren. Die entdeckten Mutationen/Gene lassen sich grob in vier Kategorien einteilen: Proteine des äußeren Kinetochors, des SCFCdc4-Ubiquitin-Ligase-Komplexes, eines Hauptregulators des Spindel Assembly Checkpoints (SAC): MPS1 und des CPC selbst. Die Suppressormutationen reduzierten die CIN um somit die schädlichen Auswirkungen der Aneuploidie zu verbessern. Auch die nützlichen Aneuploidien aus den teilweise angepassten (bir1Δ-ad) Zellen wurden reduziert. Zusammen zeigen diese Daten eine Zeitachse der Adaptation an den Verlust der CPC-Funktion. Zunächst selektieren Zellen mit mangelhafter CPC-Aktivität nach nützlichen vorteilhaften Aneuploidien, aber im Laufe der Zeit akkumulieren sie schließlich Suppressormutationen, die spezifisch auf die Quelle der CIN abzielen und daher den Bedarf an solchen Aneuploidien reduzieren können. Diese Experimente geben uns ein besseres Verständnis dafür, wie sich gesunde Zellen möglicherweise an CIN und Aneuploidie anpassen können, wenn sie sich verändern und zu Krebszellen entwickeln.

1. Introduction: Mitotic segregation fidelity is essential for maintaining a stable genotype

The equal distribution of genetic information into daughter cells is a strictly controlled process known as chromosomal segregation. The reason segregation must be so strictly controlled is because it is essential for establishing a new generation of cells with the same genotype as the previous generation. Without the ability to maintain a stable genetic template between generations, life as we know it could not exist. In eukaryotes the physical separation of genetic information is mediated mechanistically by a combination of structural and regulatory components.

When the structural and/or regulatory components which mediate mitosis are dysregulated, this results in missegregation (**Figure 1**). High rates of missegregation from one generation to another (known as chromosomal instability, CIN) leads to daughter cells that are unable to maintain a stable karyotype and do not inherit the appropriate amount of genetic information. When a cell does not have the correct chromosomal complement, this is known as aneuploidy. In humans, loss of any autosome results in embryonic lethality, and very few chromosome gains are viable (Hassold & Hunt 2001; Brewer *et al.,* 2002). Additionally, studies have shown that inducing either high rates of CIN or aneuploidy in healthy tissues result in poor proliferation and/or cell death (Gropp *et al.,* 1983; Torres *et al.,* 2007; Pfau & Amon, 2012; Giam & Rancati, 2015). It is therefore surprising that cancer cells, which can grow very well, often show elevated rates of missegregation (reviewed in Ben-David and Amon, 2020). Additionally, approximately 90% of solid tumors and 70% of hematopoietic cancers possess aneuploidy (Weaver & Cleveland, 2006). This makes aneuploidy one of the most common characteristics found in cancers. The explanation for why CIN and aneuploidy is enriched in cancer, yet are highly detrimental in healthy cells, remains mysterious. Determining the mechanisms which underlie the contributions CIN and aneuploidy have in cancer evolution will help future efforts in diagnosing and treating disease.

In order to fully understand how cells can adapt to missegregation, the components which establish and control kinetochore-microtubule attachments must be discussed in greater detail. The most signifcant structural components involved in segregation include microtubules and a large proteinaceous hierarchical complex called the kinetochore (reviewed in Biggins, 2013). The kinetochore is assembled at a specific genetic locus known as the centromere. The kinetochore acts as the interface that connects chromatin to microtubules. It can be divided into two parts: the inner kinetochore, which is most proximal to the centromere, and the outer kinetochore, which is most proximal to the microtubules. Microtubules begin polymerization at the microtubule organizing center (MTOC), called the Spindle Pole Body (SPB) in yeast or centrosomes in higher organisms, and then polymerize towards kinetochores to which they form attachments (Jin *et al.,* 2000; Jasperen & Winey, 2004; Marco *et al.,*

2013). Interestingly, microtubules are also able to nucleate at kinetochores which can help catch microtubules emanating from MTOCs (Maiato *et al.,* 2004). Additionally, the cohesin complex is a signifcant structural component as it physically holds sister chromatids together (Peters *et al.,* 2008; 2012; Oliveira & Nasmyth, 2010; Skibbens, 2019).

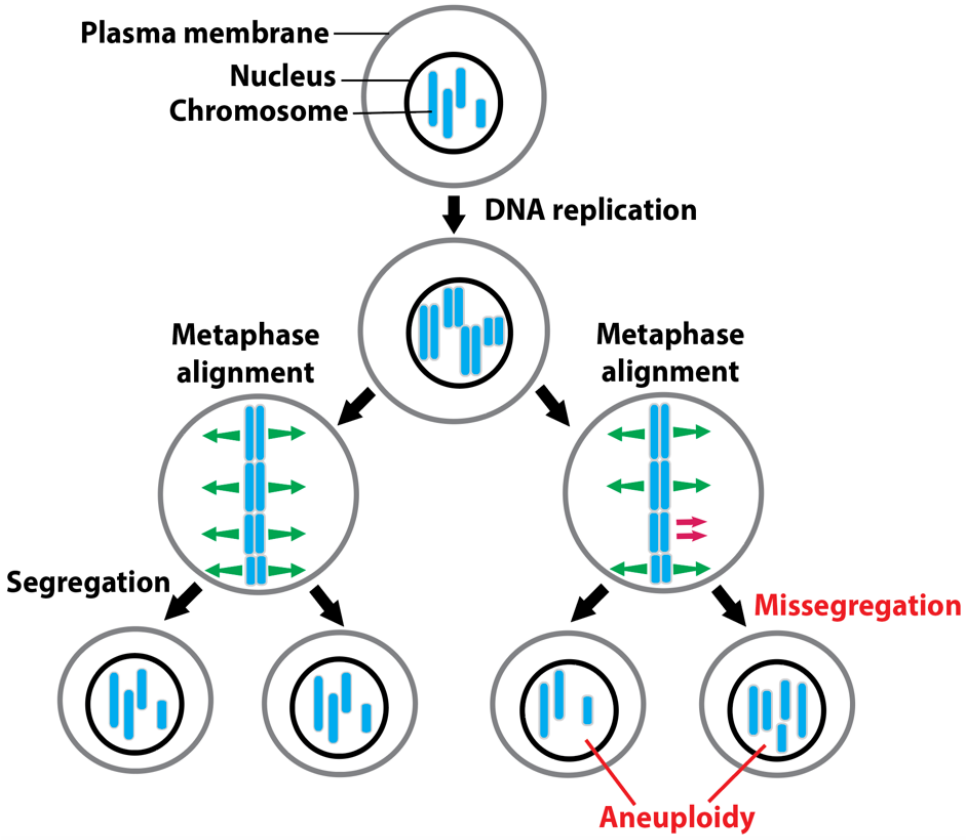

Figure 1. Missegregation leads to aneuploidy
Schematic showing different stages of the cell cycle, as well as how missegregation results in aneuploidy. This example shows four chromosomes (blue) which undergo replication and then cell division.

The regulation of cell division and segregation is highly complex and largely mediated by enzymatic protein complexes as well as signaling cascades known as “checkpoints”. One of the most relevant components is the Chromosomal Passenger Complex (CPC). The CPC is composed of four different subunits, one of which is the kinase subunit, Ipl1/Aurora B. This kinase is essential for phosphorylating specific residues in the kinetochore thereby reducing the kinetochore’s electrostatic attraction and binding affinity for microtubules (Welburn *et al.,* 2010; DeLuca *et al.,* 2011; Carmena *et al.,* 2012; Sarangapani *et al.,* 2013; Kalantzaki *et al.,* 2015).

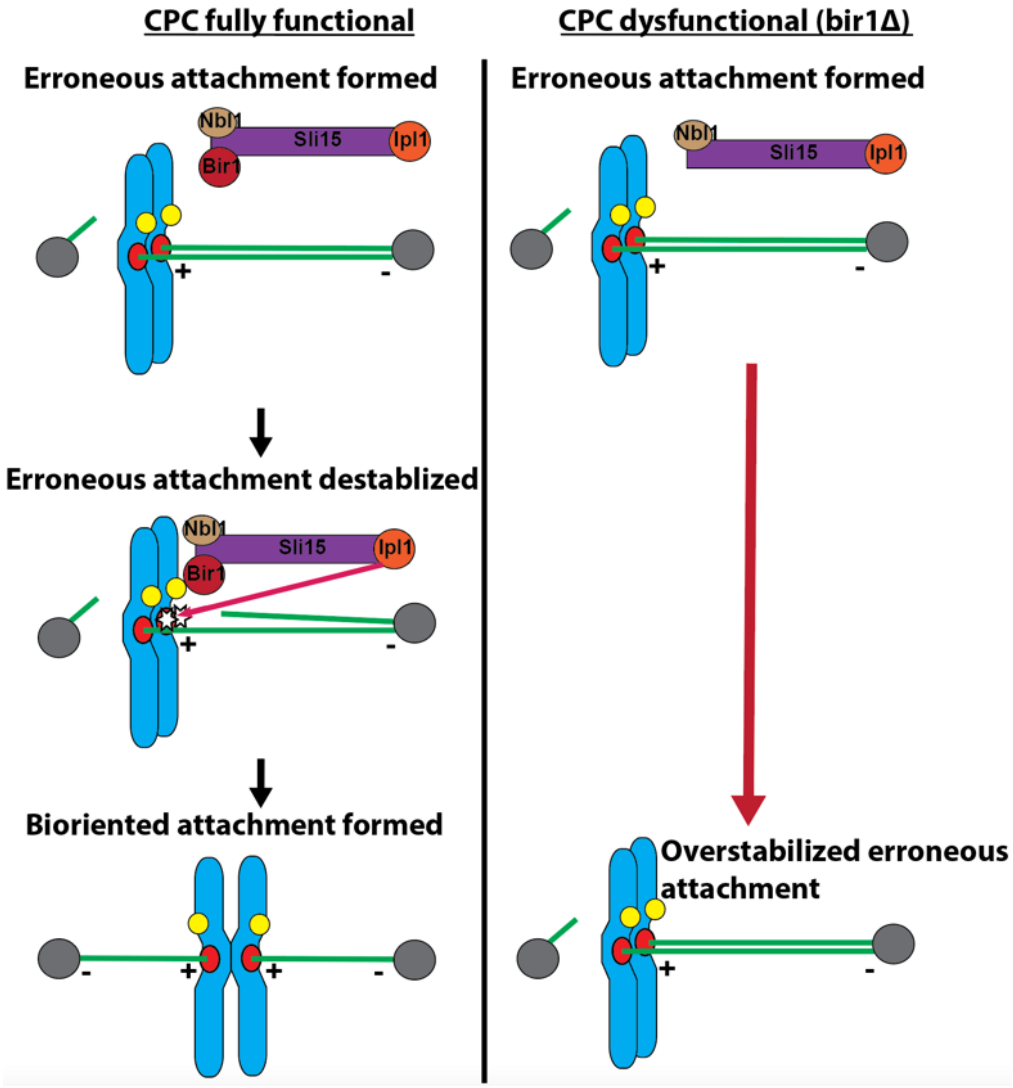

Figure 2. Loss of Bir1 leads to overstabilized attachments
(Left)Schematic showing an erroneous attachment where the kinetochores (red circles) of both sister chromatids (blue) are connected to the same SPB (grey circle) by microtubules (green). The plus end of the microtubule is most proximal to kinetochores. Next, during cell division, the CPC localizes to the inner centromere via Bir1 directly associating with Sgo1 (yellow circle). Using Ipl1, the CPC then phosphorylates (white stars) kinetochore subunits which destabilizes the attachment. Eventually the formation of stable bioriented attachments occur, thus facilitating segregation fidelity. (Right) Schematic showing an erroneous attachment. In this case however the loss of Bir1 impairs localization of the CPC to the inner centromere. This results in erroneous attachments becoming overstabilized due to the loss of the CPC's destabilizing activity. This inevitably leads to CIN and aneuploidy.

Another subunit, Bir1/Survivin, is essential for localizing the CPC to the inner centromere in early mitosis (Vader *et al.,* 2006; Jeyaprakash *et al.,* 2007; Vanoosthuyse *et al.,* 2007; Storchova *et al.,* 2011; Campbell & Desai, 2013). During the later stages of cell division, the CPC localizes to the spindle midzone (Pereira *et al.,* 2003; Mirchenko & Uhlmann, 2010; Tsukahara *et al.,* 2010; Storchova *et al.,* 2011; Campbell & Desai, 2013). Once each chromatid is bound to microtubules from

opposite spindle poles this is known as a bioriented attachment (**Figure 2**). This is the desired attachment state because then one copy of each sister chromatid will be segregated toward opposite poles (Tanaka, 2010). The formation of attachments between microtubules and kinetochores is stochastic, and therefore the formation of erroneous attachments is guaranteed. The CPC functions by destabilizing incorrect attachments until, through successive rounds of attachment and detachment, all the attachments become bioriented (**Figure2**) (Santaguida & Musacchio, 2009; Sarangapani *et al.,* 2013). Once the attachments are bioriented, the tension generated between the opposite spindles result in the stable formation of this attachment state. Applying tension to sister chromatids has been shown in literature to stabilize attachments (Nicklas, 1967; Tanaka *et al*., 2002; Joglekar *et al,* 2009). Only once each pair of chromatids is in a bioriented state is the cohesin complex degraded and the chromatids allowed to separate. The migration of chromatids towards cellular poles is physically driven by the active depolymerization of microtubules. This facilitates the separation of sister chromatids. Other key regulatory components relevant to this thesis include the Spindle Assembly Checkpoint (SAC) pathway, the anaphase promoting complex or cyclosome (APC), and the Skp1-Cullin-F-box (SCF) complex.

The reason we believe CIN and aneuploidy are enriched in cancer is because they are required for cancer progression as well as resistance to cancer therapies and evasion of the immune system (Davoli *et al.,* 2017; Ben-David & Amon, 2020). Studies have shown that the acquisition of certain aneuploidies through CIN can provide selective advantages against particular stresses including hypoxia, starvation and chemotherapeutic drugs (Rancati *et al.,* 2008; Chen *et al.,* 2012; Rutledge *et al.,* 2016; Ryu *et al.,* 2016; Sansregret *et al.,* 2017; Davoli *et al.,* 2017). Additionally, enhanced CIN and aneuploidy is associated with poor prognosis in cancer patients (Davoli *et al.,* 2017; Bakhoum & Cantley, 2018; Replogle *et al.,* 2020). Nevertheless, the negative effects of aneuploidy and/or CIN must be mitigated somehow in cancer. Consequently, a question which arises here is how can cells adapt so they are able to alleviate the growth detriments associated with CIN? To answer this question, we deleted Bir1, thereby perturbing CPC localization to the inner centromere, for long periods of time to determine how cells adapt to persistent CIN (**Figure 2**). The data from this thesis suggest that first cells adapt by obtaining beneficial aneuploidies. Over longer durations of time, cells accumulate mutations which ameliorate the source of persistent CIN by perturbing multiple distinct pathways.

In order to fully appreciate the work done in this project this first chapter will review the structural and regulatory molecular processes which control and mediate cell-division, specifically chromosome biorientation in mitosis and cancer. It is also pertinent to review the molecular pathways, and the genes/proteins therein, which were found to be involved in CIN suppression.

1.1 Cancer cells adapt to overstablized kinetochore-microtubule attachments and aneuploidy

In cancer, control over the cell cycle, particularly cell division and chromosome segregation, is lost. Hence, the mechanisms put in place to control segregation become dysregulated and some chromosomes lag behind others during segregation. This is a major problem for the cell because this often leads to increased amounts of failed segregation, and therefore CIN. CIN inevitably leads to cells which possess too little or too many chromosomes, a state known as aneuploidy. Lagging chromosomes are seen often in cancer cells and are indicative of missegregation as well as aneuploidy (Bakhoum *et al.,* 2009). Studies have shown that usually the more lagging chromosomes, and therefore CIN, a cell possesses the more aneuploidy it possesses too (Duesberg *et al.,*1998; Nicholson & Cimini, 2013). While the precise mechanisms which cause CIN in cancer remain elusive, one of the leading causes for lagging chromosomes and CIN in cancer is the formation of erroneous kinetochore-microtubule (KT-MT) attachments that cannot be destabilized (Bakhoum *et al.,* 2009;2011; Gordon *et al.,* 2012; Sansregret *et al.,* 2018). Such kinds of attachments are referred to as overstabilized attachments. Indeed, it has been shown in literature via a fluorescence dissipation after photoactivation assay that KT-MT attachments in various cancer derived cell-lines tend to be more stable than wild-type attachments (Bakhoum *et al.,* 2009). In order to improve medical cancer interventions, we must better understand how overstabilization facilitates cancer progression. Although so far there has been limited success, there are currently clinical trials underway using Aurora kinase inhibitors (reviewed in Du *et al*., 2021).

Cancer cells all start out as healthy cells. Usually, such cells are highly sensitive to the genetic detriments enriched in cancer: CIN and aneuploidy (Gropp *et al.,* 1983; Torres *et al.,* 2007; Sheltzer *et al.,* 2011; Pfau & Amon, 2012; Giam & Rancati, 2015; Passerini *et al.,* 2016). How then do cells start out sensitive to lagging chromosomes, CIN and aneuploidy, but later specifically select for these same characteristics? In short, we still do not have a full explanation as to how cells progress from healthy cells to cancer cells. Studies suggest that cells develop adaptations which allow them to ameliorate the detriments of CIN and aneuploidy so that they can reap the benefits of loss of proliferative control and enhanced genetic diversity (Davoli *et al.,* 2017). However, it is still debated as to whether the adaptations used by cells suppress the negative effects of aneuploidy directly, or if the suppressors act on the source of CIN itself, thus reducing aneuploidy indirectly. Work by Torres *et al.,* (2010) in a budding yeast model has shown that certain mutations improve growth fitness in strains with specific chromosome gains. Additionally, multiple studies have shown that certain aneuploidies are beneficial under specific stress conditions in human cancer cell-lines (Rutledge *et al.,* 2016;

Sansregret *et al.,* 2017; Davoli *et al.,* 2017). This data suggest that cells can 1) utilize aneuploidy to adapt to specific stresses and 2) utilize certain mutations to enhance resistance to the detrimental effects of specific aneuploidies themselves (Torres *et al.,* 2010; Rancati *et al.,* 2008) (**Figure3A**). One of the main mechanisms proposed to be involved in aneuploidy tolerance is an overactive proteasome. Ubp6 is a protein involved in 26S proteasome modulation.

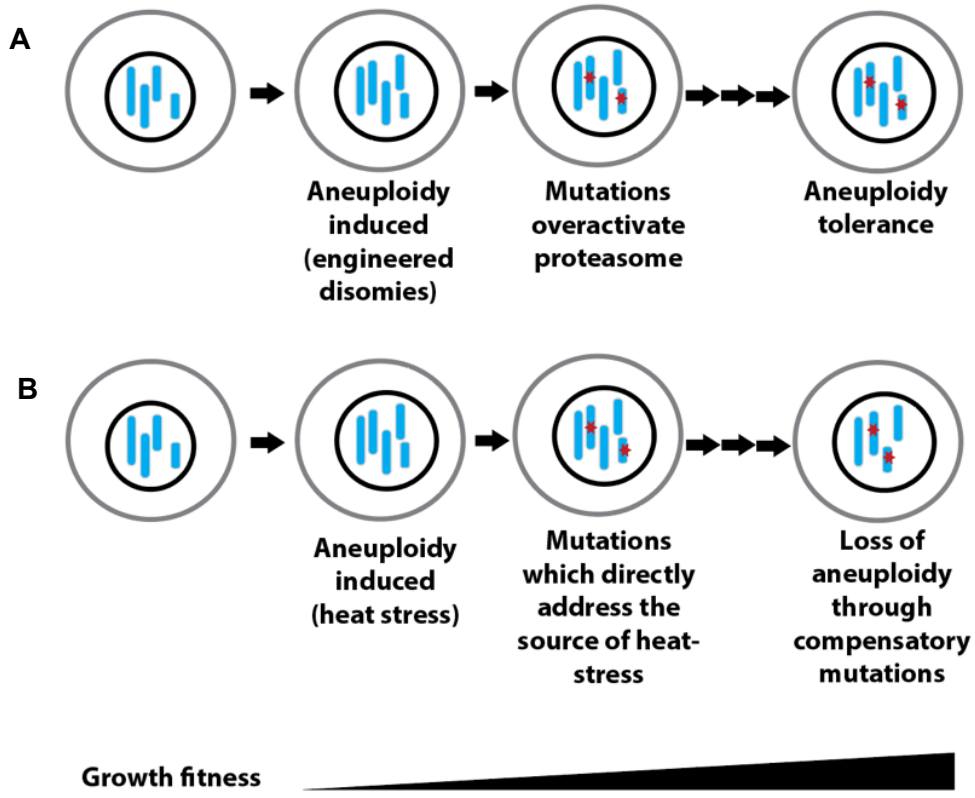

Figure 3. Multiple routes to CIN and aneuploidy adaptation exist
(**A**)Schematic showing how cells adapt and grow better overtime by accumulating mutations which enhance the degradation of excess proteins thus counteracting the effects of aneuploidy (Torres *et al.,* 2010)
(**B**) Schematic showing how cells adapt and grow better by accumulating mutations which directly address the source of CIN (heat stress). The presence of these mutations allows for the cell to refine or lose the aneuploidy which has now become obsolete for growth fitness (Yona *et al.,* 2012).

Ubp6 negatively regulates the proteasome, therefore the impairment of Ubp6 results in accelerated ubiquitin mediated protein degradation. Aneuploid cells often produce too many proteins and therefore an overactive proteasome is believed to help reduce the toxicity induced by excessive protein accumulation (Torres *et al.,* 2007; 2010; Sheltzer *et al.,* 2012; Yona *et al.,* 2012; Pavani *et al.,* 2021). Indeed, studies show that the nonsense mutant *ubp6(E256X)* enables tolerance of gains of chromosomes 5, 8, 9, and 11 (Torres *et al.,* 2010). Additionally, another study found

that when Ubp3, a deubiquitinase vital for proteasome function, is impaired, proteotoxicity already inherent in aneuploid cells increases. This fits with the idea that increased protein degradation is utilized by cells to become resistant to aneuploidy (Dodgson *et al.,* 2016). The same study suggested that Ubp3 could provide a potential new drug target for anti-cancer therapies (Dodgson *et al.,* 2016).

Another model postulated by researchers is that aneuploidy provides a source for rapid adaptation to specific stresses. Adaptation experiments involving the exposure of budding yeast to heat stress resulted in the gain of an extra copy of chromosome 3. The strains which possessed chromosome 3 trisomy grew better than wild-type strains at the same elevated temperature. However, over many generations, the cell eventually lost chromosome 3 trisomy and instead upregulated the expression of 17 specific genes on chromosome 3. Additionally, when the trisomic strains were grown once again at the permissive temperature, the trisomy was lost. Altogether, this suggests that overtime the detriments of this aneuploidy must still be mitigated. Consequently, the cell develops suppressors which directly address the source of CIN, which eliminate the need for the aneuploidy altogether (**Figure3B**) (Yona *et al.,* 2012; Pavani *et al.,* 2021).

Despite whichever route the cancer cell uses to adapt, cancer utilizes the genetic diversity provided by missegregation and aneuploidy to evolve improved growth fitness and metastasis (Davoli et al., 2017; Carter *et al.,* 2006; McGranahan *et al.,* 2012; Shukla *et al.,* 2020). Furthermore, the genetic diversity provided by CIN and aneuploidy aids adaptation to various anti-tumor factors, including evasion of the immune system and resistance to anti-cancer drugs. In a retrospective analysis of data from clinical trials, a study found that tumors which possessed more aneuploidy were less likely to benefit from immune based therapies (Davoli *et al.,* 2017).

Furthermore, proteolysis-targeting chimeras (PROTACs) are a type of anticancer drug currently being used in clinical trials. A study has shown evidence that cancer cell-lines can become resistant to PROTAC drugs through overexpression of the drug efflux pump MDR1, which is found on chromosome 7 (Kurimchak *et al.,* 2022). An earlier study found evidence, based on FISH assays, that ovarian cancers resistant to chemotherapy have a much higher prevalence of chromosome 7 gain, including multiple copies of MDR1. This illustrates how aneuploidy, specifically gain of chromosome 7 and therefore MDR1, can be utilized by cancer to become resistant to treatments (Zhang *et al.,* 2017). Furthermore, upregulation of efflux pumps is a common method used by cancer to circumvent anticancer drug function (reviewed in Fletcher *et al.,* 2010: Kurimchak *et al.,* 2022).

In addition to this, certain aneuploidy patterns, including gain of chromosome arms 8q and 20q, are frequently seen in many different cancer types (Beroukhim *et al.,* 2010). Other aneuploidies are only common in specific cancer types (Taylor e*t al.,* 2018). The specific reason for such gains and losses is still unclear. However, Davoli *et al.,* (2013) showed that the prevalence of tumor suppressors and oncogenes on a chromosome could predict the gain or loss of that particular

chromosome in cancer. Nevertheless, the complexity of cancer karyotypes makes it very difficult to determine why certain chromosome gains or losses provide selective advantages.

Some studies have shown that cancer may adapt to overstabilized attachments through overexpression of Kif2b or MCAK (Walczak *et al.,* 1996; Kline-Smith & Walczak, 2002). The overexpression of these kinesins increases kinetochore-microtubule turnover and decreases mitotic errors in cancer cell-lines (Bakhoum *et al.,* 2009). Other mutations, which lengthen mitotic timing, reduce errors in cancer by giving cells more time to correct erroneous attachments. Consequently, this reveals another possible pathway for CIN and aneuploidy adaptation (Wang *et al.,* 2003; Sansregret *et al.,* 2017; Alonso Y Adel *et al.,* 2022). Delayed mitotic timing is often caused by dysfunctional Anaphase Promoting Complex (APC). However, this does not always occur in cancer and many aspects of cancer progression remain unclear. Notably, aneuploidy has been shown to cause enhanced G1 arrest, which reduces the efficacy of certain anti-cancer drugs (Replogle *et al.,* 2020).

In summary, we know cancer cells start out sensitive to CIN and aneuploidy but somehow are able to adapt to overstabilized KT-MT attachments and aneuploidy (Ben-David & Amon, 2020). Although there are several known causes of CIN (overstabilized attachments being one of these) the specific mechanisms which lead to CIN in cancer remain unclear. CIN and aneuploidy are associated with increased cancer malignancy and growth, as well as increased likelihood of drug resistance (Davoli *et al.,* 2017; Replogle *et al.,* 2020). In order to further elucidate the complex role of CIN adaptation in regard to cancer development, we must look more closely at the precise mechanisms which mediate chromosome segregation; more specifically, the establishment of kinetochore-microtubule attachments and the control of mitosis.

1.2 The cell-cycle and mitosis

The cell is the smallest accepted unit of life, and one of the reasons for such a prestigious title is the cell's ability to make copies of itself. The control of the cell-cycle is one of the most fundamentally important tasks for a cell. The cell-cycle can be broken up into two main stages: interphase and cell-division. Interphase is broken up into three sub-phases: Gap 1 (G1) phase, Synthesis (S) phase and Gap 2 (G2) phase. In G1-phase the cell mostly undergoes growth. In S-phase the cell makes copies of its genetic information as well as organelles, and in G2-phase the cell continues to grow and prepares itself for cell division (reviewed in Rieder, 2011; Biggins, 2013; Cuddihy & O'Connell, 2003).

1.2.1 G1 to S-phase

There are many mechanisms which control the cell-cycle. Some of the most important of these mechanisms are known as “checkpoints”. Cell-cycle checkpoints are signaling cascades which halt the cell-cycle at specific stages **(Figure 4A)**. The control of these signaling cascades is of vital importance to the cell. Without these checkpoints, the cell would have no ability to regulate vital processes that must be completed before specific cell-cycle stages can be performed (Wenzel & Singh, 2018). In budding yeast, G1 phase is when the formation of the daughter bud begins and the physical site of division decided (Balasubramanian *et al.,* 2004). Unless a cell has undergone DNA damage, the mechanisms which control G1 to S-phase transition will not be inhibited. S-phase entry is controlled by the G1 to S checkpoint signaling cascade. This signaling cascade is controlled by the expression of cyclins and cyclin-dependent kinases (CDKs) (Bertoli *et al.,* 2018). CDK activity, coupled with the proteasomal degradation of S-phase entry inhibitors by the E3 ubiquitin ligase SCF-complex, enables the cell to transition from G1 to S-phase (Goh & Surana, 1999). Such inhibitory factors include p27Kip1 (*CDKN1B*) in humans or Sic1 in budding yeast (Berset *et al.,* 2002; Barberis *et al.,* 2005; Böhm *et al.,* 2021). These mechanisms together trigger a positive-feedback loop, accumulating G1 to S-phase transition factors that result in an irreversible commitment to cell-division. The transition to S-phase is also described as a “point of no return” in which the cell has committed to entering the cell cycle. In budding yeast this is known as the “Start” point or in humans the “restriction” point. During S-phase the cell makes a copy of its DNA as well as its organelles. Next in G2-phase, the cell continues to grow and prepares itself for cell division.

1.2.2 G2 to M-phase

Once more due to a checkpoint, the cell pauses its cycle between G2 phase and the beginning of cell-division **(Figure 4A)**. This arrest is performed so the cell is able to assess if any DNA damage has occurred, likely due to issues during S-phase (Cuddihy & O’Connell, 2003). Immunofluorescence microscopy shows evidence that ATM and ATR kinases recognize and localize to sites of damaged DNA in human cells (Burma *et al.,* 2001; Kinner *et al.,* 2008). In yeast the kinase responsible for this is known as Rad3. If the checkpoint is fully functional the cell will only enter cell-division once the damaged DNA is repaired. If the cell is damaged severely and cannot be repaired it may undergo apoptosis, otherwise known as controlled cell-death (Bunz *et al.,* 1998; Colin *et al.,* 2015). Severe damage to DNA may also result in senescence, which is also known as stable cell-cycle arrest (reviewed in Gire & Dulic, 2015; Kuilman *et al.,* 2010). If there are no issues with DNA damage then, after G2-phase, the cell proceeds to distribute copies of its chromosomes into multiple newly formed daughter cells.

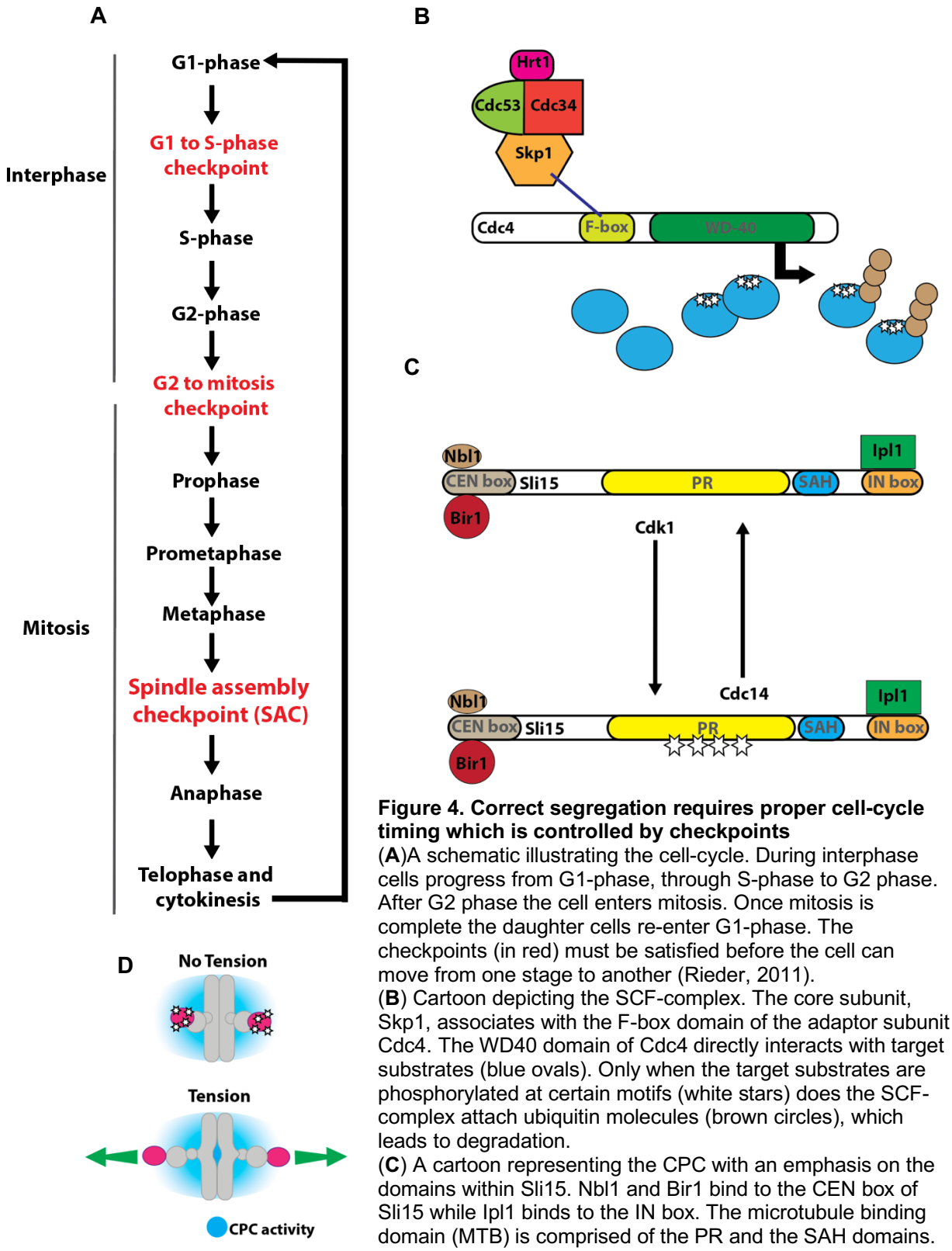

Figure 4. Correct segregation requires proper cell-cycle timing which is controlled by checkpoints
(**A**)A schematic illustrating the cell-cycle. During interphase cells progress from G1-phase, through S-phase to G2 phase. After G2 phase the cell enters mitosis. Once mitosis is complete the daughter cells re-enter G1-phase. The checkpoints (in red) must be satisfied before the cell can move from one stage to another (Rieder, 2011).
(**B**) Cartoon depicting the SCF-complex. The core subunit, Skp1, associates with the F-box domain of the adaptor subunit Cdc4. The WD40 domain of Cdc4 directly interacts with target substrates (blue ovals). Only when the target substrates are phosphorylated at certain motifs (white stars) does the SCF-complex attach ubiquitin molecules (brown circles), which leads to degradation.
(**C**) A cartoon representing the CPC with an emphasis on the domains within Sli15. Nbl1 and Bir1 bind to the CEN box of Sli15 while Ipl1 binds to the IN box. The microtubule binding domain (MTB) is comprised of the PR and the SAH domains. Cdk1 phosphorylation of phosphosites (white stars) in the PR domain enrich CPC localization at the inner centromere. During later stages of cell division Cdc14 dephosphorylates Sli15 triggering redistribution to the mitotic spindle.
(**D**)Schematic demonstrating the spatial separation model. Lack of tension results in the phosphorylation (white stars) of outer kinetochore substrates (pink ovals).

Figure 4D adapted from (Marsoner, 2022).

At this point the cell can undergo two different types of division. Mitosis is typically the division of somatic tissue that creates two genetically identical daughter cells. Meiosis is the process which governs sexual division and formation of gametes. In meiosis instead of two identical cells, four non-identical daughter cells are created. This thesis is concerned with mitotic divisions only. In mitosis the stages of division in chronological order are: prophase, prometaphase, metaphase, anaphase, telophase and then finally cytokinesis **(Figure 4A)**. The stages most important to this thesis are prometaphase and metaphase because it is at these stages that the connections between kinetochores and microtubules are finalized (Biggins, 2013; Marsoner, 2022). The control of entry to particular stages of the cell cycle requires the degradation of certain protein targets. The manner in which these substrates are degraded is largely achieved by ubiquitin-based targeting to the proteasome. This is usually mediated by E3 ubiquitin ligase complexes. As previously mentioned in this section, the SCF-complex is an example of an E3 ubiquitin ligase complex (Orlicky *et al.,* 2010). The known functions of the SCF complex include the degradation of S-phase inhibitors, centromeric nucleosomes, and inner kinetochore subunits (Schwob *et al.,* 1994; Drury *et al.,* 1997; Goh & Surana, 1999; Au *et al*., 2020; Böhm *et al.,* 2021). Based on these data, the SCF-complex has implications for control of mitotic entry as well as chromosome segregation.

1.2.2.1 The SCF-complex

The SCF complex is an E3 ubiquitin ligase complex and is composed of core subunits and one of a number of adaptor subunits (**Figure 4B**). In budding yeast, the core components include Cdc53 (scaffold protein), Cdc34 (E2 enzyme), Skp1, and Hrt1 (Mathias *et al.,* 1996; Feldman *et al.,* 1997; Goh & Surana, 1999; Au *et al*., 2020; Böhm *et al.,* 2021). Adaptor proteins of the SCF are the subunits which specify the target substrates. There are various adaptor proteins which exist. These adaptors contain an F-box domain at the N-terminus and WD40-repeat domain in the C-terminus. Structural analyses and yeast two-hybrid studies show that the F-box domain in the adaptor proteins is the region which associates with the core protein, Skp1 (**Figure 4B**) (Patton *et al.,* 1998; Orlicky *et al.,* 2010). Similar studies show that the WD40 domain forms a large beta-barrel structure, and is the part of the adaptor that directly interacts with substrates (Orlicky *et al.,* 2010). The SCF recognizes phosphodegron motifs on specific substrates, and depending on their phosphorylation state the SCF-complex will tag the protein for degradation by covalently linking ubiquitin molecules (**Figure 4B**) (Nash *et al.,* 2001; Böhm *et al.,* 2021). Not all the targets of the SCF-complex are known and the presence of multiple adaptor proteins makes this even more difficult to fully determine. The SCF adaptors most pertinent to this thesis are Cdc4 and Met30. Met30 and Cdc4 are both essential genes which are implicated in S-phase entry. Protein degradation assays

show Cdc4 degrades Cdc6 and Sic1 (Drury *et al.,* 1997). Similar assays show Met30 is responsible for the degradation of Swe1 (Kaiser *et al.,* 1998).

In budding yeast, the Cdc4 adaptor has mostly been studied by temperature sensitive mutants characterized in the 1980s (Yochem & Byers, 1987; Schwob *et al.,* 1994; Goh & Surana, 1999). Most Cdc4 temperature sensitive mutants are known to cause cell-cycle arrest at restrictive temperatures. Additionally, studies have shown that certain temperature sensitive Cdc4 alleles can rescue loss of Pds1/Securin. Pds1/Securin is also a major target of the APC. Additionally, loss of Cdc4 function can rescue anaphase arrest caused by Cdc20 mutants (Goh & Surana, 1999). Loss of Pds1/Securin function causes premature loss of sister chromatid cohesion and is a source of CIN. This suggests that inhibition of SCF^{cdc4} can rescue premature loss of sister cohesion.

Additionally, the human homolog of Cdc4 (hCdc4/FBXW7) has been implicated in the degradation of oncogenes including c-Myc and cyclin E. Indeed, mutations in FBXW7 are enriched in certain cancer types including endometrium and intestinal cancers (reviewed in Yeh *et al.,* 2018). Additionally, loss of FBXW7 promotes resistance to certain chemotherapeutics (Gasca *et al.,* 2016). This suggests that hCdc4/FBXW7 is a tumor suppressor. To summarize, the SCF-complex degrades certain factors important for chromosome segregation, S-phase entry and transition from G2 phase to mitosis.

1.2.3 Prophase

The cell begins mitosis by organizing its duplicated genetic information into a highly condensed state. This condensation process is also known as supercoiling. The control of chromosomal condensation is attributed to two complexes: condensin I and condensin II. These are both conserved in eukaryotes. The main purpose of condensins is to organize chromatin into a physically compact state (Martinez-Garcia *et al.,* 2023). The condensin II complex resides within the nucleus and is partly responsible for the condensation of chromatin during prophase. The exact mechanism behind the compaction of chromatin is still not well understood and highly debated. However, it is currently believed that condensin complexes facilitate DNA loop extrusion, a process which mediates supercoiling (reviewed in DeWit & Nora, 2023). In brief, loop extrusion is the physical formation of DNA loops which in turn form Topologically Associated Domains (TADs) (Fudenberg *et al.,* 2016). Another well characterized extrusion factor which aids compaction is the cohesin complex (reviewed in Skibbens, 2019; Ryu *et al.,* 2022).

The cohesin complex is also very important for holding sister chromatids together until they are allowed to separate during anaphase (Blow & Tanaka, 2005; Peters *et al.,* 2008;2012). The cohesin complex is an evolutionary conserved protein complex. In yeast, it is composed from the subunits: Smc1, Smc3, Mcd1/Scc1 and Irr1/Scc3 (Kothiwal *et al.,* 2021). Current literature suggests that the cohesin

complex acts by using its ring structure to encircle both sister chromatids, thereby holding them together. This is based on studies which show, firstly, that Smc3 and Scc1 are essential for sister chromatid cohesion, and lastly that these same proteins do not form covalent bonds with DNA (Gruber *et al.,* 2003). During prophase, cohesin becomes redistributed. Instead of being localized along the whole chromosome cohesin begins to dissociate from chromosomal arms and remains enriched at centromeres (Blow & Tanaka, 2005). The physical act of holding sister chromatids together, and the appropriate timing of cohesin complex degradation and sister chromatid release, are highly important for mediating correct segregation.

At this point a key difference between yeast and human mitosis must be highlighted. In yeast, unlike vertebrate cells, cell division is “closed” due to the fact that the nuclear envelope does not undergo breakdown (also known as nuclear envelope breakdown, NEBD). Only in the final stages of cell division does the nucleus divide into two new daughter cells, and finishes budding completely from the mother cell. In human cells, mitosis is “open” due to the dissolution of the nuclear envelope. Another feature of prophase in mammalian cells is that centrosomes begin to mature and form bipolar spindles. In mammalian cells, the breakdown of the nuclear membrane signals the end of prophase (Boettcher & Barral, 2013). However, in yeast, the nucleus does not break down therefore establishing end of prophase in budding yeast is more difficult. Also, the MTOCs of yeast (SPBs) are embedded within the nuclear membrane and microtubules form within the nucleus itself. This allows yeast to form kinetochore-microtubule attachments already during S-phase (Marco *et al.,* 2013; Smoyer & Jaspersen, 2014).

1.2.4 Prometaphase and metaphase

For the purposes of this thesis, prometaphase and metaphase are the most relevant phases of all the stages of mitotic division. The reason for this is because by the end of metaphase kinetochore-microtubule attachments are finalized. Prometaphase begins after NEBD in open mitosis. In human cells, condensin I complex lies outside the nucleus in the cytoplasm and is only able to interact with chromatin after NEBD (Shintomi & Hirano, 2011; Lee *et al.,* 2011; Nishide & Hirano, 2014). After this, both condensin I and condensin II help to form the rod like structures that form the sister chromatids. Condensins I and II are therefore vital for establishing the chromatid structure before cell division and segregation. In both yeast and humans, early prometaphase includes the migration of sister chromatids to the center of the cell along the metaphase plate. The movement of sister chromatids towards the center of cells is very important as it allows for an equal chance of capture by microtubules from opposite poles (Maiato *et al.,* 2017). It has been demonstrated in both yeast and metazoan cells that lateral connections are formed between microtubules and kinetochores initially (Hayden *et al.,* 1990; Merdes & DeMey, 1990; Rieder & Alexander, 1990; Tanaka *et al.,* 2005). These lateral connections are later converted

into end-on attachments. In budding yeast, the control of the transition from lateral to end-on attachments has been connected with the phosphorylation of specific serine residues (S13, S49, S217, S218 and S232) in Dam1. The kinase responsible for this is Mps1. Loss of this phosphorylation leads to dysregulation of the transition from lateral to end-on attachments. Such dysregulation has been associated with missegregation and has been demonstrated in both mitotic and meiotic divisions (Shimogawa *et al.,* 2006; 2010; Meyer *et al.,* 2018).

When only one chromatid is bound to microtubules this is an erroneous attachment called a monotelic attachment. When both sister chromatids are attached to the same pole this is an erroneous attachment called a syntelic attachment. A third kind of erroneous attachment occurs when microtubules emanating from both poles bind to one kinetochore; this is known as a merotelic attachment. These can only occur when multiple microtubules bind to the same kinetochore, which means that merotelic attachments are impossible in budding yeast where only one microtubule binds per kinetochore. Additionally, merotelic attachments are often responsible for the lagging chromosomes which are seen in human cell-lines (Gregan *et al.,* 2011).

It should be emphasized that the mechanism behind kinetochore-microtubule capture is a random process. During cell division erroneous connections between kinetochores and microtubules are inevitable. It is the job of the CPC to recognize and destabilize erroneous attachments (Vader *et al.,* 2006; Carmena *et al.,* 2012; van der Horst & Lens, 2014; Hadders & Lens, 2022). The CPC is composed of four subunits including Sli15/INCENP, Bir1/Survivin, Nbl1/Borealin, and Ipl1/Aurora B (**Figure 4C)**. Sgo1 (also known as Shuogoshin 1 or SGO1 in humans) is a highly conserved protein important for recruiting the CPC, specifically Bir1, to the inner centromeric chromatin. Localization of Sgo1 to the inner centromere is dependent on the phosphorylation of histone H2A by the kinase Bub1 (Kitajima *et al.,* 2005; 2006). Also, Sgo1 plays an important role in protecting the cohesin complex during cell division (Kitajima *et al.,* 2006).

Bir1 directly associates with Sgo1 in yeast. Bir1 also associates with the N-terminal CEN-box of the Sli15 scaffold protein. It should be noted that Nbl1 also localizes to the CEN-box in the CPC, and is important for maintaining CPC integrity (Nakajima *et al.,* 2009). At the C-terminus of Sli15 there is an IN-box region to which Ipl1/Aurora B kinase binds. During prometaphase, the phosphoregulated domain (PR), a part of the Microtubule Binding (MTB) domain of Sli15, remains phosphorylated by Cdk1 (**Figure 4C**) (Pereira *et al.,* 2003; Mirchenko & Uhlmann, 2010; Tsukahara *et al.,* 2010; Storchova *et al.,* 2011; Campbell & Desai, 2013). This phosphorylation prevents spindle localization and the CPC mainly localizes to the inner centromere. Another signifcant part of the MTB is the Single Alpha Helix (SAH) domain. This domain is vital for viability and has recently been shown to be important for CPC localization (Marsoner *et al.,* 2022).

Although it is known that the CPC can distinguish between erroneous and bioriented attachments, it is still heavily debated as to how this is actually achieved. One of the most prevalent models that explains how it does this is known as the "spatial separation" model (**Figure4D**) (Tanaka *et al.*, 2002; Joglekar et al., 2009; Lampson & Cheeseman, 2011). When sister chromatids are erroneously attached there is a lack of tension between the centromeres of the sister chromatid pairs (Nicklas & Koch, 1969; Li & Nicklas, 1995; Nicklas, 1997). Due to this lack of tension, the kinetochore substrates of the CPC remain close enough to where the CPC localizes so that Ipl1/Aurora B can phosphorylate and destabilize kinetochore-microtubule attachments (Biggins *et al.,* 1999; Cheeseman *et al.,* 2001;2002; Tanaka *et al.,* 2002). Once a bioriented attachment is made, the sister-chromatids experience tension. Tension has been shown to be sufficient for KT-MT stabilization (Tanaka *et al.,* 2002). During metaphase, when KT-MT attachments are bioriented and under tension, FRET assays have demonstrated that Aurora B kinase activity is limited to the inner centromeric region, and does not affect the outer-kinetochore. However, when there are no KT-MT connections formed, Aurora B phosphorylates subunits found within the inner centromere as well as the outer-kinetochore (Liu *et al.,* 2009; Welburn *et al.,* 2010). Altogether, this suggests that the physical act of tension moves the main kinetochore targets of the CPC away from Ipl1/Aurora B. Consequently, this results in the stabilization of the attachment (**Figure 4D**).

However, it has been shown by Campbell & Desai (2013) that the inner centromeric recruitment of the CPC is not essential for segregation and viability. This suggests that in yeast the localization of the CPC to the inner centromere is not essential for segregation. Instead there must be another locus where the CPC is still sufficient to correct erroneous attachments. Another main site of CPC localization is at the mitotic spindle. As the cell transitions from metaphase to anaphase the phosphatase Cdc14 dephosphorylates the PR region of CPC triggering loss of CPC at the inner centromere and redistribution along the mitotic spindle (Pereira *et al.,* 2003; Tsukahara *et al.,* 2010; Storchova *et al.,* 2011; Campbell & Desai, 2013; Marsoner *et al.,* 2022). The loss of any part of the mitotic binding domain (MTB) of the CPC results in lethality. It has been recently demonstrated by Marsoner *et al* (2022) that the CPC has multiple localizations essential for function: the inner centromere, the inner kinetochore and the mitotic spindle.

Additionally, Campbell & Desai (2013) showed that deleting the N-terminus of Sli15 (*sli15-Δ2-228* or *sli15-ΔNT*), including the CEN box, rescued loss of Bir1. Western blots of CPC components show that Bir1 deletion also inhibits the stability of Sli15 and, by extension, the entire CPC (Campbell & Desai, 2013). It is speculated that by deleting the Bir1 binding site of Sli15 (ie. the CEN box) the CPC no longer experiences perturbed stability. This same study also showed an increased amount of CPC at microtubules after *sli15-ΔNT* expression as well as improved segregation fidelity. Similarly, the unphosphorylatable *sli15-6A* allele, which enhances CPC localization to microtubules (Pereira *et al.,* 2003), also rescues the growth detriment

caused by loss of Bir1 (Campbell & Desai, 2013). This together suggests that the microtubule binding activity of Sli15 is vital for CPC function and enhanced binding at microtubules can rescue loss of Bir1.

To summarize, the CPC destabilizes those connections which are erroneous and has multiple localization sites. The biorientation of chromosomes in humans begins in prophase and continues in prometaphase and is completed by the end of metaphase. In budding yeast, the nucleus does not break down during mitosis therefore the biorientation of chromosomes already starts during S-phase (Marco *et al.,* 2013). It is very important that the cell does not proceed to anaphase until all chromosomes are properly bioriented. Even the presence of a single pair of erroneously attached chromatids triggers arrest (Zich & Hardwick, 2010; Murray, 2011; Musacchio, 2011). During prometaphase and up to the end of metaphase, the cell cycle is arrested until there are no longer unattached kinetochores. By creating unattached kinetochores, the CPC indirectly activates the SAC thereby preventing anaphase onset.

1.2.4.1 The Spindle Assembly Checkpoint (SAC) is initiated by Mps1 and monitors the attachment state of kinetochores

As has been previously mentioned, the SAC is a highly important molecular surveillance system which monitors the attachment state of kinetochores. If any of the kinetochores within a eukaryotic cell are not attached to a microtubule (monotelic or completely without attachments) the SAC ensures the cell does not move from metaphase to anaphase before every sister chromatid has formed bioriented KT-MT attachments (Rieder & Palazzo, 1992; Weiss & Winey, 1996; Pinsky *et al.,* 2006; Zich & Hardwick, 2010; Murray, 2011; Musacchio, 2011). This allows the cell more time to form bioriented attachments. It is important to again emphasize that it is the job of the CPC to recognize erroneous attachments in budding yeast, and destabilize such attachments so that the connection between the kinetochore and microtubule is broken. CPC activity therefore indirectly keeps the SAC signal active by breaking erroneous connections to form unattached kinetochores. This has been shown by experiments where the CPC is rendered dysfunctional and yet the SAC is not activated by these mutants, meaning the loss of CPC function does not activate the SAC (Biggins & Murray, 2001). The proteins involved in the control of the SAC have been identified by genetic screens in budding yeast (Hoyt *et al.,* 1991; Li & Murray, 1991; Hardwick *et al.,* 1999). In yeast the chief players include Mps1, Bub1, Bub2, Bub3, Mad1, Mad2, and Mad3 (Weiss & Winey, 1996). It needs to be stated that while most of these checkpoint genes are non-essential in yeast (with the exception of Mps1 which is vital for SPB duplication) they are all essential genes in animal cells (Winey *et al.,* 1991; Jones *et al.,* 2001; Basu *et al.,* 1999; Kitagawa & Rose, 1999; Dobles *et al.,* 2000; Kalitsis *et al.,* 2000; Gillett *et al.,* 2004). What this suggests is

that during a typical cycle, without any added stress, a yeast cell does not require extra time to properly orientate its chromosomes. However, this pause during mitosis is essential in animal cells (Basu *et al.,* 1999; Kitagawa & Rose, 1999; Dobles *et al.,* 2000; Kalitsis *et al.,* 2000; Gillett *et al.,* 2004; Biggins, 2013). While these checkpoint genes may be dispensable for viability in yeast, their loss does increase the rate of missegregation. Also, loss of such checkpoint proteins can cause segregation defects in yeast and also sensitizes yeast cells to drugs that disrupt microtubule dynamics (such as benomyl) (Li & Murray, 1991; Pangilinan & Spencer, 1996; Warren *et al.,* 2002; Storchova *et al.,* 2011). The SAC begins when Mps1 associates with unbound kinetochores (Pinsky *et al.,* 2006) (**Figure 5**). Mps1 is a kinase and is the main regulator of the SAC. After Mps1 phosphorylates MELT repeats at the outer kinetochores of unattached kinetochores, Bub1 and Bub3 associate with phosphorylated Spc105 (**Figure 5**). It should be noted that the phosphorylation of Spc105 by Mps1 is essential for checkpoint activation (London *et al.,* 2012; Yamagishi *et al.,* 2012). Mps1 autophosphorylation is essential for its kinase function as well as localization to the kinetochore in certain organisms (Kang *et al.,* 2007; Mattison *et al.,* 2007; Xu *et al.,* 2009). It should be noted that Mps1 has also been implicated in the phosphorylation of Ndc80 and Mad1 (Hardwick et al., 1996; Kemmler et al., 2009).

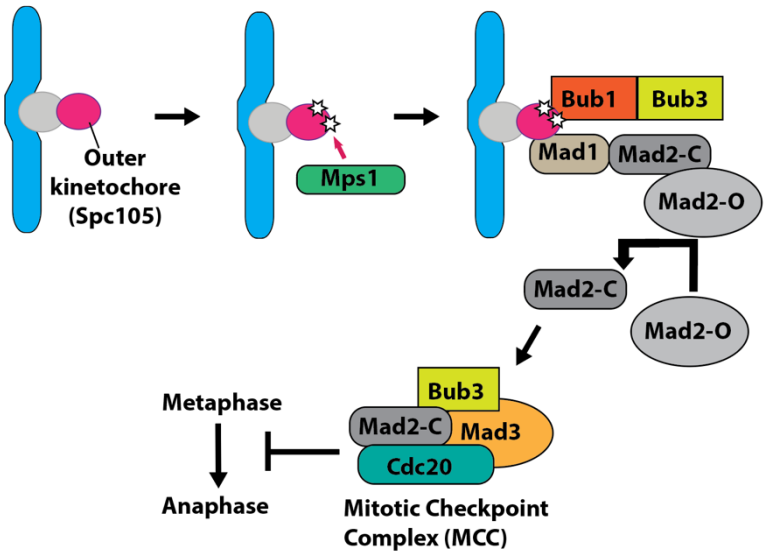

Figure 5. Phosphorylation of Spc105 is essential for activating the SAC and formation of the MCC
This schematic illustrates the process by which Mps1 activates the SAC. The outer-kinetochore (pink oval) is linked to the chromatid (blue) by the inner kinetochore (grey circle). Mps1 recognizes unattached kinetochores and phosphorylates (white stars) Spc105. After Spc105 is phosphorylated, Bub1/Bub3 associates. Next, Mad1 and Mad2 bind too. This leads to the establishment of the Mitotic Checkpoint Complex (MCC) which sequesters Cdc20 thus preventing APC activation. This in turn leads to inhibition of metaphase to anaphase transition.

Adapted from (Biggins, 2013 p.835)

The recruitment of Bub1 to phosphorylated Spc105 also contributes to the localization of the CPC to the inner centromere. This is because Bub1's kinase activity is important for the recruitment of Sgo1 (Kitajima *et al.,* 2005; 2006; Campbell & Desai, 2013). After this, Mad1 and Mad2, forming a complex, associate with the phosphorylated Spc105 and Bub1/Bub3 complex (**Figure 5**). Mad2 can be stably bound to Mad1 or cycle on and off the kinetochore (Howell *et al.,* 2000). When Mad2 is free in the cytoplasm, it exists in an "open" state (Mad2-O). Mad2 bound to kinetochores becomes converted to an alternate "closed" state (Mad2-C) in which direct association with Cdc20 can be made (Luo *et al.,* 2000; 2002; Sironi *et al.,* 2002; DeAntoni *et al.,* 2005; Mapelli *et al.,* 2007). Additionally, Mad2-C is a receptor for Mad2-O and upon binding the Mad2-O molecules are converted to Mad2-C. Next, Mad2-C not stably bound to Mad1 can associate with Mad3, Cdc20 and Bub3. Together this forms the Mitotic Checkpoint Complex (MCC) (**Figure 5**).

The SAC halts progression to anaphase by inhibiting a significant activator of the Anaphase Promoting Complex (APC): Cdc20. To briefly review, the APC is an E3-uqiquitin ligase complex responsible for targeting cyclin B and Pds1/Securin for proteosomal degradation. Such degradation leads to the activation of seperase and the cleavage of the cohesin complex (specifically Scc1) joining sister chromatids together. This is all required to allow the cell to enter anaphase (Li *et al.,* 1997; Fang *et al.,* 1998; Hwang *et al.,* 1998; Kim *et al.,* 1998; Kim & Yu 2011). The APC is highly functionally conserved between yeast and humans. The core subunits of the APC associate with multiple distinct activator subunits (Höckner *et al.,* 2016).

The inhibition of APC activity is facilitated mainly by the Mitotic Checkpoint Complex (MCC). The proteins which directly bind to Cdc20, thus keeping it from activating the APC, are Mad2 and Mad3 (Chao *et al.,* 2012; Lau & Murray, 2012). The MCC assembles and localizes at unattached kinetochores. While the MCC remains formed, the Cdc20 subunit remains unavailable to the APC.

Many rounds of kinetochore-microtubule capture are usually required to allow for the eventual stabilization of bioriented connections. Only once the kinetochore-microtubule attachments are bioriented and no longer destabilized by the CPC can the SAC be silenced (Zich & Hardwick, 2010; Murray, 2011; Musacchio, 2011).

It is appropriate to note that SAC silencing is required for cell cycle progression. The manner in which the SAC is silenced is mostly through the dephosphorylation of SAC targets, including Spc105/Knl1 (Pinsky *et al.,* 2009; Vanoosthuyse & Hardwick, 2009; London *et al.,* 2012). This is facilitated by the phosphatase Glyc7 (or PP1 in humans). Additionally, Aurora B has been implicated in modulating the SAC by disrupting PP1 phosphatase activity, thereby preventing SAC silencing (Rosenberg *et al.,* 2011).

Summarily, the control of chromosome biorientation and segregation by the CPC and SAC has been the main focus of the most recent section. The CPC acts to destabilize erroneous attachments thereby triggering the SAC which provides the cell with enough time to obtain bioriented attachments.

1.2.5 Anaphase entry

Once the chromosomes have been correctly aligned and bioriented, the Spindle Assembly Checkpoint (SAC) is silenced (Pinsky *et al.,* 2006; 2009). The silencing of the SAC is mediated by a combination of Glyc7/PP1 phosphatase activity and lack of unbound kinetochores. This disables the MCC allowing Cdc20 to activate the APC and target securin for degradation. Loss of securin activates separase, an enzyme that cleaves the cohesin complex rings that hold sister chromatids together at the centromeric region (Li *et al.,* 1997; Fang *et al.,* 1998; Hwang *et al.,* 1998; Kim *et al.,* 1998; Kim & Yu 2011). The loss of cohesion between sister chromatids allows anaphase to truly begin as they are pulled apart and segregated. The physical forces which drive chromosomes toward the cellular poles is mediated by the depolymerization of kinetochore-bound microtubules (Asbury *et al.,* 2011). Notably, at anaphase onset Cdc14 dephosphorylates the CPC and it becomes redistributed from the inner centromere to the spindle microtubules (Mirchenko & Uhlmann, 2010; Tsukahara *et al.,* 2010; Storchova *et al.,* 2011; Campbell & Desai, 2013).

1.2.6 Telophase and cytokinesis

The final phases of mitosis include the decompaction of chromosomes, and in the case of open mitosis, the reformation of nuclear envelopes around the recently segregated chromosomes (Schellhaus *et al.,* 2016). Also, the sites of transcription known as nucleoli reform as well (Boisvert *et al.,* 2007). The site of abscission is decided in earlier stages of the cell-cycle (Balasubramanian, Bi and Glotzer, 2004). In both yeast and human cells, the physical act of cellular separation is performed by a ring formed from actin and myosin II, which tightens around the cellular membrane, forming what is known as the cleavage furrow (Bhavsar-Jog & Bi, 2017). This ring eventually pinches the cells off into two daughter cells. Notably, the division of cytoplasm as well as cellular organelles also occurs at this later stage and is known as cytokinesis (Glotzer, 2005). Additionally, CPC function is essential for cytokinesis in metazoan cells but not in yeast cells (Ainsztein *et al.,* 1998; Kitagawa & Lee, 2015). In summary, this section reviewed the stages of mitotic division highlighting the importance of the SCF complex in segregation fidelity. The significance of the CPC, APC and Mps1 in controlling the SAC was also reviewed. Now that we have had a general overview of the cell-cycle, we can focus more on how chromosomes become attached to microtubules at a molecular level.

1.3 Protein complexes required for chromosome biorientation and segregation

In order to address the complexities associated with missegregation, a sound understanding of the major mechanistic components behind segregation is vital. To this end, the main structural components important for mediating chromosomal segregation are discussed in this section.

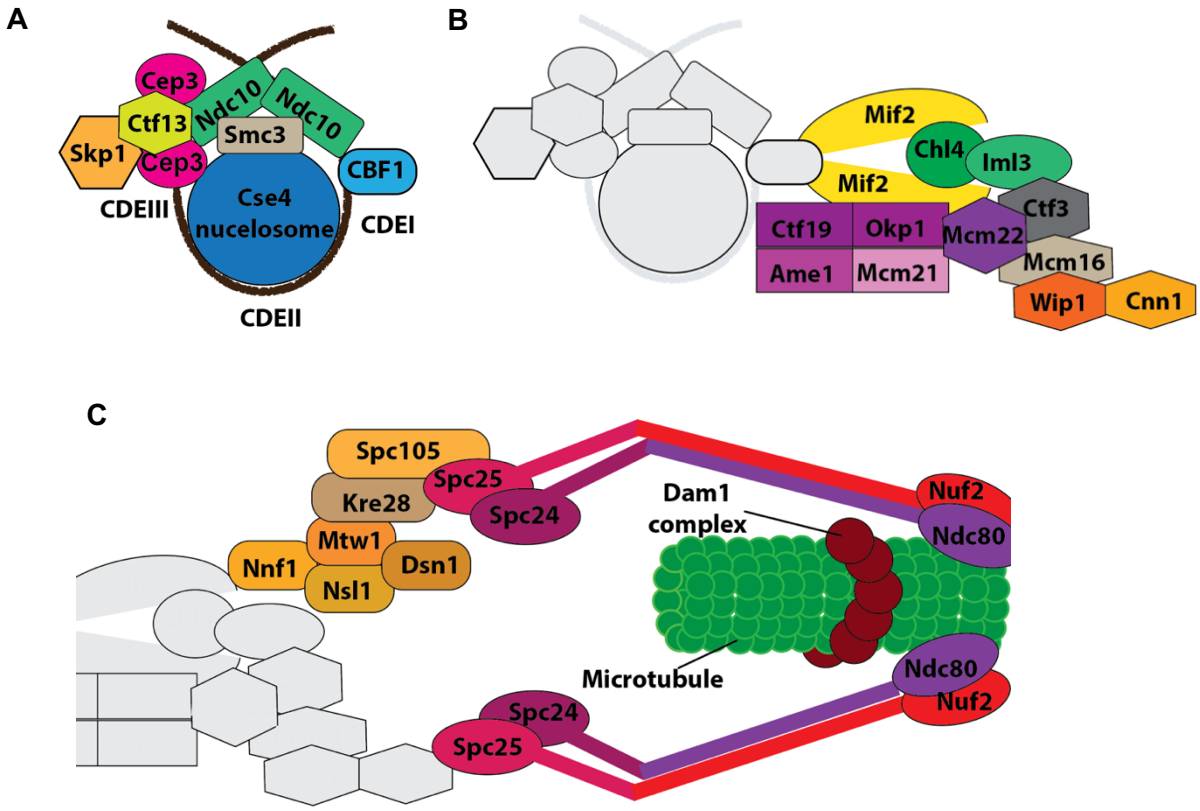

Figure 6. The kinetochore is assembled at centromeric chromatin in a stepwise manner (**A**)Schematic depicting DNA (black line) wound around the Cse4 nucleosome and inner-centromere binding subunits, including the CBF3 complex. Centromere determining elements (CDE) are also shown. Cse4 is deposited by the Smc3 chaperone (**B**)Schematic illustrating the inner kinetochore complexes including the CCAN (**C**) Schematic showing members of the outer-kinetochore including the KMN as well as the Dam1 complex.

Figure 6A adapted from (Biggins, 2013 p.827). **Figure 6B** and **6C** adapted from (Marsoner, 2022)

1.3.1 The centromere

In order to physically separate one's genetic information it is essential that a structure, upon which forces can be applied, forms connected to the chromatids directly. This physical structure is known as the centromere. In yeast this was first identified by Clarke and Carbon (1980) as being the region of the chromosomes that allows mitotic stability of plasmids. In most eukaryotes these loci are composed of

very large repetitive regions. In human cells these are known as alpha-satellites, and they consist of 170-bp long tandem repeat sequences. These types of centromeres are known as “regional” centromeres, because they are defined by a large region (ranging up to 4Mb) of the chromosome (Burrack & Berman, 2012). However, in budding yeast, the genetic elements that control the localization of the centromere are much smaller in length. The budding yeast centromere is defined as a 200-bp nuclease resistant region. Within this region is a 125bp “point” centromere. Comprising this genetic sequence are three conserved centromere-determining elements (CDEs). CDEI associates with Cbf1, a yeast specific protein which is nonessential, and CDEIII binds to the CBF3 complex, a yeast specific inner kinetochore subcomplex composed of four subunits: Ndc10, Ctf13, Skp1, and Cep3. CDEII is slightly longer than the other CDEs and is an AT-rich region (Clarke, 1998) (**Figure 6A**).

It should be noted that budding yeast relies more on genetic factors to control centromere assembly than epigenetic factors, which are utilized more commonly by eukaryotes (Black *et al.,* 2010; Henikoff & Furuyama, 2010). Most nucleosomes are made from histone octamers composed of two copies of four different subunits: H2A, H2B, H3 and H4. H2A is the histone phosphorylated by Bub1 kinase, which is required for Sgo1 localization (Indejeian *et al.,* 2005; Kitajima *et al.,* 2005; 2006; Fernius & Hardwick, 2007; Indjeian & Murray, 2007). At eukaryotic centromeres an H3-histone variant is used instead to form the nucleosomes at centromeres. This H3 variant is known as Cse4 in budding yeast, or CENP-A in humans, and was among the first centromeric proteins discovered in the 1980s (Earnshaw & Rothfield 1985; Palmer *et al.* 1987) (**Figure 6A**). Chromatin immunoprecipitation experiments showed that Cse4 is associated with centromeres (Stoler *et al.,* 1995; Meluh *et al.,* 1998; Stellfox *et al.,* 2013). Understanding the mechanisms that control the stoichiometry of Cse4-nucleosomes are very important for clarifying how centromeres form, as well as how this contributes to segregation fidelity. When the stoichiometry of Cse4 is disrupted this leads to CIN (Au *et al.,* 2020). The mechanism by which Cse4 is deposited into chromatin is still debated, but it is highly likely this involves a histone chaperone protein called Scm3 in budding yeast (Dunleavy *et al.,* 2009; Foltz *et al.,* 2009). In budding yeast, the specific deposition of Cse4 at the centromeres is mediated by Ndc10, a part of the CBF3 complex, which interacts with Smc3 (Camahort *et al*., 2007). The phosphorylation of Cse4 by Ipl1 has been linked to increased KT-MT attachment instability (Boeckmann *et al.,* 2013). Some of these phosphosites are found in the N-terminal part of Cse4, which associates with specific key members of the inner-kinetochore. This suggests that the phosphoregulation of Cse4 by the CPC is important for controlling kinetochore formation and subsequently segregation fidelity. The proteolytic degradation of Cse4 is tightly controlled by Psh1 E3 ubiquitin ligase. Additionally, it has been shown by Au *et al.,* (2020) that the $SCF^{cdc4/met30}$ complex is also responsible for the proteolytic degradation of Cse4.

It should be noted that in yeast one of the core-members of the SCF-complex is Skp1, which is also a part of the CBF3 inner kinetochore complex (Sorger *et al.,* 1995; Connelly & Hieter, 1996). Another point to highlight is that biochemical and protein degradation assays show that the SCF-complex is involved in the degradation of Ctf13. This same study also highlights that SCF-complex activity is modulated by phosphorylation of the target substrate (Kaplan *et al.,* 1997). These data further emphasize the significant connection between the SCF-complex and control of Cse4 as well as CBF3 stoichiometry, which is essential for segregation fidelity.

1.3.2 The inner kinetochore

Although the centromere forms the foundation on which a connection to chromatin can be made, it does not directly connect with the microtubules itself. Instead a large, intermediary complex acts as a middleman that connects the microtubules to the centromere and by extension the chromatin within the nucleus. This complex uses the centromere as a platform on which to build itself, and is known as the kinetochore. The kinetochore is a very large complex made out of several subcomplexes. For the sake of simplicity, the kinetochore can be broken into two pieces: the inner kinetochore and the outer-kinetochore (Biggins, 2013). The inner kinetochore comprises those subcomplexes most biochemically associated with, and therefore most proximal to, the centromere **(Figure 6B)** (Stoler *et al.,* 1995; Meluh *et al.,* 1998; Stellfox *et al.,* 2013). The CBF3 complex is a member of the inner kinetochore and was mentioned earlier. However, the CBF3 complex is not conserved in other eukaryotes (Biggins, 1999; 2013).

In the past it was challenging to find conserved inner kinetochore proteins because of low sequence similarities. Despite this, there are now several accepted inner kinetochore proteins conserved between yeast and humans which form the constitutive centromere associated network (CCAN) (Biggins, 2013; Westermann & Schleiffer, 2013; Musacchio & Desai, 2017). The CCAN is present at centromeres in both humans and yeast for most of the cell-cycle, and is momentarily only briefly absent during S-phase (Kitamura *et al.,* 2007). Otherwise the inner kinetochore (CCAN and CBF3 in yeast) is constitutively formed (Nevaro & Cheeseman, 2021).

Mif2 (CENP-C in humans) was one of the first members of the CCAN to be discovered and characterized. Mif2 is a conserved inner kinetochore protein that forms a homodimer and binds directly to CDEIII and associates specifically with Cse4 nucleosomes (Cohen *et al.,* 2008; Xiao *et al.*, 2017; Fischböck-Halwachs *et al.*, 2019). The COMA complex is another member of the CCAN, and is made up of four subunits: Ctf19, Okp1, Mcm21 and Ame1. The COMA complex has too been found to associate with Cse4 specific nucleosomes (Fischböck-Halwachs *et al.*, 2019). Crosslinking experiments have shown that Okp1 binds to an N-terminal domain within Cse4 (Fischböck-Halwachs *et al.*, 2019). Only Okp1 and Ame1 are essential

for mitosis and *in vitro* experiments show an interaction with Mif2 (Hornung et al., 2014). Additionally, this interaction is also important for outer-kinetochore assembly, further explaining why these two proteins are essential. It is also pertinent to add that Ame1 has been shown to be degraded by the SCF^{cdc4} E3 ubiquitin ligase complex (Böhm *et al.,* 2021). Disruption of this degradation leads to missegregation. This reveals another link between the SCF-complex and the control of kinetochore stoichiometry and segregation fidelity.

Despite Mcm21 and Ctf19 being disposable for mitotic divisions, they are essential for establishing cohesion during meiotic divisions (Agarwal *et al.,* 2015). The remaining members of the CCAN are non-essential for viability, and comprise the Iml3/Chl4 complex, the Ctf3 complex (composed of Ctf3, Mcm16 and Mcm22), and the Cnn1 complex (composed of Wip1 and Cnn1) (Bock et al., 2012; Schleiffer et al., 2012) (**Figure 6B**).

The Iml3/Chl4 complex interacts with the COMA complex, and the Mif2 homodimer (Hinshaw & Harrison, 2013). It has also been shown via cryo-EM that the Iml3/Chl4 complex (specifically Iml3) interacts with Ctf3, a member of the Ctf3 inner kinetochore subcomplex (Hinshaw *et al.,* 2019). Ctf3 also binds directly to the Cnn1 complex. The Cnn1 complex forms a heterodimer and is located in the outermost part of the inner-kinetochore. The Cnn1 complex is partly responsible for recruiting the outer-kinetochore Ndc80 subcomplex; a complex essential for viability (**Figure6B** and **6C**) (Malvezzi *et al.,* 2013; Lang *et al.,* 2018). Despite being an interface between the inner and outer kinetochore, the Cnn1 complex remains non-essential. This implies that the Ndc80 complex is recruited by an alternative mechanism. The formation of the outer-kinetochore will be further discussed in the next part of this chapter.

1.3.3 The outer kinetochore

The outer-kinetochore is comprised of those sub-complexes most proximal to the microtubule (**Figure6C**). It is at this part of the kinetochore the microtubules directly bind. In yeast, the inner and outer kinetochore complexes remain assembled and present at the centromeres for most of the cell cycle (Nevaro & Cheeseman, 2021).

1.3.3.1 The KMN network

The subcomplexes comprising the outer-kinetochore include the Mis12-complex, the Kln1-complex, and the Ndc80-complex. These are all conserved between yeast and humans and form the KMN network (Kln1, Mis12, and Ndc80 complex network) (Cheeseman *et al.,* 2006). While the Ndc80-complex is highly important for binding to microtubules, especially in humans, a yeast specific complex called the Dam1-complex is also a part of the outer-kinetochore and contributes significantly to microtubule binding (**Figure 6C**) (Enquist-Newman *et al.,* 2001; Cheeseman *et al.,*

2001; 2002). After the establishment of the centromere and essential inner kinetochore components, the Mis12 complex (composed of the protein subunits Mtw1, Dsn1, Nnf1 and Nsl1) is responsible for recruiting the Ndc80 and Kln1 complexes to the kinetochore (**Figure 6C**) (Maskell *et al.,* 2010; Lang *et al.,* 2018). The Mis12 complex is formed by two heterodimers made from Mtw1/Nnf1 and Dns1/Nsl1. Ipl1 is responsible for phosphorylating two sites in Dsn1 which are crucial for outer kinetochore assembly. In Xenopus it was shown that phosphorylation of Dns1 by Aurora B is vital for outer kinetochore assembly (Bonner *et al.,* 2019). When Dsn1 is unphosphorylated, it cannot interact with Mif2 (CENP-C) (Dimitrova *et al*., 2016). Unsurprisingly, mutating three phosphosites to non-phosphorylate alanines (*dsn1-3A*) resulted in reduced levels of Ndc80 and Kln1 complex proteins. Relevant to this, it was previously mentioned that the Cnn1 complex is also responsible for recruiting Ndc80-complex. Consequently, loss of Cnn1 complex function (*cnn1Δ*) coupled with loss of Mis12 function (*dsn1-3A*) is synthetic lethal (Lang *et al.,* 2018). This suggests that the Mis12 complex and the Cnn1 complex are both responsible for recruiting Ndc80, and in this regard are redundant. The loss of both these complexes however is not viable. Mis12 complex recruits Ndc80 complex and also the Spc105 complex. The Spc105 complex is made from Kre28 and Spc105, which form a heterotrimeric complex (two Kre28 molecules to one Spc105 molecule). *In vitro* the Spc105/Kln1 complex binds microtubules, but its main function *in vivo* is SAC regulation (Lara-Gonzalez *et al.,* 2021).

In a number of model organisms, the main complex in the outer kinetochore responsible for binding to microtubules is the Ndc80 complex. There are four subunits which comprise the Ndc80 complex: Spc24, Spc25, Ndc80 and Nuf2. These four subunits form two subcomplexes: a Spc24/Spc25 heterodimer, and a Ndc80/Nuf2 heterodimer. Each of these contains globular head domains and they interact with each other through their coiled coil domains. The final orientation of this complex is such that the Spc34/Spc25 globular domains associate with Dsn1 (in the Mis12 complex) and the globular domains of Ndc80/Nuf2 bind directly to microtubules (**Figure6C**) (Wei *et al.,* 2005; Ciferri *et al.,* 2007). Ndc80 contains multiple Ipl1 phosphorylation sites within its N-terminus. It is well established in literature that phosphoregulation of Ndc80 is highly important for modulating microtubule binding affinity and consequently segregation fidelity (DeLuca *et al.,* 2006; Sarangapani *et al.,* 2013). The phosphorylation of Ndc80 has been shown *in vivo* as well as *in vitro*. Phosphorylation of the Ndc80 reduces the electrostatic attraction between the Ndc80 complex and negatively charged domains within tubulin (Miller *et al.,* 2008). For vertebrate cell-lines, Ndc80 appears to be the main mediator for microtubule binding in the outer-kinetochore. Indeed, when Ndc80 is rendered unphosphorylatable, chromosomal biorientation is highly perturbed (DeLuca *et al.,* 2006). However, in yeast Ndc80 non-phosphorylatable mutants do not show signs of missegregation under conditions where mitosis is not disrupted

(Akiyoshi *et al.,* 2009). This means that yeast do not solely rely on the Ndc80 complex to bind to microtubules directly.

1.3.3.2 The Dam1 complex

In the late 90s some of the first subunits of the yeast specific Dam1-complex were identified and characterized (Chen *et al.,* 1997; Hofmann *et al.,* 1998; Jones *et al.,* 1999; Cheeseman *et al.,* 2001; 2002; Enquist-Newman *et al.,* 2001; Janke *et al.,* 2002; Li *et al.,* 2002). These subunits included Duo1 and Dam1, which both proved to be essential for yeast viability (Enquist-Newman *et al.,* 2001). Based on crosslinking and yeast two-hybrid assays, it has been demonstrated that Duo1 and Dam1 both interact and bind with microtubules directly (Shang *et al.,* 2003). It is now known that the Dam1 complex is composed of several decamers, which multimerize together to form the Dam1 complex ring (**Figure7A**). The Dam1 decamer can be subdivided into two "arms". Each of these arms consists of five subunits each (**Figure7B**). Arm 2 contains Duo1 and Dam1, and is the arm which directly interacts with microtubules. Live fluorescence microscopy assays, which labelled different subunits from the different arms, show that the microtubule binding activity of arm 2 does not require prior oligomerization with arm 1. However, in order to facilitate robust coupling to dynamic microtubule ends against applied mechanical loads, the oligomerization of the arms is vital (Umbreit *et al.,* 2014). After the decamer is formed by the oligomerization of the two arms, the ring structure can be assembled. Approximately 13 independent decameric complexes multimerize together to form a ring-shaped complex. *In vitro* cryo-EM images have shown that these Dam1-complex rings form spontaneously around microtubules and that even partially formed rings are able to bind to microtubules (Gonen *et al.,* 2012; Ng *et al.,* 2019).

Structural analyses show the Dam1 decameric complex contains two main interfaces essential for the multimerization of the assembly (**Figure7A**) (Jenni & Harrison, 2018). It is still debated whether Dam1-complex rings are partial or full rings *in vivo*. It is also not known what effect partial rings may have on chromosome segregation fidelity *in vivo*. One study found that only 40% of the Dam1-complex assemblies on microtubules were fully formed rings at metaphase (Ng *et al.,* 2019). Besides Duo1 and Dam1, the other members of the Dam1-complex include: Spc34, Dad1, Dad2, Dad3, Hsk3, Dad4, Ask1, and Spc19 (Chen *et al.,* 1997; Hofmann *et al.,* 1998; Jones *et al.,* 1999; Cheeseman *et al.,* 2001; 2002; Enquist-Newman *et al.,* 2001; Janke *et al.,* 2002; Li *et al.,* 2002). Similar to the Ndc80 complex, the Dam1 complex's stability and microtubule binding affinity are controlled by phosphorylation (Cheeseman *et al.,* 2002; Sarangapani *et al.,* 2013; Jin & Wang, 2013). The main essential sites for this phosphorylation occur within Dam1 itself. Dam1 possesses several phosphosites. Some are phosphorylated by Mps1 (S13, S49, S217, S218 and S232) others by Ipl1(S20, S257, S265, and S292) (Shimogawa *et al.,* 2006; 2010; Sarangapani *et al.,* 2013; Meyer *et al.,* 2018). These four Ipl1-phospho sites

are known to be vital for controlling kinetochore-microtubule stability. This has been shown by testing the viability of yeast strains with non-phosphorylatable Dam1 mutants. Only when all four Ipl1 sites are turned from serines to alanines does the yeast cell die (Cheeseman *et al.,* 2002; Sarangapani *et al.,* 2013). A study using optical trap assays demonstrated that mutations which mimic the negative charge generated by phosphorylation (phosphomimics) significantly reduced KT-MT stability. Furthermore, non-phosphorylatable mutants (*dam1*-S20A, *dam1-3A* or *dam1-4A*) do not cause any decrease in KT-MT connection stability (Sarangapani *et al.,* 2013). Additionally, it has been speculated that mutation of Dam1 serine 20 also results in defects in Dam1 complex oligomerization (Jenni & Harrison, 2018). In contrast to this, the *dam1(S257D, S265D, and S292D)* mutant, also known as the *dam1-3D* mutant, does not disrupt attachment strength. More intriguingly, *dam1-3D* is associated with slow growth and anaphase arrest (Cheeseman *et al.,* 2002; Jin & Wang, 2013). Studies from literature have explained these phenotypes by showing enhanced levels of SAC signaling within *dam1-3D* cells (Jin & Wang, 2013). Other experiments show that if Mad1 or Mad2 (key members of the SAC) are deleted, the overactive SAC signaling and anaphase arrest is lost in *dam1-3D* cells. Surprisingly, chromosomal missegregation assays have revealed that *dam1-3D* does not cause missegregation (Jin & Wang, 2013). Based on this, the *dam1-3D* mediated overactivation of the SAC is not related to decreased KT-MT stability (Jin and Wang, 2013). Instead, it is speculated that the *dam1-3D* mutant inhibits SAC silencing.

A complex in humans has been proposed as a putative functional counterpart to the Dam1-complex: the spindle and kinetochore associated (Ska)-complex (Sauer *et al.,* 2005; Welburn *et al.,* 2009). Besides the fact that the Ska-complex has Ipl1/Aurora B phosphosites, there is no apparent sequence or structural similarity between them (Theis *et al.,* 2009; Jeyaprakash *et al.,* 2012). Although it does not form a ring around microtubules like Dam1-complex, the Ska complex can bind and move along depolymerizing microtubules (Welburn *et al.,* 2009). Biological and biochemical assays have shown that loss of Ska-complex activity leads to microtubule attachment defects, delayed chromosome compaction, and delayed SAC silencing (Gaitanos *et al*., 2009; Raaijmakers *et al*., 2009; Welburn *et al.,* 2009; Daum *et al.,* 2009). The Ska-complex is essential in humans for forming microtubule attachments *in vivo.* RNAi experiments against Ska subunits result in missegregation, metaphase arrest and cohesion fatigue (Gaitanos *et al.,* 2009; Raaijmakers *et al.,* 2009; Welburn *et al.,* 2009). Similar to the Dam1-complex, the Ska-complex requires Ndc80 and microtubules to localize to kinetochores *in vivo*. Another similarity between the Dam1 complex and Ska complex is the presence of Mps1 phosphosites. Using a kinetochore targeting assay it was shown that Mps1 can destabilize kinetochore-microtubule attachments (Maciejowski *et al.,* 2017). Furthermore, the Ska-complex may aid anaphase onset by facilitating the activity of the anaphase promoting complex (APC) and recruitment of Protein Phosphatase 1 (PP1) (Sivakumar *et al.,*

2014; 2016). Intriguingly, the overexpression of the Ska complex is associated with poor prognosis of various cancers. The precise mechanism as to how the Ska complex does this is not known (reviewed in Yu, 2022).

In summary, the kinetochore comprises several essential complexes that are required for connecting chromosomes to microtubules, thereby facilitating segregation fidelity. The kinetochore is an interface which connects microtubules to centromeric chromatin. The ability of the kinetochore complexes to form connections with microtubules is largely dependent on the structure and electrostatic properties of the proteins which form the complexes. Many of these regulatory proteins either add or remove phosphate groups from specific substrates. This allows the activity of specific structures to be modulated. Lastly, another factor highly relevant to forming kinetochore-microtubule attachments, and segregation fidelity, includes microtubule organizing centers (MTOCs) where microtubules nucleate.

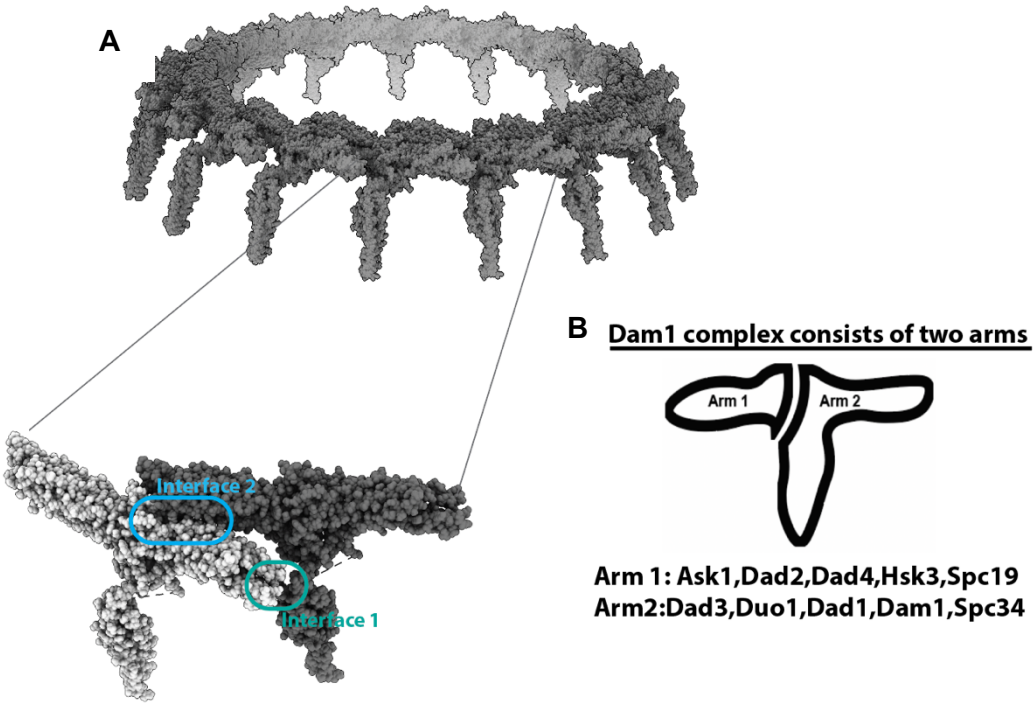

Figure 7. Multiple Dam1 decameric complexes multimerize to form a ring
(**A**) Sphere representation of the crystal structure of *C. thermophilum* Dam1 complex homologues. The image at the top depicts the entire ring. The image below shows two Dam1 decamers which oligomerize via interfaces 1 and 2. The interfaces are shown here with a blue and green box (Jenni and Harrison, 2018) (**B**) The Dam1 decamer is composed from two separate “arms”. Each arm comprises five subunits.

Figure 7A adapted from (Clarke *et al.,* 2022) and made from PDB: 6CFZ from (Jenni & Harrison, 2018) using Chimera-X software version 1.5 (Pettersen *et al.,* 2021).

1.3.4 Microtubule nucleation, as well as the structure of the SPB, are vital for segregation fidelity

Under physiological conditions microtubules have a very low likelihood to polymerize spontaneously. It is therefore not surprising that platforms upon which microtubules can be nucleated are required within cells. Gamma-tubulin (Tub4 in budding yeast) is essential for microtubule nucleation at the Spindle Pole Body (SPB) (Wigge *et al.,* 1998; Kollman *et al.,* 2008; 2010; Gombos *et al.,* 2013). Tub4 is recruited to the SPB and, once there, acts as a template upon which alpha and beta tubulin dimers can begin nucleation of microtubule filaments. Tub4 also acts as a cap at the minus-end of the microtubule; the plus end remains free to polymerize. In yeast, the MTOC is called the Spindle Pole Body (SPB) (**Figure 8**) (Knop *et al.,* 1999; Jaspersen & Winey, 2004). This MTOC is quite different from metazoan centrosomes. In budding yeast, both SPBs are embedded in the nuclear membrane and have very a different structural composition to centrosomes. In centrosomes the central protein structures are called centrioles. Usually centrosomes contain two centrioles positioned perpendicular to each other. A myriad of scaffold and regulatory proteins interact and form a layer around the centrioles. This layer later matures to form the pericentriolar material (Garbrecht *et al.,* 2021; Vasquez-Limeta *et al.,* 2021; Blanco-Ameijeiras *et al.,* 2022). It is this layer that forms the scaffold upon which microtubules can begin nucleation and polymerization.

Supernumerary centrosomes have been identified as a source of CIN (Sansregret *et al.,* 2018; Gheghiani *et al.,* 2021). Supernumerary centrosomes can also be found in cancer cell lines. The control of centrosome structure and duplication is therefore relevant to understanding segregation fidelity. In contrast to centrosomes in humans, SPBs in yeast do not possess centrioles (Winey & Bloom, 2012). Instead SPBs are embedded within the nuclear membrane and contain an outer plaque layer which connects to cytoplasmic microtubules. These help to position the nucleus during the cell-cycle.

The SPB is a large macromolecular assembly comprised of many subunits. There are multiple layers to the SPB: the outermost plaque layer, two intermediate layers, a central layer, and then an inner plaque layer that nucleates and associates with nuclear microtubules (**Figure8**). The core proteins of the SPB contain coiled-coil domains and form various homodimers and heterodimers. One of the main core components is Spc42, which is essential for SPB duplication and assembly. Spc42 is found in the central plaque layer of the SPB and associates with two other essential proteins that localize to the SPB: Spc110 and Spc29 (**Figure8**) (Alonso *et al.,* 2020). Additionally, the size of the SPB's diameter increases during mitosis (Greenland *et al.,* 2010). The diameter of SPBs limits the number of microtubule interactions that are possible. Other proteins essential for microtubule nucleation include Spc98, Spc97 and gamma-tubulin (Tub4), which localize at the inner and outer plaque layers of the SPB (**Figure8**). At the inner plaque layer, the microtubules which

connect with the kinetochores are nucleated. The SPB must be duplicated once per cell cycle as two SPBs are needed to form bioriented spindles. The kinase Mps1 is also essential for SPB duplication (Winey *et al.,* 1991; Straight *et al.,* 2000; Jones *et al.,* 2001). The duplication of the SPB is completed before DNA replication (Rüthnick & Schiebel, 2016). Summarily, the structure, duplication and size of MTOCs is highly relevant to chromosome biorientation. Although some of the details differ between yeast and humans in terms of structure, the overall function and significance of this organelle is conserved. The final part of the introduction will review the main technical differences between human cells and budding yeast relevant to this project.

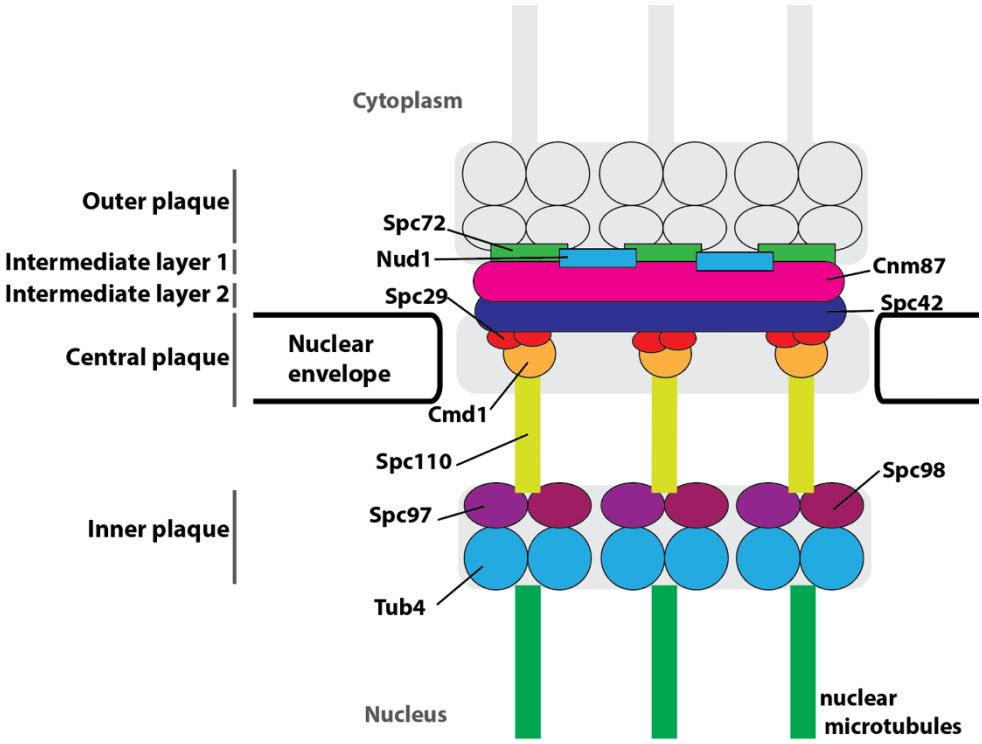

Figure 8. SPBs are embedded in the nuclear envelope and form microtubules within the nucleus
This schematic depicts the structure of the SPB. The outer-plaque (grey) is established proximal to the cytoplasm and can nucleate cytoplasmic-microtubules. However, the more relevant microtubules form within the nucleus at the inner plaque.

Adapted from (Rayment, 2023).

1.4 Advantages and disadvantages – using budding yeast as a model to investigate adaptation to CIN and aneuploidy

Now that the major components which control chromosome biorientation have been reviewed in detail, the technical advantages and disadvantages of using budding yeast as a model to study persistent CIN adaption should be addressed. One strength of using budding yeast as a model is that yeast can still missegregate at

rates similar to what is seen in cancer. Consequently, budding yeast can be used to study adaptation to overstablized attachments due to several highly conserved kinetochore and SAC factors that exist between yeast and humans (Storchova, 2018). As has been mentioned previously, the molecular processes which control mitosis are functionally conserved.

In order to understand how cells can adapt to CIN and aneuploidy, we need to induce CIN and aneuploidy within cells, and then analyze the mechanisms utilized to adapt. This can give us a better idea about how cells adapt and potentially provide new insights, as well as new therapeutic targets, into cancer evolution. However, inducing CIN or aneuploidy in cells is a major challenge due to their sensitivity (Gropp *et al.,* 1983; Torres *et al.,* 2007;2010; Sheltzer *et al.,* 2011; Pfau & Amon, 2012; Giam & Rancati, 2015; Passerini *et al.,* 2016; Alonso y Adel *et al.,* 2023). The complete loss of any checkpoint gene or CPC component is usually lethal in animal cells (Basu *et al.,* 1999; Kitagawa & Rose, 1999; Dobles *et al.,* 2000; Kalitsis *et al.,* 2000; Gillett *et al.,* 2004). Only partial loss of function or drug induced CIN/aneuploidy is possible. Unsurprisingly, such techniques have significant off-target effects.

One of the major benefits of using budding yeast is that the loss of Bir1/Survivin results in viable haploid (homozygous *bir1Δ*) spores 10% of the time (Campbell & Desai, 2013). Another benefit to this is that a complete homozygous deletion has no possibility of reversion. A further advantage of using budding yeast is that the CPC's only known essential function is in chromosome biorientation. This means that any lethality observed must be a result directly linked to loss of chromosome biorientation. In contrast to this, in human cells the CPC has other essential functions during cytokinesis (Ainsztein *et al.,* 1998; Kitagawa & Lee, 2015). In *Xenopus* the CPC is essential for kinetochore assembly (Bonner *et al.,* 2019)

Additionally, the doubling time of budding yeast is substantially faster than in human cells, therefore adaptation assays can be performed more quickly. Furthermore, the small genome size of yeast (approximately 6000 genes) makes sequencing the entire genome of over 100 strains relatively straight forward.

Lastly, the fact that only one microtubule binds to one kinetochore aids the interpretation of assays in which we look at attachment states; there is either an attachment or not, no "partial attachment" states (Winey *et al.,* 1995). In humans however, kinetochores have between three and thirty binding sites for microtubules. Consequently, kinetochores can be "partially" bound by microtubules.

One of the major caveats with using *Saccharomyces cerevisiae* to study cancer progression is that yeast does not form cancer per se. Tumor suppressors are genes that act to inhibit tumorigenesis (Menendez *et al.,* 2013). Usually, this is performed by activating various checkpoints, including apoptosis or stable cell-cycle arrest. In order for cancer to form, these tumor suppressors, including the well-studied p53 tumor suppressor, must be inhibited or bypassed. This allows cancer cells to undergo cell division with high rates of missegregation and aneuploidy.

Studies have shown that p53 is mutated in 50% of cancers, making it one of the most universal mutations in cancer (Smardova *et al.,* 2005; Yamamoto & Iwakuma, 2018; Mantovani *et al.,* 2019; Hu *et al.,* 2021). While tumor suppressors act as barriers to tumorigenesis, genes which facilitate cancer are referred to as oncogenes. These include certain transcription factors like c-Myc that control the activation of genes responsible for promoting growth (Meyer *et al.,* 2020). Despite the fact budding yeast does not develop cancer, it still possesses genes which either promote cell growth (like oncogenes) or inhibit cell growth (like tumor suppressors). It is this fact, in combination with the functional conservation between human and budding yeast mitosis, that makes budding yeast an appropriate model for studying adaptation to CIN in cancer.

Summarily, budding yeast is still a very useful model for studying adaptation to CIN because 1) the CPC has no other function in yeast other than chromosome biorientation 2) yeast can survive the induction of high rates of persistent CIN or aneuploidy 3) yeast has a relatively fast doubling time (90minutes) making it a suitable choice for long term adaptation studies 4) budding yeast has a relatively small genome, thereby facilitating the sequencing of the whole genome and 5) mitotic pathways associated with cancer progression are functionally conserved between yeast and humans.

2. Aim of the thesis

The main motivation behind this thesis project can to be summed up by the question: how can healthy cells, which are sensitive to genetic detriments such as CIN and aneuploidy, adapt and become not just *resistant* but actually *select* for these same genetic detriments in cancer cells? Consequently, the first objective of this thesis project was to identify candidate genes/mutations that allow for cells to cope with persistent CIN and/or aneuploidy over long periods of time. The second objective was to characterize these mutations and understand the mechanisms which allow for adaption to CIN and/or aneuploidy.

Firstly, we wished to investigate how cells initially adapt to high rates of CIN and aneuploidy. We achieved this by deleting Bir1 in several haploid budding yeast strains and then grew them for approximately 200 generations. We discovered that these strains (*bir1Δ-ad*) accumulate beneficial aneuploidies to help them cope with high amounts of CIN (Ravichandran *et al.,* 2018; 2020). Additionally, we discovered that these adapted *bir1Δ*-ad strains did not accumulate mutations which were enriched in CIN related genes. Indeed, the number of mutations in genes related to CIN were no different than what would be expected by chance. The main conclusion here is that initial adaptation is achieved by selecting for beneficial aneuploidies.

However, it is known in literature that aneuploidy of any kind, however beneficial it may be initially, will always provide a source of proteotoxic stress on the cell (Yona *et al.,* 2012; Torres *et al.,* 2010). Consequently, one of the aims was to investigate how these CPC deficient cells coped with CIN and aneuploidy over even longer periods of time. We hypothesized that eventually suppressor mutations would accumulate, and the aneuploidy burden could be subsequently reduced or refined (Yona *et al.,* 2012).

Once we allowed the CPC deficient cells to adapt to persistent CIN for another 200 generations, we harvested these strains (*bir1Δ-ad2*) and performed Next Generation Sequencing (NGS). Based on these data, we found the aneuploid karyotypes of these strains became refined and converged on an optimal karyotype. We also found an accumulation of CIN related mutations; almost twice what is expected by chance. Several mutations engineered into a parental strain rescued the growth detriment caused by *bir1Δ*. The suppressor mutations that were confirmed by the plasmid shuffle assay fell into roughly four categories: the outer-kinetochore, the SCF^{cdc4} complex, Mps1 and the CPC itself. What we also found was a reduction in total aneuploidy in those strains that possess confirmed suppressors. Additionally, we showed via a mini-chromosome loss assay that the missegregation caused by loss of Bir1 can be significantly reduced by the suppressors. Now that we had identified suppressor mutations, we proceeded to our second objective: characterizing the molecular pathways involved in rescuing loss of CPC function. To this end, we performed live fluorescence microscopy assays, growth tests, temperature sensitivity assays, and structural analysis of a major component of the

outer kinetochore: the Dam1-complex. What we discovered was that suppressor mutations in the Dam1-complex likely interrupt oligomerization, and subsequent microtubule binding. This reduces the stability of the kinetochore-microtubule attachment, thus counteracting the overstabilization caused by loss of Bir1. However, the mutations outside the outer-kinetochore (such as in SCF and Mps1) did not act by directly destabilizing kinetochore-microtubule attachments. Instead, these mutations seem to affect the CPC directly.

3. Results

3.1 Genetic interactions between specific chromosome copy number alterations dictate complex aneuploidy patterns

The following manuscript was submitted on the 1st of August 2018 to *Genes and Development*. The final revised version was accepted for publication on October 3rd 2018. In this paper the experiments and data shown in supplementary tables 3 and 4 were performed by the author of this thesis. Furthermore, the author of this thesis also contributed to discussions during the revision process and provided input on the writing process. Most of the experiments for this paper were performed by Madhwesh C. Ravichandran and the project was originally conceptualized by Christopher S. Campbell. It should be noted that a number of experiments for this paper were performed by Sarah Fink and Franziska Christina Hofer. The published version of this article can be found at: https://pubmed.ncbi.nlm.nih.gov/30463904/. The DOI is: 10.1101/gad.319400.118

Genetic interactions between specific chromosome copy number alterations dictate complex aneuploidy patterns

Madhwesh C. Ravichandran, Sarah Fink, Matthew N. Clarke, Franziska Christina Hofer, and Christopher S. Campbell

Department of Chromosome Biology, Max F. Perutz Laboratories, University of Vienna, Vienna Biocenter, Vienna 1030, Austria

Cells that contain an abnormal number of chromosomes are called aneuploid. High rates of aneuploidy in cancer are correlated with an increased frequency of chromosome missegregation, termed chromosomal instability (CIN). Both high levels of aneuploidy and CIN are associated with cancers that are resistant to treatment. Although aneuploidy and CIN are typically detrimental to cell growth, they can aid in adaptation to selective pressures. Here, we induced extremely high rates of chromosome missegregation in yeast to determine how cells adapt to CIN over time. We found that adaptation to CIN occurs initially through many different individual chromosomal aneuploidies. Interestingly, the adapted yeast strains acquire complex karyotypes with specific subsets of the beneficial aneuploid chromosomes. These complex aneuploidy patterns are governed by synthetic genetic interactions between individual chromosomal abnormalities, which we refer to as chromosome copy number interactions (CCNIs). Given enough time, distinct karyotypic patterns in separate yeast populations converge on a refined complex aneuploid state. Surprisingly, some chromosomal aneuploidies that provided an advantage early on in adaptation are eventually lost due to negative CCNIs with even more beneficial aneuploid chromosome combinations. Together, our results show how cells adapt by obtaining specific complex aneuploid karyotypes in the presence of CIN.

[*Keywords*: chromosomes; aneuploidy; chromosomal instability; CIN; adaptation; chromosomal passenger complex]

Supplemental material is available for this article.

Received August 1, 2018; revised version accepted October 3, 2018.

Accurate distribution of replicated genetic material to daughter cells is one of the most fundamental requirements of cell division. Errors in chromosome segregation lead to the loss or gain of chromosomes, a state called aneuploidy. In many cases, cancer cells have highly aberrant chromosome copy numbers and extremely complex karyotypes (Mitelman Database of Chromosome Aberrations and Gene Fusions in Cancer, http://cgap.nci.nih.gov/Chromosomes/Mitelman). The complexity of these cancer karyotypes makes it difficult to retroactively piece together the steps in their formation.

Aneuploidy is generally associated with decreased cellular fitness. Experiments using yeast or human cell lines engineered with specific aneuploidies have revealed that doubling the copy number of single chromosomes leads to increased expression of nearly all of the genes on that chromosome (Torres et al. 2007; Stingele et al. 2012). This creates imbalances in the expression levels between genes on different chromosomes. These imbalances lead to proteotoxic stress and increased rates of mutation and chromosome missegregation (Sheltzer et al. 2011; Oromendia et al. 2012; Zhu et al. 2012; Passerini et al. 2016).

In contrast, in certain cases, aneuploidy provides a selective advantage. Specific aneuploidies have been shown to provide resistance to stress conditions in yeast (Selmecki et al. 2006; Chen et al. 2012). Aneuploidy can also act as a suppressor of certain mutations (Rancati et al. 2008; Liu et al. 2015; Ryu et al. 2016). Although aneuploid chromosomes alter the stoichiometry of many genes, the selective advantage can often be attributed to the change in expression of one or two genes (Hughes et al. 2000; Rancati et al. 2008; Ryu et al. 2016). This indicates that, similar to other types of mutations, aneuploidy is typically detrimental but can be beneficial to cellular growth in specific cases. These results also suggest that the selective force on aneuploidy for a particular chromosome is determined mainly by the specific advantage of altered expression of a few genes. These advantages are tempered by the general disadvantage of expression imbalances for many other genes.

Corresponding author: christopher.campbell@univie.ac.at

Article published online ahead of print. Article and publication date are online at http://www.genesdev.org/cgi/doi/10.1101/gad.319400.118. Freely available online through the *Genes & Development* Open Access option.

Aneuploidy arises from errors in cell division that result in the uneven distribution of the chromosomes between the two daughter cells. The increased rate of the formation of aneuploidy resulting from chromosome missegregation errors is called chromosomal instability (CIN). Importantly, both aneuploidy and CIN are hallmarks of cancer and are indicators of poor prognosis (for review, see Sansregret et al. 2018). Some cancer cell lines have chromosome segregation errors as high as 1% per chromosome per cell division, which would be detrimental to the growth of normal cells (Thompson and Compton 2008). Little is known about how cancer cells adapt to thrive with high levels of CIN.

In this study, we induced extremely high rates of chromosome missegregation in yeast to determine how they adapt to CIN over time. We found that the yeast adapted primarily through the accumulation of beneficial aneuploidies of many different chromosomes. The adapted yeast acquired complex karyotypes that consisted of specific subsets of the beneficial aneuploid chromosomes. By engineering the observed complex aneuploidy patterns in the absence of CIN, we demonstrate that distinct patterns of complex karyotypes are created by genetic interactions between individual aneuploid chromosomes. Given enough time to adapt, divergent complex karyotype patterns eventually converge on an "optimal" complex karyotype that maximizes the selective advantage of individual chromosomal aneuploidies while minimizing the negative genetic interactions between aneuploidies. This process often involves the loss of beneficial aneuploidies in order to gain other, incompatible aneuploid chromosomes. Overall, our results show that complex aneuploid karyotypes result from CIN in a stepwise manner that is heavily influenced by genetic interactions between aneuploid chromosomes.

Results

Yeast cells adapt to CIN through frequent accumulation of specific aneuploidies

To induce high rates of CIN in haploid budding yeast, we deleted the Survivin homolog Bir1. Bir1 is a member of the chromosomal passenger complex (CPC), which prevents chromosome missegregation by detecting and correcting improper connections between chromosomes and the mitotic spindle. Following tetrad dissection of a *BIR1*/*bir1Δ* heterozygous diploid, only ~10% of the *bir1Δ* spores are able to form colonies (Sandall et al. 2006). The cells in the surviving 10% of colonies have extremely high rates of chromosome missegregation, making *bir1Δ* a strong candidate for inducing complex aneuploidy (Campbell and Desai 2013). To obtain strains in a semistable state amenable to further analysis, >100 isolated cells from 19 individual *bir1Δ* spores were allowed to adapt over 10 clonal expansions by selecting a single colony every 2 d. These haploid adapted strains, now called *bir1Δ-ad,* grow faster than the *bir1Δ* strains prior to adaptation; however, their growth rates remain lower than that of wild-type strains (Fig. 1A,B). To directly measure the rate of chromosome missegregation of the *bir1Δ* strains after adaptation, we monitored a fluorescently labeled chromosome by live microscopy. The missegregation rate of chromosome 4 for a subset of the *bir1Δ-ad* strains was found to vary from 0.5% to 4.2% per cell division (Supplemental Fig. S1A). In contrast, chromosome missegregation rates for four unadapted strains were significantly higher, ranging from 2.8% to 7.7% ($P = 0.0013$). As an additional assay for CIN, we measured the growth of the *bir1Δ-ad* strains on plates with a moderate amount of the microtubule-depolymerizing drug benomyl (10 µg/mL). The adapted strains maintained strong sensitivity to the drug (Supplemental Fig. S1B,C). Taken together, the above results demonstrate the adapted *bir1Δ* yeast display a partial decrease in CIN rates yet maintain a strong CIN phenotype.

To determine the degree of aneuploidy in the adapted strains, the DNA content of the *bir1Δ-ad* strains was measured by flow cytometry. All 102 adapted strains had substantially increased DNA content, with increases ranging from 10% to 40% over wild type, demonstrating large amounts of aneuploidy consistent with approximately one to six extra chromosomes in each strain. Although the *bir1Δ-ad* strains display a remarkable heterogeneity in both growth rate and degree of aneuploidy, there was no clear correlation between the two (Fig. 1B). This lack of correlation indicates that there is not a simple relationship between the induced CIN, the resultant aneuploidy, and their impact on cellular fitness.

To determine the degree to which the growth defects in the *bir1Δ-ad* strains result from either ongoing CIN (from the continued lack of Bir1) or the resulting aneuploidy, we added the *BIR1* gene back into the adapted strains via single-copy insertions. *BIR1* add-back fully rescued the benomyl sensitivity for nearly all of the adapted strains, demonstrating a rescue of the CIN phenotype (Supplemental Fig. S1B,C). The growth rates of the add-back strains only partially recovered with readdition of the *BIR1* gene, indicating that aneuploidy also contributes directly to the growth defects in the *bir1Δ-ad* strains (Supplemental Fig. S1D). Most of the *bir1Δ-ad* strains had decreased levels of aneuploidy following *BIR1* add-back (Supplemental Fig. S1E), suggesting that the absence of *BIR1* was an ongoing source of selection for specific aneuploidies. To specifically assess the effect of aneuploidy on the cellular fitness, we analyzed only those strains that maintained similar levels of aneuploidy after *BIR1* add-back (28 out of 102 *bir1Δ-ad* strains) (Supplemental Fig. S1E). These aneuploid *BIR1* add-back strains showed a partial (~50% median) rescue in growth (Supplemental Fig. S1F). We conclude from these results that the growth defects in the *bir1Δ-ad* strains are caused by a combination of ongoing CIN as well as the resulting aneuploidy.

Disomy of different chromosomes can contribute directly to CIN adaptation

For detailed determination of the types of aneuploidy acquired in the adapted strains, their genomes were sequenced, and the relative chromosome copy numbers

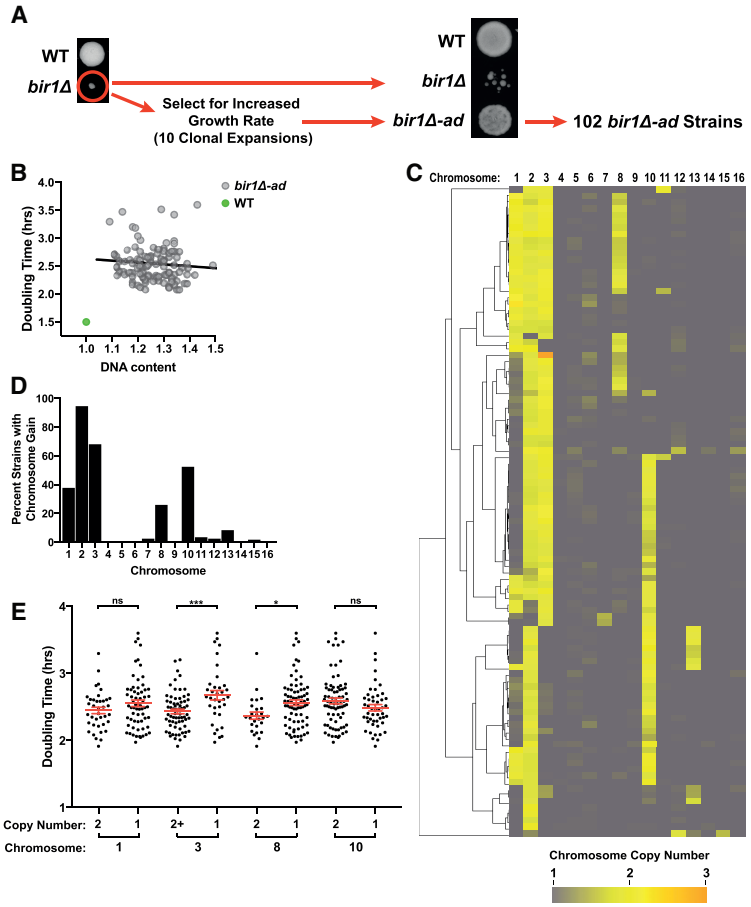

Figure 1. Adaptation to *BIR1* deletion generates complex aneuploid karyotypes. (*A*) Schematic for the generation of 102 strains adapted to *BIR1* deletion (*bir1Δ-ad*). At the *left*, colonies from wild-type and *bir1Δ* spores are shown 4 d after tetrad dissection of a *BIR1*/*bir1Δ* diploid onto rich (YPA plus 2% dextrose [YPAD]) medium. The *bir1Δ* cells were then grown for ~200 generations through 10 clonal expansions. At the *right*, equal optical densities of a wild-type strain, a *bir1Δ* strain, and its corresponding *bir1Δ-ad* strain were spotted on YPAD plates. (*B*) Lack of correlation between growth rates and degree of aneuploidy for the *bir1Δ-ad* strains. Doubling times in liquid YPAD of all 102 *bir1Δ-ad* strains were measured by optical density and plotted against the DNA content as measured by flow cytometry. Pearson's correlation coefficient = −0.09. Two-tailed *P*-value = 0.38. (*C*) Heat map visualization of chromosome copy number data for the *bir1Δ-ad* strains as measured by read counts from whole-genome sequencing. Each of the 102 *bir1Δ-ad* strains is represented as a row and clustered to show groupings of karyotype patterns. (*D*) Frequency of aneuploidy for each chromosome in the haploid *bir1Δ-ad* strains based on binarization of the data in *C*. (*E*) Comparison of the growth rates of haploid *bir1Δ-ad* strains with and without extra copies of chromosomes 1, 3, 8, and 10. The mean doubling time and the standard error of each group are shown. (*) $P \leq 0.01$; (***) $P \leq 0.0001$; (ns) not significant, unpaired *t*-test.

were determined from the read counts. The *bir1Δ-ad* strains frequently had extra copies of chromosomes 1, 2, 3, 8, and 10 (traditionally referred to as the roman numerals I, II, III, VIII, and X in yeast), each of which was seen in over a quarter of the strains (Fig. 1C,D). No chromosome rearrangements or large insertions or deletions were present in any of the adapted strains. Although nearly all of the strains acquired point mutations during adaptation (average of approximately two mutations per strain), the nonsynonymous mutations in coding regions were not significantly enriched for genes reported to be involved in CIN ($P = 0.53$). Of the genes mutated in *bir1Δ-ad* strains, 15.8% (30 of 190 genes) (Supplemental Table S3) were CIN genes, which is similar to the 14.5% of genes in the yeast genome (874 of 6000 genes). Additionally, no gene ontology (GO) terms were significantly enriched for in the list of genes mutated in the *bir1Δ-ad* strains (false discovery rate [FDR] < 0.05). We additionally identified 41 heterozygous gene mutations on disomic chromosomes (Supplemental Table S4). These mutations were also not significantly enriched for GO terms. The above result suggests that improved growth from adaptation was generally not a result of mutations in certain genes. Together, these results point to aneuploidy being the most substantial genomic alteration in the *bir1Δ-ad* strains.

To determine the degree to which the growth benefits from adaptation could be attributed to certain types of aneuploidy, we compared the doubling times of *bir1Δ-ad* strains with and without gains of chromosomes 1, 3, 8, and 10. There was an insufficient number of strains without chromosome 2 aneuploidy (six out of 102) to make a meaningful comparison (Fig. 1C). Adapted strains with gains of chromosomes 3 or 8 had significantly improved fitness over those that carry only one copy of those chromosomes (Fig. 1E). Chromosome 1 disomy was correlated with a small insignificant increase in fitness ($P = 0.14$). Surprisingly, disomy of chromosome 10 was not correlated with any increase in fitness despite over half of the adapted *bir1Δ* strains containing an extra copy of chromosome 10 (Fig. 1D,E). This discrepancy could be explained by one of the following: (1) Disomy of chromosome 10 in the background of *BIR1* deletion is fitness-neutral, in which case, over a long enough period of time, half of the strains would be expected to have one copy, and half would have two, or (2) disomy of chromosome 10 provides an initial adaptive advantage that decreases with time. To test this second possibility, we engineered strains with individual disomies prior to removal of the *BIR1* gene (Fig. 2A). Aneuploidy was induced via expression of a strong centromere-proximal galactose-inducible promoter and selected for by stochastic recombination events that restore the function of a

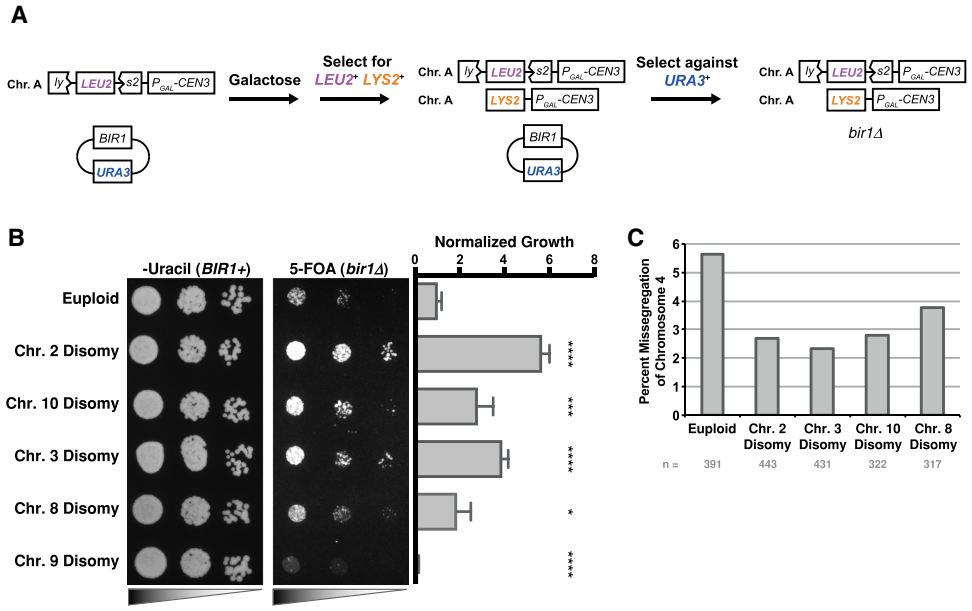

Figure 2. Disomy of specific chromosomes provides an initial advantage to *BIR1* deletion. (*A*) Schematic of a galactose-inducible system to engineer disomy of specific chromosomes prior to *BIR1* deletion. Strains transformed with a construct (P_{GAL}*CEN3 lys2::LEU2*) and a minichromosome containing *BIR1* and *URA3* were grown in medium containing galactose to induce chromosome nondisjunction during cell division. Disomy of the desired chromosome was then selected for on minimal medium plates lacking leucine and lysine. Disomic strains for the chromosome of interest were grown on plates containing the drug 5-FOA to select for loss of the *URA3* gene, creating *bir1Δ* yeast that are disomic for the chromosome of interest. (*B*) Tenfold dilution series of disomic strains on minimal medium plates with 5-FOA (selecting against *URA3*) or lacking uracil (selecting for *URA3*) plates. The graph shows the quantification of the growth of each strain after selection against *BIR1* with 5-FOA. All values were normalized to the initially euploid strain. (*) $P \leq 0.05$; (***) $P \leq 0.0001$; (****) $P \leq 0.00001$, unpaired *t*-test. (*C*) Missegregation rates of GFP-labeled chromosome 4 for *bir1Δ* strains from 5-FOA plates as in *B*. The total numbers of quantified segregation events (*n*) are indicated *below* the graph. See Supplemental Figure S1A for examples of segregation and missegregation events.

selectable marker (Anders et al. 2009). *BIR1* was subsequently lost by counterselection of the plasmid-linked *URA3* gene with the drug 5-fluoroorotic acid (5-FOA) (Fig. 2A). Strains with disomy of chromosomes 2, 3, 8, and 10 had significantly increased growth relative to the euploid control on 5-FOA plates selecting for *bir1Δ* mutants (Fig. 2B). In contrast, a strain with disomy of chromosome 9, which was never observed in the adapted strains, had drastically impaired growth in the absence of *BIR1*. All five strains grew similarly on nonselective (*BIR1*$^+$) plates. The increase in initial fitness following *bir1Δ* for the beneficial aneuploidies corresponded with a decrease in the missegregation rate of chromosome 4, indicating that disomy of these chromosomes partially suppresses the CIN phenotype (Fig. 2C). We conclude that high frequencies of certain chromosome gains in adapted *bir1Δ* strains, including chromosome 10, result from an initial benefit in fitness shortly after CIN initiation.

Chromosome 2 disomy had the strongest rescue of the *bir1Δ* phenotype and was the most frequent aneuploidy in the *bir1Δ-ad* strains, indicating that there is a gene or set of genes on that chromosome that contributes strongly to survival following *BIR1* deletion. Notably, the gene for the CPC subunit Sli15 is on chromosome 2. We therefore put an additional copy of *SLI15* on chromosome 5 to determine whether it would partially rescue the *bir1Δ* phenotype (Supplemental Fig. S2A). *SLI15* duplication had levels of growth similar to chromosome 2 disomy immediately following *BIR1* deletion (Supplemental Fig. S2B). Furthermore, adapted *bir1Δ* strains with *SLI15* duplication had drastically reduced amounts of chromosome 2 disomy and significantly improved growth rates (Supplemental Fig. S2C,D). Sequencing of 12 *SLI15*-duplicated *bir1Δ-ad* strains showed that these strains still accumulated the other four frequent disomies seen in the original *bir1Δ-ad* strains (chromosomes 1, 3, 8, and 10) when chromosome 2 disomy is absent, demonstrating that the other four disomies are selected for independently of chromosome 2 (Supplemental Fig. S2E). Attempts to create *bir1Δ* strains with the sole copy of *SLI15* on chromosome 5 failed to produce any viable spores. This indicates that *SLI15* duplication is an essential initial step in adaptation to *BIR1* deletion and is not possible on a chromosome whose disomy is associated with severe growth defects (Torres et al. 2007). We therefore relocated *SLI15* as the only copy on a chromosome that we knew could be duplicated: chromosome 8. None of the adapted relocated *SLI15* strains had disomy of chromosome 2 (zero out of seven strains) (Supplemental Fig. S2F,G), further demonstrating that increased expression of Sli15 is the sole basis behind the frequent disomy of chromosome 2 in *bir1Δ-ad* strains.

Positive and negative correlations occur between chromosome copy number alterations

If disomy of chromosome 10 gives an initial growth advantage, why does it not correlate with increased fitness in the adapted strains? Up to this point, we analyzed each chromosomal aneuploidy independently. However, 96% of the *bir1Δ-ad* strains had complex karyotypes, as defined by containing more than one chromosome copy number alteration (Fig. 1C). We next determined whether there were any correlations between the copy numbers of different chromosomes. The most striking pattern is a negative correlation between disomy of chromosomes 8 and 10. Seventy-six percent (78 of 102) of adapted strains have an elevated copy number of either chromosome 8 or 10, but only one strain has an increased copy number of both chromosomes ($P = 2.6 \times 10^{-9}$, hypergeometric test) (Fig. 3A). Conversely, a strong positive correlation is seen between chromosomes 8 and 3. Ninety-two percent of strains (24 of 26) with chromosome 8 gains have increases in chromosome 3 as well, while only 59% (45 of 76) of strains with a single copy of chromosome 8 have an extra copy of chromosome 3 ($P = 0.001$, hypergeometric test) (Fig. 3B). Comprehensive pairwise correlations between all aneuploid chromosomes in the *bir1Δ-ad* strains revealed five highly significant ($P < 0.001$) correlations (Fig. 3C). We conclude that aneuploidies of individual chromosomes do not act independently, which could help explain why aneuploidy of some chromosomes, such as chromosome 10, improved initial growth following *BIR1* deletion (Fig. 2B) but did not correlate with increased fitness in the adapted strains (Fig. 1E).

Chromosome copy number correlations result from genetic interactions between aneuploid chromosomes

The strong anti-correlation between disomy of chromosomes 8 and 10 could result from functional redundancy in their adaptive advantage to *BIR1* deletion, resulting in a loss of positive selection for the second disomic chromosome. Alternatively, combination of both disomies could result in a synthetic negative genetic interaction independently of *BIR1* deletion. To test for genetic interactions between specific pairs of disomic chromosomes, we modified the aneuploidy induction system to engineer two chromosomal aneuploidies simultaneously (Fig. 3D). After induced missegregation via addition of galactose, disomy of both chromosomes was selected for on plates lacking histidine, uracil, leucine, and lysine. We engineered pairwise combinations of all five chromosomes that showed significant positive or negative copy number

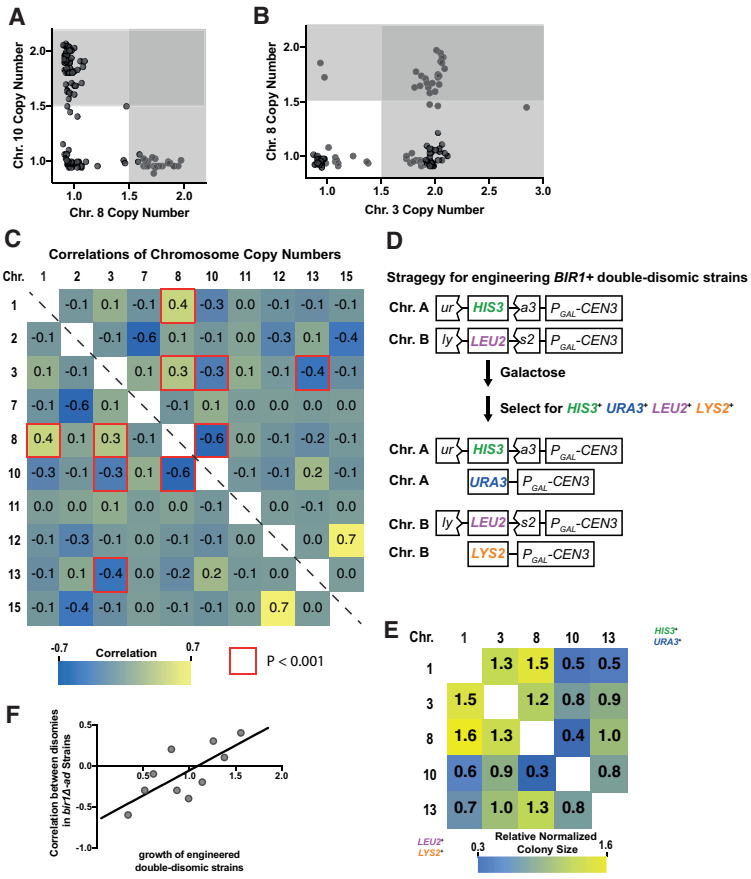

Figure 3. Genetic interactions between whole-chromosome disomies dictate patterns in complex aneuploidy. (*A*,*B*) Scatter plot of specific chromosome copy numbers of 102 *bir1Δ-ad* strains demonstrating positive (*B*) and negative (*A*) correlations between different chromosomal disomies. Copy number data are from read frequencies as in Figure 1C. The darker-gray regions contain strains that are aneuploid for both of the plotted chromosomes. (*C*) Heat map of the correlations between chromosome copy numbers in the 102 haploid *bir1Δ-ad* strains. Only correlations between chromosomes where aneuploidy was observed are shown. Each cell of the matrix contains the correlation coefficient between the two chromosomes written in the row and column. The red highlighted border represents correlations with $P < 0.001$ in the hypergeometric test. (*D*) Schematic of a system to engineered strains (*BIR1*$^+$) that harbor two chromosome disomies. Strains were transformed with the construct P_{GAL}-*CEN3 ura3::HIS3* on one chromosome (chromosome A) and P_{GAL}-*CEN3 lys2::LEU2* on another chromosome (chromosome B). Chromosome nondisjunction was induced with galactose, and disomy of both chromosomes was selected for with all four auxotrophic markers (*URA3*, *HIS3*, *LYS2*, and *LEU2*). (*E*) Relative colony sizes of double-disomic strains on YPAD plates were normalized to the other values in their respective rows and columns. Colony sizes without normalization are shown in Supplemental Figure S2I. (*F*) Comparison of the correlation coefficients of the chromosome copy numbers in *bir1Δ-ad* strains (from *C*) and the relative fitness of engineered double-disomic strains (from *E*). Relative values are the average of the two values in *E* (column:row and row:column for each chromosome pair). Pearson's correlation coefficient = 0.73. Two-tailed *P*-value = 0.016.

correlations in the *bir1Δ-ad* strains (Fig. 3E). The presence of an extra copy of both chromosomes was confirmed by quantitative PCR (qPCR). Colony sizes for each pair were measured and normalized to account for growth differences in individual aneuploidies (Fig. 3E; Supplemental Fig. S2I). Colony sizes ranged from 70% smaller to 60% larger than expected, demonstrating strong positive and negative genetic interactions between aneuploid chromosomes. These genetic interactions were not simply a result of increasing amounts of extra DNA, as there was no significant correlation between combined chromosome size and relative growth for the chromosome combinations that we tested ($P = 0.48$) (Supplemental Fig. S2J). We call these whole-chromosome-level genetic interactions chromosome copy number interactions (CCNIs).

To determine the degree to which CCNIs could explain the complex karyotype patterns observed in the *bir1Δ-ad* strains, we directly compared the colony sizes of the engineered double-disomic strains (Fig. 3E) with the chromosome copy number correlations in the *bir1Δ-ad* strains (Fig. 3C). The combination of disomies with the highest significant positive correlation in the *bir1Δ-ad* strains, chromosomes 1 and 8, had the largest relative colony sizes in engineered double-disomic strains. Similarly, the disomy pair with the highest significant negative correlation, chromosomes 8 and 10, had the smallest relative colony sizes (Fig. 3C,E,F; Supplemental Fig. S3A). Results were similar if the selection markers used for the two chromosomes were reversed (Fig. 3E). No negative interactions were seen with chromosome 2 disomy (Supplemental Fig. S2H,I).

Overall, the correlation between growth of engineered disomic pairs and frequency of co-occurrence in *bir1Δ-ad* strains was significant ($r = 0.73$, $P = 0.016$) (Fig. 3F), demonstrating that aneuploidy patterns observed in complex karyotypes are directly affected by positive and negative genetic interactions between specific aneuploid chromosome pairs. This indicates that CCNIs play a key role in governing the formation of complex aneuploid karyotypes.

The complexity of aneuploidy correlates with the severity of CIN induction

We next tested how varying the level of induced CIN affects the resulting complex aneuploidy. To alter the amount of CIN induced, we used mutants that affect different aspects of the kinetochore–microtubule attachment error correction pathway (Fig. 4A). Deletions in *NBL1*, *BUB1*, and *SGO1* (Borealin, BUB1, and Shugoshin in humans) were adapted via clonal expansion in the same manner as the *BIR1* deletion strains. The growth rates of adapted strains demonstrate that *bir1Δ-ad* and *nbl1Δ-ad* have the strongest growth defects, followed by *bub1Δ-ad* strains, and the *sgo1Δ-ad* strains had the weakest phenotype (Fig. 4B). These results are consistent with previously published measurements of missegregation rates for mutants in *BIR1* and *SGO1* (Storchova et al. 2011; Campbell and Desai 2013). Whole-genome sequencing to determine the chromosome copy numbers for the adapted strains revealed very similar aneuploidy patterns for all four deletion mutants. The four mutants

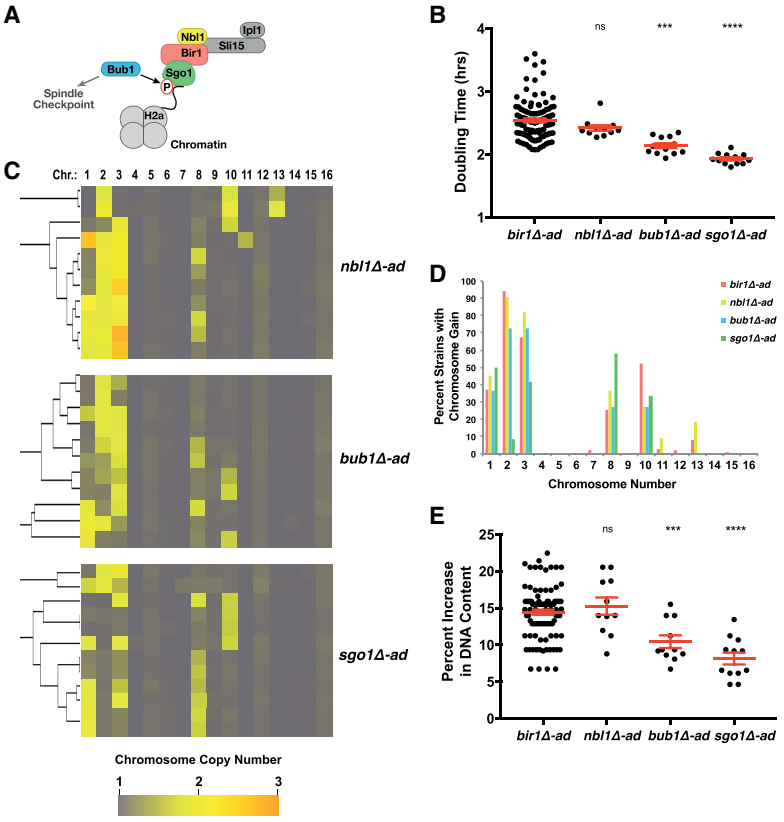

Figure 4. The degree of aneuploidy correlates with the severity of induced CIN. (*A*) Cartoon of the CPC and the regulators of its localization to chromatin. (*B*) Cell doubling times for each of the indicated strain types. (*C*) Heat map visualization of the clustered chromosome copy numbers of the *nbl1Δ-ad*, *bub1Δ-ad*, and *sgo1Δ-ad* strains. (*D*) Plot of the percentage of strains with a gain of a specific chromosome based on binarization of the data shown in *C* and Figure 1C. (*E*) Percentage change in overall DNA content as measured by taking the binarized copy number values of each chromosome, subtracting 1, multiplying each by the fraction of the genome represented by that chromosome, and then summing all of the chromosomes. Mean values and the standard errors are in red. (***) $P \leq 0.0001$; (****) $P < 0.00001$.

resulted in aneuploidy predominantly in the same five chromosomes (chromosomes 1, 2, 3, 8, and 10) (Fig. 4C, D). Additionally, the negative correlation between chromosome 8 and 10 disomy is also observed in these strains, although one *sgo1Δ-ad* strain did display disomy of both chromosomes (Fig. 4C). Although the general patterns of aneuploidy remained the same in the different adapted deletion strains, the degree of aneuploidy varied. *nbl1Δ-ad* and *bir1Δ-ad* had very similar increases in aneuploidy, whereas *bub1Δ-ad* and *sgo1Δ-ad* strains averaged comparatively less aneuploidy (Fig. 4E; Supplemental Fig. S3B). This trend correlates well with the degree of CIN observed in these strains. Together, these results suggest that increased karyotype complexity can result directly from elevated rates of chromosome missegregation.

Ploidy greatly affects the patterns of chromosome copy number correlations

We next sought to determine how changes in ploidy affect patterns in complex karyotypes. Compared with haploid genomes, diploids have a greater number of potential aneuploidy types to exploit for adaptation, such as chromosome loss (monosomy) and gain (trisomy) of only 50% more copies of a chromosome. In theory, this would provide more avenues to fine-tune adaptation through aneuploidy. To test this, we generated 25 diploid *bir1Δ* yeast strains, adapted them through clonal expansion, and subjected them to whole-genome sequencing (Fig. 5A). Similar to the adapted haploid strains, the diploids frequently accumulated extra copies of chromosomes 2, 3, 8, and 10 (Fig. 5B). In addition, the diploids had a much higher frequency of chromosome 13 gain (64% in diploids vs. 8% in haploids) (Figs. 1D, 5B). Although chromosomes 2, 3, 8, and 10 all had instances of tetrasomy, this was not the case for chromosome 13 (Fig. 5A). These data suggest that a 50% increase in chromosome 13 copy number provides a much better balance of growth benefit to fitness deficit when compared with a 100% increase in *bir1Δ-ad* strains. In addition to chromosome gains, losses of chromosomes 1 and 9 were also observed. Intriguingly, chromosome 1 was lost in some strains and gained in others, suggesting that the presence or absence of additional copies of this chromosome is largely inconsequential in adaptation to *BIR1* deletion. The percentage change of DNA content (normalized to the basal ploidy) for *bir1Δ-ad* strains was very

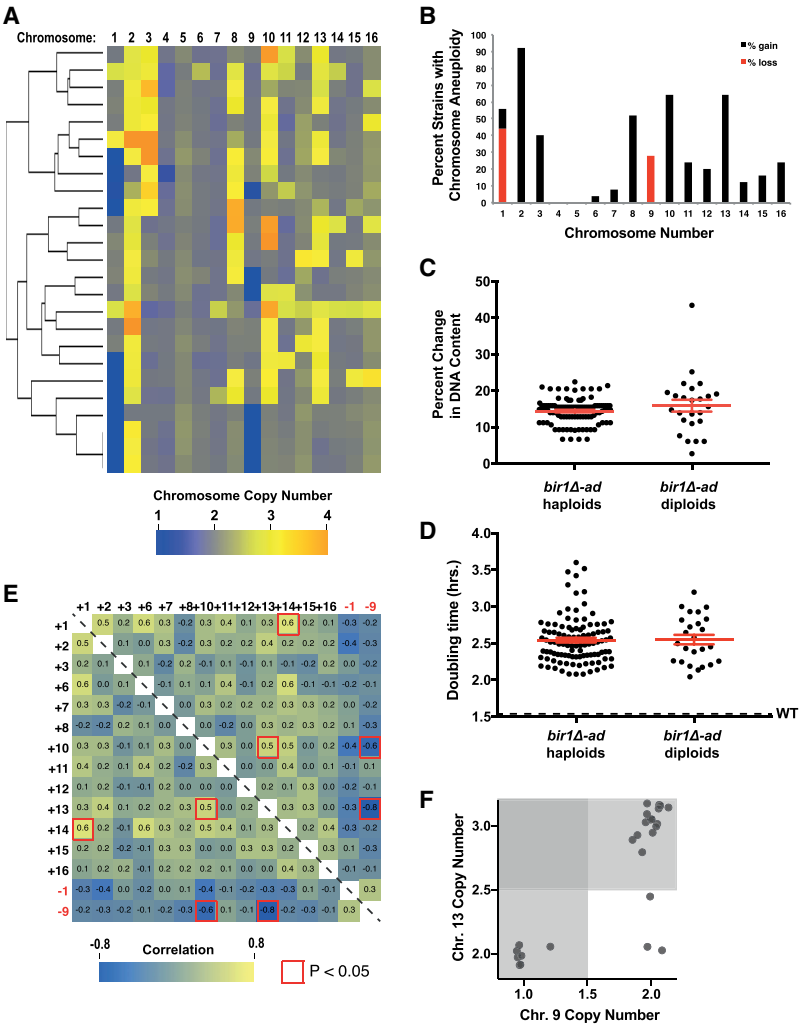

Figure 5. Ploidy greatly affects chromosome copy number correlations. (*A*) Heat map visualization of chromosome copy number values for diploid *bir1Δ-ad* strains clustered by similarity. Each of the 25 diploid *bir1Δ-ad* strains is represented as a row. (*B*) Frequency of the aneuploid chromosomes in the diploid *bir1Δ-ad* strains from binarization of the data shown in *A*. (*C*) Percentage change in overall DNA content as measured by taking the binarized copy number values of each chromosome, subtracting the basal ploidy 2, multiplying each by the fraction of the genome represented by that chromosome, and then summing the absolute values for all of the chromosomes. There was no significant difference between the two groups. $P = 0.16$. (*D*) Cell doubling times for the haploid and diploid *bir1Δ-ad* strains. There was no significant difference between the two groups. $P = 0.91$. (*E*) Heat map of the correlations between chromosome copy numbers for the 25 diploid *bir1Δ-ad* strains. Only correlations between chromosomes where aneuploidy was observed are shown. Each cell of the matrix contains the correlation coefficient between the two chromosomes written in the rows and columns. The red highlighted border represents correlations that had a $P < 0.05$ in the hypergeometric test. (*F*) Scatter plot of specific chromosome copy numbers of 25 diploid *bir1Δ-ad* strains demonstrating a negative correlation between monosomy of chromosome 9 and trisomy of chromosome 13. Copy number data are from read frequencies as in *E*. The darker-gray region contains strains that are aneuploid for both of the plotted chromosomes. Mean values and the standard error of each group are indicated in red with error bars.

similar for haploids and diploids (Fig. 5C), demonstrating that the aneuploidy burden that is tolerated by a cell scales with its ploidy. Curiously, there was no significant difference between the mean doubling times of *bir1Δ-ad* haploids and diploids despite the diploids having more avenues for adaptation (Fig. 5D). Overall, these data show that initial ploidy is an important determinant in complex aneuploidy patterns.

We next determined the pairwise correlations between specific chromosome aneuploidy types in diploid *bir1Δ-ad* strains (Fig. 5E). Surprisingly, the most significant negative correlation in haploids, between gain of chromosomes 8 and 10, was not present in the diploids. Instead, the most significant correlations are between the loss of chromosome 9 and the gain of chromosome 10 or 13 ($P = 0.003$ and $P = 7 \times 10^{-5}$, respectively). Although 92% (23 out of 25) of strains had either chromosome 13 gain or chromosome 9 loss, none of them had both (Fig. 5E,F). As with chromosomes 8 and 10 in haploids, the anti-correlation between chromosome 13 trisomy and chromosome 9 monosomy is associated with a negative CCNI. The growth of cells engineered with both trisomy of chromosome 13 and monosomy of chromosome 9 was approximately half the size of those with chromosome 9 monosomy alone ($P < 0.0001$, Supplemental Fig. S3C). This demonstrates that CCNIs also play a role in shaping complex karyotypes with a diploid base ploidy. We conclude that chromosome copy number correlations and CCNIs are observed in multiple ploidy states, but the patterns change dramatically.

Chromosome copy number correlations are seen in cancer karyotypes

To determine whether cancer karyotypes have patterns similar to those that we observed in adapted CIN yeast strains, we analyzed competitive genome hybridization (CGH) data from The Cancer Genome Atlas (TCGA) database. Cancer karyotypes for 15 different cancer types were analyzed with a matrix of pairwise correlations between different aneuploidies. The cancers with the five highest percentages of predominantly whole-chromosome or whole-arm complex aneuploidy were analyzed in higher detail (Fig. 6A; Supplemental Fig. S4; Supplemental Table S2). Strong correlations were observed in all five cancer types (Fig. 6A; Supplemental Fig. S4). Correlation patterns in lower-grade glioma (LGG) stood out as being especially similar to the *bir1Δ-ad* strains, with both strong positive and negative correlations for a subset of

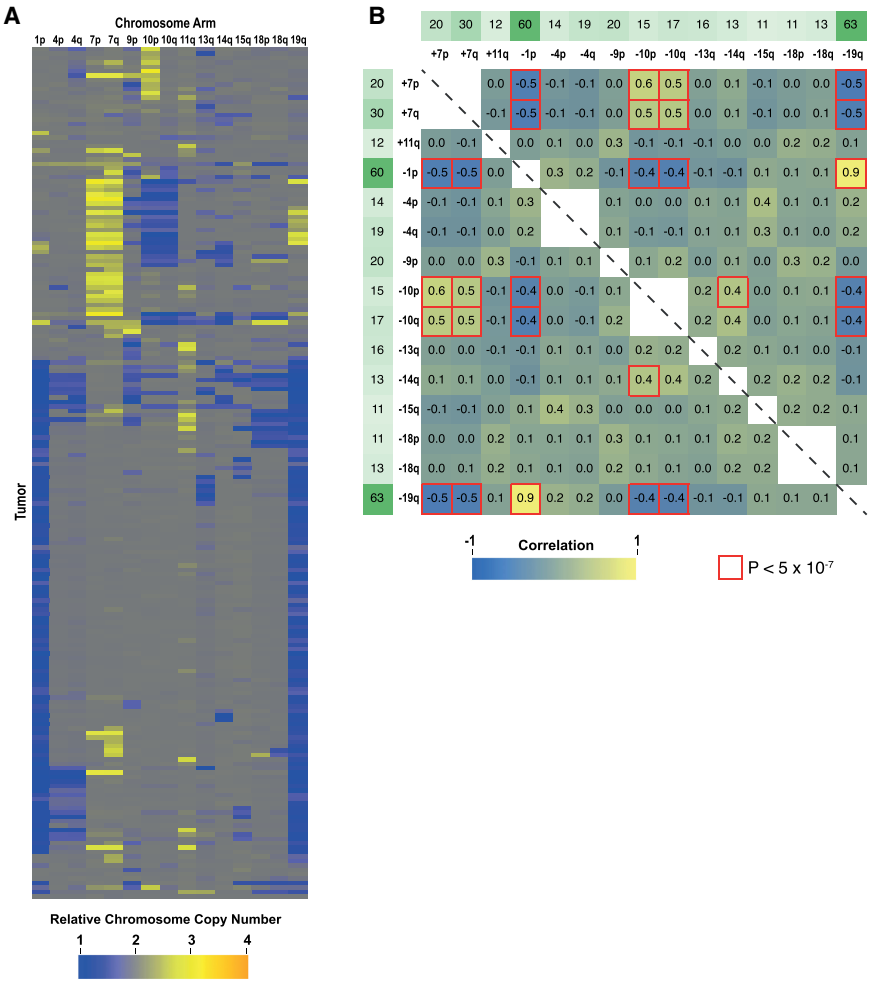

Figure 6. Identification of chromosome copy number correlations in brain LGG tumors. (*A*) Visualization of the chromosome arm karyotypes from brain LGG tumor samples. Cancer karyotype data was acquired from the CGH data from the TCGA database. Each of the 193 LGG karyotypes is represented as a row, with the column indicating the chromosome copy number of chromosome arms. Only chromosome arms where aneuploidy was present in >10% of the tumor samples are shown. (*B*) Pairwise correlation coefficients for chromosome arm aneuploidy are shown as a heat map. The frequency of each aberration is shown in green as a percentage. The red highlighted border indicates $P < 5 \times 10^{-7}$ in the hypergeometric test. See Supplemental Figure S4 for similar analysis of four additional tumor types.

chromosomes (Fig. 6A,B). LGG karyotypes largely fell into two categories: those with (1) loss of 1p and 19q or (2) gain of chromosome 7 and loss of chromosome 10 (Fig. 6B). The combined loss of 1p and 19q is the result of a frequent translocation between those two chromosomes. Intriguingly, strains that harbor this translocation almost never have a gain of chromosome 7 or loss of chromosome 10 (Fig. 6B). Other common chromosome aberrations such as loss of chromosome 18 did not have any strong correlations, suggesting specificity in the negative correlation between the two main karyotype classes. We conclude that chromosome copy number correlations are also present in cancer karyotypes and may reflect genetic interactions between different aneuploid chromosomes (CCNIs).

Additional competitive adaptation of bir1Δ-ad *strains leads to convergent optimized complex karyotypes*

Given that certain patterns in the karyotypes of *bir1Δ-ad* strains had strong correlations with increased growth rates, it is somewhat surprising that not all of the strains adapted to have the most advantageous patterns. We reasoned that perhaps if the adapted *bir1Δ* strains were given more time to adapt in a more competitive environment, they might converge on an "ideal" karyotype. Alternatively, further adaptation could allow the strains to find alternate ways to independently obtain the advantages conferred by the aneuploidy and then eliminate the disadvantages by returning to the euploid state (Yona et al. 2012). We therefore selected 16 haploid and 16 diploid strains for further adaptation for an additional ~200 generations in rich liquid medium (Fig. 7A). We refer to these further adapted strains as *bir1Δ-ad2*. The adaptation in liquid medium did not greatly affect the CIN phenotype of the further adapted strains, as the 16 *bir1Δ-ad2* diploids had little to no change in benomyl sensitivity when compared with the *bir1Δ-ad* strains (Supplemental Fig. S5A). In the haploid *bir1Δ-ad2* strains, aneuploidy of chromosomes 8 and 10 was almost completely lost (Fig. 7B,C). This resulted in strains with more similar karyotypes, as the pooled standard deviation decreased from 0.18 to 0.13 after liquid adaptation. In contrast, levels for chromosomes 1 and 2 were largely unchanged. Notably, all four strains that started with chromosome 10 disomy and chromosome 3 monosomy lost a copy of chromosome 10 and gained a copy of chromosome 3. This suggests that, in haploids, the "optimal" *bir1Δ* karyotype is disomy of chromosomes 2 and 3, with chromosome 10 disomy being excluded due to the negative CCNI between aneuploidy of chromosomes 3 and 10 (Fig. 3C,E). Interestingly, the diploid *bir1Δ-ad2* strains became much more homogenous in their karyotypes, with a decrease in pooled standard deviation from 0.36 to 0.17 after liquid adaptation. Trisomy of chromosomes 2, 3, 10, and 13 is now present in nearly all of the further adapted strains (Fig. 7D,E). Strikingly, all three *bir1Δ-ad* strains that started off with chromosome 9 monosomy regained a copy of chromosome 9 and acquired an extra copy of chromosome 13. Both of these changes occurred within 1 wk of each other in all three strains and occurred within the first 2 wk of liquid adaptation (Supplemental Fig. S5B). We conclude that certain types of aneuploidy that give an initial growth advantage, such as gain of chromosome 10 in haploids and loss of chromosome 9 in diploids, will eventually be lost due to the comparatively better fitness increases of other, incompatible types of aneuploidy (chromosome 3 gain in haploids and chromosome 13 gain in diploids). Together, these results suggest that although there are often many different, sometimes conflicting paths to obtaining an ideal karyotype, cell populations with high levels of CIN will eventually converge on a common complement of aneuploid chromosomes.

Discussion

In this study, we developed a system for studying how complex karyotypes arise from extremely high rates of CIN. Mutations in the kinetochore–microtubule error correction pathway provide an increase in the frequency of aneuploidy while simultaneously creating the selective pressure to adapt via aneuploidy. We identified strong correlations and anti-correlations between specific aneuploid chromosome pairs in the resulting complex karyotypes and hypothesized that these patterns result from genetic interactions between certain aneuploid chromosomes. We then identified genetic interactions between whole-chromosome copy number alterations (CCNIs) in engineered double-aneuploid strains that match the patterns observed in the adapted CIN strains. After additional competitive adaptation of the CIN strains, we observed an increase in homogeneity of the strains as they converged on an optimal karyotype.

We present a model of the different paths that yeast take in order to get to a final ideal aneuploid state that minimizes the growth defects resulting from *BIR1* deletion (Fig. 7F). These paths of adaptation were based on (1) comparing cellular fitness with the different aneuploid states in the adapted strains (Figs. 1E, 2B), (2) comparing the karyotypes before and after liquid adaptation (Fig. 7B–E), and (3) the CCNIs observed between aneuploid chromosomes (Fig. 3E; Supplemental Fig. S3A,C). While the paths of adaptation are quite different for haploid and diploid cells, they have several things in common. For both ploidies, there are stepwise increases in aneuploidy and corresponding increases in fitness. The paths always start with the gain of chromosome 2, which is required for initial survival. After that, the cultures can acquire a number of different aneuploidies that all provide some selective advantage. These aneuploidies will sometimes lead down a direct route that quickly leads to the final optimal karyotype, such as the gain of chromosome 3 in haploids. Alternatively, the cultures will instead take a detour via an aneuploidy that is initially advantageous but, paradoxically, also provides a temporary barrier to obtaining the ideal complement of aneuploid chromosomes. Examples of this include gain of chromosome 10 in haploids or loss of chromosome 9 in diploids. These aneuploidies are eventually replaced due to negative CCNIs with copy number alterations

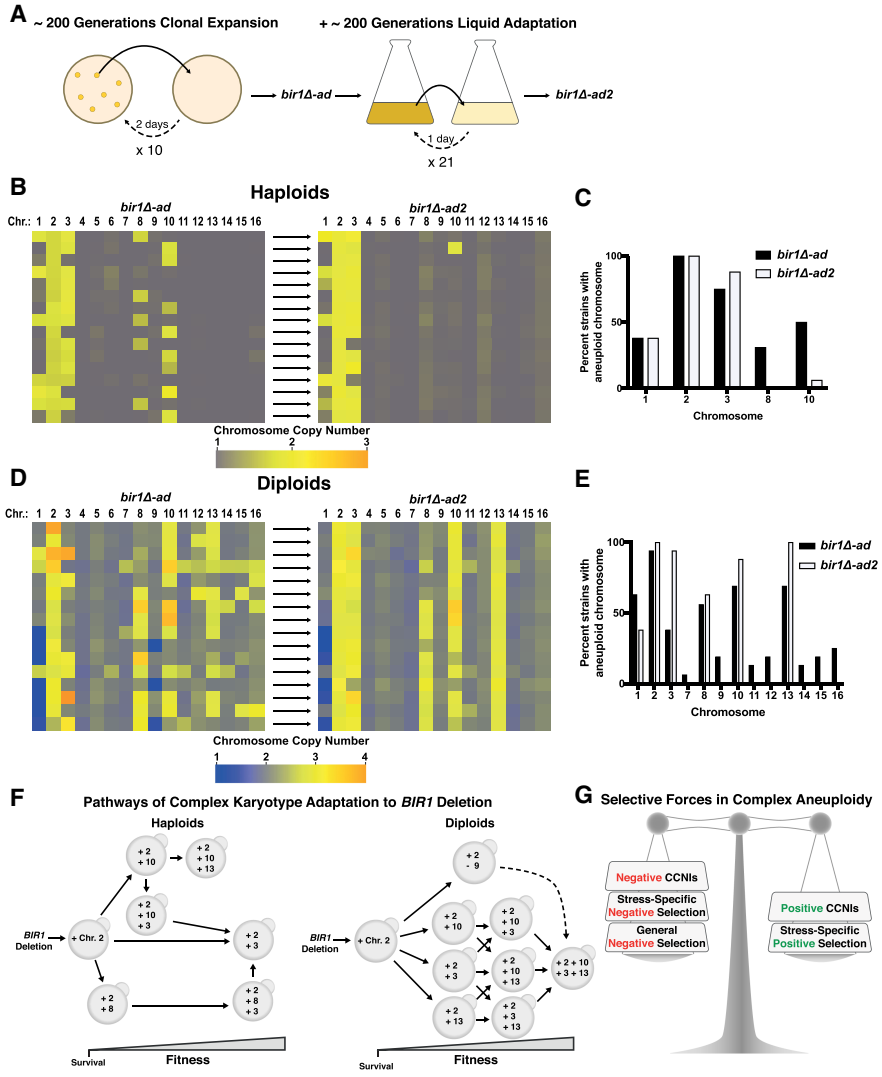

Figure 7. Additional adaptation leads to convergence on "ideal" karyotypes in *BIR1* deletion strains. (*A*) Graphical representation of the adaptation process on solid (see Fig. 1A) followed by liquid medium. On solid medium, the *bir1Δ* strains were struck out for single colonies and allowed to grow for 2 d at 30°C. After 10 rounds of growth on solid medium, a subset of *bir1Δ-ad* strains, selected to represent a diverse set of karyotypes, was grown for an additional ~200 generations in liquid medium. Liquid cultures were diluted each day for 21 d, generating further adapted haploid/diploid *bir1Δ-ad2* strains. (*B*) Heat map visualization of chromosome copy number values for the haploid *bir1Δ* strains before (see Fig. 1C) and after adaption in liquid medium. The *bir1Δ-ad* strains at the *left* directly correspond to the *bir1Δ-ad2* strains at the *right*. (*C*) Frequency of aneuploidy for each chromosome in the haploid *bir1Δ-ad* and *bir1Δ-ad2* strains based on binarization of the data in *B*. (*D*) Heat map visualization of chromosome copy number values for the diploid *bir1Δ* strains before (see Fig. 5A) and after adaption in liquid medium. The *bir1Δ-ad* strains at the *left* directly correspond to the *bir1Δ-ad2* strains at the *right*. (*E*) Frequency of aneuploidy for each chromosome in the diploid *bir1Δ-ad* and *bir1Δ-ad2* strains based on binarization of the data in *D*. (*F*) An empirical model depicting the pathways of adaptation to *BIR1* deletion based on synthesizing data from Figures 1, 2, 3, and 5 and this figure. Adaptation starts with the gain of chromosome 2, which appears to be essential for initial survival. Following chromosome 2 gain, many different possible paths can be taken by haploid and diploid yeast during the formation of complex karyotypes. Note that some chromosome aneuploidies (disomy of chromosome 10 in haploids and monosomy of chromosome 9 in diploids) provide a growth advantage early in adaptation but must become euploid again to achieve the "optimal" complex karyotype. (*G*) Illustration of the selective forces that determine whether the aneuploidy of a chromosome is advantageous.

that are even more advantageous. Our results demonstrate that aneuploidy can provide a surprisingly versatile mechanism of adaptation, with many different chromosomal aneuploidies able to provide an initial competitive advantage under selective conditions. Despite these divergent starting points, chromosomally unstable cell populations settle on an ideal complex karyotype through the gain and loss of chromosomes over time.

Synthetic genetic interactions between chromosomes have been reported before, as disomy of chromosome 6 is tolerated only in conjunction with a concomitant gain of chromosome 13. This interaction is due to imbalanced

expression of the *TUB2* gene on chromosome 6 and can be compensated for by increased expression of *TUB1* from chromosome 13 (Torres et al. 2007; Anders et al. 2009). Here we demonstrate that both positive and negative whole-chromosome genetic interactions are potentially quite common and have strong effects on shaping complex aneuploid karyotypes. As of yet, we do not know the basis behind these genetic interactions and whether they typically result primarily from genetic interactions between pairs of genes, as with chromosomes 6 and 13, or due to cumulative effects of many genes, as has been reported for the growth defects that result from aneuploidy in general (Bonney et al. 2015). However, the specificity of the CCNIs among different chromosomes would suggest that they are likely the result of imbalances in a few specific genes. Another open question is whether cells frequently adapt to maintain the beneficial aspects of aneuploidy while finding ways to minimize the negative effects of genetic interactions between chromosomes.

Whether aneuploidy of a particular chromosome is advantageous depends on the balance between positive and negative selective forces (Fig. 7G). The key positive selective pressure for aneuploidy is the increased expression of genes on a chromosome that specifically relate to the selective forces acting on the cell population (Hughes et al. 2000; Rancati et al. 2008; Ryu et al. 2016). Negative selective pressure can come from the aberrant expression of many different genes simultaneously as well as stress-specific negative selection (Bonney et al. 2015; Chen et al. 2015). Here, we show that specific genetic interactions between aneuploid chromosomes can contribute either positively or negatively to the selective forces on aneuploidy. Additionally, the selective advantage for aneuploidy is heavily influenced by the original ploidy of the cells, as haploid and diploid yeast display largely divergent aneuploidy patterns. Furthermore, we found that the degree of aneuploidy resulting from CIN in diploids is, on average, doubled in comparison with haploids. These results are in agreement with the observation that gaining an extra chromosome in diploids causes much weaker phenotypes than gaining an extra chromosome in haploids (Beach et al. 2017). On the extreme end, tetraploidy in yeast has been shown to greatly encourage adaptation via aneuploidy (Selmecki et al. 2015). Together, these results highlight how subtle changes in the forces that select for and against aneuploidy can have a strong impact on the aneuploidy landscape in a cell population.

In cancer cell lines, higher amounts of aneuploidy are directly correlated with increased CIN rates, as measured by the frequency of lagging chromosomes (Duesberg et al. 1998; Nicholson and Cimini 2013). Since engineered aneuploid cells often display CIN (Sheltzer et al. 2011; Zhu et al. 2012; Passerini et al. 2016), this correlation has often been interpreted as aneuploidy being upstream of CIN (Nicholson and Cimini 2013). Here we show that the reciprocal relationship also exists. Yeast mutants with higher rates of CIN adapt to have proportionally more aneuploidy following adaptation. This may also explain why we observed much more complex karyotypes than previous studies that induced lower amounts of CIN and examined the resulting aneuploidy (Chen et al. 2012).

By analyzing the karyotypes of many different tumor cell populations, we identified that certain cancer types have strong correlations between specific somatic copy number alterations (SCNAs). A previous pan-cancer analysis of complex karyotypes revealed many positive correlations between whole-chromosome copy number changes (Ozery-Flato et al. 2011). Here, we found that restricting the analysis to certain cancer types allows for SCNAs at frequencies high enough to identify strong negative correlations in addition to positive correlations. These correlations are quite frequent and are suggestive of chromosome-level synthetic genetic interactions. Correlations between different aneuploidies in cancer identified in this manner could provide a starting point for identifying CCNIs in human cells. Additionally, our discovery that multiple distinct paths can lead to refined adaptive karyotypes provide a first glimpse into the paths of complex karyotype formation in cancer.

Materials and methods

Yeast strains and media

All yeast strains and plasmids used in this study are listed in Supplemental Table S1. Strains were grown in yeast extract/peptone supplemented with 40 µg/mL adenine-HCl (YPA) and 2% sugars. Benomyl (Sigma-Aldrich, 381586) and 5-FOA (Chempur, 220141-70-8) were used at concentrations of 10 µg/mL and 1 mg/mL, respectively. Cultures were incubated at 30°C. Genetic manipulations such as gene deletions were carried out as described (Longtine et al. 1998). Haploid strains with deletions of CIN genes were generated via tetrad dissection of heterozygous diploids. Homozygous diploid *BIR1* deletion mutants were made one of two ways. Two heterozygous diploids were deleted of either the MATa or MATα locus to allow for mating between diploids. The resulting tetraploid strains were then sporulated, and tetrads were dissected. Alternatively, both copies of the endogenous *BIR1* locus in a diploid strain were deleted in the presence of *BIR1* linked to *URA3* on a minichromosome. The minichromosome was then selected against using 5-FOA. Single disomic strains (N + 1 aneuploid strains) were constructed using a conditional centromere as described in Anders et al. (2009). In this system, the function of the centromere is repressed by the galactose-inducible promoter, causing frequent chromosome missegregation. Endogenous centromeres were targeted using recombination sites both upstream of and downstream from the centromere and subsequently replaced by the galactose-repressable centromere P_{GAL1}-CEN3 and either *URA3* or *LYS2*. This insert was then disrupted by insertion of plasmids with pieces of *URA3* or *LYS2* linearized with the Stu2 or EcoRV restriction enzymes, respectively, and selected for with *HIS3* or *LEU2* genes also present on the plasmid. Haploid strains containing P_{GAL1}-CEN3 *ura3*::*HIS3* and/or P_{GAL1}-*CEN3 lys2*::*LEU2* constructs were grown to log phase in YPA plus 2% dextrose (YPAD) and transferred to YPA plus 1% galactose and 1% raffinose (YPAGR) medium for 3 h. The cells were subsequently plated onto selection plates with complete synthetic medium (CSM) lacking either uracil and histidine or lysine and leucine. The resulting aneuploid strains were verified by qPCR. For double-disomic strains (N + 2 aneuploid strains), P_{GAL1}-CEN3 *ura3*::*HIS3* and P_{GAL1}-*CEN3 lys2*::*LEU2* were inserted on separate chromosomes.

After induction for 3 h in YPAGR, the cultures were first plated on CSM lacking uracil and histidine. Single colonies were then selected on CSM plates lacking lysine and leucine. For engineering simultaneous loss and gain of chromosomes in diploid strains, P_{GAL1}-CEN3 *URA3* and P_{GAL1}-*CEN3 lys2*::*LEU2* were inserted into separate chromosomes to be lost and gained, respectively. The cells were induced as stated above and selected first on plates containing 5-FOA. Subsequently, single colonies were grown on CSM plates lacking lysine and leucine. The respective aneuploidies of the selected strains were verified using qPCR.

Adaptation through clonal expansion

Fresh *BIR1*-deleted haploids were obtained by tetrad dissection of heterozygous diploids on YPAD. After 4 d of growth, small colonies (*bir1Δ*) from tetrads with two large colonies (*BIR1*$^+$) were streaked out for singles on fresh YPAD plates. Six colonies from each initial colony were then selected for further analysis by clonal expansion. Every 2 d, one large colony from each strain was streaked out on a fresh plate. After 10 clonal expansions, the strains were kept frozen at −80°C in 25% glycerol. Subsequent experiments were performed from these frozen stocks. The *bir1Δ* genotype was confirmed by hygromycin resistance as well as genome sequencing of the adapted strains.

Doubling time measurements

Overnight cultures were diluted to an optical density (OD) at 600 nm of 0.01 in YPAD. OD measurements were taken 3, 4, 5.5, 7, and 8.5 h after induction. The measurements were fit to logarithmic curves using Microsoft Excel to calculate doubling times.

Colony size measurements

Yeast strains were streaked for single colonies on YPAD plates and incubated for 40 h. The plates were imaged using an SPimager (S&P Robotics, Inc.) fitted with a Canon Rebel XSi dSLR camera, and the images were analyzed using ImageJ. After thresholding, colony sizes were measured using the "analyze particles" function with the following settings: particle size: 0.03–3 mm^2; circularity: 0.90–1. Median colony sizes from multiple plates were averaged for each strain.

Flow cytometry

Log-phase cultures ($OD_{600} \sim 1.0$) were pelleted and resuspended in 50 mM sodium citrate and sonicated to disperse cell clumps. Subsequently, the cells were treated with 250 µg/mL RNase A (Sigma-Aldrich, R6513) and 1 mg/mL Proteinase K (Sigma-Aldrich, P2308) overnight at 37°C. Finally, the cells were resuspended in 50 mM sodium citrate solution containing 1 µM SYTOX green (Thermo Fisher, 10768273). Samples were run on BD FACSCallibur flow cytometer equipped with a 15-mW 488-nm laser. Maximum count peaks for fluorescence intensities were calculated using the BD FACSDiva 8.0.1 software.

Next-generation sequencing and data analysis

DNA from saturated overnight cultures was isolated using the Wizard genomic DNA purification kit (Promega). The samples were then fragmented to ~500 base pairs (bp) using the Bioruptor Pico sonicator for two to three cycles (30 sec on/off). The samples were subsequently run on a 0.8% agarose gel to verify the fragment length. DNA libraries were prepared using the NEBNext Ultra II DNA library preparation kit for Illumina (New England Biosciences). AMPure XP beads were used for size selection. Twelve to 16 strains per run were multiplexed with NEBNext Multiplex oligos (96 index primers) and mixed at equimolar ratios. The multiplexed samples were sequenced using the 50-bp paired-end setting on an Illumina HiSeq 2500 system at the Vienna Biocenter Next-Generation Sequencing Facility (VBCF). The demultiplexed data sets were then aligned to the yeast genome using Bowtie2 (version 2.2.9; http://bowtie-bio.sourceforge.net/bowtie2) and converted to bed files using SAMtools (version 1.3.1; http://samtools.sourceforge.net) and Bedtools (version 2.14, http://bedtools.readthedocs.io). The resulting bed files were used to calculate chromosome copy numbers for read densities using custom-made Python2 scripts. To normalize for differences in chromosome sizes, only the 15 kb closest to the telomeres were used. The value for the second-lowest quartile chromosomes was used for normalization. Mutations in the *bir1Δ-ad* strains were identified by taking the output from Bowtie2 and running mpileup function in SAMtools. The data were filtered by quality score and read depth. Next, BCFtools (version1.3.1) was implemented to convert the bcf files generated by mpileup to variant call format (.vcf) files. Subsequently, VCFtools (version0.1.13) was used to compare all mutations found in our test strains with mutations already identified in the diploid parent strain. Last, a custom-made Python script generated lists containing the strain identity, the coordinates of the mutation (in base pairs), and the type of mutation (coding/noncoding). We generated a list of CIN genes in the yeast genome from the *Saccharomyces* Genome Database associated with six specific GO terms: colony sectoring: increased; chromosome segregation: abnormal; chromosome/plasmid maintenance: decreased rate; chromosome/plasmid maintenance: abnormal; chromosome segregation: premature; and chromosome segregation: decreased. GO term enrichment tests were conducted using the Panther Classification System Web site (http://pantherdb.org) with the settings model organism: "*S. cerevisiae*"; "statistical overrepresentation test"; and "GO biological process complete."

Microscopy

Strains were grown overnight, subsequently diluted 100-fold, and grown for 5 h to mid-log phase. Cells were pelleted by brief centrifugation, washed, and resuspended in 100 mM phosphate buffer (pH 7.4). They were then placed on 1% agarose pads supplemented with complete synthetic medium, covered with a coverslip, and sealed around the edges with VALAP (a 1:1:1 mixture of petroleum jelly [Vaseline], lanolin, and paraffin [Thermo Fisher Scientific] by weight). Time-lapse imaging was performed on an Olympus cellSens microscopy system (Olympus Corporation) fitted with an Olympus cellVivo system for temperature control at 30°C. A 60× 1.42 NA oil immersion Olympus plan apochromat objective and an ORCA-Flash4.0 V2 sCMOS camera (Hamamatsu) were used for imaging. *Z*-sections were taken with 11 0.7-µm steps with Olympus cellSens version 1.18 software (Olympus Corporation). Images were collected every 15 min for a period of 4 h. Image analyses, including maximum intensity projections and contrast adjustments, were performed using ImageJ. The images shown were collected on the same day, and contrast was adjusted identically. For quantification of the missegregation rates the GFP-labeled chromosome 4, foci were followed over time through chromosome segregation. When both foci ended up in either the mother or daughter cell after complete nuclear division (judged by the background nuclear fluorescence), the division was scored as an event of missegregation. The percentage of all missegregation events in a strain out of the total number of nuclear divisions is reported as the missegregation rate.

qPCR

Small amounts of cells from plates were lysed in 0.02 N NaOH for 10 min at 100°C in a thermocyler. The lysates were then centrifuged to pellet cellular debris, and the supernatants were collected. Each 20-µL reaction contained 10 µL of GoTaq qPCR master mix (Promega), 1 µL of lysate, and 1 µM each primer. Primers were in noncoding regions on each arm of the chromosome. The reactions were set up in 96-well plates (Eppendorf twin.tec real-time PCR 96-well plate) and cycled using a Mastercycler RealPlex^2 (Eppendorf). Cycling conditions were for 5 min at 95°C followed by 40 cycles of 15 sec at 95°C and 1 min at 60°C. Dissociation curves were performed to verify that no secondary products had been amplified. C_t values were determined using the automatic thresholding of the Eppendorf RealPlex^2 software. All reactions were run in duplicate along with the appropriate wild-type or parental controls. Chromosome copy numbers were calculated using a slightly modified $\Delta\Delta C_t$ method (Schmittgen 2001). The C_t values from duplicates were averaged and used to obtain the ΔC_t, which was subsequently raised to the negative power of 2 to give the fold change. The ratio of fold change of the test strains to that of a wild-type strain was calculated to obtain the values for the chromosome copy numbers.

Cancer genome databases and data analysis

Copy number variation (CNV) files were downloaded from the Genomic Data Commons (GDC) data portal (https://portal.gdc.cancer.gov) on October 19, 2017. Relative copy numbers were determined from each chromosome arm using a custom Python2 script. Tumor samples containing chromosome arms with large insertions or deletions (mean and median copy numbers differed by >0.2) were excluded from analysis. Karyotypes with no complex aneuploidy (fewer than two copy number aberrations) were not included in the statistical analyses.

Liquid adaptation

Overnight saturated cultures were first diluted to OD_{600} of 0.1. Subsequently, the cultures were diluted 1000-fold into 200 µL of YPAD in 96-well plates (Nunc 96 deep-well plates: 2-mL volume) and covered with a Breathe-Easier strip (Sigma, 2763624). These plates were fixed onto an incubator (New Brunswick Innova 4000 benchtop incubator shaker) using custom-made holders and incubated with shaking at 300 revolutions per minute for 24 h at 30°C. Each day, the cultures were diluted 1000-fold into fresh medium.

Statistics

Unpaired *t*-tests were performed in Prism 7 (Graphpad). Hypergeometric tests were performed in Python2 using the "hypergeom.pmf" function in the scipy.stats module. Pearson correlation coefficients were calculated using either the "pearsonr" function in the scipy.stats module in Python2 or the "correl" function in Microsoft Excel.

Acknowledgments

We thank all members of the Campbell and Dammermann laboratories for helpful discussions; Alexander Dammermann, Franz Klein, and Manish Grover for comments on the manuscript; Claudia Stadler for help with strain construction; Christopher D. Putnam for assistance with next-generation sequencing data analysis; and Kirk Anders for the gifts of plasmids. This work was supported by Vienna Science and Technology Fund (WWTF) grant VRG14-001 and Austrian Science Fund (FWF) grants Y944-B28 and W1238-B20 to C.S.C., and a University of Vienna Uni:docs Fellowship to M.C.R.

Author contributions: S.F., M.N.C., and F.C.H. conducted the experiments. C.S.C. and M.C.R. designed and conducted the experiments and wrote the paper.

References

Anders KR, Kudrna JR, Keller KE, Kinghorn B, Miller EM, Pauw D, Peck AT, Shellooe CE, Strong IJT. 2009. A strategy for constructing aneuploid yeast strains by transient nondisjunction of a target chromosome. *BMC Genet* **10:** 36.

Beach RR, Ricci-Tam C, Brennan CM, Moomau CA, Hsu P-H, Hua B, Silberman RE, Springer M, Amon A. 2017. Aneuploidy causes non-genetic individuality. *Cell* **169:** 229–242.e21.

Bonney ME, Moriya H, Amon A. 2015. Aneuploid proliferation defects in yeast are not driven by copy number changes of a few dosage-sensitive genes. *Genes Dev* **29:** 898–903.

Campbell CS, Desai A. 2013. Tension sensing by Aurora B kinase is independent of survivin-based centromere localization. *Nature* **497:** 118–121.

Chen G, Bradford WD, Seidel CW, Li R. 2012. Hsp90 stress potentiates rapid cellular adaptation through induction of aneuploidy. *Nature* **482:** 246–250.

Chen G, Mulla WA, Kucharavy A, Tsai H-J, Rubinstein B, Conkright J, McCroskey S, Bradford WD, Weems L, Haug JS, et al. 2015. Targeting the adaptability of heterogeneous aneuploids. *Cell* **160:** 771–784.

Duesberg P, Rausch C, Rasnick D, Hehlmann R. 1998. Genetic instability of cancer cells is proportional to their degree of aneuploidy. *Proc Natl Acad Sci* **95:** 13692–13697.

Hughes TR, Roberts CJ, Dai H, Jones AR, Meyer MR, Slade D, Burchard J, Dow S, Ward TR, Kidd MJ, et al. 2000. Widespread aneuploidy revealed by DNA microarray expression profiling. *Nat Genet* **25:** 333–337.

Liu G, Yong MYJ, Yurieva M, Srinivasan KG, Liu J, Lim JSY, Poidinger M, Wright GD, Zolezzi F, Choi H, et al. 2015. Gene essentiality is a quantitative property linked to cellular evolvability. *Cell* **163:** 1388–1399.

Longtine MS, McKenzie A, Demarini DJ, Shah NG, Wach A, Brachat A, Philippsen P, Pringle JR. 1998. Additional modules for versatile and economical PCR-based gene deletion and modification in *Saccharomyces cerevisiae*. *Yeast* **14:** 953–961.

Nicholson JM, Cimini D. 2013. Cancer karyotypes: survival of the fittest. *Front Oncol* **3:** 148.

Oromendia AB, Dodgson SE, Amon A. 2012. Aneuploidy causes proteotoxic stress in yeast. *Genes Dev* **26:** 2696–2708.

Ozery-Flato M, Linhart C, Trakhtenbrot L, Izraeli S, Shamir R. 2011. Large-scale analysis of chromosomal aberrations in cancer karyotypes reveals two distinct paths to aneuploidy. *Genome Biol* **12:** R61.

Passerini V, Ozeri-Galai E, de Pagter MS, Donnelly N, Schmalbrock S, Kloosterman WP, Kerem B, Storchova Z. 2016. The presence of extra chromosomes leads to genomic instability. *Nat Commun* **7:** 10754.

Rancati G, Pavelka N, Fleharty B, Noll A, Trimble R, Walton K, Perera A, Staehling-Hampton K, Seidel CW, Li R. 2008. Aneuploidy underlies rapid adaptive evolution of yeast cells deprived of a conserved cytokinesis motor. *Cell* **135:** 879–893.

Ryu H-Y, Wilson NR, Mehta S, Hwang SS, Hochstrasser M. 2016. Loss of the SUMO protease Ulp2 triggers a specific multichromosome aneuploidy. *Genes Dev* **30:** 1881–1894.

Sandall S, Severin F, McLeod IX, Yates JR, Oegema K, Hyman A, Desai A. 2006. A Bir1-Sli15 complex connects centromeres to microtubules and is required to sense kinetochore tension. *Cell* **127:** 1179–1191.

Sansregret L, Vanhaesebroeck B, Swanton C. 2018. Determinants and clinical implications of chromosomal instability in cancer. *Nat Rev Clin Oncol* **15:** 139–150.

Schmittgen TD. 2001. Real-time quantitative PCR. *Methods* **25:** 383–385.

Selmecki A, Forche A, Berman J. 2006. Aneuploidy and isochromosome formation in drug-resistant *Candida albicans*. *Science* **313:** 367–370.

Selmecki AM, Maruvka YE, Richmond PA, Guillet M, Shoresh N, Sorenson AL, De S, Kishony R, Michor F, Dowell R, et al. 2015. Polyploidy can drive rapid adaptation in yeast. *Nature* **519:** 349–352.

Sheltzer JM, Blank HM, Pfau SJ, Tange Y, George BM, Humpton TJ, Brito IL, Hiraoka Y, Niwa O, Amon A. 2011. Aneuploidy drives genomic instability in yeast. *Science* **333:** 1026–1030.

Stingele S, Stoehr G, Peplowska K, Cox J, Mann M, Storchova Z. 2012. Global analysis of genome, transcriptome and proteome reveals the response to aneuploidy in human cells. *Mol Syst Biol* **8:** 608.

Storchova Z, Becker JS, Talarek N, Kögelsberger S, Pellman D. 2011. Bub1, Sgo1, and Mps1 mediate a distinct pathway for chromosome biorientation in budding yeast. *Mol Biol Cell* **22:** 1473–1485.

Thompson SL, Compton DA. 2008. Examining the link between chromosomal instability and aneuploidy in human cells. *J Cell Biol* **180:** 665–672.

Torres EM, Sokolsky T, Tucker CM, Chan LY, Boselli M, Dunham MJ, Amon A. 2007. Effects of aneuploidy on cellular physiology and cell division in haploid yeast. *Science* **317:** 916–924.

Yona AH, Manor YS, Herbst RH, Romano GH, Mitchell A, Kupiec M, Pilpel Y, Dahan O. 2012. Chromosomal duplication is a transient evolutionary solution to stress. *Proc Natl Acad Sci* **109:** 21010–21015.

Zhu J, Pavelka N, Bradford WD, Rancati G, Li R. 2012. Karyotypic determinants of chromosome instability in aneuploid budding yeast. *PLoS Genet* **8:** e1002719.

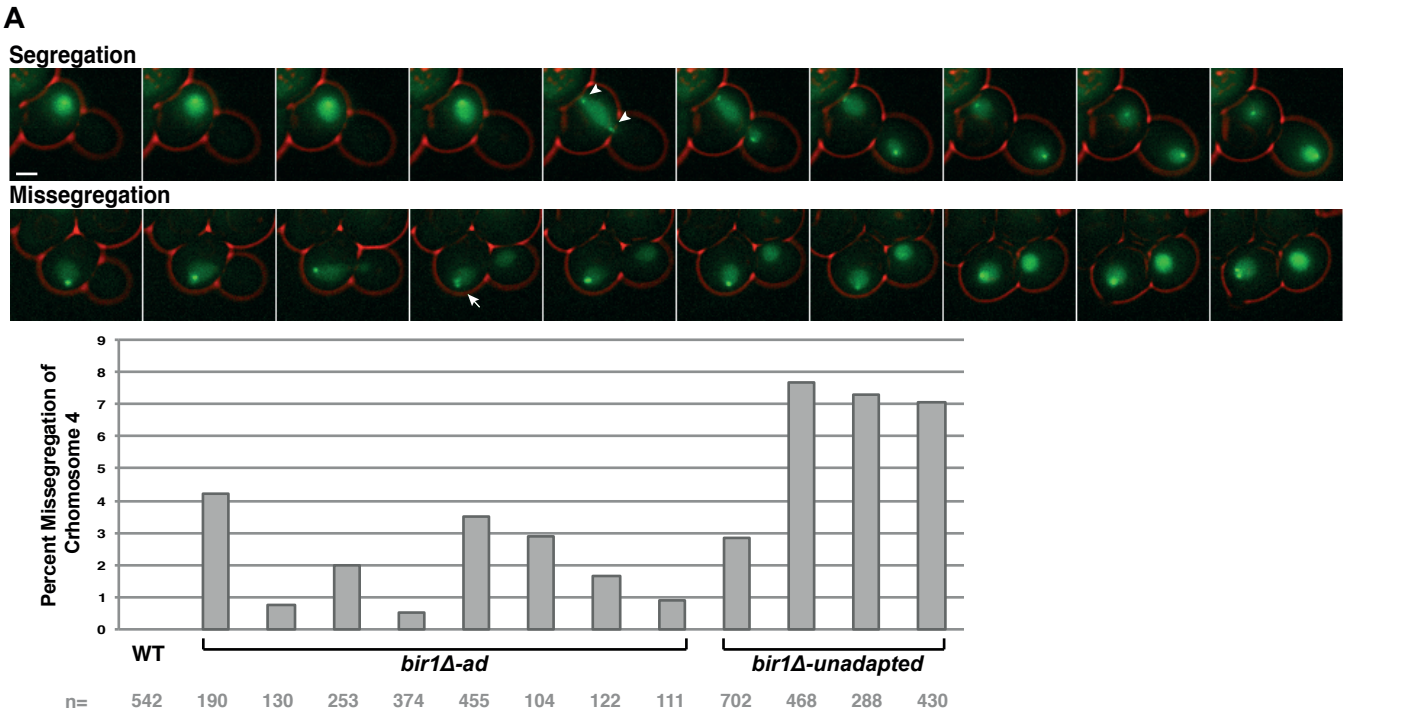
A
Segregation
Missegregation
Percent Missegregation of Chromosome 4
WT
bir1Δ-ad
bir1Δ-unadapted
n= 542 190 130 253 374 455 104 122 111 702 468 288 430

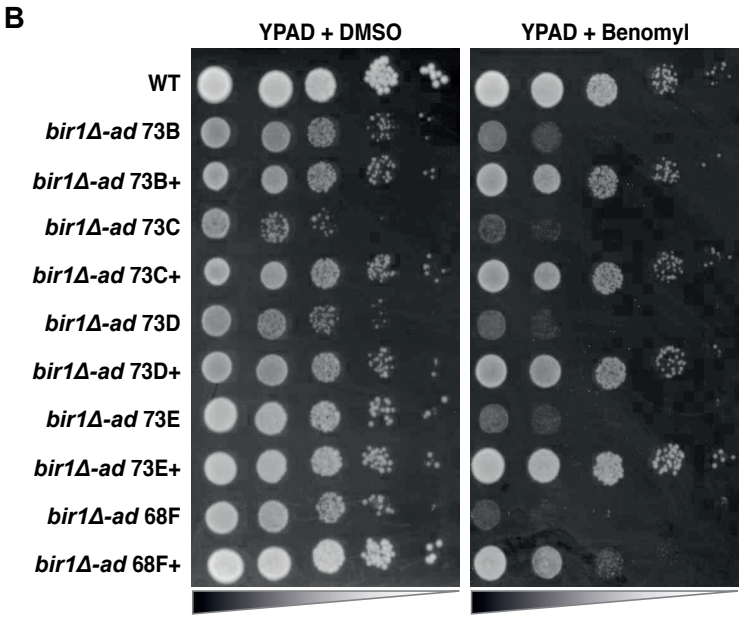
B
YPAD + DMSO
YPAD + Benomyl
WT
bir1Δ-ad 73B
bir1Δ-ad 73B+
bir1Δ-ad 73C
bir1Δ-ad 73C+
bir1Δ-ad 73D
bir1Δ-ad 73D+
bir1Δ-ad 73E
bir1Δ-ad 73E+
bir1Δ-ad 68F
bir1Δ-ad 68F+

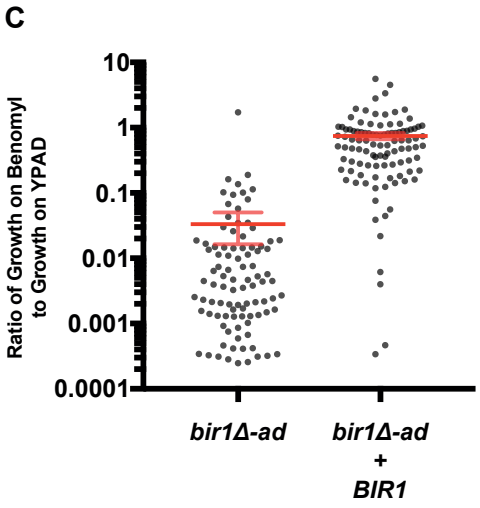
C
Ratio of Growth on Benomyl to Growth on YPAD
bir1Δ-ad
bir1Δ-ad + BIR1

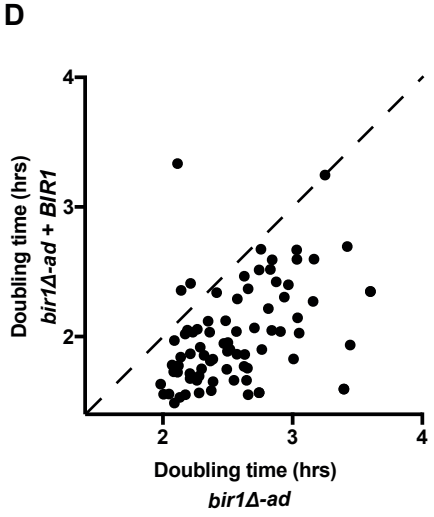
D
Doubling time (hrs) bir1Δ-ad + BIR1
Doubling time (hrs) bir1Δ-ad

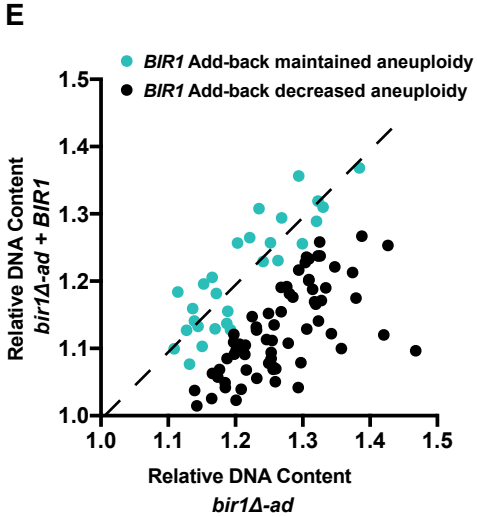
E
BIR1 Add-back maintained aneuploidy
BIR1 Add-back decreased aneuploidy
Relative DNA Content bir1Δ-ad + BIR1
Relative DNA Content bir1Δ-ad

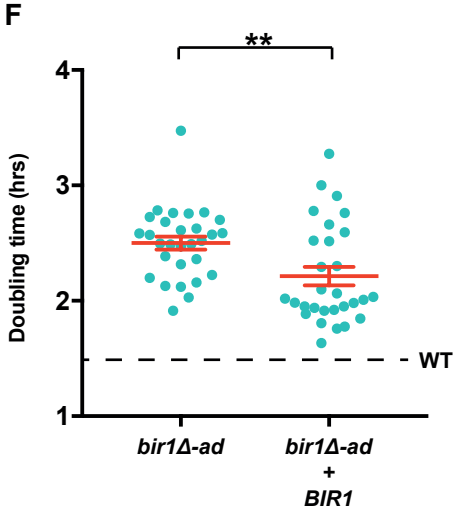
F
**
Doubling time (hrs)
WT
bir1Δ-ad
bir1Δ-ad + BIR1

Figure S1: Readdition of *BIR1* to *bir1Δ-ad* strains.

A) Missegregation rates of GFP-labeled chromosome 4 for *bir1Δ-ad* strains. The time lapse images show examples of properly segregated (arrowheads) and missegregated (arrow) chromosome 4. The time interval between images is 6 minutes and the scale bar is 2 μm long. The graph below shows the quantification of the missegregation rates per chromosome of wild-type (WT), eight different *bir1Δ-ad* strains, and four different unadapted *bir1Δ* strains. No missegregation events were observed for the wild-type cells. The total number of segregation events quantified (n) are indicated below the graph.
B) Sensitivity to a moderate (10 μg/ml) amount of the microtubule-depolymerizing drug Benomyl in *bir1Δ-ad* and *bir1Δ-ad* + *BIR1* add-back strains. 10-fold dilutions spotted for wildtype and 5 representative *bir1Δ-ad* and their respective *BIR1* add-back strains on YPAD + DMSO plates with and without Benomyl.
C) Ratio of growth for all 102 *bir1Δ-ad* and *bir1Δ-ad* + *BIR1* with vs. without Benomyl. The mean values and the standard errors are shown in red.
D) Plot of the doubling times for *bir1Δ-ad* strains vs. *bir1Δ-ad* + *BIR1* add-back strains.
E) Plot of the DNA content as measured by flow cytometry for *bir1Δ-ad* strains vs. *bir1Δ-ad* + *BIR1* add-back strains. The blue dots indicate strains that maintained a similar degree of aneuploidy after the add-back of *BIR1*.
F) Doubling times of *bir1Δ-ad* and *bir1Δ-ad* + *BIR1* add-back strains for strains that maintained similar amounts of aneuploidy (blue dots from panel **E)** after the readdition of *BIR1*. Doubling times were measured by optical density. The mean values and the standard errors are shown in red. ** $p < 0.001$.

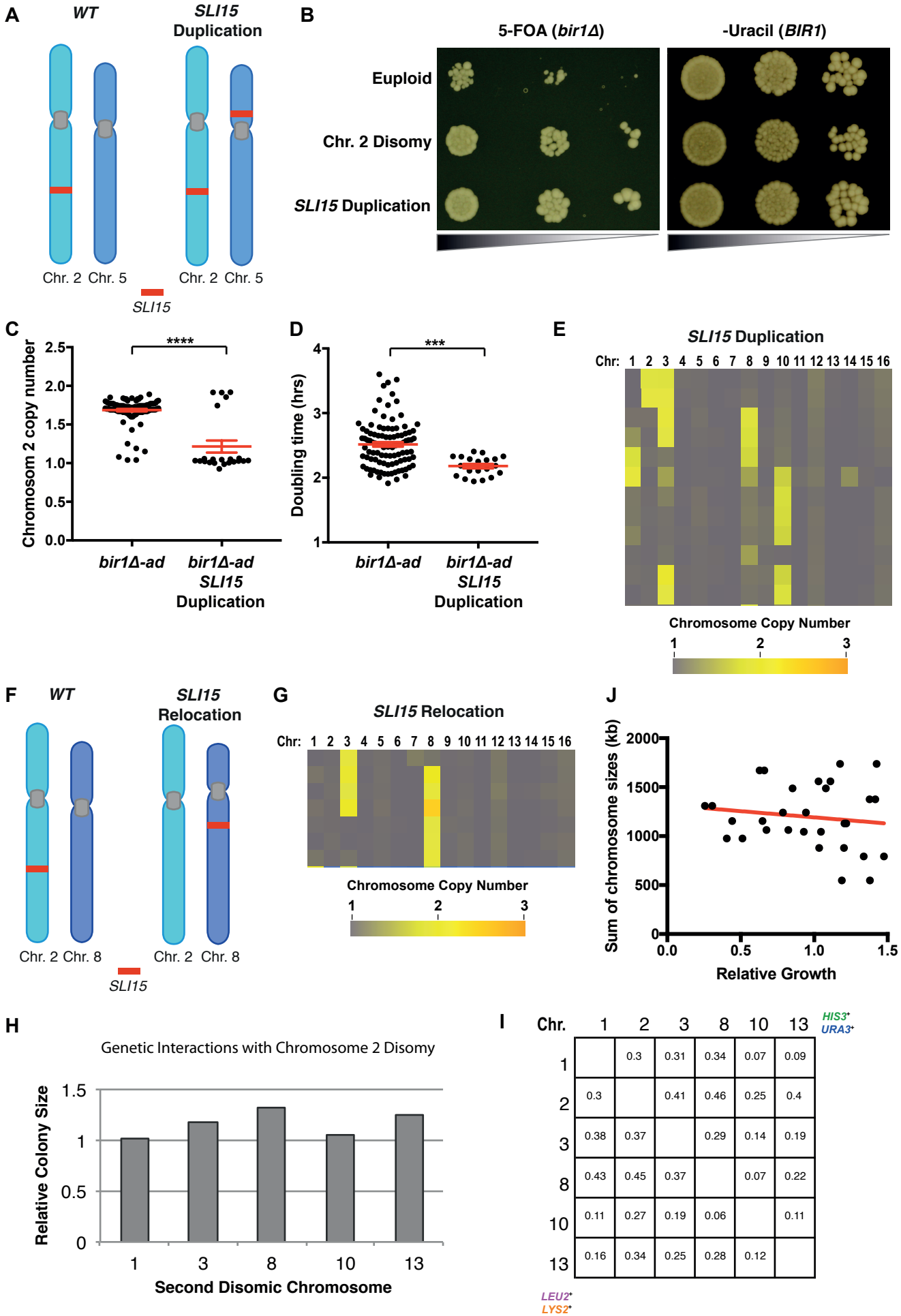

Chr.	1	2	3	8	10	13
1		0.3	0.31	0.34	0.07	0.09
2	0.3		0.41	0.46	0.25	0.4
3	0.38	0.37		0.29	0.14	0.19
8	0.43	0.45	0.37		0.07	0.22
10	0.11	0.27	0.19	0.06		0.11
13	0.16	0.34	0.25	0.28	0.12	

Figure S2: Chromosome 2 disomy contributes to adaptation to *BIR1* deletion by increasing the copy number of the *SLI15* gene.

A) Schematic for the duplication of the *SLI15* gene. One copy of *SLI15* was added to chromosome 5.
B) 10-fold dilution series of strains on 5-FOA (selecting against *URA3*) and -uracil (selecting for *URA3*) plates. Selection against *URA3* eliminates the copy of *BIR1* present on a minichromosome, resulting in *bir1Δ* cells.
C) Chromosome 2 copy numbers in *bir1Δ-ad* strains and *bir1Δ-ad* strains with *SLI15* duplication prior to adaptation as measured by qPCR. Mean values and the standard errors are shown in red.
D) Doubling times for *bir1Δ-ad* strains and *bir1Δ-ad* strains with *SLI15* duplication prior to adaptation as measured by optical density in rich liquid media. Mean values and the standard errors are shown in red.
E) Heat-map visualization of the chromosome copy numbers for the *bir1Δ-ad* + *SLI15* duplication strains. Each of the strains is represented as a row.
F) Schematic for the relocation of the *SLI15* gene, with the sole copy of *SLI15* now on chromosome 8.
G) Heat-map visualization of the chromosome copy numbers for the *bir1Δ-ad* + *SLI15* relocation strains. Each of the strains is represented as a row.
H) Relative colony sizes for strains that contain an extra copy of chromosome 2 and one of the other indicated chromosomes. Values were normalized as in Figure **3E**.
I) Median colony sizes in square millimeters of double disomic strains on YPAD plates. Normalized values are in Figure **3E**.
J) Scatter plot of relative colony sizes obtained from Figures **3E** and **S2H** plotted against the sum of the chromosome sizes of the two induced disomic chromosomes ($r = -0.1368$, $p = 0.48$).

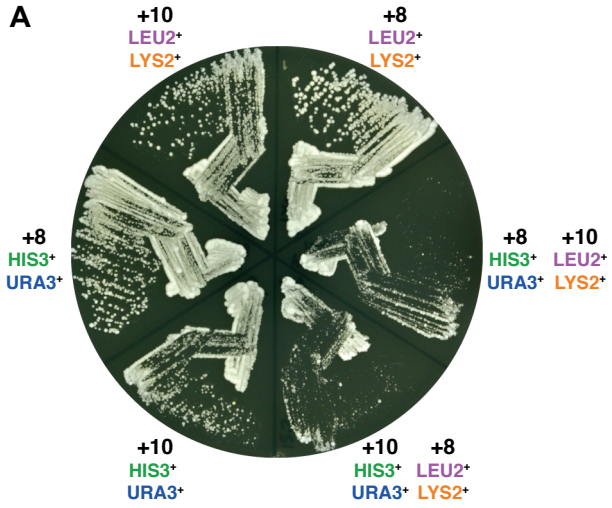
A
+10
LEU2+
LYS2+
+8
LEU2+
LYS2+
+8
HIS3+
URA3+
+8
HIS3+
URA3+
+10
LEU2+
LYS2+
+10
HIS3+
URA3+
+10
HIS3+
URA3+
+8
LEU2+
LYS2+

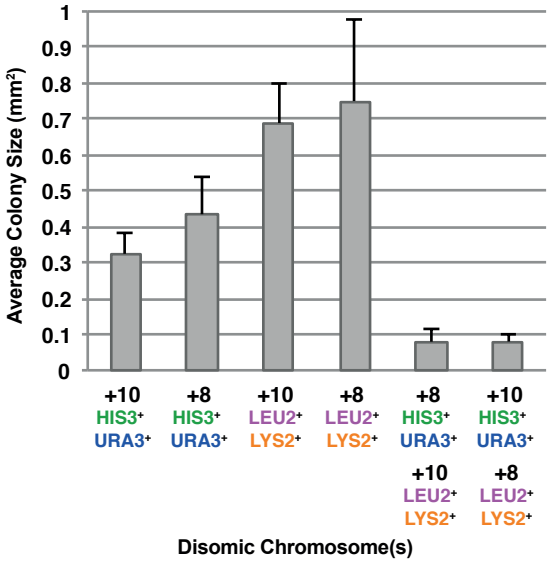
Average Colony Size (mm²)
1
0.9
0.8
0.7
0.6
0.5
0.4
0.3
0.2
0.1
0
+10 HIS3+ URA3+
+8 HIS3+ URA3+
+10 LEU2+ LYS2+
+8 LEU2+ LYS2+
+8 HIS3+ URA3+
+10 HIS3+ URA3+
+10 LEU2+ LYS2+
+8 LEU2+ LYS2+
Disomic Chromosome(s)

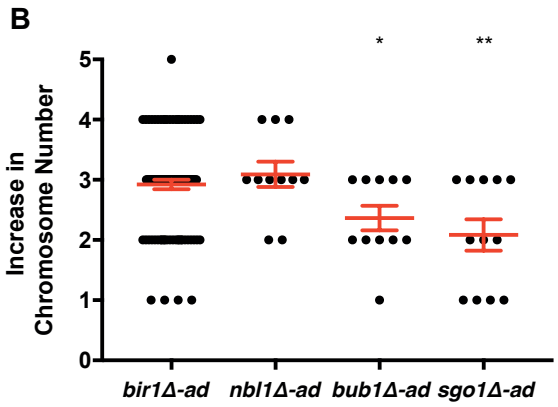
B
Increase in Chromosome Number
5
4
3
2
1
0
*
**
bir1Δ-ad
nbl1Δ-ad
bub1Δ-ad
sgo1Δ-ad

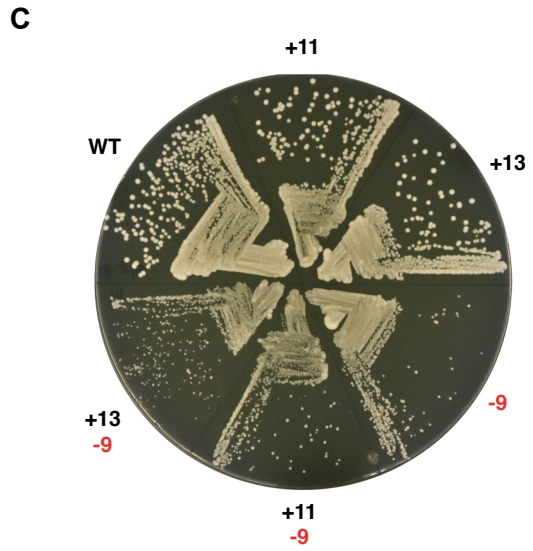
C
+11
WT
+13
+13
-9
-9
+11
-9

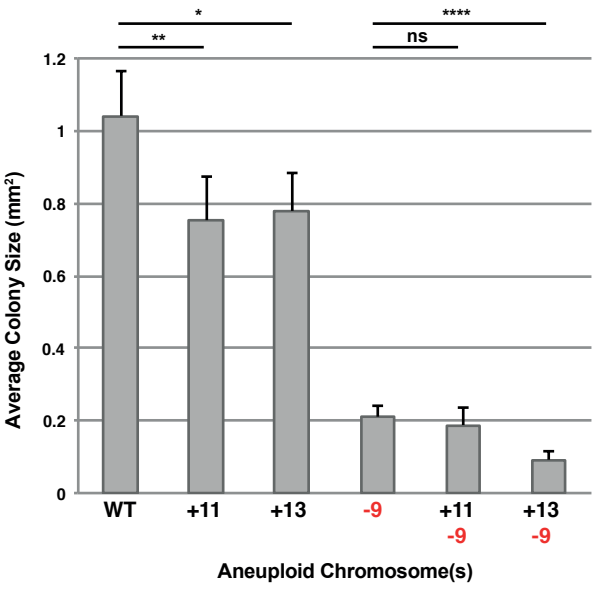
*
**
****
ns
Average Colony Size (mm²)
1.2
1
0.8
0.6
0.4
0.2
0
WT
+11
+13
-9
+11 -9
+13 -9
Aneuploid Chromosome(s)

Figure S3: Synthetic negative genetic interaction between chromosome 8 and 10 disomy and growth rates for different diploid *bir1Δ-ad* karyotypes.

A) Strains with disomy of chromosomes 8, 10, or both were struck out for single colonies on a YPAD plate. The graph on the right shows the measured colony sizes (mm^2). Error bars represent the standard deviation for average colony sizes of three independently generated strains (n = 3).
B) Increase in the number of total chromosomes for adapted strains with the indicated mutations. Mean values and the standard errors are in red. $*p \leq 0.05$, $**p < 0.001$.
C) Strains with either aneuploidy of chromosomes 13, 11, 9 or a combination of 11 and 9 or 13 and 9 were struck out for single colonies on a YPAD plate. The graph on the right shows the measured colony sizes. Error bars represent the standard deviation for average colony sizes for 2 replicates of three independently generated strains (n = 6). $*p \leq 0.05$, $**p < 0.001$, $***p < 0.0001$.

Ravichandran et al. Figure S4

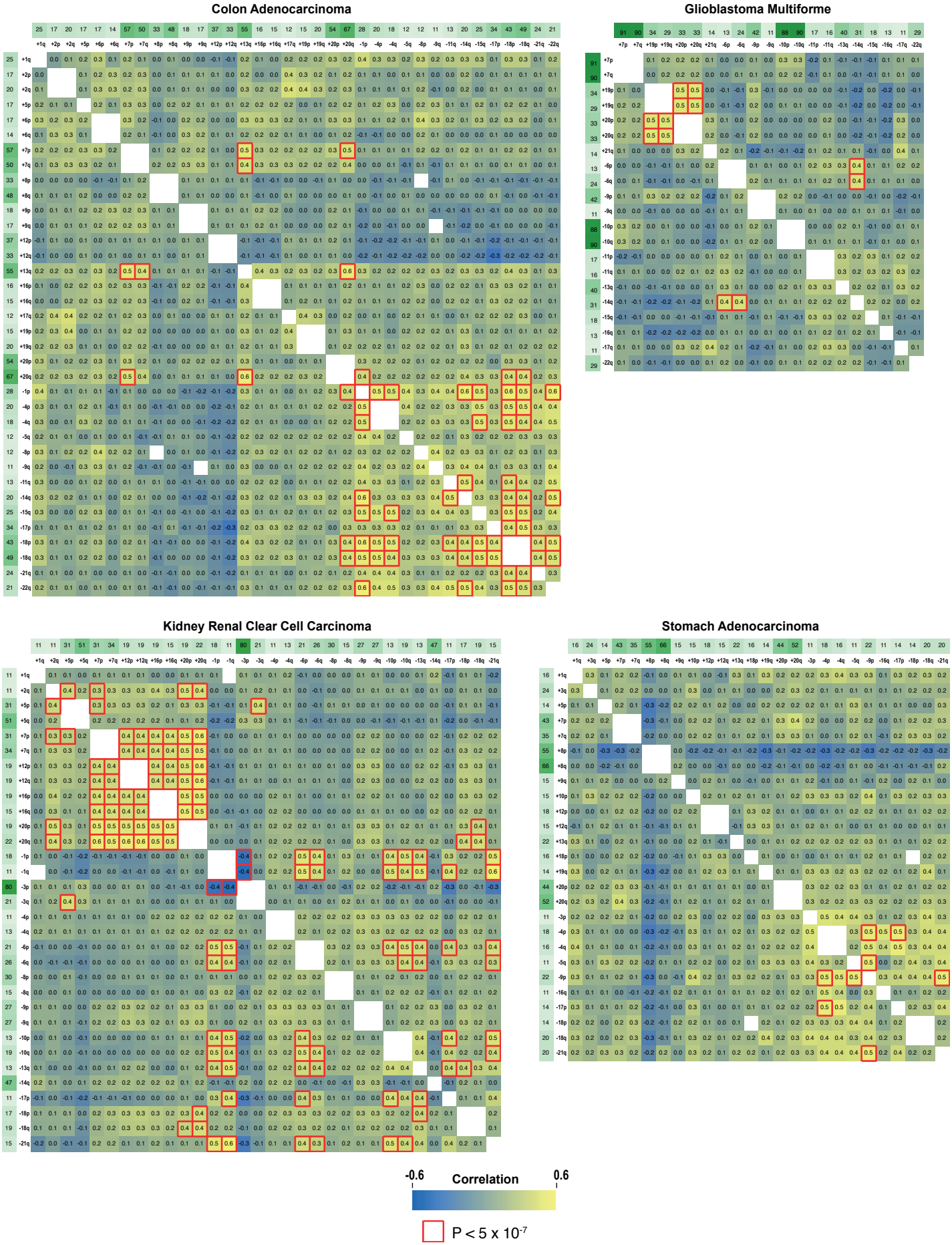

Figure S4: Chromosome arm copy number correlations in four different cancer types.

Pairwise correlation coefficients for chromosome arm aneuploidy are shown as a heat map for 138 Colon Adenocarcinoma, 160 Glioblastoma Multiforme, 253 Kidney Renal Clear Cell Carcinoma, and 119 Stomach Adenocarcinoma tumors. The frequency of each aberration is shown in green as a percentage. The red highlighted border indicates a $P < 5 \times 10\text{-}7$ in the hypergeometric test.

A

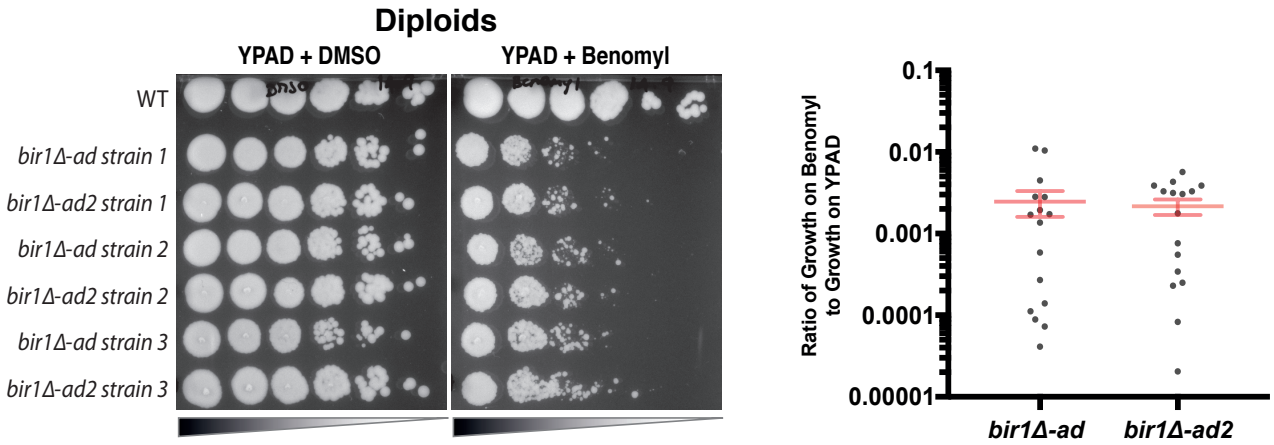

B

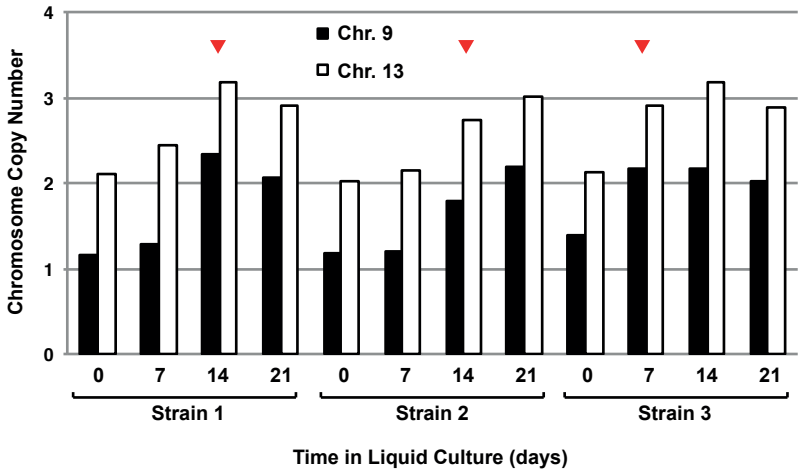

Figure S5: Further of adaptation in liquid media for three diploid *bir1Δ-ad* strains.

A) Sensitivity to a moderate (10 μg/ml) amount of the microtubule-depolymerizing drug Benomyl in *bir1Δ-ad* and *bir1Δ-ad2* strains (Further adapted for 21 days). 10-fold dilutions spotted for wildtype and 3 representative *bir1Δ-ad* and their respective *bir1Δ-ad2* strains on YPAD + DMSO plates with and without Benomyl. Mean values and the standard errors are in red.
B) The copy number of chromosome 9 (black) and 13 (white) for 3 *bir1Δ-ad* strains after 0, 7, 14, and 21 days of further liquid adaptation. The chromosome copy numbers on the 0 and 21 days are from relative read counts in whole-genome sequencing data while those for the 7 and 14 day time points are from qPCR. Red arrowheads signify the point at which both chromosomes 9 and 13 gained copies.

Table S1. Plasmids and Yeast Strains used in this study.

Strain	Genotype	Source	Background	Figure(s)
CCY747	*MATα, leu2,3-112, lys2Δ, ura3-1, his3-11:pCUP1-GFP12-lacI12:HIS3, trp1-1:256lacO:TRP1*	a	W303	1B
CCY149	*MATa/MATα, ura3-1/ura3-1, LEU2/leu2,3-112, LYS2/lys2Δ, ADE2/ade2-1, can1-100, bar1Δ, his3-11:pCUP1-GFP12-lacI12:HIS3/his3-11:pCUP1-GFP12-lacI12:HIS3 trp1-1:256lacO:TRP1/ trp1-1:256lacO:TRP1, BIR1/bir1Δ::hphNT1*	a	W303	1
bir1Δ-ad haploids	*All 102 strains were derived from tetrad dissection of CCY149*	c	W303	1B, 1C, 1D, 1E, 3A, 3B, 3C, 3F, S1
bir1Δ-ad2 haploids	*All haploid strains were derived from bir1Δ-ad haploids*	c	W303	7B, 7C
BY4741	*MATa, his3Δ1, leu2Δ0, ura3Δ0, met15Δ0*	b	S288c	-
BY4742	*MATα, his3Δ1, leu2Δ0, ura3Δ0*	b	S288c	-
CCY1865	*MATa, his3Δ1, leu2Δ0, ura3Δ0*	c	S288c	-
CCY1905	*MATa, leu2,3-112, lys2Δ, ura3-1, his3-11:pCUP1-GFP12-lacI12:HIS3, trp1-1:256lacO:TRP1, bir1Δ::hphNT1, pCC598:URA3*	c	W303	-
CCY1976	*CCY1905 + cen2::p-$_{GAL1}$-CEN3:LYS2/cen2::p-$_{GAL1}$-CEN3:lys2::pCC644:LEU2*	c	W303	2B
CCY1947	*CCY1905 + cen10::p-$_{GAL1}$-CEN3:LYS2/cen10::p-$_{GAL1}$-CEN3:lys2::pCC644:LEU2*	c	W303	2B
CCY2161	*CCY1905 + cen3::p-$_{GAL1}$-CEN3:LYS2/cen3::p-$_{GAL1}$-CEN3:lys2::pCC644:LEU2*	c	W303	2B
CCY1943	*CCY1905 + cen8::p-$_{GAL1}$-CEN3:LYS2/cen8::p-$_{GAL1}$-CEN3:lys2::pCC644:LEU2*	c	W303	2B
CCY2284	*CCY1905 + cen9::p-$_{GAL1}$-CEN3:LYS2/cen9::p-$_{GAL1}$-CEN3:lys2::pCC644:LEU2*	c	W303	2B
CCY1924	*CCY1865 + cen8::p-$_{GAL1}$-CEN3:URA3/cen8::p-$_{GAL1}$-CEN3:ura3::pCC644:HIS3*	c	S288c	S3A
CCY1927	*CCY1865 + cen10::p-$_{GAL1}$-CEN3:URA3/cen10::p-$_{GAL1}$-CEN3:ura3::pCC644:HIS3*	c	S288c	S3A
CCY2122	*CCY1865 + cen10::p-$_{GAL1}$-CEN3:LYS2/cen10::p-$_{GAL1}$-CEN3:lys2::pCC644:LEU2*	c	S288c	S3A
CCY2125	*BY4742 + cen8::p-$_{GAL1}$-CEN3:LYS2/cen8::p-$_{GAL1}$-CEN3:lys2::pCC644:LEU2*	c	S288c	S3A
CCY2073	*BY4742 + cen3::p-$_{GAL1}$-CEN3:URA3/cen3::p-$_{GAL1}$-CEN3:ura3::pCC644:HIS3, cen8::p-$_{GAL1}$-CEN3:LYS2/cen8::p-$_{GAL1}$-CEN3:lys2::pCC644:LEU2*	c	S288c	3E, 3F
CCY2074	*BY4742 + cen2::p-$_{GAL1}$-CEN3:URA3/cen2::p-$_{GAL1}$-CEN3:ura3::pCC644:HIS3, cen8::p-$_{GAL1}$-CEN3:LYS2/cen8::p-$_{GAL1}$-CEN3:lys2::pCC644:LEU2*	c	S288c	S2H
CCY2075	*BY4742 + cen3::p-$_{GAL1}$-CEN3:URA3/cen3::p-$_{GAL1}$-CEN3:ura3::pCC644:HIS3, cen10::p-$_{GAL1}$-CEN3:LYS2/cen10::p-$_{GAL1}$-CEN3:lys2::pCC644:LEU2*	c	S288c	3E, 3F

CCY2076	*BY4742 + cen10::p-$_{GAL1}$-CEN3:URA3/cen10::p-$_{GAL1}$-CEN3:ura3::pCC644:HIS3, cen8::p-$_{GAL1}$-CEN3:LYS2/cen8::p-$_{GAL1}$-CEN3:lys2::pCC644:LEU2*	c	S288c	3E, 3F
CCY2077	*BY4742 + cen2::p-$_{GAL1}$-CEN3:URA3/cen2::p-$_{GAL1}$-CEN3:ura3::pCC644:HIS3, cen10::p-$_{GAL1}$-CEN3:LYS2/cen10::p-$_{GAL1}$-CEN3:lys2::pCC644:LEU2*	c	S288c	S2h
CCY2078	*BY4742 + cen8::p-$_{GAL1}$-CEN3:URA3/cen8::p-$_{GAL1}$-CEN3:ura3::pCC644:HIS3, cen10::p-$_{GAL1}$-CEN3:LYS2/cen10::p-$_{GAL1}$-CEN3:lys2::pCC644:LEU2*	c	S288c	3E, 3F
CCY2260	*BY4741 + cen1::p-$_{GAL1}$-CEN3:URA3/cen1::p-$_{GAL1}$-CEN3:ura3::pCC644:HIS3, cen8::p-$_{GAL1}$-CEN3:LYS2/cen8::p-$_{GAL1}$-CEN3:lys2::pCC644:LEU2*	c	S288c	3E, 3F
CCY2261	*BY4741 + cen1::p-$_{GAL1}$-CEN3:URA3/cen1::p-$_{GAL1}$-CEN3:ura3::pCC644:HIS3, cen10::p-$_{GAL1}$-CEN3:LYS2/cen10::p-$_{GAL1}$-CEN3:lys2::pCC644:LEU2*	c	S288c	3E, 3F
CCY2264	*BY4741 + cen3::p-$_{GAL1}$-CEN3:URA3/cen3::p-$_{GAL1}$-CEN3:ura3::pCC644:HIS3, cen8::p-$_{GAL1}$-CEN3:LYS2/cen8::p-$_{GAL1}$-CEN3:lys2::pCC644:LEU2*	c	S288c	3E, 3F
CCY2266	*BY4742 + cen13::p-$_{GAL1}$-CEN3:URA3/cen13::p-$_{GAL1}$-CEN3:ura3::pCC644:HIS3, cen10::p-$_{GAL1}$-CEN3:LYS2/cen10::p-$_{GAL1}$-CEN3:lys2::pCC644:LEU2*	c	S288c	3E, 3F
CCY2364	*BY4742 + cen13::p-$_{GAL1}$-CEN3:URA3/cen13::p-$_{GAL1}$-CEN3:ura3::pCC644:HIS3, cen3::p-$_{GAL1}$-CEN3:LYS2/cen3::p-$_{GAL1}$-CEN3:lys2::pCC644:LEU2*	c	S288c	3E, 3F
CCY2366	*BY4741 + cen2::p-$_{GAL1}$-CEN3:URA3/cen2::p-$_{GAL1}$-CEN3:ura3::pCC644:HIS3, cen3::p-$_{GAL1}$-CEN3:LYS2/cen3::p-$_{GAL1}$-CEN3:lys2::pCC644:LEU2*	c	S288c	S2H
CCY2368	*BY4742 + cen8::p-$_{GAL1}$-CEN3:URA3/cen8::p-$_{GAL1}$-CEN3:ura3::pCC644:HIS3, cen3::p-$_{GAL1}$-CEN3:LYS2/cen3::p-$_{GAL1}$-CEN3:lys2::pCC644:LEU2*	c	S288c	3E, 3F
CCY2369	*BY4741 + cen10::p-$_{GAL1}$-CEN3:URA3/cen10::p-$_{GAL1}$-CEN3:ura3::pCC644:HIS3, cen3::p-$_{GAL1}$-CEN3:LYS2/cen3::p-$_{GAL1}$-CEN3:lys2::pCC644:LEU2*	c	S288c	3E, 3F
CCY2370	*BY4742 + cen13::p-$_{GAL1}$-CEN3:URA3/cen13::p-$_{GAL1}$-CEN3:ura3::pCC644:HIS3, cen3::p-$_{GAL1}$-CEN3:LYS2/cen3::p-$_{GAL1}$-CEN3:lys2::pCC644:LEU2*	c	S288c	3E, 3F
CCY2372	*BY4741 + cen2::p-$_{GAL1}$-CEN3:URA3/cen2::p-$_{GAL1}$-CEN3:ura3::pCC644:HIS3, cen1::p-$_{GAL1}$-CEN3:LYS2/cen1::p-$_{GAL1}$-CEN3:lys2::pCC644:LEU2*	c	S288c	S2H
CCY2374	*BY4741 + cen3::p-$_{GAL1}$-CEN3:URA3/cen3::p-$_{GAL1}$-CEN3:ura3::pCC644:HIS3, cen1::p-$_{GAL1}$-*	c	S288c	3E, 3F

	CEN3:LYS2/cen1::p-$_{GAL1}$-CEN3:lys2::pCC644:LEU2			
CCY2376	*BY4741 + cen8::p-$_{GAL1}$-CEN3:URA3/cen8::p-$_{GAL1}$-CEN3:ura3::pCC644:HIS3, cen1::p-$_{GAL1}$-CEN3:LYS2/cen1::p-$_{GAL1}$-CEN3:lys2::pCC644:LEU2*	c	S288c	3E, 3F
CCY2378	*BY4742 + cen10::p-$_{GAL1}$-CEN3:URA3/cen10::p-$_{GAL1}$-CEN3:ura3::pCC644:HIS3, cen1::p-$_{GAL1}$-CEN3:LYS2/cen1::p-$_{GAL1}$-CEN3:lys2::pCC644:LEU2*	c	S288c	3E, 3F
CCY2379	*BY4742 + cen13::p-$_{GAL1}$-CEN3:URA3/cen13::p-$_{GAL1}$-CEN3:ura3::pCC644:HIS3, cen1::p-$_{GAL1}$-CEN3:LYS2/cen1::p-$_{GAL1}$-CEN3:lys2::pCC644:LEU2*	c	S288c	3E, 3F
CCY1480	*MATa/MATα, ura3-1/ura3-1, LEU2/leu2,3-112, LYS2/lys2Δ, ADE2/ade2-1, can1-100, bar1Δ, his3-11:pCUP1-GFP12-lacI12:HIS3/his3-11:pCUP1-GFP12-lacI12:HIS3 trp1-1:256lacO:TRP1/ trp1-1:256lacO:TRP1, NBL1/nbl1Δ::hphNT1*	c	W303	-
nbl1Δ-ad haploids	*All nbl1Δ-ad strains were derived from tetrad dissection of CCY1480*	c	W303	4B, 4C, 4D, 4E
CCY1482	*MATa/MATα, ura3-1/ura3-1, LEU2/leu2,3-112, LYS2/lys2Δ, ADE2/ade2-1, can1-100, bar1Δ, his3-11:pCUP1-GFP12-lacI12:HIS3/his3-11:pCUP1-GFP12-lacI12:HIS3 trp1-1:256lacO:TRP1/ trp1-1:256lacO:TRP1, SGO1/sgo1Δ::hphNT1*	c	W303	-
sgo1Δ-ad haploids	*All sgo1Δ-ad strains were derived from tetrad dissection of CCY1482*	c	W303	4B, 4C, 4D, 4E
CCY1484	*MATa/MATα, ura3-1/ura3-1, LEU2/leu2,3-112, LYS2/lys2Δ, ADE2/ade2-1, can1-100, bar1Δ, his3-11:pCUP1-GFP12-lacI12:HIS3/his3-11:pCUP1-GFP12-lacI12:HIS3 trp1-1:256lacO:TRP1/ trp1-1:256lacO:TRP1, BUB1/bub1Δ::hphNT1*	c	W303	-
bub1Δ-ad haploids	*All bub1Δ-ad strains were derived from tetrad dissection of CCY1484*	c	W303	4B, 4C, 4D, 4E
CCY1739	*tetradploid, MATa/MATaΔ::natNT2/Matα/MatαΔ::kanMX4, ura3-1, lys2Δ, LEU2/leu2,3-112, his3-11:pCUP1-GFP12-lacI12:HIS3 trp1-1:256lacO:TRP1 ADE2/ade2-1, can1-100, bar1Δ, BIR1/BIR1/bir1Δ::hphNT1/bir1Δ::hphNT1*	c	W303	-
CCY1743	*MATa/MATα, ura3-1/ura3-1, lys2Δ/lys2Δ, LEU2/leu2,3-112, his3-11:pCUP1-GFP12-lacI12:HIS3, trp1-1:256lacO:TRP1, ADE2/ade2-1, can1-100, bar1Δ, bir1Δ::hphNT1/bir1Δ::natNT2, pCC599::URA3*	c	W303	-
CCY1744	*MATa/MATα, ura3-1/ura3-1, lys2Δ/lys2Δ, LEU2/leu2,3-112, his3-11:pCUP1-GFP12-lacI12:HIS3, trp1-1:256lacO:TRP1, ADE2/ade2-1, can1-100, bar1Δ, bir1Δ::hphNT1/bir1Δ::kanMX4, pCC599::URA3*	c	W303	-
bir1Δ-ad diploids	*All 25 strains were derived from tetrad dissection of strains with the genotype of CCY1739, or from counter-selection of URA3 plasmid of CCY1743,*	c	W303	5, S3B

	CCY1744			
bir1Δ-ad2 diploids	*All bir1Δ-ad2 diploid strains were derived from bir1Δ-ad diploids*	c	W303	7D, 7E
CCY1295	*CCY149 + SLI15/sli15Δ:natNT2*	c	W303	-
CCY1320	*CCY1295 + ura3-1:pCC411:URA3*	c	W303	-
bir1Δ-ad SLI15 Duplication	*All bir1Δ-ad SLI15 Duplication strains were derived from spores of CCY1320*	c	W303	S2C, S2D, S2E
CCY2761	*CCY1295 + cup1-1:pCC607:URA3*	c	W303	-
bir1Δ-ad SLI15 Relocation	*All bir1Δ-ad SLI15 Relocation strains were derived from spores of CCY2761*	c	W303	S2G
CCY2115	*CCY1905 + trp1-1:pCC272:TRP1*	c	W303	S2B

Plasmid	**Description**	**Source**		
pRS306	*pBluescript URA3*	d		
pCC272	*SLI15 + 1kb upstream in pRS304*	c		
pCC283	*BIR1 + 1kb upstream in pRS306*	a		
pKA52	*HIS3 integration plasmid with part of URA3 inserted at the MCS. Can insert HIS3 into a URA3 locus. Used for making disomic strains.*	e		
pGALCEN-JC3-13	*For replacing centromeres with CEN3 under the GAL-10 promoter (URA3)*	e		
pCC658	*For replacing centromeres with CEN3 under the GAL-10 promoter (LYS2)*	c		
pCC644	*LEU2 integration vector with bases 3043-3538 of LYS2 for Disruption of the LYS2 gene. Used for making disomic strains.*	c		
pCC598	*BIR1 + 1kb upstream in pRS306*	c		
pCC411	*SLI15 + 1kb upstream in pRS306*	c		
pCC607	*pCC411 + sequence from Cup1-1 gene for integrating Sli15 plus promoter into that location of chromosome 8*	c		

Key	**Source**
a	Campbell and Desai, Nature 497: 118–121 (2013)
b	Brachmann CB et al., Yeast. (1998)
c	This study
d	Sinorski and Hieter Genetics 122: 19-27 (1989)
e	Anders et. al., BMC Genetics (2009)

Table S2. Filtering of cancer karyotypes based on type of aneuploidy. Related to Figure 6.

Cancer type	Number of samples	Samples with only whole chromosome/ arm aneuploidy	Number with complex whole chromosome/arm aneuploidy	Percent with complex whole chromosome/ arm aneuploidy
Breast Invasive Carcinoma	1096	214	177	16
Glioblastoma Multiforme	593	170	161	27
Ovarian Serous Cystadenocarcinoma	573	13	11	2
Lung Adenocarcinoma	518	114	97	19
Uterine Corpus Endometrial Carcinoma	547	323	137	25
Kidney Renal Clear Cell Carcinoma	532	273	253	48
Head and Neck Squamous Cell Carcinoma	531	120	98	18
Brain Lower Grade Glioma	514	225	193	38
Thyroid Carcinoma	505	468	42	8
Lung Squamous Cell Carcinoma	504	59	49	10
Prostate Adenocarcinoma	498	198	75	15
Skin Cutaneous Melanoma	470	91	78	17
Colon Adenocarcinoma	458	198	138	30
Stomach Adenocarcinoma	443	159	119	27
Bladder Urothelial Carcinoma	412	65	47	11

Table S3. List of genes mutated in the *bir1Δ-ad* strains.

Systematic	Standard	Mutant	Residue	CIN gene
tS(UGA)I	SUP17	missense	A18G	no
tV(AAC)G2	None	nonsense	E15*	no
YAL051W	OAF1	missense	V939I	no
YAR028W	None	missense	D32N	no
YCR017C	CWH43	missense	E250G	no
YCR021C	HSP30	missense	R11C	no
YCR033W	SNT1	missense	F870I	yes
YDL101C	DUN1	missense	A307V	yes
YDL137W	ARF2	missense	S147C	no
YDL145C	COP1	missense	I307S	no
YDL156W	CMR1	missense	L27F	yes
YDL171C	GLT1	missense	D1583V	no
YDL190C	UFD2	missense	Q88E	no
YDL243C	AAD4	indel	70	no
YDR104C	SPO71	missense	D814N	no
YDR142C	PEX7	missense	L253I	no
YDR159W	SAC3	missense	I1097L	no
YDR180W	SCC2	missense	N63Y	yes
YDR189W	SLY1	missense	D151N	yes
YDR190C	RVB1	missense	T322K	no
YDR238C	SEC26	missense	F555L	no
YDR302W	GPI11	missense	R29L	no
YDR304C	CPR5	missense	V188L	no
YDR321W	ASP1	missense	R55I	no
YDR325W	YCG1	missense	G677R	yes
YDR333C	RQC1	indel	565	no
YDR335W	MSN5	missense	H426Y	no
YDR387C	CIN10	missense	S311T	yes
YDR389W	SAC7	missense	L511F	no
YDR422C	SIP1	missense	E357D	no
YDR440W	DOT1	missense	H142N	no
YDR451C	YHP1	missense	A273T	no
YDR492W	IZH1	missense	E35K	no
YDR523C	SPS1	missense	F248S	no
YDR527W	RBA50	missense	G22V	no
YEL060C	PRB1	missense	G304R	no
YER002W	NOP16	missense	D122V	no
YER008C	SEC3	missense	Q495R	no
YER027C	GAL83	missense	P78S	no
YER043C	SAH1	missense	R241C	no
YER053C	PIC2	missense	N49Y	no
YER066W	RRT13	missense	G93S	no
YER095W	RAD51	missense	G40V	yes
YER109C	FLO8	missense	A529T	no
YER116C	SLX8	missense	P150S	yes
YER154W	OXA1	missense	D239H	no
YER155C	BEM2	missense	H2114Q	no

YER167W	BCK2	missense	S414P	no
YER172C	BRR2	missense	K351N	no
YER172C	BRR2	missense	N352Y	no
YER173W	RAD24	missense	T622A	yes
YER176W	ECM32	indel	781	no
YFL002C	SPB4	missense	R207S	no
YFL013C	IES1	missense	D309V	no
YFL013C	IES1	nonsense	Y572*	no
YFL021W	GAT1	missense	H182Y	no
YFL024C	EPL1	indel	Q790	no
YFL024C	EPL1	indel	Q790	no
YFR015C	GSY1	missense	A639T	no
YFR029W	PTR3	missense	D19E	no
YFR040W	SAP155	missense	D780H	no
YGL017W	ATE1	missense	A274S	no
YGL203C	KEX1	missense	P43S	no
YGL206C	CHC1	missense	P1463Q	no
YGL207W	SPT16	missense	W54R	yes
YGL207W	SPT16	missense	T713A	yes
YGR054W	None	missense	P242Q	no
YGR070W	ROM1	missense	V248A	no
YGR080W	TWF1	missense	E51D	no
YGR090W	UTP22	missense	S819L	no
YGR130C	None	indel	190	no
YGR142W	BTN2	indel	310	no
YGR208W	SER2	missense	A271T	no
YGR241C	YAP1802	indel	514	no
YGR253C	PUP2	missense	D71N	yes
YGR257C	MTM1	indel	344	no
YGR271C-A	EFG1	missense	L118F	no
YGR271W	SLH1	missense	N924K	no
YHL008C	None	indel	449	no
YHL034C	SBP1	missense	V44I	no
YHL041W	None	missense	S101F	no
YHR030C	SLT2	missense	L159F	no
YHR042W	NCP1	missense	L315M	no
YHR046C	INM1	missense	G112V	no
YHR072W	ERG7	missense	S612F	no
YHR078W	None	missense	C408Y	no
YHR106W	TRR2	missense	C165F	no
YHR117W	TOM71	missense	T293A	no
YHR138C	None	missense	V27A	no
YIL010W	DOT5	missense	S14F	yes
YIL042C	PKP1	missense	R97K	no
YIL073C	SPO22	nonsense	Q38*	no
YIL078W	THS1	missense	P174S	no
YIL090W	ICE2	missense	C364R	yes
YIL166C	SOA1	indel	394	no
YIL169C	CSS1	indel	942	no

YIR016W	None	missense	D252H	no
YJL005W	CYR1	missense	H1984L	no
YJL080C	SCP160	missense	R152G	no
YJL158C	CIS3	missense	S191N	no
YJR062C	NTA1	missense	S424G	no
YJR109C	CPA2	missense	A1049P	no
YKL021C	MAK11	missense	C252R	no
YKL040C	NFU1	missense	M213I	no
YKL078W	DHR2	missense	G161A	no
YKL080W	VMA5	missense	L130S	no
YKL182W	FAS1	missense	A632T	no
YKL183W	LOT5	missense	D54V	no
YKL191W	DPH2	missense	N386K	no
YKL215C	OXP1	missense	T310A	no
YKR021W	ALY1	missense	L621M	no
YKR039W	GAP1	missense	A527T	no
YKR054C	DYN1	missense	N2915I	no
YKR095W	MLP1	missense	Q1040P	no
YLL061W	MMP1	missense	H550N	no
YLR020C	YEH2	missense	Q479L	no
YLR024C	UBR2	missense	S1400C	no
YLR024C	UBR2	nonsense	S1483*	no
YLR045C	STU2	missense	P146S	no
YLR067C	PET309	missense	G350D	no
YLR096W	KIN2	indel	730	no
YLR145W	RMP1	missense	C132Y	no
YLR196W	PWP1	missense	E129D	yes
YLR332W	MID2	missense	I359L	no
YLR369W	SSQ1	missense	K303R	no
YLR383W	SMC6	missense	M270V	yes
YLR410W	VIP1	missense	K262T	yes
YLR417W	VPS36	missense	A412G	no
YLR422W	DCK1	missense	S370L	no
YLR454W	FMP27	missense	M1621I	no
YML072C	TCB3	missense	D168E	no
YML097C	VPS9	missense	C260Y	no
YML100W	TSL1	missense	M121I	no
YMR026C	PEX12	missense	T241M	no
YMR092C	AIP1	missense	Y515H	no
YMR129W	POM152	missense	G1069S	no
YMR154C	RIM13	missense	A93G	no
YMR178W	None	missense	S234T	no
YMR207C	HFA1	missense	G110D	yes
YMR246W	FAA4	missense	F356C	yes
YMR317W	None	indel	270	yes
YMR317W	None	indel	270	yes
YNL054W	VAC7	missense	P143S	no
YNL077W	APJ1	missense	P107Q	no
YNL078W	NIS1	indel	4	no

YNL082W	PMS1	missense	T92M	no
YNL178W	RPS3	missense	A80T	no
YNL258C	DSL1	missense	K615N	no
YNL261W	ORC5	missense	D323G	yes
YNL287W	SEC21	missense	S405Y	no
YNR016C	ACC1	missense	A1019V	yes
YNR030W	ALG12	missense	N477K	no
YNR059W	MNT4	nonsense	W285*	no
YOL039W	RPP2A	missense	G74A	no
YOL075C	None	missense	C506F	no
YOL081W	IRA2	missense	A1845S	yes
YOL110W	SHR5	missense	R113P	no
YOR076C	SKI7	missense	D430V	no
YOR101W	RAS1	missense	R109T	no
YOR107W	RGS2	missense	H71Q	no
YOR151C	RPB2	missense	G888C	yes
YOR168W	GLN4	missense	F61Y	yes
YOR195W	SLK19	missense	N291S	yes
YOR204W	DED1	missense	H93Q	no
YOR241W	MET7	missense	E306D	no
YOR275C	RIM20	nonsense	E269*	no
YOR291W	YPK9	missense	E1231V	no
YOR301W	RAX1	missense	Q179H	no
YOR335C	ALA1	missense	K611M	no
YOR354C	MSC6	missense	T562R	no
YPL045W	VPS16	missense	V617I	no
YPL056C	LCL1	missense	V55L	no
YPL086C	ELP3	missense	L512F	no
YPL100W	ATG21	missense	K32N	no
YPL106C	SSE1	missense	L278F	yes
YPL116W	HOS3	missense	Q578P	no
YPL184C	MRN1	missense	E91Q	no
YPL249C	GYP5	missense	M472I	no
YPL264C	None	missense	M273I	no
YPL272C	PBI1	missense	G25R	no
YPR014C	None	missense	V39G	no
YPR029C	APL4	missense	H64N	no
YPR043W	RPL43A	missense	C12S	no
YPR095C	SYT1	missense	Y1058N	no
YPR097W	None	missense	V368L	no
YPR116W	RRG8	nonsense	S86*	no
YPR120C	CLB5	missense	D43N	yes
YPR138C	MEP3	missense	A26P	no
YPR173C	VPS4	missense	E126Q	no
YPR192W	AQY1	missense	F62S	no

Table S4. List of heterozygous mutations in the *bir1Δ-ad* strains.

Chromosome	Systematic name	Standard name	Mutant type	Residue change
1	YAL048C	GEM1	missense	H356N
1	YAL034C	FUN19	missense	A286S
2	tL(UAA)B1	None	missense	V15F
2	YBL098W	BNA4	missense	G313C
2	YBL079W	NUP170	missense	F669Y
2	YBL066C	SEF1	missense	H42Y
2	YBL063W	KIP1	missense	P1070L
2	YBL061C	SKT5	missense	A378T
2	YBL050W	SEC17	missense	R73M
2	YBL047C	EDE1	missense	R387K
2	YBL022C	PIM1	missense	A851V
2	YBL019W	APN2	missense	F31L
2	YBR045C	GIP1	missense	S233R
2	YBR066C	NRG2	missense	K68Q
2	YBR092C	PHO3	missense	S132P
2	YBR133C	HSL7	missense	S29C
2	YBR136W	MEC1	missense	S1709*
2	YBR162C	TOS1	missense	G449A
2	YBR180W	DTR1	missense	A202V
2	YBR222C	PCS60	missense	S217N
2	YBR236C	ABD1	missense	T313I
2	YBR272C	HSM3	missense	Y73*
2	YBR285W	None	missense	F123L
2	YBR289W	SNF5	missense	D315Y
3	YCR032W	BPH1	missense	H1648Q
3	YCR061W	None	missense	G442A
3	YCR093W	CDC39	missense	V511M
8	YHL030W	ECM29	missense	F1508C
8	YHR070W	TRM5	missense	V30M
8	YHR193C	EGD2	missense	K100N
10	YJL208C	NUC1	missense	L265F
10	YJL165C	HAL5	missense	E20K
10	YJL090C	DPB11	missense	G284D
10	YJL051W	IRC8	missense	N728I
10	YJL039C	NUP192	missense	K567E
10	YJL034W	KAR2	missense	P162T
10	YJR045C	SSC1	missense	K579N
10	YJR052W	RAD7	missense	L444Q
10	YJR094C	IME1	missense	H243N
10	YJR113C	RSM7	missense	E36D
10	YJR117W	STE24	missense	D52N

3.2 Adaptation to high rates of chromosomal instability and aneuploidy through multiple pathways in budding yeast

The following manuscript was submitted on 22nd April 2022 to *EMBOJ*. The final revised version was accepted for publication on the 24th of November 2022. The project was originally conceptualized by Christopher S. Campbell. The author of this thesis performed most of the experiments for this paper. The following contributions from co-authors must be noted: Theodor Marsoner performed experiments for figures 6B, EV4A, EV4B and EV4C. Manuel Alonso Y Adell performed the experiments for figures EV5 and 6C. Madhwesh C. Ravichandran performed the experiments for figures 1B and 1C. Furthermore, the author of this thesis, as well as Theodor Marsoner, Christopher S. Campbell and Manuel Alonso Y Adell contributed to key discussions before and during the revision process, and helped edit the manuscript during the writing process. The published version of this article can be found at: https://www.embopress.org/doi/full/10.15252/embj.2022111500. The DOI is: https://doi.org/10.15252/embj.2022111500. An earlier version was put on bioArxiv: https://www.biorxiv.org/content/10.1101/2022.04.21.489003v1. (accessed: 25.11.2022).

Article

TRANSPARENT PROCESS OPEN ACCESS

THE EMBO JOURNAL

Adaptation to high rates of chromosomal instability and aneuploidy through multiple pathways in budding yeast

Matthew N Clarke, Theodor Marsoner, Manuel Alonso Y Adell, Madhwesh C Ravichandran & Christopher S Campbell*

Abstract

Both an increased frequency of chromosome missegregation (chromosomal instability, CIN) and the presence of an abnormal complement of chromosomes (aneuploidy) are hallmarks of cancer. To better understand how cells are able to adapt to high levels of chromosomal instability, we previously examined yeast cells that were deleted of the gene *BIR1*, a member of the chromosomal passenger complex (CPC). We found *bir1Δ* cells quickly adapted by acquiring specific combinations of beneficial aneuploidies. In this study, we monitored these yeast strains for longer periods of time to determine how cells adapt to high levels of both CIN and aneuploidy in the long term. We identify suppressor mutations that mitigate the chromosome missegregation phenotype. The mutated proteins fall into four main categories: outer kinetochore subunits, the SCF^{Cdc4} ubiquitin ligase complex, the mitotic kinase Mps1, and the CPC itself. The identified suppressor mutations functioned by reducing chromosomal instability rather than alleviating the negative effects of aneuploidy. Following the accumulation of suppressor point mutations, the number of beneficial aneuploidies decreased. These experiments demonstrate a time line of adaptation to high rates of CIN.

Keywords aneuploidy; Aurora B; chromosomal instability; kinetochore; SCF complex

Subject Categories Cell Cycle; DNA Replication, Recombination & Repair

DOI 10.15252/embj.2022111500 | Received 22 April 2022 | Revised 8 November 2022 | Accepted 24 November 2022

The EMBO Journal (2022) e111500

Introduction

The accurate distribution of chromosomes to daughter cells is a fundamental requirement of cell division. An increase in the frequency of errors in chromosome segregation is called chromosomal instability (CIN). Chromosomal instability leads to abnormal karyotypes through the gain or loss of chromosomes, a state called aneuploidy. Aneuploidy and CIN are both hallmarks of cancer that have causative roles in cancer development, cancer progression, and resistance to chemotherapy (reviewed in Ben-David & Amon, 2020). Despite the promotion of cell proliferation in cancer, aneuploidy and CIN have consistently been demonstrated to decrease cell growth and division (Gropp *et al*, 1983; Torres *et al*, 2007). Cancers therefore likely develop adaptations to ameliorate the negative effects of CIN and aneuploidy.

Different models for how cells adapt to CIN and aneuploidy have been proposed. Cells could adapt via compensatory mutations that decrease the levels of CIN after the accumulation of beneficial aneuploidies (Cahill *et al*, 1999; Kwon *et al*, 2008; Sansregret *et al*, 2017). Alternatively, researchers postulated that cancer cells could adapt to CIN and aneuploidy through mutations that lead to aneuploidy tolerance (Torres *et al*, 2010). Additionally, it was suggested that CIN and aneuploidy provide for a fast, but transient mechanism of adaptation. In this model, aneuploidy provides a short-term benefit that outweighs its downsides but would eventually be superseded by more targeted genome alterations (Yona *et al*, 2012). How aneuploidy and more specific types of mutations affect each other during the course of adaptation is currently unknown.

The molecular mechanisms that lead to CIN in cancer cells have long been elusive (Gordon *et al*, 2012). However, one relevant phenotype that is frequently observed across many cancer types is the overstabilization of connections between microtubules and kinetochores, which are the binding sites for microtubules at the centromeres of chromosomes (Bakhoum *et al*, 2009a). These overstabilized attachments lead to the accumulation of misattached chromosomes where both of the sister chromatids are attached to microtubules emanating from the same spindle pole (merotelic and syntelic attachments). One or both of the kinetochores must then be detached from the microtubules in order to properly distribute one sister chromatid to each daughter cell. Although the basis behind this phenotype in cancer cells is currently unknown, the central player in destabilizing erroneous kinetochore–microtubule attachments is the chromosomal passenger complex (CPC). The CPC contains a kinase, Aurora B, that phosphorylates kinetochores to lower their affinity for microtubules (Tanaka *et al*, 2002; Cheeseman *et al*,

Department of Chromosome Biology, Max Perutz Labs, Vienna Biocenter (VBC), University of Vienna, Vienna, Austria
*Corresponding author. Tel: +43 1 4277 74418; Fax: +43 1 4277 9562; E-mail: christopher.campbell@univie.ac.at

2006; Sarangapani *et al*, 2013; Kalantzaki *et al*, 2015). Inhibition of Aurora B in mammalian cells leads to an increased frequency of lagging chromosomes in anaphase due to the inability to detach microtubules from kinetochores that are attached to both spindle poles (Cimini *et al*, 2006). This lagging chromosome phenotype is also frequently observed in cancers (Bakhoum *et al*, 2014).

In addition to Aurora B, the CPC contains the subunits INCENP, Survivin, and Borealin. The C-terminus of INCENP binds to and activates Aurora B, while the N-terminus binds to Survivin and Borealin (Ainsztein *et al*, 1998; Bishop & Schumacher, 2002; Honda *et al*, 2003; Sessa *et al*, 2005; Klein *et al*, 2006; Jeyaprakash *et al*, 2007). Survivin and Borealin target the complex to centromere-proximal chromatin through an interaction with Shugoshin. This interaction was shown to promote the activity of the CPC in correcting erroneous kinetochore–microtubule attachments through phosphorylation of substrates at the outer kinetochore (Gassmann *et al*, 2004; Kawashima *et al*, 2007, 2010; Vanoosthuyse *et al*, 2007).

The budding yeast *Saccharomyces cerevisiae* is a valuable model organism for studying CIN and aneuploidy as it can tolerate high levels of CIN that are similar to what is frequently observed in cancer. We previously determined how cells initially adapt to extremely high rates of chromosome missegregation by growing budding yeast cells carrying mutations that decrease CPC function (Ravichandran *et al*, 2018). The budding yeast homologs of the CPC subunits Aurora B, INCENP, Survivin, and Borealin are Ipl1, Sli15, Bir1, and Nbl1, respectively (Fig 1A). By sequencing populations of yeast that were grown in the absence of the CPC subunit Survivin/Bir1, we found that the yeast adapted by acquiring specific aneuploidies that decreased the rate of CIN (Ravichandran *et al*, 2018). The compositions of karyotypes were further refined over time until the cells acquired certain combinations of beneficial aneuploid chromosomes. However, these adapted cells were still substantially less fit than wild-type due to a combination of the negative effects of the acquired aneuploidies and residual chromosomal instability. It is currently not known how cells with high rates of CIN and aneuploidy further adapt after the initial optimization of their karyotypes.

In this study, we have now monitored these CPC-deficient cells for longer periods of time to determine how cells evolve to cope in the long term with increased levels of both CIN and aneuploidy. We aimed to determine whether they adapt through genetic changes that either (i) allow for better aneuploidy tolerance, (ii) decrease the levels of CIN, or (iii) further optimize their karyotypes. We found that cells evolved through hypomorphic mutations in essential genes that decreased the levels of CIN. The lower levels of CIN then allowed the cells to decrease their levels of aneuploidy, as the beneficial effects of the extra chromosomes no longer outweighed the fitness costs. The identified mutations fall into two broad functional categories. The first category of mutations destabilizes kinetochore–microtubule interactions, counteracting the overstabilization created by decreased CPC activity. These mutations were found in outer kinetochore proteins that directly interact with microtubules. The second category of mutations affect the function of the CPC more directly. These include mutations in the CPC itself, the mitotic kinase Mps1, and the ubiquitin ligase SCF^{Cdc4} complex. SCF^{Cdc4} mutations increase the recruitment of the CPC to key regulatory regions in both yeast and human cells. We conclude that cells generally adapt to high levels of CIN and aneuploidy through mutations that alleviate the CIN phenotype. Furthermore, we have identified specific pathways of adaptation to defects in CPC function.

Results

Adaptation to high levels of CIN and aneuploidy occurs through point mutations that reduce the rate of CIN

To determine how cells adapt to high rates of CIN and aneuploidy, we started with a collection of haploid yeast strains that were previously cultured for 21 days via clonal expansion following *BIR1* deletion (Ravichandran *et al*, 2018). We call these partially adapted strains *bir1Δ-ad*. These strains have a high frequency of specific aneuploidies that decrease the rate of CIN. However, they are not enriched for mutations that are related to CIN. We adapted 68 of these strains for an additional 21 or 42 days (*bir1Δ-ad2*) in liquid culture to determine how cells continue to evolve after their initial adaptation through aneuploidy (Fig 1B). In comparison with the clonal expansion of the initial adaptation, liquid culture adaptation allows time for rarely occurring beneficial genomic changes to take over the population competitively. This additional adaptation greatly improved the growth of some strains but did not result in a significant level of growth improvement for all of the adapted populations combined (Fig 1C). Cells with impaired chromosome segregation are especially sensitive to microtubule-depolymerizing drugs. Consistent with this, *BIR1* deletion results in a strong sensitivity to moderate amounts of the microtubule-depolymerizing drug benomyl

Figure 1. Strains with high levels of CIN and aneuploidy adapt by decreasing CIN.

A Schematic summarizing the main localization of the CPC and its role in phosphorylating the Dam1 complex (Dam1c) to destabilize microtubule attachments.

B Summary of the adaptation time-line. *bir1*Δ strains from tetrads were grown clonally for 21 days to produce *bir1*Δ-*ad* strains. Colonies from the *bir1*Δ-*ad* strains were then grown in liquid media for 21 or 42 additional days to produce the *bir1*Δ-*ad2* strains.

C, D Growth comparisons of wild-type (WT, $n = 16$), unadapted (*bir1*Δ, $n = 14$), partially adapted (*bir1*Δ-*ad*, $n = 15$), and further adapted (*bir1*Δ-*ad2*, $n = 15$) strains as measured by area of growth after serial dilution. The serial dilutions of all these strains were carried out once in parallel. Examples of dilutions series such as those used in the quantification for *bir1*Δ-*ad* and *bir1*Δ-*ad2* strains can be found in Fig EV1C. Ten-fold serial dilutions were made on YPAD plates containing either 0.1% DMSO (C) or 10 μg/ml of benomyl (D). The mean (red line) is shown. Growth was normalized to WT.

E Comparison of the mean number of aneuploid chromosomes per strain for the *bir1*Δ-*ad* ($n = 45$ strains) and *bir1*Δ-*ad2* ($n = 51$ strains) collections. Only data from *bir1*Δ-*ad* strains that were subjected to additional adaptation are shown. Means and standard deviations are shown.

F Histogram showing the proportion of strains that are aneuploid for specific chromosomes in partially adapted (*bir1*Δ-ad) and further adapted (*bir1*Δ-*ad2*) strains.

G Eight hundred and seventy-four genes out of 6,002 total yeast genes (14.5%) have phenotypes related to CIN. The percentage of newly identified mutations in the *bir1*Δ-*ad2* (26 out of 98) and *bir1*Δ-*ad* (37 out of 246) strains that are related to CIN are shown.

Data information: (ns) not significant; (*) $P < 0.05$; unpaired *t*-test.

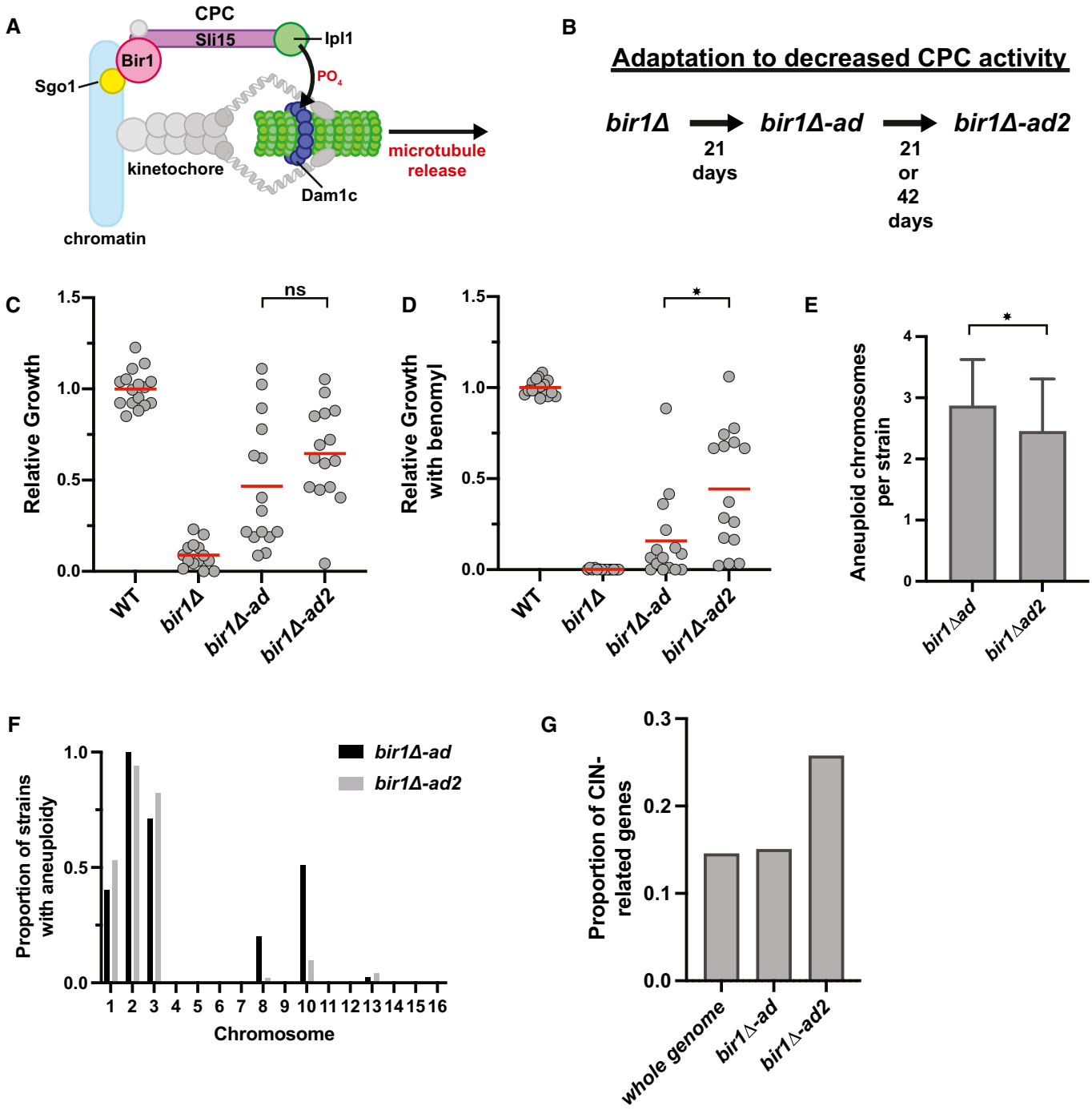

Figure 1.

(Makrantoni & Stark, 2009). Many of the *bir1Δ-ad2* strains have strongly decreased benomyl sensitivity in comparison with the *bir1Δ-ad strains*, suggesting that they have acquired additional changes that suppress the CIN phenotype (Fig 1D). To determine whether this additional adaptation occurs through further increased aneuploidy, we measured chromosome copy numbers via read counts from whole-genome sequencing. Two strains that were observed to have large segmental amplifications of chromosomes 2 and 13 were excluded from this analysis. Overall, the *bir1Δ-ad2* strains have decreased numbers of aneuploid chromosomes, suggesting that these strains do not adapt through further increases in aneuploid chromosomes that attenuate CIN (Fig 1E and F). We conclude that the additional adaptation to CIN in the further adapted CPC-deficient strains likely comes from specific mutations rather than chromosome copy number alterations.

Adaptation to CIN and aneuploidy could potentially come from mutations that either decrease CIN or increase aneuploidy tolerance. To determine whether mutations in the adapted strains fall into

these categories, we searched for nonsynonymous mutations that arose during liquid culture adaptation in the whole-genome sequencing data. We identified 97 such mutations in 68 strains. These mutations were enriched in genes related to CIN (Fig 1G). Mutations that increase aneuploidy tolerance were previously reported in budding yeast (Torres *et al*, 2010). However, there was no overlap between the 22 genes identified in the aneuploidy tolerance screen and the genes mutated in the *bir1Δ-ad2* strains. We therefore used the most heavily characterized gene whose loss leads to aneuploidy tolerance, the ubiquitin-specific protease *UBP6* (Torres *et al*, 2010). We tested whether a mutation in *UBP6* that was previously reported to increase aneuploidy tolerance would increase resistance to *bir1Δ*. The mutation was introduced into a haploid strain whose only copy of *BIR1* is on a minichromosome that also contains the *URA3* gene. This minichromosome can be selected against using 5-Fluoroorotic acid (5-FOA), which is converted into a toxin by the *URA3* gene product. The addition of the *ubp6(E256X)* mutation did not increase viability after *BIR1* was deleted (Fig EV1A). This result suggests that aneuploidy tolerance does not lead to CIN tolerance following *BIR1* deletion. We note that we used the same strain background as the studies that identified and characterized the role of *UBP6* in tolerating aneuploidy (W303), which has been shown to have a mutation in the *SSD1* gene that makes them more sensitive to aneuploidy (Hose *et al*, 2020). We conclude that cells with high levels of CIN and aneuploidy adapt primarily through mutations that mitigate CIN rather than aneuploidy.

bir1Δ suppressor mutations fall into four major categories

To determine which categories of mutations are most prevalent in our adapted strains, we searched for the enrichment of functional gene ontology (GO) terms. We found significant enrichment of genes related to "chromosome segregation" (FDR = 3.53×10^{-5}) and "SCF-dependent proteasomal ubiquitin-dependent protein catabolic process" (FDR = 1.3×10^{-1}, Table EV2). Further refinement of these categories revealed that the mutations fall largely into four categories (Table 1).

The first category is in proteins that form the outer kinetochore, including mutations in the Dam1 complex, the Ndc80 complex, and Spc105/KNL1. All three of these proteins/protein complexes directly bind to microtubules. The Dam1 complex was the most heavily represented in the data set with mutations in five of the 10 subunits.

Table 1. Candidate mutations identified in *bir1Δ-ad2*.

Gene mutated	Residue changes	Tested	Chromosome	Days of liquid adaptation	Essential	Basic function
DUO1	P17L	Yes	7	21	Yes	Kinetochore–microtubule attachment
DAD1	N43S	Yes	4	21	Yes	
DAD2	K11Q	Yes	11	21	Yes	
ASK1	S216F	Yes	11	21	Yes	
SPC34	D119A	Yes	11	21	Yes	
NDC80	K181N	Yes	9	42	Yes	
SPC105	R583G[a]	Yes	7	21	Yes	
SLI15	L71S	Yes	2[b]	21	Yes	CPC subunit
SLI15	P109A	No	2[b]	21	Yes	
SLI15	G334S	Yes	2[b]	21	Yes	
CDC53	K448E	No	4	21	Yes	S-phase entry
CDC53	A486P	No	4	21	Yes	
CDC34	M64T[a]	Yes	4	21	Yes	
CDC4	S438G	Yes	6	21	Yes	
CDC4	G439S	Yes	6	21	Yes	
CDC4	G652D	No	6	21	Yes	
MPS1	R596H	Yes	4	21	Yes	Initiation of SAC
MPS1	W629S	No	4	21	Yes	
MPS1	V631M	Yes	4	21	Yes	
MIF2	D241N	Yes	11	42	Yes	Inner kinetochore
RTG2	G154S	Yes	7	21	Yes	Mitochondrial sensor
RTG2	H425L	No	7	21	Yes	
RTG2	A433P	No	7	21	Yes	
SPC97	S816X	Yes	8[b]	21	Yes	Spindle pole body

[a]Identified in the same strain.
[b]Chromosomes that are commonly aneuploid in bir1Δ strains.

Mutations in the Dam1 complex subunit Dam1 that mimic Ipl1 phosphorylation were previously shown to suppress CPC mutations (Cheeseman *et al*, 2002). However, none of the mutations identified in the *bir1Δ-ad2* strains were in the Dam1 protein itself, indicating that they do not directly mimic similar phosphorylation events (Fig 2A). The mutation of lysine 181 in the Ndc80 complex resides in the microtubule binding CHD domain and is similar to the lysine 146 mutation in human Ndc80 that was previously shown to reduce microtubule binding (Ciferri *et al*, 2008).

The second category of mutations are in the CPC subunit Sli15. Mutations in Sli15 that disrupt binding to Bir1 or prevent Cdc28 (cyclin-dependent kinase) phosphorylation were both previously shown to suppress *BIR1* deletion (Campbell & Desai, 2013). All three of the observed mutations are consistent with these previous observations, as two were in the CEN box that interacts with Bir1 (L71S and P109H) and one was directly adjacent to the main Cdc28 phosphorylation site (G334S).

The third category of common mutations in the adapted strains is in subunits of the SCF ubiquitin-protein ligase complex. The SCF is primarily involved in the initiation of S-phase, but it also has roles in mitosis (Goh & Surana, 1999). We identified mutations in the core SCF subunits Cdc53 and Cdc34 as well as the F-box adaptor protein Cdc4. F-box proteins dictate the substrate specificity of the SCF complex (Jonkers & Rep, 2009). Important substrates of SCF^{Cdc4} include the cell cycle kinase inhibitors Sic1 and Far1. No mutations in any other F-box proteins were identified, suggesting that the ability to suppress *BIR1* deletion may be specific to SCF^{Cdc4}. All three Cdc4 mutations were in the WD-40 domain, which directly interacts with SCF complex substrates (Fig 2A). No direct connection between the SCF complex and the CPC has been previously identified.

The final category of potential suppressor mutations was in the mitotic kinase Mps1. All three of the mutations in Mps1 were in the kinase domain (Fig 2A). Mps1 has functions in spindle assembly checkpoint signaling, correction of misattached chromosomes, and spindle pole body duplication (reviewed in Liu & Winey, 2012). We were surprised to identify mutations in Mps1 as the kinase would be expected to promote rather than antagonize CPC activity, and mutations in Mps1 that suppress CPC deficiency have not previously been identified.

Intriguingly, all of the mutations in Table 1 are in essential genes, so they are most likely to be hypomorphic alleles. To determine whether the identified mutations are sufficient to rescue *bir1Δ*, we introduced mutations from each category prior to *BIR1* deletion. In addition, we included mutations identified in the adapted strains in three other potentially interesting proteins: the inner kinetochore protein Mif2, the spindle pole body protein Spc97, and the mitochondrial signaling protein Rtg2. Rtg2 was selected because we identified three independent mutations in this protein. After selection of *bir1Δ* on 5-FOA plates, all of the tested mutations at least partially rescued growth with the exception of *mif2*, *rtg2*, and *ask1* (Fig 2B). We identified multiple mutations that suppress the *BIR1* deletion growth phenotype for each of the four major categories. To determine whether the mutants were able to rescue the chromosome missegregation phenotype of *BIR1* deletion, we measured the fidelity of minichromosome transmission with representative suppressor mutations from the outer kinetochore, SCF complex, and Mps1 categories. We did not perform any further experiments with the Sli15 mutations, as we previously characterized similar mutations (Campbell & Desai, 2013). For the SCF complex, we analyzed mutations that we identified in Cdc4, as mutations in the F-box subunit are less likely to have pleiotropic effects. Minichromosome transmission fidelity was higher than the *bir1Δ* control for mutations in all three categories, although the degree of rescue for the Mps1 mutation was not significant ($P = 0.1$, Fig 2C). We have therefore identified four categories of mutations—in the outer kinetochore, the CPC, the SCF, and Mps1—that are frequently mutated to suppress the chromosome missegregation phenotype of yeast with impaired CPC activity.

We next wanted to test whether the suppressor mutations could affect aneuploidy tolerance in addition to CIN tolerance. Suppressor mutations in the Dam1 complex, SCF complex, and Mps1 did not suppress the growth defects caused by an extra copy of either chromosome 8 or 10 (Fig EV1B). In addition, a combination of these mutations with *ubp6(E256X)* did not show any synergistic effects (Fig EV1A). To determine whether the remaining growth impairment in the further adapted strains was primarily due to aneuploidy or CIN, we added wild-type *BIR1* to a subset of the *bir1Δ-ad* and *bir1Δ-ad2* strains and tested their growth. Even in the further adapted strains, re-addition of BIR1 greatly improved their fitness (Fig EV1C). We conclude that even though the suppressor mutations act exclusively by suppressing the CIN phenotype, the residual CIN is still the primary contributor to the growth defects in the further adapted strains.

We next wanted to determine the degree to which the identified mutations contribute to adaptation. We compared the growth of

Figure 2. Four main categories of mutations rescue *BIR1* deletion.

A Schematics showing the location of mutations from Table 1 (red lines). Domains of interest were identified using the Saccharomyces Genome Database.

B Serial dilutions of strains engineered with the indicated mutations identified in *bir1Δ-ad2* strains were tested for rescue of *BIR1* deletion. Ten-fold serial dilutions on the indicated media are shown. The mutations colored in blue, green, or red were selected for additional characterization.

C Top: schematic summarizing how loss of the *URA3*-containing plasmid is used to measure relative missegregation rates. Bottom: Proportion of colonies that grow on plates with restrictive (lacking uracil) versus permissive (YPAD) media. Many of the suppressor mutants significantly increase the segregation fidelity of the minichromosome in a *bir1Δ* background. *ctf19Δ* serves as a positive-control for decreased minichromosome transmission fidelity. Statistical significance is relative to *bir1Δ* alone for three independent experiments. Means and standard deviations are shown.

D, E Growth comparisons of *bir1Δ-ad2* strains that contain (18 strains) or do not contain (28 strains) confirmed suppressor mutations as measured by area of colony growth after serial dilution. The mean (red line) is shown. 10-fold serial dilutions were made on YPAD plates containing either 0.1% DMSO (D) or 10 μg/ml of benomyl (E).

F Comparison of the mean number of aneuploid chromosomes per strain for *bir1Δ-ad2* with and without identified suppressor mutations.

Data information: (ns) not significant; (*) $P < 0.05$; (**) $P < 0.01$; (***) $P < 0.001$; (****) $P < 0.0001$; unpaired *t*-test.

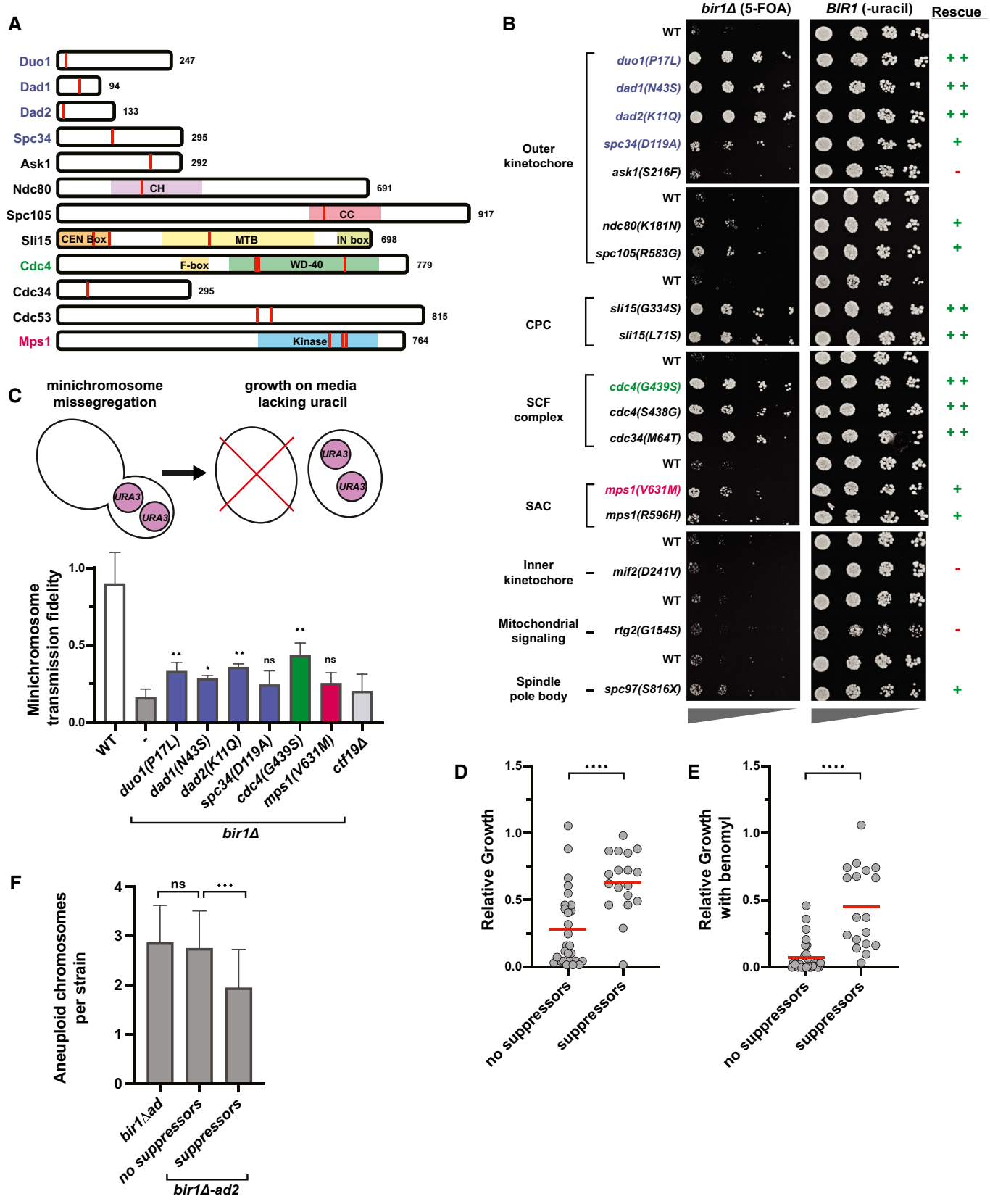

Figure 2.

bir1Δ-ad2 strains that either do or do not contain identified suppressor mutations. All mutations listed in Table 1 were considered suppressors for this analysis, with the exception of genes with mutations that did not rescue the *BIR1* deletion growth phenotype (*MIF2*, *RTG2*, and *ASK1*). On average, adapted strains that contain identified suppressor mutations grew substantially better than those without suppressors, suggesting that we identified most of the impactful mutations and that they contributed greatly to the adaptation (Fig 2D and E). This difference was significant either with or without the addition of benomyl. Other genetic or epigenetic changes that alter protein abundance could also contribute to adaptation under these conditions; however, the strong correlation between the identified suppressor mutations and the growth phenotype indicates that these alterations would have a relatively small contribution. Furthermore, the degree of aneuploidy is significantly reduced in the strains with suppressor mutations, indicating that these mutations decreased the need for aneuploid chromosomes to suppress the *bir1Δ* phenotype (Fig 2F). This decrease was seen across all of the observed aneuploid chromosomes (Fig EV1D). The aneuploidy burden in the further adapted strains was therefore reduced by decreasing the requirement for aneuploidy rather than decreasing the impact of aneuploidy on cellular fitness. These results provide a time line of events for adaptation to high rates of CIN. First, the cells acquire specific aneuploidies that suppress the CIN phenotype. The cells then acquire optimal combinations of aneuploidies (Ravichandran *et al*, 2018). Next, point mutations arise that more specifically target the source of the CIN leading to a reduction in CIN. Finally, the level of aneuploidy decreases to relieve the fitness burden placed on the cell.

Suppressor mutations in the Dam1 complex create unattached kinetochores

We next sought to determine where in the chromosome biorientation pathway each of these categories of mutations falls. Defects in CPC activity lead to the overstabilization of kinetochore–microtubule attachments and the failure to correct attachments where both sister chromatids attach to microtubules emanating from the same pole (syntelic attachments; Biggins *et al*, 2001; Pinsky *et al*, 2006). Mutations that rescue CPC defects are therefore likely to restore the higher turnover of kinetochore–microtubule attachments. This could occur either by increasing the activity of the CPC or by decreasing the microtubule binding activity of kinetochores. To determine whether the mutations act downstream of the CPC, we tested whether they could rescue a temperature-sensitive mutation in the CPC kinase Ipl1/Aurora B. Of the mutations tested, only the Dam1c mutants significantly rescued *ipl1-321* at the restrictive temperature (Fig 3A). Although the Dam1c suppressor mutations rescue the temperature-sensitive *IPL1* mutation, they could not rescue a full deletion of *SLI15*, suggesting that they do not completely bypass the need for CPC activity (Fig EV2A). These results indicate that the Dam1c mutations affect the pathway downstream of the CPC, whereas the SCF complex and Mps1 potentially affect the CPC itself.

If the mutations rescue by globally destabilizing kinetochore–microtubule attachments, then the number of unattached kinetochores should increase even in the presence of Bir1. Since unattached kinetochores trigger the spindle assembly checkpoint, we first determined whether the mutations induce a delay in mitosis. None of the identified mutations showed substantial changes in cell cycle duration, as measured by the sustained accumulation of large budded cells over time after release from synchronization in G1 (Fig EV2B). These mutations therefore do not maintain sustained checkpoint activity. As a more sensitive assay, we monitored the presence of unattached kinetochores by measuring the frequency of cells with foci of the checkpoint protein Bub3 that colocalize with kinetochore clusters. For this assay, we only counted cells that have two kinetochore clusters that are separated yet still in close proximity, indicative of a stage around the prometaphase to metaphase transition. At this stage, three of the four Dam1c mutations resulted in significantly more cells with Bub3-mNeonGreen foci than the wild-type control (Fig 3B). By contrast, suppressor mutations in Cdc4 and Mps1 did not increase the frequency of Bub3 foci. We conclude that suppressor mutations in the Dam1 complex transiently increase the number of unattached kinetochores, likely through increased kinetochore–microtubule attachment turnover.

The suppression of the *bir1Δ* chromosome missegregation phenotype through an increase in unattached kinetochores in Dam1 complex mutants suggests that there is a restoration of the balance between microtubule attachment and detachment when both mutations are combined. If this were the mechanism of rescue, then we would expect that in the absence of *BIR1* deletion, the increase in kinetochore–microtubule attachment turnover in the Dam1 mutants would overly destabilize attachments and increase the chromosome missegregation rate. To test this, we measured the rate of minichromosome transmission in strains that have suppressor mutations and wild-type *BIR1*. Similar to the results of the Bub3 foci counts, three of the four Dam1c mutants showed a significant decrease in minichromosome transmission fidelity (Fig 3C). The Cdc4 and Mps1 mutations had no measurable effect. The Dam1c mutation that did not show a significant result in either the unattached kinetochore or chromosome segregation assays, *spc34*(G439S), also had the weakest rescue of growth following *BIR1* deletion (Fig 2B). Overall, these results demonstrate that mutations in outer kinetochore proteins rescue deficient CPC activity by destabilizing kinetochore–microtubule attachments. By contrast, Cdc4 and Mps1 suppressor mutations act through an alternative mechanism that does not directly affect the stability of kinetochore–microtubule attachments.

Dam1c suppressor mutations have similar phenotypes to a phosphomimic mutation that decreases Dam1c microtubule binding

Phosphomimics of Ipl1 phosphorylation sites on the Dam1 subunit of the Dam1 complex were previously shown to partially rescue *ipl1-ts* mutants (Cheeseman *et al*, 2002). These phosphosites include serine 20 (*dam1(S20D)*) near the N-terminus and three serines (S257, S265, S292, *dam1(3D)*) closer to the C-terminus of the protein (Fig 4A). The two phosphomimic mutants change the serines to negatively charged aspartic acid residues. The S20D mutation has been demonstrated to reduce microtubule binding *in vitro*, whereas the 3D mutant results in activation of the mitotic checkpoint (Jin & Wang, 2013; Sarangapani *et al*, 2013). To determine whether the identified suppressor mutations function similarly to the phosphomimics, we first determined whether the *dam1*

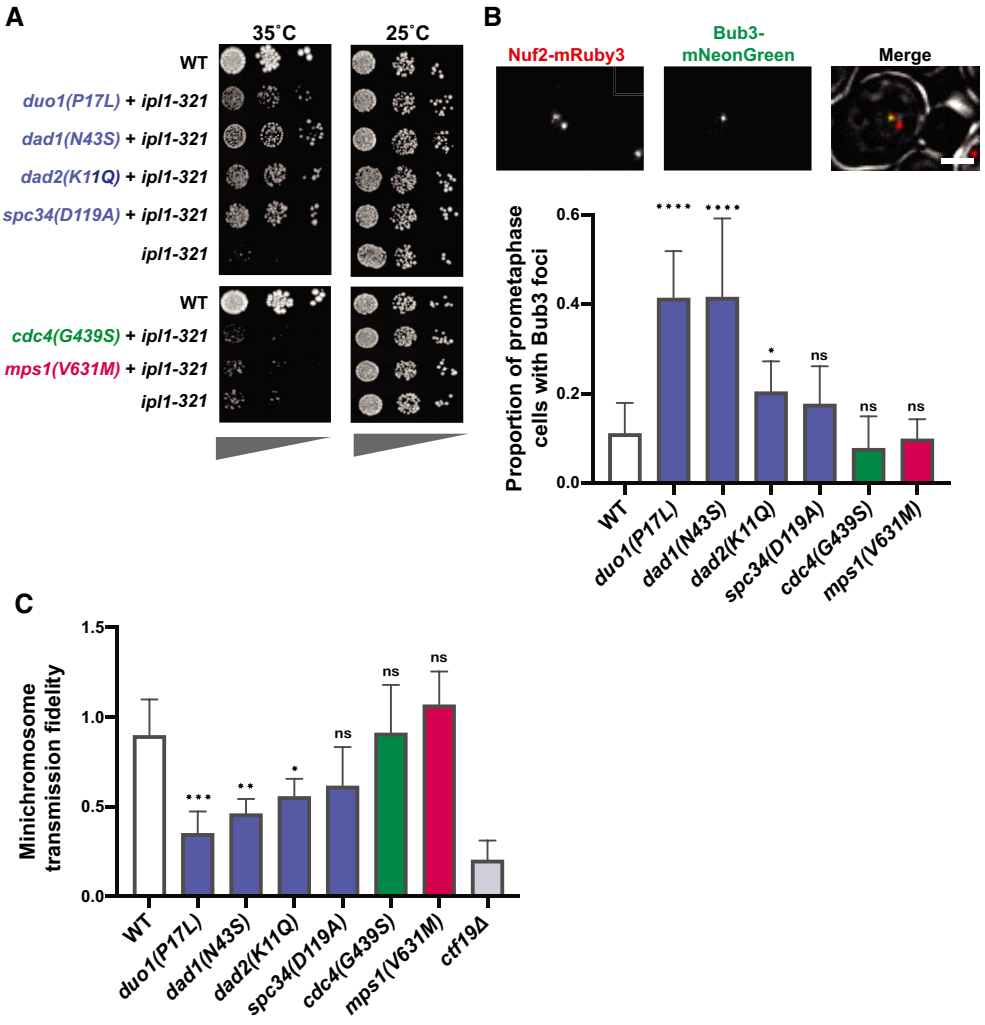

Figure 3. Suppressor mutations in the Dam1 complex result in elevated spindle assembly checkpoint activity and minichromosome missegregation.

A Serial dilutions on YPAD media at the permissive (25°C) or restrictive (35°C) temperatures for the *ipl1-321* mutation. The suppressor mutations from the Dam1c (blue) were the only mutants that rescued viability at the restrictive temperature.

B Top: representative images showing Bub3-mNeonGreen localization to kinetochores (Nuf2-mRuby3), indicating spindle assembly checkpoint activation in wild-type yeast. Scale bar is 2 μm. Bottom: quantification of the proportion of prometaphase cells with Bub3-mNeonGreen foci. Only the mutations in Dam1 complex (blue) show a significant increase in SAC activity. Data are from at least five independent experiments. Means and standard deviations are shown.

C Proportion of colonies that grow on plates with restrictive (lacking uracil) versus permissive (YPAD) media after 24 h growth under permissive conditions with a *URA3*-containing plasmid. The suppressor mutations in the Dam1c (blue) show a significant reduction of minichromosome segregation fidelity. Data are from three independent experiments. Means and standard deviations are shown.

Data information: (ns) nonsignifcant; (*) $P < 0.05$; (**) $P < 0.01$; (***) $P < 0.001$; (****) $P < 0.0001$; unpaired *t*-test.

(S20D) or *dam1(3D)* mutations rescue *BIR1* deletion. Intriguingly, *dam1(S20D)* rescues *BIR1* deletion but *dam1(3D)* does not, indicating that these mutants are mechanistically distinct (Fig 4B). Both mutations increase the frequency of Bub3 foci in prometaphase cells, similarly to the Dam1c suppressor mutations that we identified (Fig 4C). However, the *3D* mutant shows a strong cell cycle delay, further indicating that it differs from the other Dam1c mutants in either mechanism or severity (Fig 4D). Despite the delay, the *3D* mutant does not affect minichromosome transmission fidelity (Fig 4E). This mitotic delay without any decrease in chromosome segregation fidelity has been previously reported for the *dam1(3D)* mutation and may indicate a defect in SAC silencing after chromosome biorientation (Jin & Wang, 2013). The *dam1 (S20D)* mutation, however, does show a decrease in minichromosome transmission in line with the suppressor mutations (Fig 4E). We conclude that the mutations in the Dam1 complex that adapt to suppress *BIR1* deletion have a similar phenotype to the *dam1 (S20D)* mutation. Intriguingly, the *S20D* phosphomimic mutation was shown to disrupt microtubule binding of kinetochores *in vitro*, whereas the triple serine phosphomimic (*3D*) mutant maintained wild-type microtubule binding activity (Sarangapani *et al*, 2013). The similarity in phenotype between the suppressor mutations and *dam1(S20D)* suggests that the suppressor mutations may also directly decrease kinetochore–microtubule affinity.

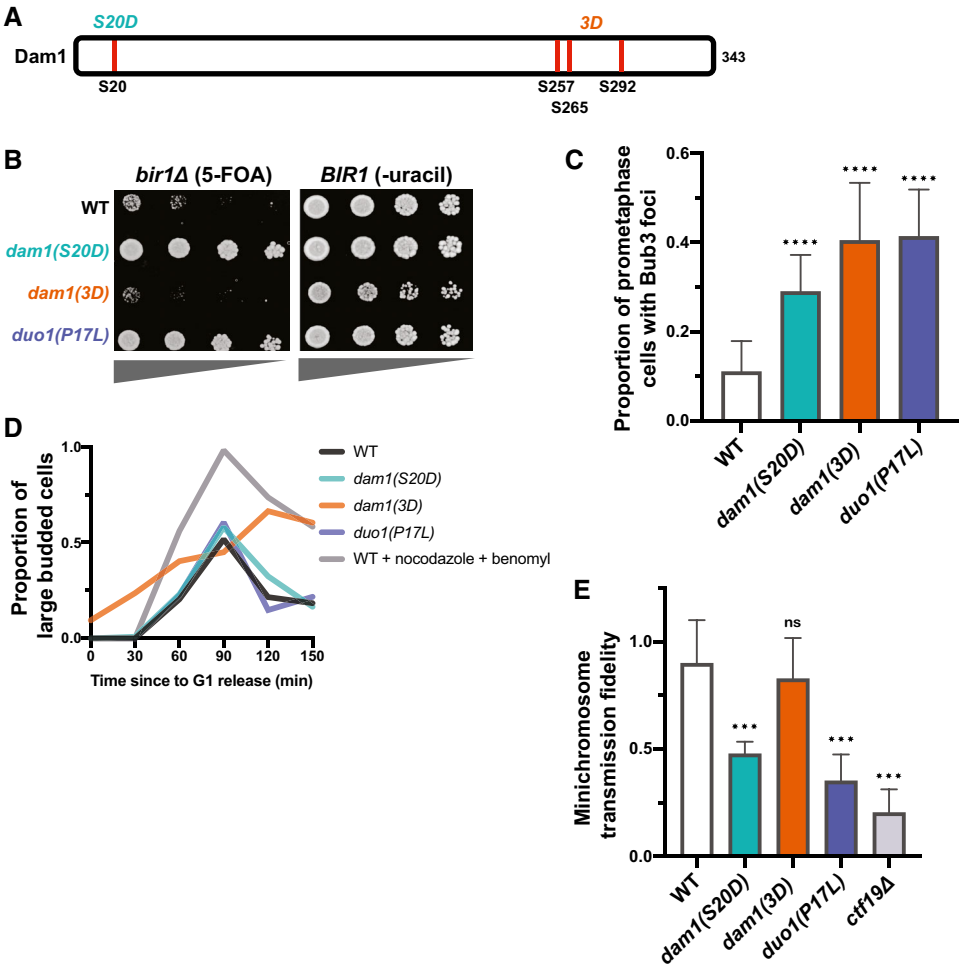

Figure 4. Suppressor mutations in the Dam1 complex have phenotypes similar to the *dam1(S20D)* phosphomimic mutation.

A A schematic showing the relative locations of the Ipl1 phosphosites in Dam1 that are mutated to aspartic acid in the phosphomimics.

B Serial dilutions of strains engineered with the indicated mutations were tested for rescue of *BIR1* deletion. Ten-fold serial dilutions on the indicated media are shown. *dam1(S20D)* rescues loss of CPC activity to a similar extent as a suppressor mutant in Duo1.

C Quantification of the proportion of prometaphase cells with Bub3-mNeonGreen foci localized to kinetochores (Nuf2-mRuby3), indicating SAC activation in all three mutant strains. Data are from at least five independent experiments. Means and standard deviations are shown.

D Degree of cell cycle delay as measured by percentage of large budded cells over time after release from G1 arrest. Wild-type (WT) cells treated with nocodazole and benomyl were used as a positive control for mitotic arrest.

E Proportion of colonies that grow on plates with restrictive (lacking uracil) versus permissive (YPAD) media after 24 h growth under permissive conditions with a *URA3*-containing plasmid. Minichromosome segregation fidelity is reduced in the *dam1(S20D)* strain, similar to the *duo1(P17L)* strain. Data are from three independent experiments. Means and standard deviations are shown.

Data information: (ns) nonsignifcant; (***) $P < 0.001$; (****) $P < 0.0001$; unpaired *t*-test.

If both the Dam1c suppressor mutations and *dam1(S20D)* act through destabilizing kinetochore–microtubule attachments, we hypothesized that combining the two mutants might destabilize the connections to a greater extent. Indeed, combination of either *duo1(P17L)* or *dad2(K11Q)* with *dam1(S20D)* resulted in zero viable spores after 3 days of growth (Fig EV2C). For the *duo1(P17L), dam1(S20D)* double mutant, rare colonies grew up after 5 days. These double-mutant cells displayed severe minichromosome loss and a strong metaphase delay, as expected for high rates of unattached kinetochores (Fig EV2D and E). Intriguingly, the double mutant was able to rescue loss of *IPL1* activity to an extent even greater than the single mutants (Fig EV2F). However, the reverse interaction was not observed, as the *ipl1-321* mutation did not improve the growth of the *duo1(P17L), dam1(S20D)* double mutant at the restrictive or permissive temperature. This could potentially be due to Ipl1 mutations preferentially stabilizing specific kinetochore–microtubule attachment states, whereas mutations in the kinetochore would destabilize all attachments indiscriminately. We conclude that the suppressor mutations in the Dam1 complex and the *dam1(S20D)* mutant both act by destabilizing kinetochore–microtubule attachments. The combination of the mutants increases the severity of the phenotype to create an extended spindle assembly checkpoint arrest and cell death.

Dam1c suppressor mutations lie proximal to multimerization interfaces and decrease spindle localization *in vivo*

To determine a potential mechanism of action for the Dam1c suppressor mutations, we mapped them onto the existing crystal structure of the *Chaetomium thermophilum* version of the complex (Jenni & Harrison, 2018). Three of the mutations are in helices that lie near interfaces of oligomerization between Dam1c decamers. *spc34(D119A)* is found in a region that corresponds to a short helix that forms part of interface 1. The *dad1(N43S)* mutation affects a highly conserved residue that lies on the surface of interface 2 (Fig 5A). The *dad2(K11Q)* mutation affects a highly conserved lysine that is also proximal to interface 2 but is not directly on the surface. The *duo1(P17L)* mutation lies in a region outside of the crystal structure. However, the affected residue would likely be near the N-terminal part of Duo1, which resides in interface 1. These interfaces are proposed to be important for the ring formation that allows the complex to encircle microtubules. It has been noted that serine 20 of the Dam1 protein is potentially also located in the vicinity of interface 1 (Jenni & Harrison, 2018). These results suggest that the suppressor mutants could act by limiting higher order oligomerization of the Dam1 complex.

The oligomerization of the Dam1 complex into rings is primarily associated with microtubule binding (Miranda *et al*, 2005; Westermann *et al*, 2005). We therefore determined whether the Dam1c mutants affect the localization of the complex to microtubules and kinetochores. We measured the amount of the Dam1 complex member Dad3 labeled with the fluorophore mNeonGreen at prometaphase and anaphase spindles in the presence of the suppressor mutants. The intensity of Dad3-mNeonGreen was significantly reduced at both prometaphase kinetochores/spindles and anaphase spindles for the three Dam1c suppressor mutations with the strongest rescue phenotypes (Fig 5B and C). The *dam1(S20D)* mutation also has a significant decrease in Dad3 localization in prometaphase. No significant decreases in Dad3 spindle localization were observed for *cdc4(G439S)* or *mps1(V631M)*. Interestingly, the decrease in localization for the Dam1c mutants was much more pronounced along the anaphase spindle than at anaphase kinetochores (Fig 5D). The maintenance of strong localization at kinetochores suggests that the localization phenotypes could result from defects in microtubule binding rather than kinetochore association. We conclude that the Dam1c suppressor mutations decrease the amount of Dam1 complex at microtubules and this potentially occurs by decreasing the ability of the complex to oligomerize.

Mps1 suppressor mutations do not act through previously established pathways

We next wanted to determine how the Mps1 mutations rescue *BIR1* deletion. Mps1 kinase functions in activating the spindle assembly checkpoint at unattached kinetochores and recruiting the CPC to the inner centromere for chromosome biorientation (Weiss & Winey, 1996; van der Waal *et al*, 2012). In yeast, it also has an essential function in spindle pole body duplication (Winey *et al*, 1991). Disruption of any of these functions would be expected to decrease, rather than increase, the ability of cells to function with reduced CPC activity. One possible explanation for this would be if the Mps1 suppressor mutations have a gain-of-function phenotype that increases the kinase's activity. We therefore tested whether the Mps1, Cdc4, and Dam1c suppressors have gain-of-function activity by determining whether they have a dominant phenotype in the heterozygous state. Only the Dam1c mutation *duo1(P17L)* had any improved growth when heterozygous, indicating that neither the Cdc4 nor the Mps1 mutations are gain of function (Fig EV3A). To determine whether the suppressor mutations affect the ability of Mps1 to activate the spindle assembly checkpoint, we measured the percentage of cells with Bub3-mNeonGreen foci either with or without the addition of nocodazole to depolymerize microtubules and create unattached kinetochores. The levels of Bub3 foci were unaffected by the *mps1(V631M)* mutation in either the presence or the absence of nocodazole, demonstrating that the mutant cells are capable of activating the spindle assembly checkpoint (Fig EV3B).

Since the Mps1 suppressor alleles have a recessive, partial loss-of-function phenotype and the mutations are located in the kinase domain, we next tested whether a partial loss of Mps1 kinase activity can rescue *BIR1* deletion. We used a mutation in the kinase domain that renders it sensitive to ATP analogs (Jones *et al*, 2005). This mutation, *mps1-as1*, decreased the doubling time of *bir1Δ* cells

Figure 5. Suppressor mutations in the Dam1 complex reduce spindle localization.

A View of the *Chaetomium thermophilum* Dam1c-ring, with focus on two adjacent protomers (labeled decamers 1 and 2). Interfaces 1 and 2 between adjacent decamers are shown with the blue dashed boxes as previously identified by Jenni & Harrison (2018). Mutations in the *Saccharomyces cerevisiae* proteins have been labeled based on sequence homology with *C. thermophilum*. Mutations within the structure are depicted as solid circles. Those that are located outside of the structured domains are shown as open-circles. Suppressor mutations identified in this study are colored magenta, and the residues mutated in the Dam1 phosphomimics are colored green. The marked residues are the closest approximations of the residues mutated in *S. cerevisiae*. N43 of Dad1 is conserved in *C. thermophilum*. The Dad2 residue K11 in *S. cerevisiae* is homologous to K35 in *C. thermophilum*. D119 of Spc34 maps to a short helix that contains H117 in *C. thermophilum*. The bottom right shows the location of the Dad1 residue N43 on the surface of interface 2. Images were made using ChimeraX (Pettersen *et al*, 2021).

B Left: representative images showing the localization of Dad3-mNeonGreen (Dam1c member) and Nuf2-mRuby3 (kinetochore marker) in prometaphase cells. Scale bar is 2 μm. Right: quantification of the intensity of Dad3-mNeonGreen at kinetochores/spindles in prometaphase cells. Each individual point on the graph represents a single measurement of Dad3-mNeonGreen intensity; up to 10 measurements per replicate. Data are from five independent experiments.

C Left: representative images showing the localization of Dad3-mNeonGreen (Dam1c member) and Nuf2-mRuby3 (kinetochore marker) in anaphase cells. Scale bar is 2 μm. Right: quantification of the intensity of Dad3-mNeonGreen at the spindle in anaphase cells. The intensity was measured in the middle of the spindle using a perpendicular line-scan. Each individual point on the graph represents a single measurement of Dad3-mNeonGreen intensity; up to 10 measurements per replicate. Data are from five independent experiments.

D Quantification of the intensity of Dad3-mNeonGreen at kinetochores in anaphase cells. Kinetochore position was based on Nuf2-mRuby3 localization. The differences in localization at the anaphase kinetochores are much weaker than those measured along the spindle (Fig 5C). Each individual point on the graph represents a single measurement of Dad3-mNeonGreen intensity; up to 10 measurements per replicate. Data are from five independent experiments. The mean (red line) is shown.

Data information: (ns) nonsignifcant; (*) $P < 0.05$; (**) $P < 0.01$; (***) $P < 0.001$; (****) $P < 0.0001$; unpaired *t*-test.

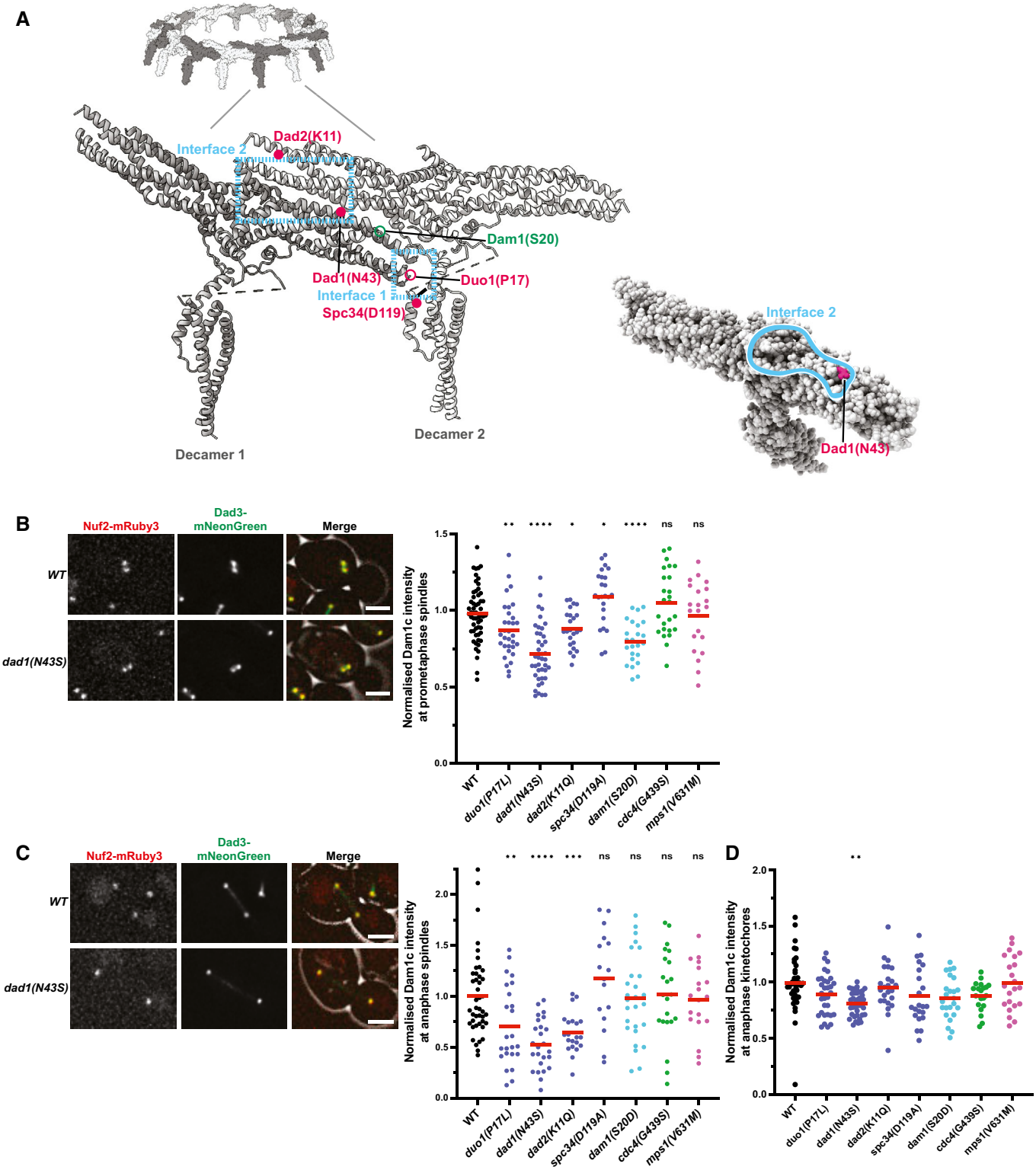

Figure 5.

to a similar extent to the suppressor mutation *mps1(V161M)* even in the absence of the small molecule inhibitor (Fig EV3C). This result suggests that the analog-sensitive mutation partially decreases kinase activity on its own, as was previously observed for similar alleles in other kinases (Bishop *et al*, 2000; Pinsky *et al*, 2006) and, furthermore, that the Mps1 suppressor mutations affect its kinase activity to a comparable extent. The addition of higher concentrations of the analog inhibitor decreased growth in *mps1-as1,bir1Δ*

cells, demonstrating that too little Mps1 activity is detrimental to growth even in the absence of Bir1.

We next tested whether the Mps1 mutations are suppressing CPC activity though its phosphorylation of the Dam1 complex subunit Dam1. Mutations that prevent phosphorylation of Dam1 at S218 and S221 by Mps1 kinase decrease kinetochore–microtubule stability and partially rescue temperature-sensitive Ipl1 mutations (Shimogawa *et al*, 2006, 2010). However, we did not observe any rescue of *BIR1* deletion with these mutants (Fig EV3D). This result agrees with our experiments demonstrating that the Mps1 and Dam1c suppressor mutations act through different mechanisms (Fig 3A–C). We conclude that partial disruption of Mps1 kinase activity results in rescue of *BIR1* deletion through a currently unknown mechanism.

The SCF^{Cdc4} complex affects CPC localization to the spindle/kinetochores in prometaphase in yeast and human cells

Finally, we wanted to determine how the SCF mutations rescue *BIR1* deletion. We first tested whether a previously identified temperature-sensitive mutation in *CDC4*, *cdc4-1*, is capable of rescuing loss of Bir1. We also tested a temperature-sensitive version of another F-box protein, Met30. Both Cdc4 and Met30 affect the stability of the yeast CENP-A homolog Cse4 (Au *et al*, 2020). The *cdc4-1* mutation shows a degree of rescue nearly as strong as the suppressor mutation *cdc4 (G439S)* (Fig 6A). By contrast, a temperature-sensitive mutation in Met30 failed to show any rescue of *BIR1* deletion, demonstrating the specificity of the suppression phenotype for SCF^{Cdc4}. We conclude that rescue of *bir1Δ* results from decreased SCF^{Cdc4} activity and is not unique to the mutations identified in our screen.

To determine how Cdc4 activity affects CPC function, we first determined whether the ubiquitin ligase directly degrades the CPC subunits Sli15 or Ipl1. We monitored Sli15 and Ipl1 protein levels in cells that were prevented from expressing new protein by the addition of cycloheximide. Sli15 and Ipl1 protein levels were unchanged by the presence of the *cdc4(G439S)* suppressor mutation, indicating that this mutation does not rescue *BIR1* deletion by increasing the levels of Sli15 or Ipl1 (Fig EV4A). We next tested whether the Cdc4 suppressor mutations change the localization of the CPC. The *cdc4 (G439S)* mutation significantly increased CPC localization to prometaphase spindles/kinetochores by ~50% (Fig 6B). Sli15 expression levels were also unaffected by the mutation at this cell cycle stage, suggesting that the SCF specifically affects CPC localization (Fig EV4B). We wanted to determine whether this mutant also rescues CPC localization in *bir1Δ* cells. However, *bir1Δ* greatly reduces Sli15 expression (Campbell & Desai, 2013), so we instead determined whether *cdc4(G439S)* rescues localization after depletion of Sgo1, the upstream recruiter of Bir1 to the inner centromere (Fig 1A). When compared to wild-type *CDC4*, mNeonGreen-Sli15 localization in *cdc4 (G439s)* mutant cells was significantly increased in prometaphase after Sgo1 depletion, demonstrating that this increase in CPC localization is independent of the Sgo1 recruitment pathway that acts through Bir1 (Fig. 6B). Intriguingly, the effect of *cdc4(G439S)* on Sli15 localization is only observed prior to anaphase, as the localization differences are no longer observed later in mitosis (Fig EV4C). This suggests that the SCF complex specifically affects CPC localization during chromosome biorientation.

We next tested whether mutations in the human homolog of Cdc4, FBXW7, also affect the accumulation of the CPC at the inner centromere. We therefore engineered the sole copy of FBXW7 in the haploid HAP1 chronic myeloid leukemia cell line with the equivalent of the G439S point mutation in the WD-40 domain that we identified in adapted *bir1Δ* cells (Fig EV5A and B). Of note, mutations in this region of the protein are frequently observed in uterine and colon cancer (Yeh *et al*, 2018). This mutation (G437S in humans) resulted in a slight increase in colony size, consistent with the function of FBXW7 as a suppressor of cell cycle entry (Fig EV5C). Intriguingly, all three cell lines engineered with this mutation showed an increase in Aurora B staining at the inner centromere in prometaphase (Fig 6C). This ~50% increase is similar to what we observe in yeast, indicating that this function of the SCF complex in CPC localization is conserved. We conclude that $SCF^{Cdc4/FBXW7}$ activity limits the recruitment of the CPC to the spindle and/or kinetochores and that reduction of this function partially restores CPC localization when the inner centromere recruitment pathway is disrupted.

Discussion

In cancers, cells with high levels of CIN and aneuploidy often have overstabilized kinetochore–microtubule connections (Bakhoum *et al*, 2009a). Although the mechanisms that cause this phenotype are still largely unclear, one way to decrease microtubule turnover at the kinetochore is through decreased CPC activity (Cimini *et al*, 2006). In this study, we identify multiple mechanisms that cells use to adapt to the overstabilization of microtubules resulting from the deletion of the CPC subunit Bir1/Survivin. We determined that *bir1Δ* suppressor mutations act through two distinct mechanisms. The first mechanism involves mutations in proteins that directly attach the kinetochore to microtubules; such mutations were identified in five of 10 subunits of the Dam1 complex. The second

Figure 6. Cdc4 limits CPC localization in prometaphase independently of Sgo1.

A Serial dilutions of strains engineered with the indicated mutations were tested for rescue of *BIR1* deletion. Ten-fold serial dilutions on the indicated media are shown. The *met30-6* and *cdc4-1* alleles are temperature-sensitive. Two independent clones of each of these alleles are shown. The serial dilutions were performed at the permissive temperature (20°C).

B The amount of mNeonGreen-Sli15 (CPC member) located at kinetochores (Nuf2-mCherry) was measured in prometaphase. Sgo1 was depleted by placing it under a galactose-inducible promoter and switching to glucose-containing media (YPAD). Representative images are on the left. Scale bar is 2 μm. Averages from three independent experiments are shown.

C Measurements of Aurora B intensity at the inner centromere of prometaphase kinetochores. Inner centromeres were identified as the regions directly between two centromeres (ACA staining). Images from an example WT cell are shown to the right. Scale bar is 5 μm long. Each data point is an individual chromosome. More than 15 cells for each cell line were measured across two independent experiments. The mean (red line) is shown.

D Time line of adaptation to high levels of CIN through aneuploidy and point mutations.

Data information: (ns) nonsignifcant; (*) $P < 0.05$; (***) $P < 0.001$; (****) $P < 0.0001$; unpaired *t*-test.

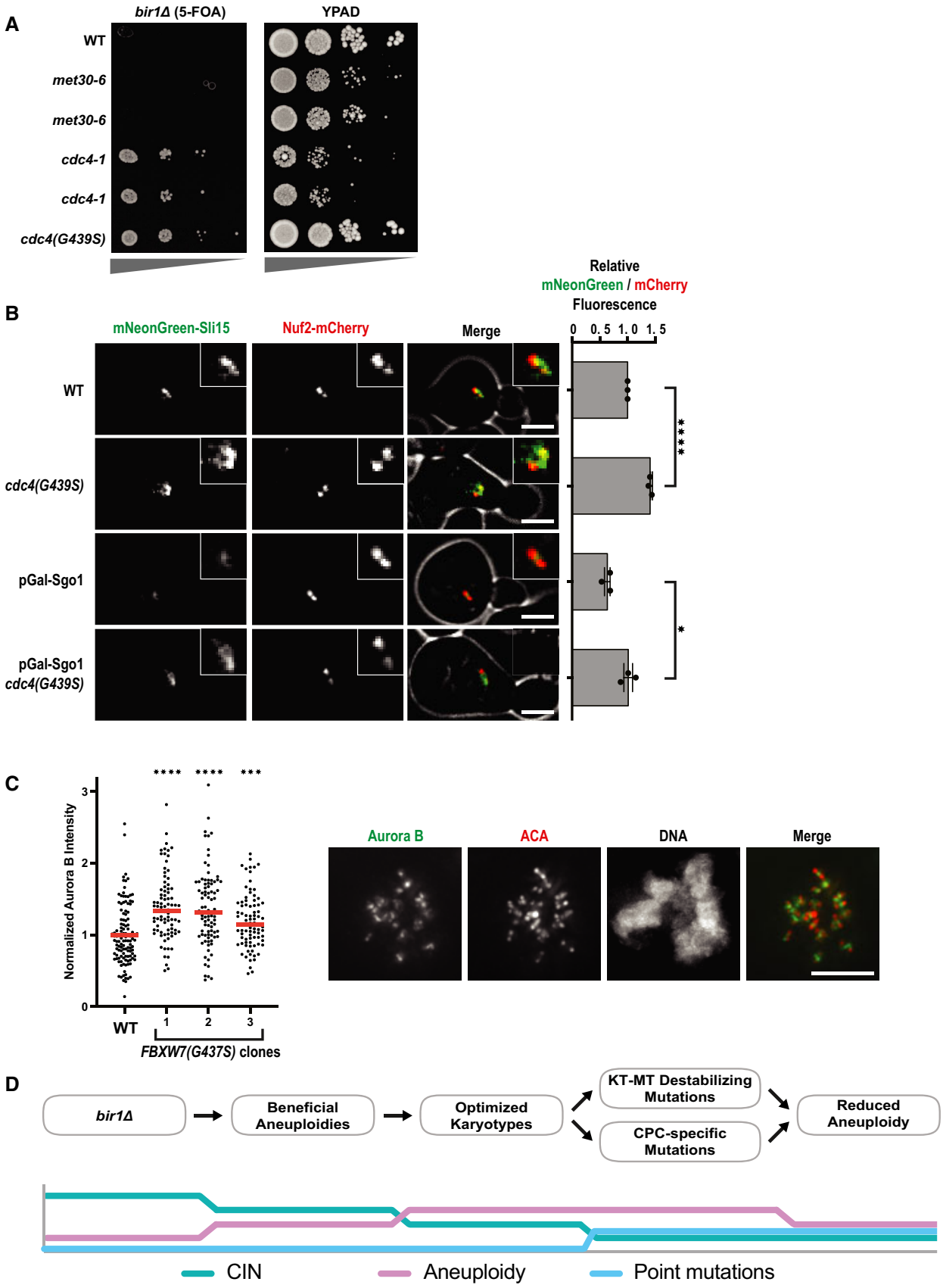

Figure 6.

mechanism results from mutations in genes that appear to affect the CPC more directly, which includes members of the SCF complex, the kinase Mps1, and the CPC member Sli15.

All of the suppressor mutations that we identified decrease the levels of CIN that result from *BIR1* deletion. Notably, we did not identify mutations whose function suggests that they allow for the greater tolerance of aneuploidy. Furthermore, a mutation in the gene *UBP6* that was previously demonstrated to reduce the negative effects of aneuploidy did not rescue *BIR1* deletion (Torres *et al*, 2010). However, mutation of *UBP6* was previously shown to improve the growth of only a subset of aneuploid chromosomes (5, 8, 9, and 11). Of these chromosomes, only aneuploidy of chromosome 8 is frequently observed in strains adapted to *bir1Δ*. Therefore, aneuploidy-tolerating mutations could potentially improve the growth of cells with other sources of CIN that adapt through different aneuploid chromosomes. In addition, the dynamics of CIN adaptation and the subsequent underlying mechanisms behind coping with CIN could vary in other strain backgrounds that may be more inherently tolerant of CIN.

In our adaptation experiments, we identified mutations in three different kinetochore complexes that directly bind to microtubules. The majority of these mutations were in the Dam1 complex. These mutations decrease the localization of the complex to microtubules and likely interfere with the complex's ability to oligomerize. The cellular phenotypes that we observe for these mutations are consistent with increased turnover of kinetochore microtubules. In vertebrates, kinetochore–microtubule turnover can be increased through the overactivation of the kinetochore-localized kinesins MCAK and Kif2b (Walczak *et al*, 1996; Kline-Smith & Walczak, 2002; Bakhoum *et al*, 2009b). Overexpression of either of these kinesins decreases the mitotic errors observed in some cancer cell lines (Bakhoum *et al*, 2009b). Furthermore, adaptation of human cells to a drug that activates MCAK resulted in cells with decreased Aurora B activity (Orr *et al*, 2016). Together, these results all point to the importance of a balance between Aurora B activity and other factors that affect the stability of connections between kinetochores and microtubules.

Mps1 is a highly conserved kinase that functions in sensing unattached kinetochores. Mps1 phosphorylates Spc105/Knl1 on MELT repeats, which recruits the spindle assembly checkpoint proteins Bub1 and Bub3/BubR1. CPC mutations have synthetic growth defects with spindle assembly checkpoint mutations, indicating that decreased SAC activity does not generally rescue CPC mutants (Ng *et al*, 2009). Bub1 binding to Spc105/Knl1 also contributes to the localization of the CPC to the inner centromere, which is one of the key locations for its function in chromosome biorientation. Bir1 is required for the CPC to bind to the inner centromere, so this targeting function of Mps1 should not affect cells with *BIR1* deletion (Makrantoni & Stark, 2009; Shimogawa *et al*, 2009). In budding yeast, Mps1 has an additional essential function in spindle pole body duplication. Interestingly, we would predict that decreased activity of any of these three functions would make the *bir1Δ* phenotype worse, not better. We conclude that the suppressor mutations partially decrease kinase activity and rescue via an unidentified mechanism. In a large-scale screen for synthetic interactions between temperature-sensitive mutations, it was found that some combinations of *MPS1* and *IPL1* alleles had positive genetic interactions, while others had negative interactions (Costanzo *et al*, 2016). These results support the idea that a balance between Mps1 activity and CPC activity is required for accurate chromosome segregation. Additional research will be required to determine which specific functions of Mps1 and which of its substrates are responsible for rescuing *BIR1* deletion.

The SCF ubiquitin ligase complex is a key regulator of many pathways related to cell cycle entry. It degrades factors that inhibit cyclins, allowing for the activation of cyclin-dependent kinases. The human homolog of the SCF F-box protein Cdc4 is FBXW7/hCDC4. FBXW7 is a tumor suppressor that is frequently mutated in many cancer types (Spruck *et al*, 2002). This function is largely attributed to the ability of FBXW7 to target important oncogenes for degradation, including MYC and Cyclin E (reviewed in Yeh *et al*, 2018). In addition to its roles in regulating cell cycle initiation, FBXW7/Cdc4 also has functions in mitosis. In yeast, certain Cdc4 mutants arrest in mitosis prior to anaphase (Goh & Surana, 1999). More recently, it was shown that Cdc4 contributes to the degradation of the inner kinetochore protein Ame1 (Böhm *et al*, 2021). In human cells, FBXW7 mutants are sensitive to inhibitors of the spindle assembly checkpoint, demonstrating a potential function in mitosis (Bailey *et al*, 2015). However, the mechanisms by which SCF^{Cdc4} regulates mitosis are still unclear. Our screen for *bir1Δ* suppressors has uncovered a connection between the SCF^{Cdc4} complex and regulation of the CPC. These suppressor mutations in the SCF complex increase the localization of the CPC to the spindle/chromosomes in the absence of inner centromere targeting, which suggests that the SCF^{Cdc4} complex may play a role in regulating alternative mechanisms of CPC localization in early mitosis. One possibility is that the SCF complex targets the degradation of a CPC recruitment factor.

Determining how cells adapt to CIN caused by the overstabilization of kinetochore-bound microtubules has important implications in cancer. Additionally, Aurora kinase inhibitors are actively being investigated in a variety of combination therapies in both preclinical and clinical trials (reviewed in Du *et al*, 2021). It is therefore important to know how cells adapt to the overstabilization of kinetochore attachments. Here, we have outlined a time line of events that cells use to adapt to decreased Aurora B activity (Fig 6D). First, cells obtain specific aneuploidies that partially decrease CIN. Next, the aneuploid karyotypes are refined to obtain an optimal complement of aneuploid chromosomes (Ravichandran *et al*, 2018). Following adaptation through aneuploidy, specific point mutations are acquired that further decrease the rate of CIN. These point mutations can affect the CPC itself or independently increase the turnover of kinetochore microtubules. Finally, point mutations that reduce CIN in a more targeted way allow for a decrease in the number of aneuploid chromosomes.

This time line of adaptation supports the theory that aneuploidy often provides a rapid but temporary form of adaptation, as has previously been observed in yeast adapted to heat stress or a tubulin mutation (Yona *et al*, 2012; Pavani *et al*, 2021). In both of those studies, a single chromosome was gained early in the adaptation process and sometimes lost again at later time points. Here, we observe the reversion toward the euploid state for many different chromosomes resulting from a wide variety of mutations. This return to the original copy number could help explain the high prevalence of whole chromosome loss of heterozygosity (LOH) in cancers. In colorectal cancers, for example, whole chromosome LOH is extremely common, even though the chromosomes are often present in multiple copies (Thiagalingam *et al*, 2001). This theory

could help explain why the bulk of LOH events do not contain known tumor suppressor genes, as the LOH itself was not the driver event, but simply a byproduct of temporary adaptation through aneuploidy (Ryland *et al*, 2015).

Materials and Methods

Yeast strains and media

All yeast strains and plasmids that were used in this study are listed in Table EV1. Strains were grown in yeast extract and peptone supplemented with 40 μg/ml adenine-HCl (YPA) and sugars (2% glucose: YPAD, 1% galactose and 1% raffinose: YPAGR). All strains used were made in the W303 background. Benomyl (Sigma-Aldrich, 381586), nocodazole (VWR, 487928), and 5-FOA (Chempur, 220141-70-8) were used at concentrations of 10 μg/ml, 15 μg/ml, and 1 mg/ml, respectively. All cultures were incubated at 30°C unless otherwise stated. Gene deletions were carried out as previously described (Longtine *et al*, 1998). The engineering of specific mutations at endogenous loci was achieved using the method established by the Boone laboratory (Li *et al*, 2011).

Tissue culture

All cell lines used in this study are listed in Table EV1. All cell lines tested negatively for mycoplasma contamination. HAP1 cell lines were cultured in a humidified growth chamber at 37°C and 5% CO_2 in Iscove's Modified Dulbecco's Medium (IMDM; Sigma-Aldrich) supplemented with 10% Fetal Bovine Serum (Thermo Fisher Scientific) and 1% (v/v) Penicillin–Streptomycin (Sigma-Aldrich).

For mutation of the endogenous FBXW7 locus in HAP1 $p53^{-}$ cells, a CRISPR/Cas9 strategy was applied. SgRNAs were cloned into pSpCas9(BB)-2A-GFP (PX458, Addgene plasmid #48138). For homologous recombination, a repair template carrying the respective mutation and 1,000 base pair (bp) homology flanks was synthesized as gBlock gene fragment (Integrated DNA Technologies IDT) and inserted into the plasmid pmScarlet_C1 (Addgene plasmid #85042). The plasmid mix of guide RNA plasmid and the repair template was transfected into HAP1 cells using FuGENE HD (Promega). Two days after transfection, cells were sorted for the presence of Cas9 (GFP positive) and repair template (mScarlet positive). Three days later, single cells were sorted into 96-well plates. Clonal populations were expanded gradually over the course of 3 weeks. The FBXW7 mutations were identified by Sanger Sequencing, and karyotypes of the cell lines were validated by flow cytometry and whole-genome sequencing.

Flow cytometry

HAP1 cells were trypsinized and stained with 10 μg/ml Hoechst 33342 (Thermo Fisher Scientific) for 30 min at 37°C. Cells were then analyzed for their ploidy state (based on G1 haploid peaks) in PBS supplemented with 5% FBS in a FACSAria III (BD) flow cytometer.

Next-generation sequencing and data analysis

Overnight cultures of each strain were made for DNA isolation. DNA was purified with the Wizard genomic DNA purification kit (Promega). The DNA was fragmented to ~500 bp using the Bioruptor Pico sonicator for three cycles (30 s on/off). AMPure XP beads were used for size selection, and DNA libraries were prepared using the NEBNext Ultra II DNA library preparation kit for Illumina (New England Biosciences). Approximately 14 strains per run were multiplexed with NEBNext Multiplex oligos (96 index primers) and mixed at equimolar ratios. The multiplexed samples were sequenced using the 50-bp paired-end setting on an Illumina HiSeq 2500 system at the Vienna Biocenter Next-Generation Sequencing Facility (VBCF). All the raw bam files are accessible in the Sequence Read Archive (SRA—Bioproject accession number: PRJNA870080, Table EV3). The demultiplexed datasets were then aligned to the yeast genome using Bowtie2 (version 2.2.9; http://bowtie-bio.sourceforge.net/bowtie2) and converted to bed files using SAMtools (version 1.3.1; http://samtools.sourceforge.net) and Bedtools (version 2.14, http://bedtools.readthedocs.io). The subsequent bed files were used to calculate chromosome copy numbers using custom-made Python scripts. To normalize for differences in chromosome sizes, only the 15 kb closest to the telomeres was used. The value for the second-lowest quartile chromosomes was used for normalization. After normalization, if the chromosome copy number of a certain chromosome was greater than 1.5, it was counted as disomic (aneuploid in a haploid cell). Larger segmental copy number changes were identified visually by binning the data into 4 kb regions. Mutations in the *bir1*Δ-*ad* and *bir1*Δ-*ad2* strains were identified by running the mpileup function with SAMtools using the output from Bowtie2 alignment. These data were filtered by quality score and read depth; the quality needed to be greater than 95 and the read depth cutoff was 300. In the next step, BCFtools (version1.3.1) was implemented to convert the bcf files generated by mpileup (SAMtools) to variant call format (.vcf) files. Subsequently, VCFtools (version0.1.13) was used to compare all mutations found in our test strains with mutations already identified in the parent strain. Last, a custom-made Python script generated lists containing the strain identity, the coordinates of the mutation (in base pairs), and the type of mutation (coding/noncoding, silent/missense/nonsense etc.; Ravichandran *et al*, 2018). GOrilla gene ontology tool (http://cbl-gorilla.cs.technion.ac.il) was used for GO enrichment tests. The target gene list was composed of all genes with nonsynonymous mutations in the adapted strains (gene repeats included), and the background list was all 6,002 genes annotated in the *S. cerevisiae* genome. The list of CIN-related genes in the yeast genome was assembled from the Saccharomyces Genome Database by searching for six specific GO terms: colony sectoring: increased; chromosome segregation: abnormal; chromosome/plasmid maintenance: decreased rate; chromosome/plasmid maintenance: abnormal; chromosome segregation: premature; and chromosome segregation: decreased. Eight hundred and seventy-four different genes satisfied these criteria.

Growth measurements

To measure growth from serial dilutions of yeast on agar plates, the images were first binarized using a threshold that distinguished the yeast colonies from the background using ImageJ. Next, a circle was placed around the first spot in the dilution series that was not saturated in the wild-type strain, and the percentage of the area above the threshold was calculated. The same dilution and circle size were used for the measurements of each other strain on the same plate.

Microscopy

Strains were grown overnight in YPAD or YPAGR, subsequently diluted 1,000-fold in the morning into fresh media, and grown for 4–6 h to midlog phase. Cells were pelleted by brief centrifugation, washed twice with 1 ml water, and resuspended in 200 µl water. Two microliters of cell suspension was spotted onto 1% agarose pads supplemented with complete synthetic media (SC) and 2% glucose. A coverslip was placed on top and sealed with 1:1:1 mixture by weight of paraffin (Merck), lanolin (Alfa Aesar), and Vaseline (Ferd. Eimermacher). Images were collected on a DeltaVision Ultra Epifluorescence Microscope system (Cytiva) at 30°C and a PlanApo N 60/1.42 Oil objective and a sCMOS sensor, 1,020 × 1,020 pixels, 6.5 µm pixel size camera. For live yeast imaging, 12 z-sections with step size of 0.5 µm were taken. Images were deconvolved using the softWoRx software (Life Sciences Software). Counting of Bub3 foci was carried out using deconvolved images. Quantification of Dad3 and Sli15 fluorescence intensity in anaphase was performed on non-deconvolved images using ImageJ and a custom-made Python script (Fink *et al*, 2017). Line scans perpendicular to the spindle were used for the entire spindle in prometaphase and either at the kinetochore or in between the kinetochores in anaphase. Spindle and kinetochore position were determined using the Nuf2 localization. A Gaussian curve was then fit to the intensity measurements and the area under the curve was calculated. Sli15 localization in preanaphase was quantified by drawing a circle around the Nuf2-mCherry signal, and measuring the intensities of both mCherry and mNeonGreen signals from the same circle. Background intensities were subtracted using the measurements in a larger circle that extends outside of the spindle. All analyses (except for Fig EV4C) were obtained from images obtained from a minimum of three different days. Microscopy measurements were taken with blinded samples. Representative images are deconvolved and were contrast adjusted identically using ImageJ.

To test the localization of Sli15 to the mitotic spindle, endogenous Sli15 was put under the control of a *Gal10-1* promoter. For synchronization and depletion of endogenous Sli15, overnight cultures grown in YPAGR were diluted 1:100 into YPAGR and shaken for 2 h at 30°C. Cells were resuspended in YPAGR containing α-factor (10 µg/ml) for 45 min at 30°C. Subsequently, the medium was exchanged with YPAD containing α-factor (10 µg/ml) and grown for 2 h and 15 min at 30°C. Cells were then released from the G1 arrest into the cell cycle by washing twice with YPAD and resuspending in YPAD containing Pronase E (Merck). Synchronized yeast cells were released into the cell cycle and grown for 45 min at 30°C. The cells were then pelleted, washed with 1 ml sterile water, resuspended in 100 µl sterile water, and 2 µl cell suspension was put onto 1% agarose SC pads.

For the immunofluorescence of human cells, mitotic cells were collected by mechanical shake-off and immobilized on adhesion slides (Marienfeld) for 30 min at 37°C. Next, cells were washed once in PBS, fixed for 15 min with 4% Formaldehyde in PBS, and subsequently permeabilized using 0.5% Triton-X-100 in PBS (0.5% PBST). Cells were blocked for 1 h in 0.01% PBST + 2% Bovine Serum Albumin and co-stained overnight with rabbit monoclonal anti-Aurora B antibody (Abcam, ab45145, 1:200) and human anti-centromere antibody (Antibodies Incorporated, 15-234, 1:200). After several washes with 0.01% PBST, cells were co-stained with goat antirabbit IgG Alexa Fluor 488 (Thermo Fisher Scientific, A32723, 1:500) and goat antihuman IgG Alexa Fluor 647 (Invitrogen, A-21445, 1:500) for 2 h. After Immunostaining, DNA was stained for 1 min with 1 µg/ml DAPI (Thermo Fisher Scientific).

Minichromosome loss assay

Yeast strains transformed with the minichromosome pRS316 were grown to saturation overnight in SC-uracil media, diluted to a starting OD^{600} of 0.05, and grown for 24 h in 2 ml of YPAD media. After 24 h of growth, these strains were diluted 10^6-fold in sterile water, and 100 µl of each strain was plated onto an SC-uracil plate and a YPAD plate. The plates were incubated at 30°C for 48 h. Pictures taken of the subsequent colonies by a Canon EOS Digital Camera. The colony numbers were counted using the "Analyze Particles" function in ImageJ. The number of colonies on the *ura*-plates were then divided by the number that grew on the YPAD plate to obtain the measurement of transmission fidelity.

ATP-analog growth assay

Strains were grown overnight in YPAD and diluted to a starting OD^{600} of 0.05 in 3 ml YPAD at 25°C. The strains were given up to 4.5 h to reach exponential phase. At time point zero, the indicated amount of ATP-analog 1NM-PP1 (Merck) or DMSO was added to the strains. Immediately after drug addition, 0.5 ml of each sample was diluted 2× in a 1 ml cuvette to analyze the OD^{600} (time point 0). This was repeated every 1.5 h thereafter, for 7.5 h.

Budding index

Strains were grown overnight in YPAD media, and 100 µl of each overnight was added to 2 ml YPAD. After allowing 1 h for recovery, 2 µl of α-factor was added every 45 min for 2 h. Strains were then washed using fresh YPAD media mixed with Pronase E (Merck; 1:10). The number of large-budded cells was counted via light-microscopy every half an hour for 2.5 h. A total of 100 cells were counted per slide per time point.

Colony formation assay

On Day 1, 600 cells were seeded into six-well plates. The plates were incubated for 12 days. Colonies were then fixed with 4% Paraformaldehyde in PBS (Sigma-Aldrich) for 20 min, washed with water, stained for 30 min with Crystal Violet, washed with water, and dried.

Protein extraction and Western blotting

For yeast protein extraction in the cycloheximide time course, saturated overnight cultures were diluted in 30 ml YPAD in order to obtain an OD^{600} of 0.25. Cells were grown at 30°C while shaking until an OD^{600} of 0.7 was reached. At this point, cycloheximide (50 µg/ml) was added (t = 0). Five milliliters aliquots was taken every 30 min for a 2 h period at 30°C. Immediately after each aliquot was taken, proteins were extracted by pelleting the cells and resuspending them in 100 µl 5% trichloroacetic acid. Following 10-min incubation at room temperature, the cells were washed once

with 1 ml ddH_2O and resuspended in 100 µl lysis buffer (50 mM Tris, pH 7.4, 50 mM dithiotreitol, 1 mM EDTA, Complete EDTA-free protease inhibitor cocktail (Roche) and Phosstop (Roche)). Cells were vortexed for 30 min at 4°C after the addition of glass beads. Subsequently, 33 µl 4× sample buffer was added and incubated at 95°C for 5 min. For protein extractions in prometaphase cells, saturated overnight cultures were diluted in 10 ml YPAGR in order to obtain an OD^{600} of 0.25. Cells were then synchronized as described as for the microscopy experiments. Sixty minutes after G1 release, proteins were extracted by resuspending cells in 100 µl 0.2 M NaOH. After 5-min incubation at room temperature, cells were resuspended in 100 µl H_2O. Thirty-three microliters of 4× sample buffer was added and incubated at 95°C for 5 min. Samples were stored at −20°C. For immunoblots, the following antibodies were used: rat anti-HA-clone 3F10 (Roche), mouse anti-PGK1 monoclonal 22C5D8 (Thermo Fisher Scientific). Membranes were probed with the corresponding secondary antibodies: antirat IgG-HRP-lined (Cell Signaling Technology) or antimouse IgG-HRP-linked (Cell Signaling Technology). Immunoblots were quantified using ImageJ.

Statistics

Statistical analysis was performed using the GraphPad Prism software. Details to the statistical tests used in a particular experiment are reported in the figure legends.

Data availability

All the raw bam files are accessible in the Sequence Read Archive (SRA-Bioproject accession number: PRJNA870080). Information on each sample ID can be found in Table EV3.

Expanded View for this article is available online.

Acknowledgements
The authors would like to thank the Campbell and Dammermann laboratories for helpful discussions and comments. We thank the Basrai and Klein laboratories for gifts of yeast strains and plasmids. The parental HAP1 p53-null cell line was kindly provided by J.I. Loizou. We acknowledge the service of the Perutz Labs BioOptics Facility, a member of the VLSI. We would also like to acknowledge the services provided to us by the VBC sequencing facility located at the VBCF. This work was supported by Vienna Science and Technology Fund (WWTF) grant VRG14-001 and Austrian Science Fund (FWF) grants Y944-B28 and W1238-B20 to CSC.

Author contributions
Matthew N Clarke: Conceptualization; data curation; formal analysis; writing – original draft; writing – review and editing. **Theodor Marsoner:** Data curation; formal analysis; writing – original draft. **Manuel Alonso Y Adell:** Data curation; formal analysis; writing – original draft. **Madhwesh C Ravichandran:** Data curation; formal analysis; writing – original draft. **Christopher S Campbell:** Conceptualization; data curation; formal analysis; supervision; funding acquisition; writing – original draft; writing – review and editing.

Disclosure and competing interests statement
The authors declare that they have no conflict of interest.

References

Ainsztein AM, Kandels-Lewis SE, Mackay AM, Earnshaw WC (1998) INCENP centromere and spindle targeting: identification of essential conserved motifs and involvement of heterochromatin protein HP1. *J Cell Biol* 143: 1763 – 1774

Au W-C, Zhang T, Mishra PK, Eisenstatt JR, Walker RL, Ocampo J, Dawson A, Warren J, Costanzo M, Baryshnikova A *et al* (2020) Skp, Cullin, F-box (SCF)-Met30 and SCF-Cdc4-mediated proteolysis of CENP-A prevents Mislocalization of CENP-A for chromosomal stability in budding yeast. *PLoS Genet* 16: e1008597

Bailey ML, Singh T, Mero P, Moffat J, Hieter P (2015) Dependence of human colorectal cells lacking the FBW7 tumor suppressor on the spindle assembly checkpoint. *Genetics* 201: 885 – 895

Bakhoum SF, Genovese G, Compton DA (2009a) Deviant kinetochore microtubule dynamics underlie chromosomal instability. *Curr Biol* 19: 1937 – 1942

Bakhoum SF, Thompson SL, Manning AL, Compton DA (2009b) Genome stability is ensured by temporal control of kinetochore–microtubule dynamics. *Nat Cell Biol* 11: 27 – 35

Bakhoum SF, Silkworth WT, Nardi IK, Nicholson JM, Compton DA, Cimini D (2014) The mitotic origin of chromosomal instability. *Curr Biol* 24: R148 – R149

Ben-David U, Amon A (2020) Context is everything: aneuploidy in cancer. *Nat Rev Genet* 21: 44 – 62

Biggins S, Bhalla N, Chang A, Smith DL, Murray AW (2001) Genes involved in sister chromatid separation and segregation in the budding yeast *Saccharomyces cerevisiae*. *Genetics* 159: 453 – 470

Bishop JD, Schumacher JM (2002) Phosphorylation of the carboxyl terminus of inner centromere protein (INCENP) by the Aurora B kinase stimulates Aurora B kinase activity. *J Biol Chem* 277: 27577 – 27580

Bishop AC, Ubersax JA, Petsch DT, Matheos DP, Gray NS, Blethrow J, Shimizu E, Tsien JZ, Schultz PG, Rose MD *et al* (2000) A chemical switch for inhibitor-sensitive alleles of any protein kinase. *Nature* 407: 395 – 401

Böhm M, Killinger K, Dudziak A, Pant P, Jänen K, Hohoff S, Mechtler K, Örd M, Loog M, Sanchez-Garcia E *et al* (2021) Cdc4 phospho-degrons allow differential regulation of Ame1CENP-U protein stability across the cell cycle. *eLife* 10: e67390

Cahill DP, Kinzler KW, Vogelstein B, Lengauer C (1999) Genetic instability and darwinian selection in tumours. *Trends Cell Biol* 9: M57 – M60

Campbell CS, Desai A (2013) Tension sensing by Aurora B kinase is independent of survivin-based centromere localization. *Nature* 497: 118 – 121

Cheeseman IM, Anderson S, Jwa M, Green EM, Kang JS, Yates JR, Chan CSM, Drubin DG, Barnes G (2002) Phospho-regulation of kinetochore–microtubule attachments by the Aurora kinase Ipl1p. *Cell* 111: 163 – 172

Cheeseman IM, Chappie JS, Wilson-Kubalek EM, Desai A (2006) The conserved KMN network constitutes the core microtubule-binding site of the kinetochore. *Cell* 127: 983 – 997

Ciferri C, Pasqualato S, Screpanti E, Varetti G, Santaguida S, Reis Dos G, Maiolica A, Polka J, De Luca JG, De Wulf P *et al* (2008) Implications for kinetochore–microtubule attachment from the structure of an engineered Ndc80 complex. *Cell* 133: 427 – 439

Cimini D, Wan X, Hirel CB, Salmon ED (2006) Aurora kinase promotes turnover of kinetochore microtubules to reduce chromosome segregation errors. *Curr Biol* 16: 1711 – 1718

Costanzo M, VanderSluis B, Koch EN, Baryshnikova A, Pons C, Tan G, Wang W, Usaj M, Hanchard J, Lee SD *et al* (2016) A global genetic interaction network maps a wiring diagram of cellular function. *Science* 353: aaf1420

Du R, Huang C, Liu K, Li X, Dong Z (2021) Targeting AURKA in cancer: Molecular mechanisms and opportunities for cancer therapy. *Mol Cancer* 20: 15 – 27

Fink S, Turnbull K, Desai A, Campbell CS (2017) An engineered minimal chromosomal passenger complex reveals a role for INCENP/Sli15 spindle association in chromosome biorientation. *J Cell Biol* 216: 911 – 923

Gassmann R, Carvalho A, Henzing AJ, Ruchaud S, Hudson DF, Honda R, Nigg EA, Gerloff DL, Earnshaw WC (2004) Borealin: a novel chromosomal passenger required for stability of the bipolar mitotic spindle. *J Cell Biol* 166: 179 – 191

Goh PY, Surana U (1999) Cdc4, a protein required for the onset of S phase, serves an essential function during G(2)/M transition in *Saccharomyces cerevisiae*. *Mol Cell Biol* 19: 5512 – 5522

Gordon DJ, Resio B, Pellman D (2012) Causes and consequences of aneuploidy in cancer. *Nat Rev Genet* 13: 189 – 203

Gropp A, Winking H, Herbst EW, Claussen CP (1983) Murine trisomy: developmental profiles of the embryo, and isolation of trisomic cellular systems. *J Exp Zool* 228: 253 – 269

Honda R, Körner R, Nigg EA (2003) Exploring the functional interactions between Aurora B, INCENP, and survivin in mitosis. *Mol Biol Cell* 14: 3325 – 3341

Hose J, Escalante LE, Clowers KJ, Dutcher HA, Robinson D, Bouriakov V, Coon JJ, Shishkova E, Gasch AP (2020) The genetic basis of aneuploidy tolerance in wild yeast. *eLife* 9: e52063

Jenni S, Harrison SC (2018) Structure of the DASH/Dam1 complex shows its role at the yeast kinetochore–microtubule interface. *Science* 360: 552 – 558

Jeyaprakash AA, Klein UR, Lindner D, Ebert J, Nigg EA, Conti E (2007) Structure of a Survivin-Borealin-INCENP core complex reveals how chromosomal passengers travel together. *Cell* 131: 271 – 285

Jin F, Wang Y (2013) The signaling network that silences the spindle assembly checkpoint upon the establishment of chromosome bipolar attachment. *Proc Natl Acad Sci USA* 110: 21036 – 21041

Jones MH, Huneycutt BJ, Pearson CG, Zhang C, Morgan G, Shokat K, Bloom K, Winey M (2005) Chemical genetics reveals a role for Mps1 kinase in kinetochore attachment during mitosis. *Curr Biol* 15: 160 – 165

Jonkers W, Rep M (2009) Lessons from fungal F-box proteins. *Eukaryot Cell* 8: 677 – 695

Kalantzaki M, Kitamura E, Zhang T, Mino A, Novak B, Tanaka TU (2015) Kinetochore–microtubule error correction is driven by differentially regulated interaction modes. *Nat Cell Biol* 17: 421 – 433

Kawashima SA, Tsukahara T, Langegger M, Hauf S, Kitajima TS, Watanabe Y (2007) Shugoshin enables tension-generating attachment of kinetochores by loading Aurora to centromeres. *Genes Dev* 21: 420 – 435

Kawashima SA, Yamagishi Y, Honda T, Ishiguro K-I, Watanabe Y (2010) Phosphorylation of H2A by Bub1 prevents chromosomal instability through localizing shugoshin. *Science* 327: 172 – 177

Klein UR, Nigg EA, Gruneberg U (2006) Centromere targeting of the chromosomal passenger complex requires a ternary subcomplex of Borealin, Survivin, and the N-terminal domain of INCENP. *Mol Biol Cell* 17: 2547 – 2558

Kline-Smith SL, Walczak CE (2002) The microtubule-destabilizing kinesin XKCM1 regulates microtubule dynamic instability in cells. *Mol Biol Cell* 13: 2718 – 2731

Kwon M, Godinho SA, Chandhok NS, Ganem NJ, Azioune A, Théry M, Pellman D (2008) Mechanisms to suppress multipolar divisions in cancer cells with extra centrosomes. *Genes Dev* 22: 2189 – 2203

Li Z, Vizeacoumar FJ, Bahr S, Li J, Warringer J, Vizeacoumar FS, Min R, VanderSluis B, Bellay J, Devit M *et al* (2011) Systematic exploration of essential yeast gene function with temperature-sensitive mutants. *Nat Biotechnol* 29: 361 – 367

Liu X, Winey M (2012) The MPS1 family of protein kinases. *Annu Rev Biochem* 81: 561 – 585

Longtine MS, McKenzie A, Demarini DJ, Shah NG, Wach A, Brachat A, Philippsen P, Pringle JR (1998) Additional modules for versatile and economical PCR-based gene deletion and modification in *Saccharomyces cerevisiae*. *Yeast* 14: 953 – 961

Makrantoni V, Stark MJR (2009) Efficient chromosome biorientation and the tension checkpoint in *Saccharomyces cerevisiae* both require Bir1. *Mol Cell Biol* 29: 4552 – 4562

Miranda JJL, De Wulf P, Sorger PK, Harrison SC (2005) The yeast DASH complex forms closed rings on microtubules. *Nat Struct Mol Biol* 12: 138 – 143

Ng TM, Waples WG, Lavoie BD, Biggins S (2009) Pericentromeric sister chromatid cohesion promotes kinetochore biorientation. *Mol Biol Cell* 20: 3818 – 3827

Orr B, Talje L, Liu Z, Kwok BH, Compton DA (2016) Adaptive resistance to an inhibitor of chromosomal instability in human cancer cells. *Cell Rep* 17: 1755 – 1763

Pavani M, Bonaiuti P, Chiroli E, Gross F, Natali F, Macaluso F, Póti Á, Pasqualato S, Farkas Z, Pompei S *et al* (2021) Epistasis, aneuploidy, and functional mutations underlie evolution of resistance to induced microtubule depolymerization. *EMBO J* 40: e108225

Pettersen EF, Goddard TD, Huang CC, Meng EC, Couch GS, Croll TI, Morris JH, Ferrin TE (2021) UCSF ChimeraX: structure visualization for researchers, educators, and developers. *Protein Sci* 30: 70 – 82

Pinsky BA, Kung C, Shokat KM, Biggins S (2006) The Ipl1-Aurora protein kinase activates the spindle checkpoint by creating unattached kinetochores. *Nat Cell Biol* 8: 78 – 83

Ravichandran MC, Fink S, Clarke MN, Hofer FC, Campbell CS (2018) Genetic interactions between specific chromosome copy number alterations dictate complex aneuploidy patterns. *Genes Dev* 32: 1485 – 1498

Ryland GL, Doyle MA, Goode D, Boyle SE, Choong DYH, Rowley SM, Li J, Bowtell DD, Tothill RW, Campbell IG *et al* (2015) Loss of heterozygosity: what is it good for? *BMC Med Genomics* 8: 1 – 12

Sansregret L, Patterson JO, Dewhurst S, López-García C, Koch A, McGranahan N, Chao WCH, Barry DJ, Rowan A, Instrell R *et al* (2017) APC/C dysfunction limits excessive cancer chromosomal instability. *Cancer Discov* 7: 218 – 233

Sarangapani KK, Akiyoshi B, Duggan NM, Biggins S, Asbury CL (2013) Phosphoregulation promotes release of kinetochores from dynamic microtubules via multiple mechanisms. *Proc Natl Acad Sci USA* 110: 7282 – 7287

Sessa F, Mapelli M, Ciferri C, Tarricone C, Areces LB, Schneider TR, Stukenberg PT, Musacchio A (2005) Mechanism of Aurora B activation by INCENP and inhibition by hesperadin. *Mol Cell* 18: 379 – 391

Shimogawa MM, Graczyk B, Gardner MK, Francis SE, White EA, Ess M, Molk JN, Ruse C, Niessen S, Yates JR *et al* (2006) Mps1 phosphorylation of Dam1 couples kinetochores to microtubule plus ends at metaphase. *Curr Biol* 16: 1489 – 1501

Shimogawa MM, Widlund PO, Riffle M, Ess M, Davis TN (2009) Bir1 is required for the tension checkpoint. *Mol Biol Cell* 20: 915 – 923

Shimogawa MM, Wargacki MM, Muller EG, Davis TN (2010) Laterally attached kinetochores recruit the checkpoint protein Bub1, but satisfy the spindle checkpoint. *Cell Cycle* 9: 3619 – 3628

Spruck CH, Strohmaier H, Sangfelt O, Müller HM, Hubalek M, Müller-Holzner E, Marth C, Widschwendter M, Reed SI (2002) hCDC4 gene mutations in endometrial cancer. *Cancer Res* 62: 4535 – 4539

Tanaka TU, Rachidi N, Janke C, Pereira G, Galova M, Schiebel E, Stark MJR, Nasmyth K (2002) Evidence that the Ipl1-Sli15 (Aurora kinase-INCENP)

complex promotes chromosome bi-orientation by altering kinetochore-spindle pole connections. *Cell* 108: 317 – 329

Thiagalingam S, Laken S, Willson JK, Markowitz SD, Kinzler KW, Vogelstein B, Lengauer C (2001) Mechanisms underlying losses of heterozygosity in human colorectal cancers. *Proc Natl Acad Sci USA* 98: 2698 – 2702

Torres EM, Sokolsky T, Tucker CM, Chan LY, Boselli M, Dunham MJ, Amon A (2007) Effects of aneuploidy on cellular physiology and cell division in haploid yeast. *Science* 317: 916 – 924

Torres EM, Dephoure N, Panneerselvam A, Tucker CM, Whittaker CA, Gygi SP, Dunham MJ, Amon A (2010) Identification of aneuploidy-tolerating mutations. *Cell* 143: 71 – 83

van der Waal MS, Saurin AT, Vromans MJM, Vleugel M, Wurzenberger C, Gerlich DW, Medema RH, Kops GJPL, Lens SMA (2012) Mps1 promotes rapid centromere accumulation of Aurora B. *EMBO Rep* 13: 847 – 854

Vanoosthuyse V, Prykhozhij S, Hardwick KG (2007) Shugoshin 2 regulates localization of the chromosomal passenger proteins in fission yeast mitosis. *Mol Biol Cell* 18: 1657 – 1669

Walczak CE, Mitchison TJ, Desai A (1996) XKCM1: a xenopus kinesin-related protein that regulates microtubule dynamics during mitotic spindle assembly. *Cell* 84: 37 – 47

Weiss E, Winey M (1996) The *Saccharomyces cerevisiae* spindle pole body duplication gene MPS1 is part of a mitotic checkpoint. *J Cell Biol* 132: 111 – 123

Westermann S, Avila-Sakar A, Wang H-W, Niederstrasser H, Wong J, Drubin DG, Nogales E, Barnes G (2005) Formation of a dynamic kinetochore-microtubule interface through assembly of the Dam1 ring complex. *Mol Cell* 17: 277 – 290

Winey M, Goetsch L, Baum P, Byers B (1991) MPS1 and MPS2: novel yeast genes defining distinct steps of spindle pole body duplication. *J Cell Biol* 114: 745 – 754

Yeh C-H, Bellon M, Nicot C (2018) FBXW7: a critical tumor suppressor of human cancers. *Mol Cancer* 17: 115 – 119

Yona AH, Manor YS, Herbst RH, Romano GH, Mitchell A, Kupiec M, Pilpel Y, Dahan O (2012) Chromosomal duplication is a transient evolutionary solution to stress. *Proc Natl Acad Sci USA* 109: 21010 – 21015

Expanded View Figures

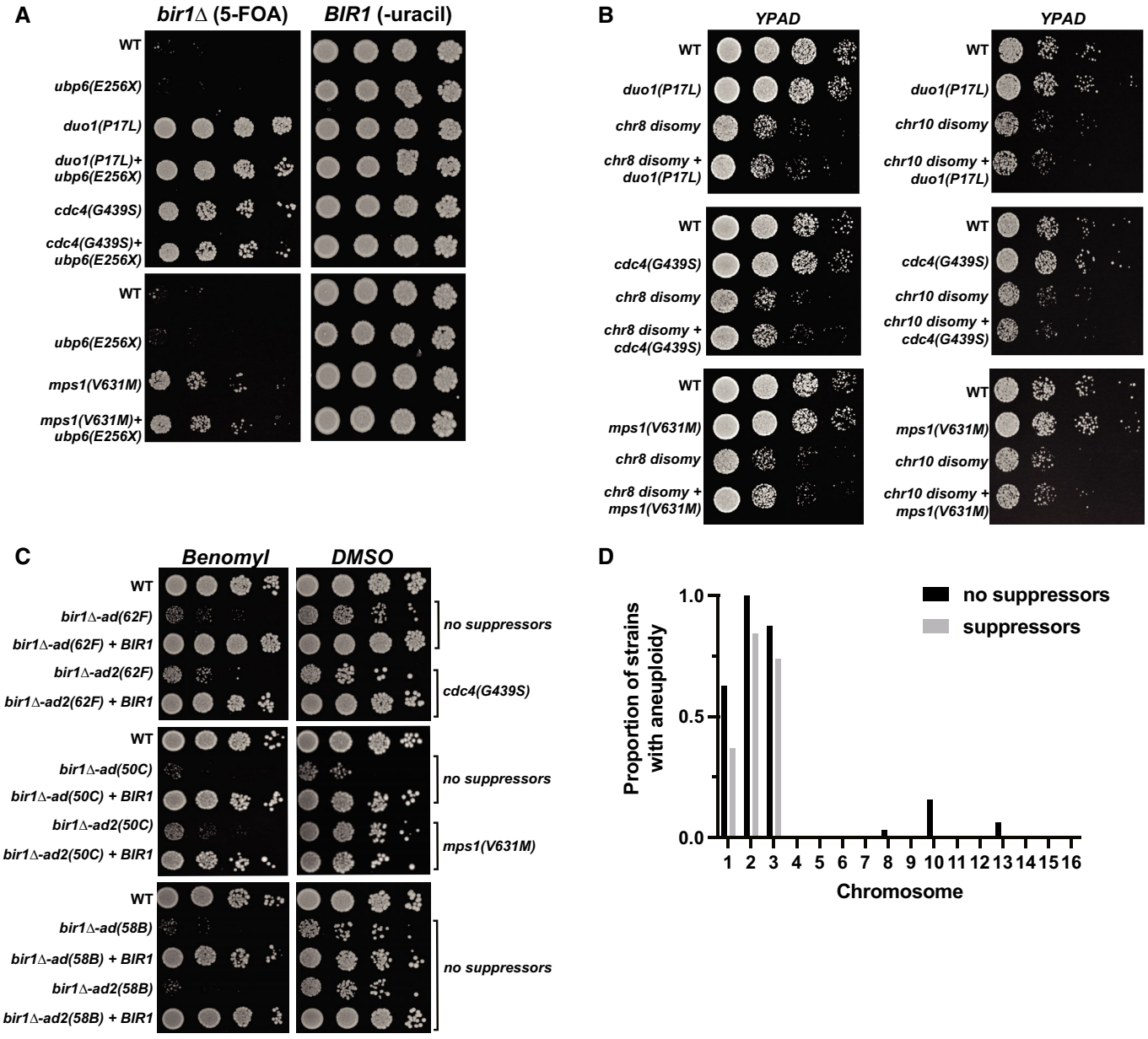

Figure EV1. CIN-related mutations in *bir1*Δ-*ad2* strains are associated with decreased aneuploidy.

A Ten-fold serial dilutions on the indicated media are shown. Strains engineered with the *ubp6(E256X)* aneuploidy tolerance mutation show no *bir1*Δ suppression. Strains with both the *ubp6(E256X)* mutation and a *bir1*Δ suppressor mutant do not additionally rescue the loss of CPC activity.

B Ten-fold serial dilutions on the indicated media are shown. Strains have disomy of either chromosome 8 (chr8) or chromosome 10 (chr10) with or without the *bir1*Δ suppressor mutations. The combination of either type of disomy with any of the three suppressors shows no change in growth.

C Ten-fold serial dilutions of the indicated strains were made on YPAD plates containing either 0.1% DMSO or 10 μg/ml of benomyl. Strains were adapted to persistent loss of CPC function for different amounts of time with or without *BIR1* then restored. Those *bir1*Δ-*ad* strains that developed suppressor mutations after the extended growth period (*bir1*Δ-*ad2*(*62F*) and *bir1*Δ-*ad2*(*50C*)) were better able to cope with benomyl than one that did not develop suppressors (*bir1*Δ-*ad2*(58B)).

D Histogram showing the proportion of strains that are aneuploid for specific chromosomes in *bir1*Δ-*ad2* strains that have identified suppressor mutations, and those that do not.

Figure EV2. Double mutants of *bir1*Δ suppressors in the Dam1 complex and the *dam1(S20D)* phosphomimic have strong synthetic phenotypes.

A Tetrad dissections performed on diploids with both *sli15*Δ and the *duo1(P17L)* did not produce any viable spores with either *sli15*Δ or a combination of *sli15*Δ and *duo1(P17L)*.

B Cell cycle progression as measured by percentage of large budded cells over time after release from G1 arrest. None of the tested suppressor mutants cause a mitotic delay.

C Tetrad dissections of diploids heterozygous for both a *bir1*Δ suppressor mutant and the *dam1(S20D)* phosphomimic mutant. Presence of either the suppressor mutant or *dam1(S20D)* was determined by antibiotic resistance conferred by a gene integrated downstream of the mutations (clonNAT and G418 respectively). Colonies from haploid spores containing either *dad2(K11Q)*, *dam1(S20D)* or *duo1(P17L)*, *dam1(S20D)* were extremely rare. Spore viability of each genotype was counted in tetrads whose type (parental ditype, nonparental ditype, or tetratype) could be distinguished. Quantification for each mutant is from a single plate, and the WT numbers are the averages from all six plates. The representative image to the right of the graph depicts six tetrads, demonstrating examples of three tetratypes, two nonparental ditypes, and a single parental ditype. In this example, the expectant *duo1(P17L)*, *dam1(S20D)* double-mutant formed a colony from 0 out of seven spores.

D Proportion of colonies that grow on plates with restrictive (lacking uracil) versus permissive (YPAD) media after 24 h growth under permissive conditions with a *URA3*-containing plasmid. *duo1(P17L)*, *dam1(S20D)* double mutants have a strong decrease in transmission fidelity. Data are from three independent experiments Means and standard deviations are shown.

E Cell cycle progression as measured by percentage of large budded cells over time after release from G1 arrest. Rare surviving *duo1(P17L)*, *dam1(S20D)* double mutants have a strong mitotic delay. Wild-type (WT) cells treated with nocodazole and benomyl were used as a positive control for mitotic arrest.

F Serial dilution showing growth of strains containing either the double-mutant (*duo1(P17L)*, *dam1(S20D)*), the *ipl1-321* temperature-sensitive allele, or a combination of all three mutations. At the restrictive temperature (34°C), the double-mutant rescues growth of the *ipl1-321* allele. Ten-fold serial dilutions were done on YPAD plates at the indicated temperatures and were grown for 48 h.

Data information: (ns) not significant; (*) $P < 0.05$; (**) $P < 0.01$; (***) $P < 0.001$; unpaired *t*-test.

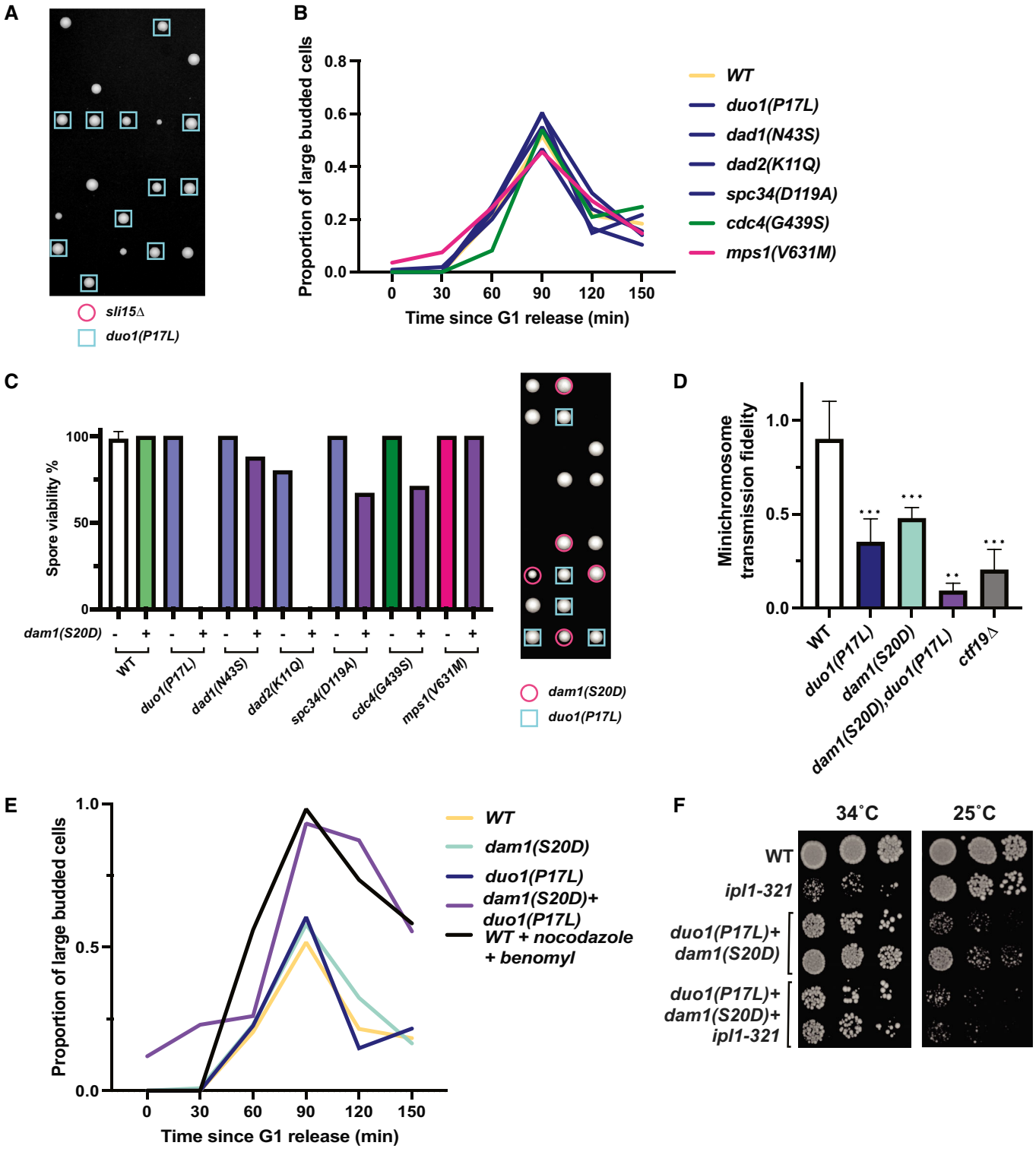

Figure EV2.

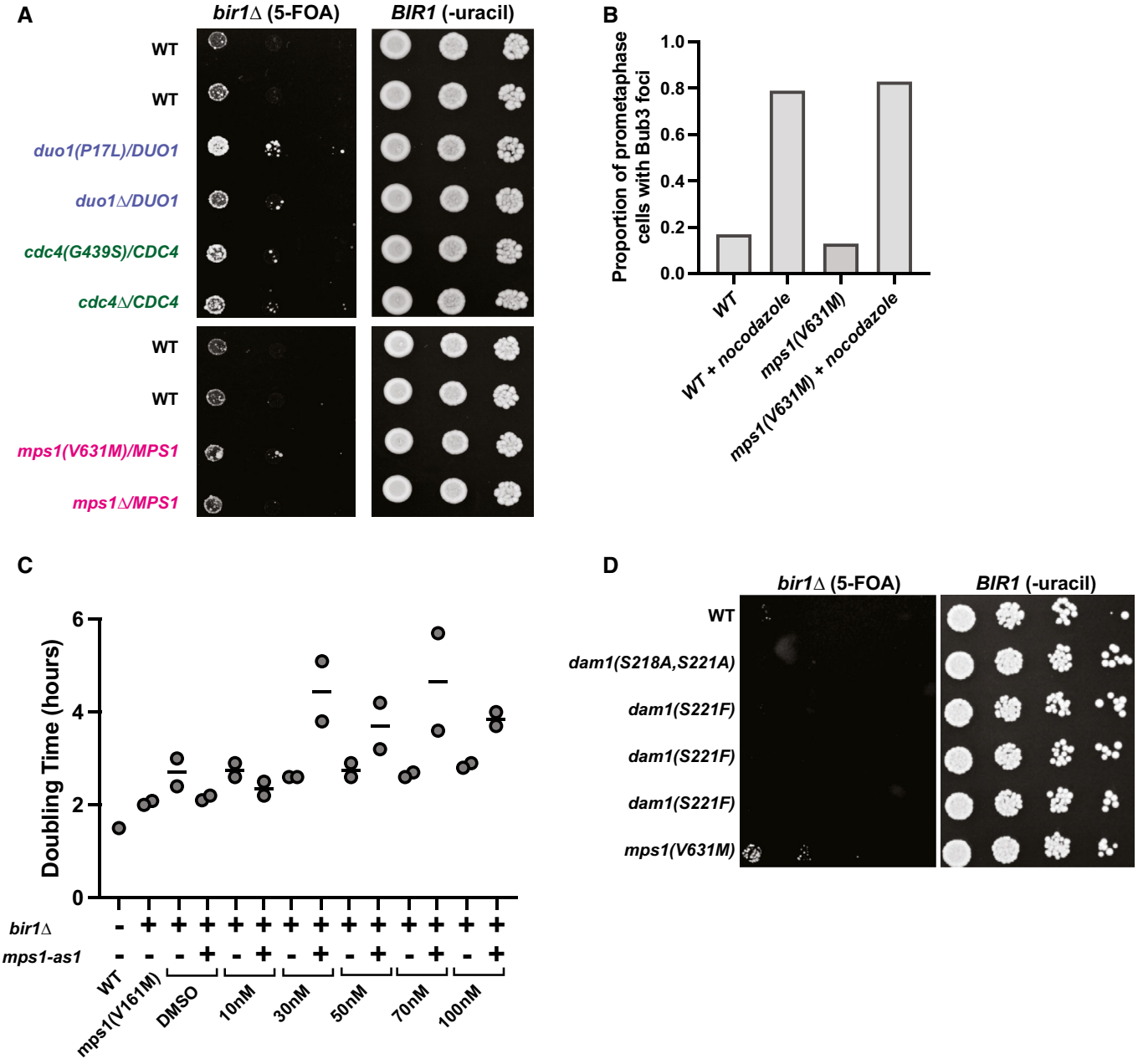

Figure EV3. Suppression of *bir1*Δ by Mps1 mutations occurs through decreased kinase activity that does not inhibit spindle assembly checkpoint activity.

A Ten-fold serial dilutions on the indicated media are shown. Strains engineered with the indicated mutations were tested for rescue of *BIR1* deletion. Diploid strains were heterozygous for either an identified suppressor mutation or a full deletion of the gene.

B Quantification of the proportion of prometaphase cells with Bub3-mNeonGreen foci with or without 15 μg/ml nocodazole. The *mps1(V631M)* mutation does not affect the percentage of cells with spindle assembly checkpoint foci. Data are from a single experiment.

C Growth assays conducted with an ATP-analog (1NM-PP1) that specifically inhibits the *mps1-as1* allele. Strains with wild-type Mps1 were not affected by the inhibitor. The WT strain is CCY1905. Data are from two independent experiments.

D Ten-fold serial dilutions on the indicated media are shown. Strains engineered with the indicated mutations were tested for rescue of *BIR1* deletion. Dam1 alleles with nonphosphorylatable mutations in Mps1 phosphosites (S218 and S221) do not rescue growth after *bir1*Δ.

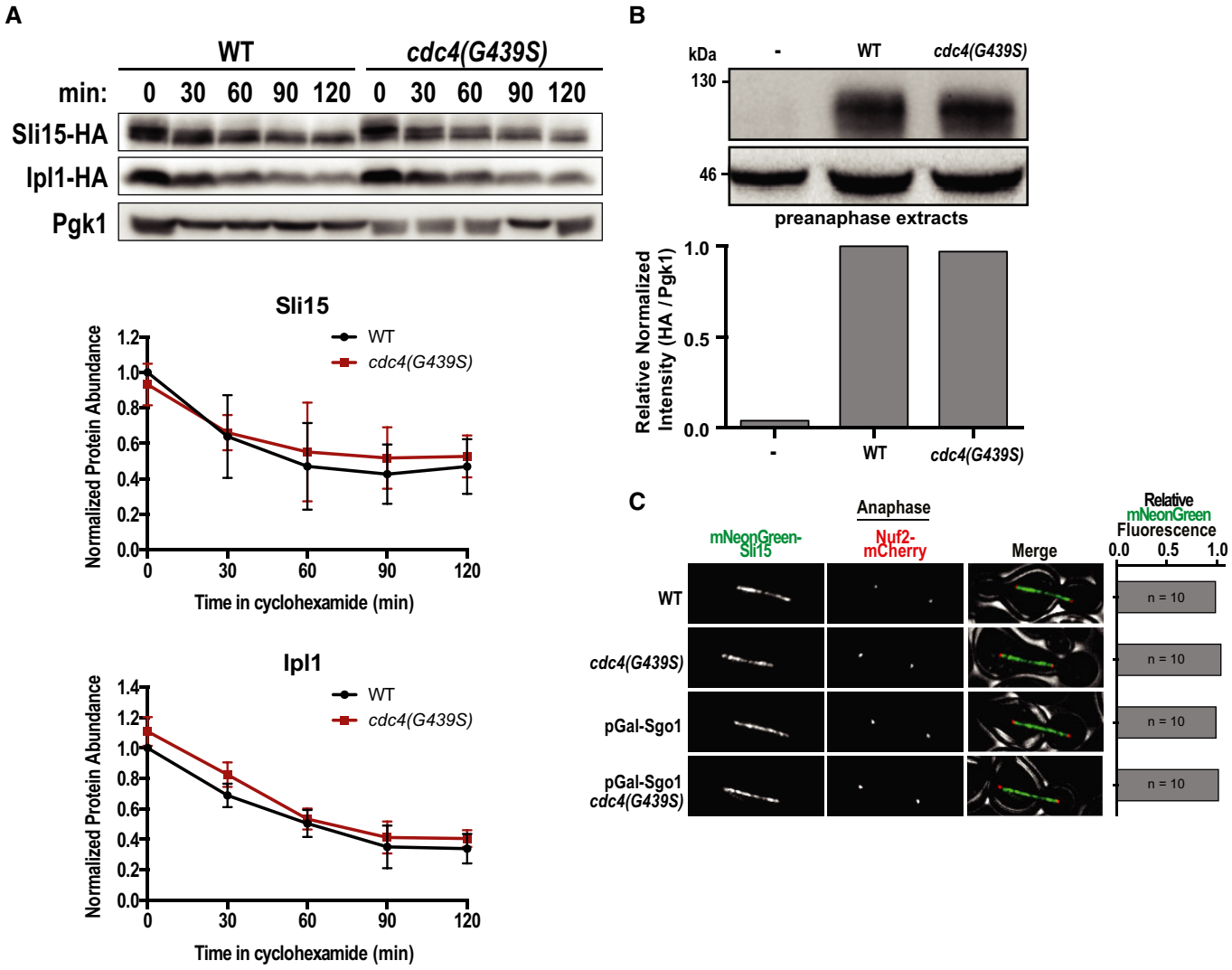

Figure EV4. *bir1*Δ suppressor mutations in Cdc4 do not affect protein stability of Sli15 or Ipl1.

A Western-blot of a time series of Ipl1 and Sli15 protein levels after inhibition of protein translation with cycloheximide. Cycloheximide was added to cells at time point 0, and cells were harvested and fixed at 30 min intervals. Representative images from one experiment are shown on top and quantification of three independent experiments is shown on bottom. Error bars represent standard deviation of three biological replicates from Western Blot quantifications.

B Western-blot and quantification of mNeonGreen-HA-Sli15 expression levels in *cdc4(G439S)* expressing cells. Pre-anaphase protein extracts were prepared as in Fig 6B and probed for Sli15 expression levels via immunoblotting using an HA antibody. Data are from a single experiment.

C The amount of mNeonGreen-Sli15 spindle localization was measured in anaphase. Sgo1 was depleted by placing the gene under a galactose-inducible promoter and switching to glucose-containing media (YPAD). For quantifications, line-scans perpendicular to the spindle were measured. Representative images are on the left. Scale bar is 2 μm. Data are from a single experiment.

Figure EV5. Engineering and characterization of FBXW7 mutant cell lines.

A Strategy implemented to introduce specific point mutations in *FBXW7* in HAP1 cells. Transfected cell lines were originally screened for a silent mutation that creates an EcoR1 restriction site.

B Sanger sequencing confirms the presence of the G437S mutation in *FBXW7*.

C Cell lines mutant for *FBXW7* have an increased colony size after 12 days of growth in comparison to a cell line with wild-type *FBXW7*. Means and standard deviations are shown. Each individual value point is the size measurement of a single clone. Data are from two independent experiments. (***) $P < 0.001$; (****) $P < 0.0001$; unpaired *t*-test.

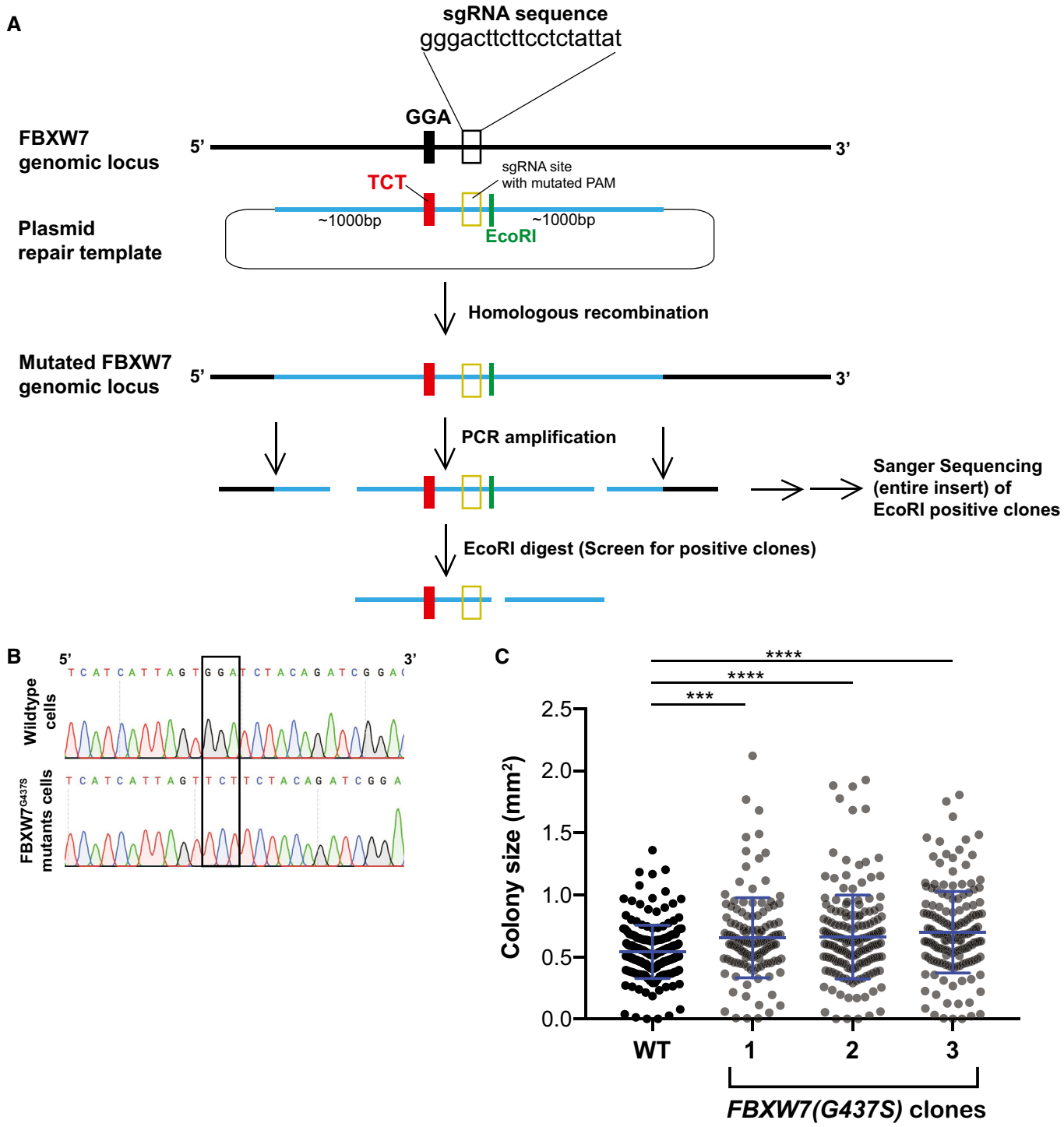

Figure EV5.

Table EV1

Table EV1. Yeast strains, Cell lines and Plasmids from this study

Strain	Genotype	Source	Background	Figure/s
CCY149	MATa/α; Bir1+/Δ::HYG; ura3-1; LEU2/leu2,3-112; his3-11:pCUP1-GFP12-lacI12:HIS3 trp1-1:256lacO:TRP1; LYS2/lys2Δ ADE2/ade2-1; can1-100; bar1Δ	a	W303	1; 2; EV1
*bir1*Δ haploids	These strains were made either through tetrad dissection of CCY149 or from single colonies of CCY1905 selected on FOA plates.	c	W303	1B;1C;1D
*bir1*Δ*-ad* haploids	All strains were derived from tetrad dissecting CCY149 (102 haploid strains)	b	W303	1B;1C;1D;1E;1F;1G;2F; EV1C
*bir1*Δ*-ad2* haploids	All strains were derived from bir1Δ-ad (68 strains)	b	W303	1B;1C;1D;1E;1F;1G;2D;2E;2F;EV1C; EV1D
*bir1*Δ*-ad3* haploids	All strains were derived from bir1Δ-ad2 (15 strains)	c	W303	1B;1C;1D;1E;1F;1G;2D;2E;2F EV1C; EV1D
CCY434	MATa; ura3-1; leu2;3-112; his3-11; trp1-1; ade2-1	a	W303	3A; 4D; EV2B; EV2E; EV2F
CCY747	MATα; his3-11:pCUP1-GFP12-lacI12:HIS3 trp1-1:256lacO:TRP1; leu2,3-112; lys2Δ; ura3-1; ADE2; trp1-1	a	W303	1C;1D;2D;2E; EV1C
CCY1744	MATa/α; Bir1Δ/Δ::G418/HYG; ura3-1; LEU2/leu2,3-112; his3-11:pCUP1-GFP12-lacI12:HIS3 trp1-1:256lacO:TRP1 LYS2/lys2Δ; ADE2/ade2-1; can1-100; bar1Δ; pCC598::URA3	a	W303	EV3A
CCY1887	MATa; ura3-1; leu2,3-112; trp1-1; ade2-1; pGalCEN8::URA3::HIS3(pCC631)	b	W303	EV1B
CCY1905	MATa; Bir1Δ:HYG; ura3-1; leu2,3-112: pCUP1-GFP12-lacI12:HIS3 trp1-1:256lacO: lys2Δ; can1-100 bar1Δ; pCC598::URA3	b	W303	2B; 4B; 6A; EV1A; EV3C; EV3D
CCY1934	CCY1905 + UBP6::ubp6(E256X):G418	c	W303	EV1A
CCY1946	Bir1Δ:HYG; ura3-1; leu2,3-112: pCUP1-GFP12-lacI12:HIS3 trp1-1:256lacO: lys2Δ; can1-100 bar1Δ; pCC598::URA3; pGalCEN10::LYS2::pCC644::LEU2	b	W303	EV1B
CCY2999	MATa Bir1Δ:HYG ; ura3-1; leu2;3-112: pCUP1-GFP12-lacI12:HIS3 trp1-1:256lacO:TRP1 lys2Δ ADE2 can1-100 bar1Δ	c	W303	EV3C
CCY3001	CCY2999 + mps1-as1:G418	c	W303	EV3C
CCY3031	CCY1905 + duo1(P17L):G418	c	W303	2B; 4B; EV1A
CCY3033	CCY1905 + cdc34(M64T):G418	c	W303	2B
CCY3035	CCY1905 + mif2(D241I):G418	c	W303	2B
CCY3037	CCY1905 + ndc80(K181N):G418	c	W303	2B
CCY3039	CCY1905 + spc105(R583G):G418	c	W303	2B
CCY3041	CCY1905 + sli15(G334S):G418	c	W303	2B
CCY3043	CCY1905 + sli15(L71S):G418	c	W303	2B
CCY3047	CCY1905 + cdc4(G439S):G418	c	W303	2B; 6A; EV1A

Table EV1

CCY3048	CCY1905 + cdc4(S438G):G418	c	W303	2B
CCY3050	CCY1905 + mps1(R596H):G418	c	W303	2B
CCY3052	CCY1905 + mps1(V631M):G418	c	W303	2B; EV1A; EV3C; EV3D
CCY3064	CCY1905 + spc34(D119A):G418	c	W303	2B
CCY3083	CCY1905 + rtg2(A433P):G418	c	W303	2B
CCY3085	CCY1905 + spc97(S816X):G418	c	W303	2B
CCY3210	MATa/α; Bir1Δ/Δ:HYG ; ura3-1/ura3-1; leu2;3-112: pCUP1-GFP12-lacI12:HIS3/leu2;3-112 trp1-1:256lacO:TRP1/trp1-1:256lacO: lys2Δ ade2-1/ADE2 can1-100/can1-100 bar1Δ/bar1Δ; pCC598::URA3 DUO1/duo1(P17L):G418	c	W303	EV3A
CCY3211	MATa/α; Bir1Δ/Δ:HYG ; ura3-1/ura3-1; leu2;3-112: pCUP1-GFP12-lacI12:HIS3/leu2;3-112 trp1-1:256lacO:TRP1/trp1-1:256lacO: lys2Δ ade2-1/ADE2 can1-100/can1-100 bar1Δ/bar1Δ; pCC598::URA3 CDC4/cdc4(G439S):G418	c	W303	EV3A
CCY3212	MATa/α; Bir1Δ/Δ:HYG ; ura3-1/ura3-1; leu2;3-112: pCUP1-GFP12-lacI12:HIS3/leu2;3-112 trp1-1:256lacO:TRP1/trp1-1:256lacO: lys2Δ ade2-1/ADE2 can1-100/can1-100 bar1Δ/bar1Δ; pCC598::URA3 MPS1/mps1(V631M):G418	c	W303	EV3A
CCY3299	MATa; ura3-1; leu2;3-112; his3-11; trp1-1; ade2-1; lys2; ipl1-321; duo1(P17L):G418	c	W303	3A
CCY3356	MATa; ura3-1; leu2;3-112; his3-11; trp1-1; ade2-1; lys2; ipl1-321; cdc4(G439S):G418	c	W303	3A
CCY3358	MATa; ura3-1; leu2;3-112; his3-11; trp1-1; ade2-1; lys2; ipl1-321; mps1(V631M):G418	c	W303	3A
CCY3439	MATa/α; Bir1Δ/Δ:HYG ; ura3-1/ura3-1; leu2;3-112: pCUP1-GFP12-lacI12:HIS3/leu2;3-112 trp1-1:256lacO:TRP1/trp1-1:256lacO: lys2Δ ade2-1/ADE2 can1-100/can1-100 bar1Δ/bar1Δ; pCC598::URA3 DUO1/duo1Δ::NAT	c	W303	EV3A
CCY3441	MATa/α; Bir1Δ/Δ:HYG ; ura3-1/ura3-1; leu2;3-112: pCUP1-GFP12-lacI12:HIS3/leu2;3-112 trp1-1:256lacO:TRP1/trp1-1:256lacO: lys2Δ ade2-1/ADE2 can1-100/can1-100 bar1Δ/bar1Δ; pCC598::URA3 CDC4/cdc4Δ::NAT	c	W303	EV3A
CCY3443	MATa/α; Bir1Δ/Δ:HYG ; ura3-1/ura3-1; leu2;3-112: pCUP1-GFP12-lacI12:HIS3/leu2;3-112 trp1-1:256lacO:TRP1/trp1-1:256lacO: lys2Δ ade2-1/ADE2 can1-100/can1-100 bar1Δ/bar1Δ; pCC598::URA3 MPS1/mps1::NAT	c	W303	EV3A
CCY3445	MATα; ura3-1; leu2;3-112; his3-11; trp1-1; ade2-1; ura3-1; leu2;3-112; his3-11; trp1-1; ade2-1; LYS2+; BUB3-mNeonGreen:NAT; NUF2-mRuby3:Hygro	c	W303	3B; 4C; EV3B
CCY3469	CCY1905 + dam1-765(S221F):G418	c	W303	EV3D
CCY3643	CCY3445 + duo1(P17L):G418	c	W303	3B; 4C
CCY3644	CCY3445 + cdc4(G439S):G418	c	W303	3B
CCY3645	CCY3445 + mps1(V631M):G418	c	W303	3B; EV3B
CCY3646	CCY3445 + dam1(3D):G418	c	W303	4C
CCY3684	MATa; ura3-1; leu2;3-112; his3-11; trp1-1; ade2-1; cdc4(G439S):G418	c	W303	EV2B
CCY3688	CCY1905 + dad1(N43S):G418	c	W303	2B

Table EV1

CCY3694	CCY1905 + ask1(S216F):G418	c	W303	2B
CCY3730	MATa; ura3-1; leu2;3-112; his3-11; trp1-1; ade2-1; LYS2+; mps1(V631M):G418	c	W303	EV2B
CCY3736	MATa; ura3-1; leu2;3-112; his3-11; trp1-1; ade2-1; LYS2+; dam1(3D):G418	c	W303	4D
CCY3745	MATa; ura3-1; leu2;3-112; his3-11; trp1-1; ade2-; LYS2+; duo1(P17L):G418	c	W303	4D; EV2B; EV2E
CCY3750	CCY1905 + dad2(K11Q):G418	c	W303	2B
CCY3808	MATα; ura3-1; leu2;3-112; his3-11; trp1-1; ade2-1; LYS2+; NUF2-mRuby3:Hygro; DAD3-mNeonGreen:NAT	c	W303	5B; 5C; 5D
CCY3809	CCY3808 + duo1(P17L):G418	c	W303	5B; 5C; 5D
CCY3813	CCY3808 + cdc4(G439S):G418	c	W303	5B; 5C; 5D
CCY3816	CCY3808 + mps1(V631M):G418	c	W303	5B; 5C; 5D
CCY3821	CCY3808 + dad1(N43S):G418	c	W303	5B; 5C; 5D
CCY3852	MATa; ura3-1;leu2;3-112;his3-11;trp1-1;ade2-1;ADE2;Nuf2-mCherry::G418;pGal-3HA-Sli15::HIS3	c	W303	EV4B
CCY3880	MATa; ura3-1; leu2;3-112; his3-11; trp1-1; ade2-1; lys2Δ; ipl1-321	c	W303	3A; EV2F
CCY3910	CCY3445 + dam1(S20D):G418	c	W303	4C
CCY3917	CCY1905 + dam1(S218A;S221A):G418	c	W303	EV3D
CCY3921	MATa; ura3-1; his3-11, ade2-1; lys2Δ; can1-100 bar1Δ; ipl1-321; PDS1-18myc::LEU2; trp1-1:lacO:TRP1; dad2(K11Q):G418	c	W303	3A
CCY3950	MATa; ura3-1; leu2;3-112; trp1-1:256lacO: lys2Δ; ade2-1; can1-100 bar1Δ; pCUP1-GFP12-lacI12:HIS3; ipl1-321; dad1(N43S):G418;	c	W303	3A
CCY4093	MATa, ura3-1; leu2;3-112; his3-11; trp1-1; dam1(S20D):G418	c	W303	4D; EV2E
CCY4106	MATa; ipl1-321; PDS1-18myc::LEU2; trp1-1:lacO:TRP1; ura3-1; leu2;3-112: pCUP1-GFP12-lacI12:HIS3 trp1-1:256lacO: lys2Δ; spc34(D119A):G418	c	W303	3A
CCY4108	CCY3808 + dad2(K11Q):G418;	c	W303	5B; 5C; 5D
CCY4201	MATα; ura3-1; leu2;3-112; his3-11; trp1-1; ade2-1; Sli15-6HA::NAT; Ipl1-3HA::HYG	c	W303	EV4A
CCY4254	CCY3808 + dam1(S20D):G418	c	W303	5B; 5C; 5D
CCY4271	MATa PDS1-18myc::LEU2; ade2-1; his3-11; dam1(S20D):G418; DAD3-mNeon:NAT; duo1(P17L):G418	c	W303	EV2E; EV2F
CCY4329	MATa; ura3-1; leu2;3-112; his3-11; trp1-1; ade2-1; Sli15-6HA::NAT; Ipl1-3HA::HYG; cdc4(G439S):G418;	c	W303	EV4A
CCY4834	MATa; ura3-1; leu2;3-112; his3-11; trp1-1; ade2-1; dad1(N43S):G418	c	W303	EV2B
CCY4854	MATα; ura3-1; leu2;3-112; his3-11; trp1-1; ade2-1; BUB3-mNeonGreen:NAT; NUF2-mRuby3:Hygro; dad1(N43S):G418	c	W303	3B
CCY4863	MATα; ura3-1; leu2;3-112; his3-11; trp1-1; ade2-1; BUB3-mNeonGreen:NAT; NUF2-mRuby3:Hygro; spc34(D119A):G418	c	W303	3B
CCY4911	MATa; ura3-1; leu2;3-112; his3-11; trp1-1; ade2-1; pRS316::URA3	c	W303	2C; 3C; 4E; EV2D
CCY4913	CCY4911 + duo1(P17L):G418	c	W303	3C; 4E; EV2D
CCY4915	CCY4911 + dad1(N43S):G418	c	W303	3C
CCY4921	CCY4911 + cdc4(G439S):G418	c	W303	3C
CCY4923	CCY4911 + mps1(V631M):G418	c	W303	3C

Table EV1

CCY4925	CCY4911 + dam1(S20D):G418	c	W303	4E; EV2D
CCY4927	CCY4911 + dam1(3D):G418	c	W303	4E
CCY4929	MATa; PDS1-18myc::LEU2; DAM1::dam1(S20D):G418; DAD3-mNeonGreen:NAT; DUO1::duo1(P17L):G418; pRS316::URA3	c	W303	EV2D
CCY4933	CCY4968 + duo1(P17L):G418	c	W303	2C
CCY4935	CCY4968 + dad1(N43S):G418	c	W303	2C
CCY4937	CCY4968 + dad2(K11Q):G418	c	W303	2C
CCY4939	CCY4968 + spc34(D119A):G418	c	W303	2C
CCY4947	CCY4968 + mps1(V631M):G418	c	W303	2C
CCY4949	CCY4968 + cdc4(G439S):G418	c	W303	2C
CCY4968	MATa; Bir1Δ:HYG; ura3-1; leu2;3-112: pCUP1-GFP12-lacI12:HIS3 trp1-1:256lacO: lys2Δ; can1-100 bar1Δ; pRS316::URA3	c	W303	2C
CCY4997	MATa; Bir1Δ:HYG; ura3-1; leu2;3-112: pCUP1-GFP12-lacI12:HIS3; can1-100; bar1Δ; pCC598::URA3; leu2;3-112; trp1-1:lacO:TRP1; lys2Δ; dam1(S20D):G418	c	W303	4B
CCY5001	MATa; Bir1Δ:HYG; ura3-1; leu2;3-112: pCUP1-GFP12-lacI12:HIS3; trp1-1; pCC598::URA3; dam1(3D):G418	c	W303	4B
CCY5101	MATa/α; ura3-1; leu2;3-112; his3-11; trp1-1; ade2-1; ura3-1; leu2;3-112; his3-11; trp1-1; DAM1/dam1(S20D):G418; DUO1/duo1(P17L):NAT	c	W303	EV2C
CCY5107	MATa/α; ura3-1; leu2;3-112; his3-11; trp1-1; ade2-1; ura3-1; leu2;3-112; his3-11; trp1-1; DAM1/dam1(S20D):G418; CDC4/cdc4(G439S):NAT	c	W303	EV2C
CCY5109	MATa/α; ura3-1; leu2;3-112; his3-11; trp1-1; ade2-1; ura3-1; leu2;3-112; his3-11; trp1-1; DAM1/dam1(S20D):G418; MPS1/mps1(V631M):NAT	c	W303	EV2C
CCY5119	MATa/α; ura3-1; leu2;3-112; his3-11; trp1-1; ade2-1; ura3-1; leu2;3-112; his3-11; trp1-1; DAM1/dam1(S20D):G418; DAD1/dad1(N43S):NAT	c	W303	EV2C
CCY5282	MATa; ura3-1; leu2;3-112; his3-11; trp1-1; ade2-1; pRS316::URA3; ctf19Δ:G418	c	W303	2C; 3C; 4E; EV2D
CCY5326	MATa; ura3-1; leu2;3-112; his3-11; trp1-1; ade2-1; ADE2; Nuf2-mCherry::G418; pGal1-3HA-Sli15::HIS3; mNeonGreen-6HA-Sli15::URA3; pGal-Sgo1::HYG	c	W303	6B; EV4C
CCY5373	CCY3445 + dad2(K11Q):G418	c	W303	3B
CCY5376	MATa; ura3-1; leu2;3-112; his3-11; trp1-1; ade2-1; spc34(D119A):G418	c	W303	EV2B
CCY5377	MATa; ura3-1; leu2;3-112; his3-11; trp1-1; ade2-1; dad2(K11Q):G418	c	W303	EV2B
CCY5420	MATa; ura3-1; leu2;3-112; his3-11; trp1-1; ade2-1; spc34(D119A):G418; pRS316::URA3	c	W303	3C
CCY5422	MATa; ura3-1; leu2;3-112; his3-11; trp1-1; ade2-1; dad2(K11Q):G418; pRS316::URA3	c	W303	3C
CCY5424	MATa/α; Bir1Δ/Bir1Δ:HYG; ura3-1; leu2,3-112: pCUP1-GFP12-lacI12:HIS3 trp1-1:256lacO: lys2Δ can1-100 bar1Δ; pCC598::URA3	c	W303	EV3A
CCY5435	MATa; ura3-1; leu2;3-112; his3-11; trp1-1; ade2-1; ADE2; Nuf2-mCherry::G418; pGal1-3HA-Sli15::HIS3; mNeonGreen-6HA-Sli15::URA3	c	W303	6B; EV4B; EV4C
CCY5469	MATa; ura3-1; leu2;3-112; his3-11; trp1-1; ade2-1; ADE2; Nuf2-mCherry::G418; pGal1-3HA-Sli15::HIS3; mNeonGreen-6HA-Sli15::URA3; pGal-Sgo1::HYG cdc4(G439S):NAT	c	W303	6B; EV4C

Table EV1

CCY5508	MATa; ura3-1; leu2;3-112; his3-11; trp1-1; ade2-1; ADE2; Nuf2-mCherry::G418; pGal1-3HA-Sli15::HIS3; mNeonGreen-6HA-Sli15::URA3; cdc4(G439S):NAT	c	W303	6B;EV4B; EV4C
CCY5512	MATa/α; ura3-1; leu2;3-112; his3-11; trp1-1; ade2-1; ura3-1; leu2;3-112; his3-11; trp1-1; dad2(K11Q):NAT; dam1(S20D):G418	c	W303	EV2C
CCY5518	MATa/α; ura3-1; leu2;3-112; his3-11; trp1-1; ade2-1; ura3-1; leu2;3-112; his3-11; trp1-1; spc34(D119A):NAT; dam1(S20D):G418	c	W303	EV2C
CCY5524	CCY3808 + spc34(D119A):G418	c	W303	5B; 5C; 5D
CCY5532	CCY1905 + met30-6:G418	c	W303	6A
CCY5535	CCY1905 + cdc4-1:G418	c	W303	6A
CCY5678	CCY1887 + duo1(P17L):NAT	c	W303	EV1B
CCY5680	CCY1887 + cdc4(G439S)NAT	c	W303	EV1B
CCY5682	CCY1887 + mps1(V631M):NAT	c	W303	EV1B
CCY5684	CCY1946 + duo1(P17L):NAT	c	W303	EV1B
CCY5686	CCY1946 + cdc4(G439S):NAT	c	W303	EV1B
CCY5688	CCY1946 + mps1(V631M):NAT	c	W303	EV1B
CCY5690	bir1Δ-ad(50C) + pCC598::URA3	c	W303	EV1C
CCY5692	bir1Δ-ad2(50C) + pCC598::URA3	c	W303	EV1C
CCY5694	bir1Δ-ad(62F) + pCC598::URA3	c	W303	EV1C
CCY5696	bir1Δ-ad2(62F) + pCC598::URA3	c	W303	EV1C
CCY5698	bir1Δ-ad(58B) + pCC598::URA3	c	W303	EV1C
CCY5700	bir1Δ-ad2(58B) + pCC598::URA3	c	W303	EV1C
CCY5706	MATa; Bir1Δ:HYG; ura3-1; leu2,3-112: pCUP1-GFP12-lacI12:HIS3 trp1-1:256lacO: lys2Δ; can1-100 bar1Δ; pCC598::URA3; DUO1::duo1(P17L):NAT; UBP6::ubp6(E256X):G418	c	W303	EV1A
CCY5708	MATa; Bir1Δ:HYG; ura3-1; leu2,3-112: pCUP1-GFP12-lacI12:HIS3 trp1-1:256lacO: lys2Δ; can1-100 bar1Δ; pCC598::URA3; CDC4::cdc4(G439S):NAT; UBP6::ubp6(E256X):G418	c	W303	EV1A
CCY5710	MATa; Bir1Δ:HYG; ura3-1; leu2,3-112: pCUP1-GFP12-lacI12:HIS3 trp1-1:256lacO: lys2Δ; can1-100 bar1Δ; pCC598::URA3; MPS1::mps1(V631M):NAT; UBP6::ubp6(E256X):G418	c	W303	EV1A
CCY5713	MATa/α; LEU2/ley2,3-112;his3-11:pCUP-GFP12-lacI:HIS3; trp1-1:256lacO:TRP1; lys2Δ; ADE2/ade2-1;can1-100 bar1D; BUB1::HYG; DUO1::duo1(P17L):G418; SLI15::NAT	c	W303	EV2A
CCY5736	CCY5678 + chr8 disomy	c	W303	EV1B
CCY5738	CCY5680 + chr8 disomy	c	W303	EV1B
CCY5740	CCY5682 + chr8 disomy	c	W303	EV1B
CCY5742	CCY5684 + chr10 disomy	c	W303	EV1B
CCY5744	CCY5686 + chr10 disomy	c	W303	EV1B
CCY5746	CCY5688 + chr10 disomy	c	W303	EV1B
CCY5752	MATα; ura3-1; leu2;3-112; his3-11; trp1-1; ade2-1; LYS2+; DUO1::duo1(P17L):NAT; ipl1-321;DAM1::dam1(S20D):G418	c	W303	EV2F
CCY5754	MATα; ura3-1; leu2;3-112; his3-11; trp1-1; ade2-1; LYS2+; DUO1::duo1(P17L):NAT; ipl1-321;DAM1::dam1(S20D):G418	c	W303	EV2F

Table EV1

CCY5755	MATα; ura3-1; leu2;3-112; his3-11; trp1-1; ade2-1; LYS2+;DUO1::duo1(P17L):NAT;DAM1::dam1(S20D):G418	c	W303	EV2F
CCY5756	CCY1887 + chr8 disomy	c	W303	EV1B
CCY5759	CCY1946 + chr10 disomy	c	W303	EV1B

Cell line	**Description**	**Source**	**Figure/s**
Clone C3	HAP1 $TP53^{-}$	e	6C; EV5C
CCH2248	HAP1 $TP53^{-}$, $FBXW7^{G437S}$(clone 1)	c	6C; EV5C
CCH2251	HAP1 $TP53^{-}$, $FBXW7^{G437S}$(clone 2)	c	6C; EV5C
CCH2254	HAP1 $TP53^{-}$, $FBXW7^{G437S}$(clone 3)	c	6C; EV5C

Plasmid	**Description**	**Source**
pRS306	pBluescript + URA3	d
pRS316	pBluescript + URA3	d
pCC598	BIR1 + 1000 bases upstream in pRS306	b
pCC-H046	Repair plasmid for $FBXW7^{G437S}$	c

a – Campbell and Desai; Nature 497: 118-121 (2013)
b – Ravichandran et al; Genes and Development (2018)
c – This study
d – Sinorski and Hieter Genetics 122: 19-27 (1989)
e – J. Loizou lab

4. Discussion and outlook

Cancer can only develop when cells bypass pathways which keep cell division under control (Kuilman *et al.,* 2010; Yamamoto & Iwakuma, 2018; Mantovani *et al.,* 2019; Hu *et al*., 2021). How this occurs exactly is still unclear, but what we do know is that cells tend to use various genetic alterations (including genetic mutations, epigenetic dysregulation, missegregation and aneuploidy) as a means to bypass the pathways which keep cell division under control. Furthermore, we know that 90% of solid tumors have complex aneuploidies and approximately 70% of hematopoietic cancers have this too (Weaver & Cleveland, 2006). This means aneuploidy is one of the most common traits found in cancer, and likely contributes to tumorigenesis. Cancers also tend to have very high rates of lagging chromosomes; a commonly accepted sign of disrupted chromosome segregation. Although the precise mechanisms behind the cause of CIN in cancer remains unknown, it is commonly accepted that a major factor is the formation of KT-MT attachments, particularly erroneous attachments, that are too stable (Bakhoum *et al*., 2009). The mechanisms normally in place to destabilize such attachments are therefore impaired in cancers. The genetic diversity provided by CIN and aneuploidy helps cancer evade detection by the immune system, as well as gain resistance to commonly used therapeutics (Davoli *et al*., 2017). In vertebrate cells, the overexpression of certain kinesins increases KT-MT turnover and can cause a decrease in mitotic errors in cancer (Walczak *et al.,* 1996; Kline-Smith and Walczak, 2002). To further elucidate the pathways that allow for tumorigenesis, the mechanisms which govern adaptation to overstabilization is of high importance.

In this study, in order to clarify how cells can adapt to CIN, we impaired CPC function through deletion of Bir1. Using NGS we analyzed the genetic changes that occurred after these *bir1Δ* cells were given time to adapt. The model we presented holds that cells can take different paths toward an ideal aneuploid karyotype. Initially, it is this aneuploid karyotype that ameliorates the detriments caused by CPC malfunction (Ravichandran *et al*., 2018;2020). In this study, both haploid and diploid yeast cells were deleted of Bir1 homozygously, and allowed to grow and adapt. The main assays used here included cellular fitness assays, NGS to determine karyotypic changes, as well as statistical analyses to determine chromosome copy number interactions (CCNIs) between aneuploid chromosomes. The paths for adaptation to *bir1Δ* were quite different for the haploid and diploid strains. For instance, the final optimal karyotype differs between haploid and diploid cells. Also, haploids did not regularly gain chromosome 13 and did not experience any chromosome losses. However, the general mode of adaptation for both ploidy types was similar. For example, both ploidies always started by gaining an extra copy of chromosome 2. We concluded that an immediate gain of chromosome 2 is vital for initial survival. The simplest explanation as to why chromosome 2 is so vital for viability is due to the

presence of Sli15. In order to test this, we created yeast strains that had an extra copy of Sli15 on chromosome 5. The addition of this extra copy resulted in the absence of chromosome 2 disomy. Next, we deleted Sli15 on chromosome 2 and added it to chromosome 8. This resulted in a complete absence of chromosome 2 disomy and the unconditional gain of chromosome 8 disomy. Based on these data, we concluded that the requirement for an extra copy of Sli15 is the reason the whole of chromosome 2 is gained. We concluded that an extra copy of Sli15 helps to rescue the stability and function of the dysfunctional CPC complex. Once the gain of chromosome 2 has been achieved, there are multiple pathways the cell can take which provide selective advantages. Ultimately, each of these pathways leads to an optimized karyotype. For haploid cells, the optimal aneuploid karyotype is the gain of chromosomes 2 and 3. Some routes of adaptation adopted by the cell allow for a faster development of the optimal karyotype. For example, the fastest route was when chromosome 3 was gained immediately after the initial gain of chromosome 2. However, some cells may take a longer route by developing aneuploidies which are only partially or transiently advantageous. Despite the advantage provided by these aneuploidies, they also slow down the progression towards the ideal karyotype. The likely reason for this is due to the negative CCNIs between those chromosomes already gained, and the chromosomes required for the optimal karyotype. In haploid cells, partially advantageous chromosomes include chromosome 8 and 10. It should be noted here that a gain of chromosome 8 and 10 together in the same cell is almost never seen. Strains which were engineered to have disomy of 8 and 10 showed a signifcant reduction in growth and cellular fitness. This suggests that there are negative synthetic genetic interactions between chromosome 8 and 10. As a consequence of this, the gain of 8 and 10 simultaneously is highly unfavorable, and does not help the cell to adapt to loss of CPC function. After gain of either chromosome 8 or 10, cells tended to gain chromosome 3, and later lose chromosome 8 or 10 disomy.

In diploids the optimal karyotype is the gain of chromosomes 2, 3, 10, and 13. As with haploids, chromosome 2 is gained initially. Similar to haploids, the cell can either follow a quick path of adaptation, or take detours by developing partially advantageous chromosome gains. Unlike the haploid cells, the diploid cells also experience chromosome losses. Sometimes, after gain of chromosome 2, diploid cells lose a copy of chromosome 9. Ultimately these cells also converge on the optimal diploid karyotype.

The overall conclusions from our study were that CIN and the resultant aneuploidy can provide a highly diverse adaptive mechanism for CPC deficient cells. Initially, cells possess divergent karyotypes but over time, and through persistent missegregation and the CCNIs between gained chromosomes, ultimately converge on an optimal karyotype. It is highly likely that the gain of chromosome 2 is due to the presence of Sli15, but the exact genes which result in the CCNIs observed for other chromosomes are still unclear. The study of CCNIs also has major medical

implications in terms of understanding cancer development. Analyses from this study show certain cancer types (including LGG brain cancers) have significant correlations, both positive and negative, between specific somatic copy number alterations (SCNAs). This suggests the existence of synthetic genetic interactions (CCNIs) between aneuploid chromosomes in cancer. Consequently, the future study of CCNIs in human cells would be invaluable to our understanding of complex aneuploidy karyotype development in cancer.

In order to further understand how CCNIs shape the evolution of specific aneuploid karyotypes in cancer, it would be prudent to elucidate which genetic factors underlie such interactions in budding yeast. Additionally, it is not yet clear if CCNIs work through one specific genetic interaction or clusters of multiple genes on aneuploid chromosomes. A potential study which could be done to clarify this would be to create gene libraries in plasmids for chromosomes 8 and 10. Once this is done, one could transform these plasmids into strains which have been engineered to possess disomy of either chromosome 8 or chromosome 10. Once a combination of genetic factors is found that results in synthetic lethality or sickness, the genes responsible for the negative CCNIs between chromosome 8 and 10 could be identified. Similarly, one could transform the plasmids from the gene library into the original adapted strains which possess multiple aneuploidies, including that of either chromosome 8 or 10. Again, the presence of negative CCNIs would cause synthetic lethality. In these experiments, one could look at the effect several genes have at once, or single genes could be tested at a time. These assays will help us understand more clearly how aneuploid chromosomes interact to trigger synthetic effects. Predicting genetic interactions is difficult and the answers gleaned from these assays could help us predict such interactions in the future. Such predictions would not be just be useful for understanding aneuploidy in yeast but also in human cancer cell-lines.

Our study also revealed a conspicuous lack of compensatory suppressor mutations within the *bir1Δ-ad* strains (Ravichandran *et al*., 2018; Clarke *et al*., 2022). We tested this by first looking for any enrichment of mutant CIN related genes. In the *bir1Δ-ad* strains we found no increase in the number of CIN-gene mutants than would be expected by chance. Next, using a plasmid shuffle assay, we tested whether any of the mutants identified could rescue loss of *bir1Δ*. Indeed, none of the mutants identified in the *bir1Δ-ad* strains we tested could rescue loss of Bir1 (own observations). Altogether, this data suggests that cells first adapt by selecting advantageous aneuploidies and do not acquire genetic suppressors of *bir1Δ* at this stage.

Another mechanism which could allow for better growth in CPC deficient cells is the accumulation of mutations which allow for the tolerance of particular aneuploidies instead of CIN itself. These have previously been described in budding yeast by Torres *et al* (2010). Instead of suppressing CIN itself, certain mutations in yeast aid in adaptation to aneuploidy of particular chromosomes. However, none of

these previously determined aneuploidy-tolerating mutants were identified in our study. One such mutation was the nonsense mutant in Ubp6 (*ubp(E256X)).* Loss of Ubp6 function leads to overactivation of the proteasomal degradation pathway. It is this overactivation that is thought to aid cells in coping with increased protein expression (Torres *et al*., 2010; Oromendia *et al*., 2012). Notably, this nonsense mutation was only associated with tolerance of disomy for chromosomes 5, 8, 9 and 11. Of all these chromosomes only chromosome 8 was commonly seen to be disomic in our studies.

Additionally, the *ubp6(E256X)* nonsense mutation was engineered in a plasmid shuffle strain, and we found that it did not rescue loss of Bir1. Furthermore, combinations of CPC suppressors together with the *ubp6(E256X)* mutant did not show any changes in growth fitness. In addition to this, when confirmed *bir1Δ* suppressors are combined with disomy of chromosome 8 or 10 they did not show any difference in growth when compared to aneuploid strains alone. Taken together, these results suggest that the strains do not adapt by developing resistance to specific aneuploidies.

It is highly intriguing that the *ubp6(E256X)* mutant only allows tolerance of certain disomies (Torres *et al*., 2010) and does not rescue loss of Bir1. Furthermore, loss of Ubp6 function does not aid the growth of those strains which have disomy of chromosome 2. In fact, it seems that strains with disomy of chromosome 2 alone grow better than when combined with *ubp6(E256X)* (Torres *et al.,* 2010). It is possible that the need for chromosome 2 disomy in *bir1Δ* cells is simply incompatible with the Ubp6 mutant. This incompatibility would explain why the *ubp6(E256X)* does not aid loss of Bir1. Furthermore, the presence of multiple disomies together with such aneuploid-tolerating mutations has not yet been studied. To help move the field forward, one could engineer double disomy of chromosomes 8 and 2 in a strain which also possesses the *ubp6(E256X)* mutant. This would quickly provide insight into whether the benefits between chromosome 8 disomy and *ubp6(E256X)* are inhibited by the presence of chromosome 2 disomy. The disomy of chromosome 2 could perturb this growth benefit either wholly, partially or not at all. The conclusions from this growth fitness assay would further our understanding of how aneuploidy-tolerating mutations function with multiple disomies.

Next, one could use the strains already engineered to have Sli15 relocated to chromosome 8 to do another fitness assay, this time with or without *ubp6(E256X)*. As we showed previously (Ravichandran *et al*., 2018), after Bir1 deletion, the presence of the relocated Sli15 leads to the unconditional gain of chromosome 8, which should be compatible with *ubp6(E256X)* (Torres *et al*., 2010). If chromosome 8 disomy (with Bir1 deletion) in combination with *ubp6(E256X)* is viable, it would mean that it is the specific gain of chromosome 2, which is incompatible with aneuploidy tolerance granted by *ubp6(E256X).* However, if the combination of chromosome 8 disomy and *ubp6(E256X)* is not viable, then the gain of chromosome 2 is not responsible for the incompatibility observed. Given the results from Torres *et al.,*

(2010) this would be surprising. Perhaps in this case the extra copy of Sli15 could be the culprit. This could be tested by adding an extra copy of Sli15 under an inducible galactose-promoter to strains with *ubp6(E256X).* After induction of the extra copy of Sli15 using galactose, one could simply test the viability of these strains. If synthetic lethality is seen between Sli15 overexpression and *ubp6(E256X)*, this could explain why the *ubp6(E256X)* mutation does not aid adaptation to disomy of chromosome 2 (*bir1Δ*). This would show that even a single gene can dictate such interactions between aneuploid chromosomes. The assays mentioned above would be vital for clarifying the mechanisms that control the benefits provided by aneuploidy-tolerating mutants. To reiterate, by investigating the mechanisms that control genetic interactions in aneuploid strains, as well as why some aneuploidy-tolerating mutants are karyotype specific, will lay the foundations for a better understanding of such interactions in cancer.

Despite the initial advantages provided by aneuploidy, studies show that aneuploidy is not a sustainable solution to stress over long periods of time. This is especially true when cells are grown in media with minimal nutrients (Yona *et al*., 2012). In short, the inherent protein production imbalances caused by aneuploidy, as well as simply having more chromosomes to segregate and higher demands on resources, leads to stresses the cell cannot ignore (Torres *et al*., 2007; 2010; Yona *et al*., 2012; Oromendia *et al*., 2012; Pavani *et al*., 2021).

As has been discussed above, the presence of Sli15 on chromosome 2 is most likely the reason it is disomic in adapted strains. However, if the cell could simply, through Sli15 dependent genetic or epigenetic alterations, restore CPC activity directly instead of gaining an extra copy of the whole chromosome, this would help the cell avoid proteotoxicity caused by the extra production of all other genes on chromosome 2. Indeed, Yona *et al* (2012) showed that in the case of heat stress, cells often cope by gaining trisomy of chromosome 3. However, over time the cell eventually favors upregulating expression levels of several genes on chromosome 3, thus rendering the need for extra chromosome 3 obsolete.

Based on this evidence, as well as the conspicuous lack of suppressor mutants in the haploid *bir1Δ-ad* strains, we decided to grow the haploid *bir1Δ-ad* strains for a further 21 days (200 generations). This allowed us to understand how these strains (*bir1Δ-ad2*) continue to adapt after initial adaptation through diverse aneuploidy karyotypes. Finally, we were able to identify an enrichment in mutant CIN-related genes in the haploid *bir1Δ-ad2* strains. Furthermore, haploid strains which were allowed to grow for longer had less total aneuploidy and grew better in the presence of a microtubule destabilizing agent: benomyl. The presence of these mutations further suggests that mutations which more specifically rescue the source of CIN are selected during later stages of adaptation.

It must be stressed that the mutations from *bir1Δ-ad2* that we identified and tested were not restricted to those known to be related to CIN by Gene Ontology

(GO) annotations. Instead, we decided to give higher priority to those mutations which 1) induced non-synonymous changes, 2) were found in essential genes, and 3) which occurred multiple times in independent strains. Indeed, not all the mutations found in the *bir1Δ-ad2* population that we tested suppressed loss of CPC function. The mutations identified in Mif2 (part of the inner kinetochore) as well as Rtg2, a protein essential for mitochondrial signaling (Jazwinski *et al*., 2005), showed no improvement in growth after Bir1 deletion. Although one might speculate that a mutation in Mif2, due to its essential involvement in kinetochore formation (Cohen *et al* 2008; Hornung *et al*., 2014; Xiao *et al*., 2017; Fischböck-Halwachs *et al*., 2019), can destabilize KT-MT attachments, it seems that the mutation identified here is not sufficient to rescue loss of CPC function. Also, despite identifying multiple distinct mutations in Rtg2, these were not able to restore growth in *bir1Δ* strains either.

Using the plasmid shuffle assay, we determined that multiple mutations in distinct pathways rescued loss of CPC function. We also noticed that the adapted strains, which harbored confirmed suppressors, possessed significantly less aneuploid chromosomes as well as increased growth fitness (with or without benomyl) in comparison to those strains that did not possess suppressors. Also, those strains, which possessed the suppressor mutations, tended to have the optimal karyotype, where as those that did not still tended to possess intermediary karyotypes. The takeaway from this is that the suppressor mutations can influence the optimal karyotype. While the NGS data we acquired showed us the karyotypes of the adapted strains, it is still not clear what aneuploid karyotypes are present in those strains engineered to have individual suppressor mutations. In order to determine whether or not these suppressors influence the optimal karyotype, one could simply use the *bir1Δ* suppressor-engineered strains to do an adaptation test. After the strains have been given time to adapt, one could test the presence of aneuploid chromosomes as well as novel mutations by using NGS. This would provide significant insight into how CIN suppressors influence the karyotypes of adapting strains. Furthermore, this would be highly medically relevant in terms of cancer evolution.

A minichromosome loss assay showed that these confirmed suppressors also significantly improve segregation fidelity in *bir1Δ* strains. One of the first set of suppressor mutations discovered was in the CPC itself; namely Sli15. It is important to note that two *bir1Δ-ad2* strains which possessed Sli15 mutants, *sli15(L71S)* and *sli15(G334S)*, were the only two adapted strains which lost disomy of chromosome 2. This is not surprising because previous studies have shown that mutations in Sli15, either by deletion of the N-terminus (*sli15(Δ2-228)* or *sli15-ΔNT*) or the mutation of Cdk1 phosphosites (*sli15-6A*), can rescue *bir1Δ* (Campbell & Desai, 2013).

The loss of Bir1 disrupts both CPC localization to the inner centromere as well as CPC stoichiometry. After loss of Bir1 western blots show Sli15 protein levels

become undetectable (Campbell & Desai, 2013). This suggests loss of Bir1 leads to increased degradation of the CPC. Assays which measure the proportion of viable spores show that combining *bir1Δ* with either *sli15-ΔNT* or *sli15-6A* rescues loss of viability (Campbell & Desai, 2013). This suggests that the loss of Bir1 now only has a limited effect on the stability of the CPC. Due to the rescue of viability it is highly likely that the *sli15-ΔNT* does indeed restore CPC stability. However, in order to verify this completely one could do a western blot for CPC subunits in *sli15-ΔNT/bir1Δ*, *sli15(L71S)*/*bir1Δ,* and *sli15(G334S)*/*bir1Δ* double-mutant strains. In *bir1Δ* strains, Sli15 is absent from the western blot. However, if the double-mutant shows the presence of Sli15 has returned, then mutating the CEN box does indeed rescue Sli15 stability in a *bir1Δ* background.

The suppressor mutation *sli15(G334S)* is adjacent to a Cdk1 phosphosite S335 (Marsoner *et al.*, 2022; Campbell & Desai, 2013). The mutation of Cdk1 phosphosites has been previously shown in literature to reduce CIN (Campbell & Desai, 2013). Furthermore, *sli15-ΔNT* and *sli15-6A* show an increased affinity for microtubule binding during cell division. It is therefore possible that the Sli15 suppressor mutants identified in the CEN box, or near the Cdk1 site, increase the amount of CPC at the mitotic spindle. This increase in CPC binding may compensate for the disomy provided by chromosome 2. In order to test this one could do live-cell fluorescence microscopy. Simply label CPC subunits and microtubules with a fluorophore in the *sli15(71S*) and *sli15(G334S)* mutant strains and then measure the amount of colocalization at the mitotic spindle during cell division. If these mutants do not cause CPC enrichment at the spindle, this would suggest they rescue *bir1Δ* independently of increased microtubule binding. These assays would clarify further whether or not CPC specific CIN suppressors function by increased microtubule binding.

While the *sli15(L71S)* mutant resulted in loss of chromosome 2 disomy, the disomy of chromosome 3 remained. Intriguingly, the only strain which completely lost all aneuploidy, and returned to a euploid state, was the same strain that contained the *sli15(G334S)* mutant. If *sli15(G334S*) does indeed increase microtubule binding, it would suggest that increasing the microtubule binding affinity of the CPC could compensate for the disomy of all chromosomes. This would make the study of such a mutant a priority. To test this further, one could engineer plasmid shuffle strains with the *sli15(6A)* mutant, the *sli15-ΔNT* mutant, and the *sli15(G334S)* mutant individually. Next, one could delete Bir1, grow the strains for 21 days and then determine the karyotypes by using q-PCR or NGS. If the increased mitotic spindle binding of Sli15 is the reason for loss of all aneuploidies than *sli15(G334S), sli15(6A)* and the *sli15-ΔNT* mutants should allow for this as well. However, if these fail to induce euploidization then the *sli15(G334S)* may be a passenger mutation rather than the specific cause of euploidization. Also, in the event these Sli15 mutations revert the karyotypes of the *bir1Δ* cells to euploid, this could potentially act as a

useful tool for euploidization of strains, which may be useful in the field of aneuploidy research.

Additionally, to further test the contribution microtubule binding has on *bir1Δ* rescue, one could swap the MTB domain in Sli15 for an MTB domain from Stu2. If it is purely the enhanced microtubule binding activity of Sli15 that rescues loss of *bir1Δ,* then overexpression of Sli15 with Stu2's MTB in a *bir1Δ* strain should also rescue growth. Elucidating how increased CPC binding at the spindle contributes to CIN suppression is highly relevant to understanding how cancers adapt to overstabilized attachments.

The next group of suppressor mutations is by far the most prominent. At least seven distinct mutations were identified in members of the outer kinetochore. A mutation in Ndc80 (*ndc80(K181N))* showed improved growth after loss of CPC function. The same results were seen with the mutation we identified in Spc105 (*spc105(R583G*)). As has been discussed in the introduction, the Ndc80 as well as Spc105 complexes are highly important for outer-kinetochore assembly, microtubule binding and SAC activation (DeLuca *et al.,* 2006; Sarangapani *et al.*, 2013). Also, the mutations identified are located in the coiled-coil (CC) domain of Ndc80 and the CH domain of Spc105. It is therefore likely that these mutations interrupt the function of the protein, which results in reduced KT-MT attachment stability. It is this reduction in KT-MT stability that rescues the overstabilization caused by *bir1Δ*.

Although the suppressors in the Ndc80 and Spc105 complexes rescue growth detriments, the mutations identified in the Dam1 complex showed a far greater improvement in both growth and segregation fidelity. The only exception to this was the mutation in Ask1 (*ask1(S216F))* which did not rescue growth. Duo1, Dad1, Dad2 and Spc34 are relatively small proteins (ranging from roughly 90kDa to 300kDa) and do not possess any known functional domains. If these mutations rescue loss of Bir1 by causing destabilization of KT-MT attachments, this would result in an increase in unattached kinetochores. This in turn would lead to an increase in SAC activity, which can be monitored using fluorescence microscopy assays. A member of the SAC, Bub3, was tagged with an mNeonGreen fluorophore and a member of Ndc80 complex, Nuf2, was tagged with an mRuby3 fluorophore. By measuring the incidence of colocalization, we found that mutations in the Dam1 complex increased the amount of SAC activity during prometaphase. Furthermore, these suppressor mutants can also rescue loss of a temperature-sensitive Ipl1 allele (*ipl1-321*). Altogether, this suggests these Dam1 complex suppressor mutants are able to substitute the loss of CPC activity. Overall, these data suggest the mutants in the Dam1 complex cause KT-MT destabilization. Now that we have sufficient evidence to show that these Dam1 complex mutations are likely functioning by destabilizing KT-MT attachments directly, the next question which arises is: how exactly is this destabilization mediated?

The Dam1-complex ring is established by the oligomerization of several decamers (Jenni & Harrison, 2018; Ng *et al*., 2014). Based on structural analyses performed by Jenni & Harrison (2018) there are two major interfaces between such decamers. These interfaces are essential for oligomerization and establishing the ring structure of the Dam1 complex. The same structural analyses revealed that the N-terminus of Duo1 resides near interface 1, which is vital for Dam1-complex oligomerization. The *bir1Δ* suppressor mutation in Duo1 (*duo1(P17L))* is located at the N-terminus. Also, the mutation *spc34(D119A)* is likely proximal to interface 1. This suggests that the mutations present in Duo1 and Spc34 interrupt interface 1.

Additionally, we discovered that mutations in Dad2 and Dad1 are near to and likely affect interface 2. The mutation we identified in Dad1 (*dad1(N43S))* affects a highly conserved residue, which resides on the surface of the decamer, and very likely disrupts Dam1-complex oligomerization. We know this based on microscopy assays which show reduced Dam1 complex microtubule binding during prometaphase and anaphase. However, only *dad1(N43S)* significantly reduced Dam1 complex levels at the kinetochore during anaphase. These data show that the mutations in the Dam1 complex result in reduced oligomerization and microtubule binding affinity in prometaphase and anaphase. These results suggest the Dam1 complex mutants interfere with Dam1 complex oligomerization and microtubule binding, thus reducing KT-MT attachment stability. It is still not clear exactly how these mutants affect Dam1 complex assembly. As mentioned in the introduction, Dam1 rings can either be whole or partial. Additionally, it is still unclear how partial rings affect the stability of KT-MT attachments as well as segregation fidelity *in vivo* (Ng *et al*., 2019). In order to test this, one could engineer mutants at a single (or both) interface and perform similar biological and structural analyses (including cryo-EM) utilized by Ng *et al.,* (2019). This would measure the proportion of partial versus whole Dam1 rings in the mutants in comparison to wild-type cells. If there is a greater prevalence of partial rings in the mutant strains, this would provide evidence that mutations at the interfaces disrupt whole ring formation. This would also suggest that partial Dam1 rings do not form as robust KT-MT attachments as wild-type Dam1-complex. If performed in parallel with microtubule pelleting assays, the structural analyses would clarify how partial ring assemblies contribute to attachment stability and segregation *in vivo*. Additionally, if the mutations proximal to the interfaces specifically perturb ring formation, this would provide further evidence that it is the specific disruption of these interfaces that results in complex instability. To further verify whether or not these mutations affect KT-MT stability, one could do an optical-trap assay and measure mean rupture force. Reduced rupture force would confirm their involvement in KT-MT instability. Altogether, these experiments would verify the manner in which such mutants affect Dam1 stability, as well as provide insight into how partial Dam1 ring assemblies affect segregation *in vivo*.

Mutations in Dam1 which affect microtubule binding affinity have been previously characterized (Cheeseman *et al*., 2002; Sarangapani *et al*., 2013). There

are four Ipl1 phosphorylation sites on Dam1 which control its binding affinity for microtubules. As previously mentioned in the introduction, mutations which mimic phosphorylation in the C-terminal phosphosites, *dam1-3D,* result in an overactive SAC, and arrested anaphase onset. However, when the most N-terminal site is mutated to a phosphomimic (*dam1(S20D)*), there is no difference in cell-cycle timing. In contrast to what one might expect, the level of SAC activity is similarly elevated in the *dam1(S20D)* mutant as it is in the *dam1-3D* mutant. What is even more striking is that all yeast strains which have mutants in the Dam1 complex show similar elevated levels of SAC activity as the *dam1-3D,* and yet none except the *dam1-3D* show any delay in anaphase onset (Jin & Wang, 2013). Additionally, data provided by our minichromosome loss assays shows us that the *dam1-3D* mutant does not cause any increase in missegregation. This helps to explain why *dam1-3D* does not rescue loss of Bir1; it may overactivate the SAC but it does not do this via enhanced KT-MT instability. Hence, the *dam1-3D* mutant triggers the SAC independently of inducing KT-MT instability. However, a more conclusive answer as to why this occurs requires further experiments which dissect the specific mechanisms which trigger anaphase delay in the *dam1-3D* mutant. It has been speculated that the *dam1-3D* mutant causes overactive SAC signal by inhibiting SAC silencing.

It is already known that loss of Mad1 or Mad2 in combination with the *dam1-3D* mutant rescues anaphase arrest (Jin & Wang, 2013). However, Mad1 and Mad2 are involved in the SAC pathway downstream of many other proteins including Mps1, Spc105, Bub1 and Bub3 (**Figure5**). To test the *dam1-3D* mutant further, one could add an inducible Spc105 mutant transgene, which cannot be phosphorylated by Mps1, and combine this with *dam1-3D*. After inducing expression of the Spc105 mutant one could test if the anaphase arrest caused by *dam1-3D* is lost. If the anaphase arrest caused by *dam1-3D* disappears this would mean that *dam1-3D* acts upstream of Spc105 to activate the SAC. The data from such experiments would finally answer exactly where in the SAC pathway the *dam1-3D* mutant acts, thereby providing insight into the mystery behind *dam1-3D* mediated anaphase-arrest.

Although the *dam1(S20D)* mutant does not trigger anaphase arrest, it does indeed have a significant destabilizing effect on KT-MT attachments. Furthermore, the Dam1(S20) site is thought to be important for Dam1 complex oligomerization (Jenni & Harrison). In our study we found, just like the other Dam1 complex suppressors, the *dam1(S20D)* mutant caused elevated levels of SAC activity at the kinetochore, and rescued loss of Bir1. Furthermore, the Dam1-complex in *dam1(S20D)* mutants showed reduced microtubule binding affinity during prometaphase. If the Dam1 complex suppressor mutants and the *dam1(S20D)* mutant function via the same mechanism, then the combination of the two mutants should result in negative genetic interactions. When combined, the *dam1(S20D)* mutant and the *duo1(P17L)* or *dad2(K11Q)* mutants result in reduced spore viability after three to five days. Rare double-mutant colonies that grew up showed severe anaphase delay and high levels of missegregation. Altogether, this evidence

supports the notion that both the *dam1(S20D)* mutants and the Dam1 complex suppressors rescue loss of Bir1 by disturbing Dam1 complex oligomerization and microtubule binding, resulting in the destabilization of KT-MT attachments.

A study by Haase *et al* (2023) used an orthogonal genetic screen in which they humanized yeast chromatin by replacing yeast nucleosomes with human nucleosomes. This resulted in an increase in missegregation. They then showed mutations in the Dam1 complex, strikingly similar to those identified in this study, that allowed for decreased microtubule binding and therefore a higher rate of KT-MT turnover. This is similar to the kind of activity we see at KT-MT attachments with our Dam1 complex suppressors. The data from their study provides evidence that mutations in the Dam1 complex tend to cause KT-MT instability, and that these can rescue both loss of centromeric and CPC function. It would be very interesting to test whether the mutants found in this study also rescue loss of *bir1Δ*. This would provide even more evidence that mutants in the Dam1 complex facilitate KT-MT instability.

One of the major differences between the outer-kinetochore of yeast and humans, is the lack of the Dam1 complex in humans. Currently, it is believed that the Ska complex serves as the human version of the Dam1 complex. As was mentioned in the introduction, the Ska complex does not have much sequence or structural similarity with the Dam1 complex, but does seem to fulfil similar functions: they both bind microtubules, they both track depolymerizing microtubule plus-ends and are highly important for modulating KT-MT attachments (Sauer *et al*., 2005; Welburn *et al*., 2009; Gaitanos *et al* 2009; Raaijmakers *et al* 2009; Helgeson *et al*., 2018). While our studies found that dysfunctional Dam1 complex helps cells to cope with CIN and aneuploidy, the loss of Ska-complex function is not known to be associated with cancer progression. Instead, in certain cancer types including glioma cells, the overexpression of Ska-complex is associated with enhanced cancer progression and poor prognosis (Yu, 2022). A question which arises here is why would human cancer cells not acquire Ska-complex mutants when, based on the data we have from CPC deficient yeast, they could potentially help the cancer cells adapt to perturbed chromosome biorientation? The answer will of course require much more study into exactly how the loss, or overexpression, of the Ska-complex affects CIN and aneuploidy levels in human cancer. Additionally, if the overexpression of the Ska complex promotes fitness in cancer, then inhibition of this overexpression should result in reduced fitness. Ska complex components could be inhibited by RNAi, a method already established in the field, to test Ska complex function (Welburn *et al*., 2009; Gaitanos *et al* 2009; Raaijmakers *et al* 2009). Finally, colony formation assays, using crystal-violet to visualize colonies, could be used to compare the growth capabilities of these cell-lines. A similar experiment would be to test the affect engineered Ska complex hypomorphic mutants have on cancer cell-line growth fitness over an extended period of time. These experiments would provide insight

into the role the Ska complex plays in cancer progression and would be medically relevant.

This study has shown that loss of attachment stability between the kinetochore and the microtubule counteracts the overstabilization of Bir1 loss, but this is just the plus end of the microtubule. At the minus end of the microtubule, the microtubule must also remain stably bound to Tub4 and other SPB components to facilitate chromosome segregation (**Figure 8**). It seems possible that loss of SPB structural stability, and therefore loss of MT-SPB attachment stability, would also result in the suppression of CPC dysfunction. This is because it should not matter at what end the instability is enhanced, as long as the overstabilized microtubule connections during cell division are disrupted. Indeed, a nonsense mutation in one of the core protein components of the SPB, *spc97(816X)*, rescued loss of Bir1 function. Despite the high likelihood this mutation also causes destabilization of attachments (albeit from the other end of the microtubule) this was not tested in this study and how exactly it operates remains unclear. In the future the *spc97(816X)* suppressor mutant, as well as other known temperature-sensitive mutants of the SPB (including *spc110-221),* could be tested by the same *bir1Δ* plasmid shuffle, SAC microscopy, *ipl1-321* temperature sensitive, and segregation fidelity assays utilized in this thesis. Additionally, another possible experiment to test turnover of the SPB-MT attachments, would be fluorescence recovery after photobleaching. If the attachments show a higher turnover rate it means they are less stable. Altogether these assays would provide new evidence that disruption of overstabilized attachments can occur from both the plus and minus ends of microtubules.

Up to this point, we have mostly discussed one of the major pathways which allows for suppression of CPC defects: the direct destabilization of KT-MT attachments independently of the CPC. However, our study confirmed suppressor mutations, in Mps1 and the SCF-complex, which must operate through a distinct pathway to the mutations found in the outer-kinetochore. The main basis for this includes: firstly, suppressor mutants in Mps1 and SCF-complex did not rescue loss of Ipl1 function. Secondly, these mutations did not increase SAC activity to the extent we see in strains with Dam1 complex mutants. Thirdly, unlike suppressor mutations in the Dam1 complex, mutations in Mps1 and the SCF-complex did not decrease segregation fidelity in a Bir1 wildtype background. As previously mentioned in the introduction, Mps1 is a master regulator of SAC onset as well as SPB duplication and CPC localization in yeast. Mps1 mutants are known to be synthetic lethal with mutations in the CPC, as well as other members of the kinetochore-microtubule error correction pathway. It is therefore very surprising, and even more intriguing, that we identified three distinct kinase-mutants in three different adapted strains. This means that in three independent instances, mutations in the Mps1 kinase were selected by CPC deficient yeast. Mps1 is essential so the mutations could not cause complete

loss of function. We tested whether or not the Mps1 mutants were hypomorphic or gain of function by comparing *bir1Δ* growth rescue in diploids with either heterozygous *mps1Δ* or heterozygous *mps1(V631M)*. Neither the heterozygous deletion nor the heterozygous mutant rescued loss of *bir1Δ.* This suggests that the *mps1(V631M)* is neither a gain of function mutant nor a complete loss of function mutant. Instead, we conclude from this that *mps1(V631M*) is likely a partial loss of function or hypomorphic mutant. Next, we decided to test this further by inhibiting Mps1 kinase activity in combination with *bir1Δ*. This was achieved by using an *mps1-as1* kinase mutant strain which is sensitive to the ATP analog 1NM-PP1 (Jones *et al*., 2005). If partial loss of Mps1 kinase function suppresses loss of Bir1, we should see increased growth fitness. However, no concentration of 1NM-PP1 tested could rescue growth of the *mps1-as1*/*bir1Δ* strains. We concluded that the Mps1 mutants partially decrease kinase activity and rescue via an unknown pathway. It has been previously described in Shimogawa *et al* (2006) and (2010) that mutations which render Dam1 non-phosphorylatable by Mps1 alter KT-MT stability. *dam1(S221F)* or *dam1(S221A)* rescue loss of Ipl1 function in *ipl1-2* mutant background at restrictive temperatures. The Mps1 phosphosite mutations in Dam1 are thought to increase KT-MT turnover by disrupting the maturation of KT-MT attachments from lateral to end-on attachment states (Tanaka *et al*., 2005; Shimogawa *et al*., 2006; Shimogawa *et al*., 2010). Although meiotic divisions are beyond the scope of this project, it must be mentioned that the *dam1(S221F)* mutant causes increased KT-MT instability during meiosis (Meyer *et al*., 2018). However, in our study we found that these non-phosphorylatable Dam1 mutants did not rescue loss of Bir1 nor loss of Ipl1 (*ipl1-321*) function. Despite this, another study has shown the presence of positive genetic interactions between Ipl1 and Mps1 mutant alleles. However, some alleles showed negative genetic interactions too (Costanzo *et al* 2016). Altogether, this only further emphasizes additional research is required to determine which functions of Mps1 as well as which specific substrates are responsible for rescuing CPC function. A large-scale phospho-proteomic analysis of the Mps1 suppressor mutants would be the vital next step in elucidating this exciting mystery further.

The final group of suppressor mutations to be discussed were found in the SCF-complex. The SCF-complex is a conserved E3 ubiquitin ligase complex responsible for entry to S-phase as well as mitotic entry in both humans and yeast. The SCF-complex is comprised of core proteins and a single adaptor protein which specifies the protein substrates. The adaptor protein is also the protein which interacts directly with the protein targets; the main targets are cyclins and other factors which regulate cell-cycle entry (Goh & Surana, 1999). Mutations were found in some of the core members of the complex, including Cdc34 and Cdc53. The only adaptor protein which we found to have any mutations was Cdc4/FBXW7. We found four distinct mutations in the WD40 domain. Similar to the Mps1 mutations, the fact we see the independent acquisition of four distinct mutations all in the same domain suggests these mutations provide a selective advantage. In yeast, temperature

sensitive mutations in Cdc4 result in anaphase arrest (Schwob *et al*., 1994; Goh & Surana, 1999). Additionally, our study showed that the *cdc4-1* temperature sensitive mutant can also rescue loss of Bir1. This suggests further that loss of SCF^{Cdc4} function leads to CIN suppression. As mentioned in the introduction, the SCF-complex also degrades Cse4, as well as inner kinetochore complex subunits including Ame1 (Böhm *et al*., 2020; Au *et al*., 2021). Multiple adaptor proteins for the SCF-complex are known, but not all adaptors have been identified. In human cells, mutants in the tumor suppressor hCdc4/FBXW7 cause sensitivity to SAC inhibitors (Yeh *et al*., 2018). Altogether this demonstrates a potential function of the SCF in mitosis, cancer and regulation of kinetochore subcomplexes. However, exactly how these regulatory mechanisms function is still unclear. It would be of great medical importance to further elucidate how the SCF-complex contributes to segregation in cancer. To this end, one could do yeast two-hybrid assays, cell cycle specific co-immunoprecipitation assays and biochemical crosslinking assays to help identify novel SCF adaptor proteins, as well as the previously unidentified SCF^{Cdc4} specific targets. Such data provided by these assays would further our understanding of the SCF^{Cdc4} complex in cell-cycle control as well as cancer.

The easiest explanation as to how the SCF-complex rescued loss of CPC function was that the SCF^{Cdc4} targets the CPC for degradation. A loss of SCF function would therefore result in increased CPC abundance, thus suppressing CIN. However, in our study we found that SCF-mutant strains do not show any decreased degradation of Sli15 or Ipl1. Next, we decided to test whether or not the SCF-complex modulates CPC localization. Using live fluorescence-microscopy we found that *cdc4(G439S)* strains showed a 50% increase in the amount of CPC at microtubules during prometaphase specifically. Using CRISPR, we engineered the equivalent mutation in the human FBXW7(G437S). Strikingly, even in human cells, a defective SCF-complex leads to a 50% increase in CPC localization during mitosis. We conclude that the SCF-complex does not act directly on the CPC itself but instead plays a role in an unknown mechanism which controls CPC localization. We speculate that the wild-type SCF complex decreases CPC spindle-localization by degrading a CPC spindle recruitment factor (eg. Cdc14). One way to test this would be by searching for negative genetic interactions between SCF mutants and microtubule recruitment factor mutants. For example, one could test the combination of Cdc14 temperature sensitive mutants and Cdc4 temperature sensitive mutants. This experiment would be important for the field as the connection between the SCF and CPC recruitment is still unclear.

Tetrad dissections revealed the Cdc4 suppressor mutant was able to rescue loss of Pds1 (own observations). This is not surprising because previous studies have shown that Cdc4 temperature sensitive mutants can rescue loss of Pds1 (Goh & Surana, 1999). Future studies could focus on evaluating whether or not enhanced CPC microtubule binding is responsible for *pds1Δ* rescue. *sli15(6A*) and *sli15-ΔNT* mutants could function as positive controls for enhanced microtubule binding. Once

again, such data would provide answers as to how Cdc4 mutants rescue various sources of CIN, which has major implications in understanding cancer progression.

Finally, the data from all these assays allow us to outline a potential time line for adaptation to persistent CIN. First, cells with loss of CPC function obtain specific aneuploid karyotypes that partially improve fitness. Second, the complex aneuploid karyotypes within the adapting strains converge on an optimal aneuploid karyotype. Third, during optimization of aneuploid karyotypes, the cell accumulates specific point mutations which either affect CPC activity and localization, or independently decrease KT-MT attachment stability. These point mutations ameliorate missegregation by targeting the source of CIN more specifically. Lastly, this reduction in CIN allows for the reduction in the number of aneuploid chromosomes. In short, the accumulative results from this thesis supports the theory that aneuploidy often provides a rapid but temporary form of adaptation.

Summarily, the data gathered from this thesis project lay the groundwork for a greater understanding of how genetic interactions and alterations are involved in adaptation to sources of CIN and aneuploidy. The assays suggested in the discussion and outlook, especially those which clarify the mysterious involvement of Mps1 kinase mutants and Cdc4 dysfunction in CIN suppression, will be important for enhancing our knowledge of cancer evolution.

5. Conclusions and summary

In this thesis key mechanisms which allow for cells to adapt to persistent CIN have been elucidated. To reiterate, overstabilization of KT-MT attachments is one of the main causes of lagging chromosomes in cancer. Understanding how cells adapt to overstabilized attachments therefore has medical implications. We deleted Bir1 in budding yeast to induce persistent CIN. After the first 21 days of adaptation *bir1Δ*-ad strains favor specific aneuploid karyotypes to adapt to CIN. Mutations which suppress *bir1Δ* were not present at this point. However, after allowing the *bir1Δ*-ad strains an additional 21 days to adapt, we identified multiple point mutations in distinct pathways which rescue growth, reduce rates of CIN, and reduce aneuploidy. The first pathway involved mutations which increased KT-MT turnover in a CPC independent manner. The second pathway involved regulation of the CPC itself. Either way, these CIN suppressor mutations lead to a reduction in aneuploidy.

6. Table of figures

7. List of abbreviations

APC = anaphase promoting complex
CC = coiled-coil
CCAN = constitutive centromere associated network
CDK = cyclin-dependent kinase
CIN = chromosomal instability
COMA = Ctf19, Okp1, Mcm21, Ame1
CPC = chromosomal passenger complex
DDR = DNA damage response
FISH = fluorescence in situ hybridization
KMN = Knl1, Mis12, Ndc80
KT-MT = kinetochore-microtubule
PR = phosphoregulated
PROTAC = proteolysis-targeting chimera
MCC = mitotic checkpoint complex
MTB = microtubule binding
MTOC = microtubule organizing center
NEBD = nuclear envelope breakdown
NGS = next generation sequencing
SAC = spindle assembly checkpoint
SCF = Skp1, Cullin, F-box
SPB = spindle pole body
SPB-MT = spindle pole body-microtubule

8. References

Agarwal, M., Mehta, G., & Ghosh, S. K. (2015). “Role of Ctf3 and COMA subcomplexes in meiosis: Implication in maintaining Cse4 at the centromere and numeric spindle poles”. *Biochimica et biophysica acta*, *1853*(3), 671–684. https://doi.org/10.1016/j.bbamcr.2014.12.032

Ainsztein, A. M., Kandels-Lewis, S. E., Mackay, A. M., & Earnshaw, W. C. (1998). “INCENP centromere and spindle targeting: identification of essential conserved motifs and involvement of heterochromatin protein HP1”. *The Journal of cell biology*, *143*(7), 1763–1774. https://doi.org/10.1083/jcb.143.7.1763

Akiyoshi, B., Nelson, C. R., Ranish, J. A., & Biggins, S. (2009). “Analysis of Ipl1-mediated phosphorylation of the Ndc80 kinetochore protein in Saccharomyces cerevisiae”. *Genetics*, *183*(4), 1591–1595. https://doi.org/10.1534/genetics.109.109041

Alonso, A., Fabritius, A., Ozzello, C., Andreas, M., Klenchin, D., Rayment, I., & Winey, M. (2020). “Yeast pericentrin/Spc110 contains multiple domains required for tethering the γ-tubulin complex to the centrosome”. *Molecular biology of the cell*, *31*(14), 1437–1452. https://doi.org/10.1091/mbc.E20-02-0146

Alonso Y Adell, M., Klockner, T.C., Höfler, R., Wallner, L., Schmid, J., Markovic, A., Martyniak, A., & Campbell, C. S., (2022) “Adaptation to spindle assembly checkpoint inhibition through the selection of specific aneuploidies” *bioarxiv*, Preprint. 1-60. https://doi.org/10.1101/2022.10.04.510607 [Accessed 20.02.2023]

Asbury, C. L., Tien, J. F., & Davis, T. N. (2011). “Kinetochores' gripping feat: conformational wave or biased diffusion?”. *Trends in cell biology*, *21*(1), 38–46. https://doi.org/10.1016/j.tcb.2010.09.003

Au, W. C., Zhang, T., Mishra, P. K., Eisenstatt, J. R., Walker, R. L., Ocampo, J., Dawson, A., Warren, J., Costanzo, M., Baryshnikova, A., Flick, K., Clark, D. J., Meltzer, P. S., Baker, R. E., Myers, C., Boone, C., Kaiser, P., & Basrai, M. A. (2020). “Skp, Cullin, F-box (SCF)-Met30 and SCF-Cdc4-Mediated Proteolysis of CENP-A Prevents Mislocalization of CENP-A for Chromosomal Stability in Budding Yeast”. *PLoS genetics*, *16*(2), e1008597. https://doi.org/10.1371/journal.pgen.1008597

Bakhoum, S. F., Genovese, G., & Compton, D. A. (2009). “Deviant kinetochore microtubule dynamics underlie chromosomal instability”. *Current biology : CB*, *19*(22), 1937–1942. https://doi.org/10.1016/j.cub.2009.09.055

Bakhoum, S. F., Danilova, O. V., Kaur, P., Levy, N. B., & Compton, D. A. (2011). “Chromosomal instability substantiates poor prognosis in patients with diffuse large B-cell lymphoma”. *Clinical cancer research : an official journal of the American Association for Cancer Research*, *17*(24), 7704–7711. https://doi.org/10.1158/1078-0432.CCR-11-2049

Bakhoum, S. F., & Cantley, L. C. (2018). “The Multifaceted Role of Chromosomal Instability in Cancer and Its Microenvironment”. *Cell*, *174*(6), 1347–1360. https://doi.org/10.1016/j.cell.2018.08.027

Balasubramanian, M. K., Bi, E., & Glotzer, M. (2004). “Comparative analysis of cytokinesis in budding yeast, fission yeast and animal cells”. *Current biology : CB*, *14*(18), 806–818. https://doi.org/10.1016/j.cub.2004.09.022

Barberis, M., De Gioia, L., Ruzzene, M., Sarno, S., Coccetti, P., Fantucci, P., Vanoni, M., & Alberghina, L. (2005). “The yeast cyclin-dependent kinase inhibitor Sic1 and mammalian p27Kip1 are functional homologues with a structurally conserved inhibitory domain”. *The Biochemical journal*, *387*(Pt 3), 639–647. https://doi.org/10.1042/BJ20041299

Basu, J., Bousbaa, H., Logarinho, E., Li, Z., Williams, B. C., Lopes, C., Sunkel, C. E., & Goldberg, M. L. (1999). “Mutations in the essential spindle checkpoint gene bub1 cause chromosome missegregation and fail to block apoptosis in Drosophila”. *The Journal of cell biology*, *146*(1), 13–28. https://doi.org/10.1083/jcb.146.1.13

Ben-David, U., & Amon, A. (2020). “Context is everything: aneuploidy in cancer”. *Nature reviews. Genetics*, *21*(1), 44–62. https://doi.org/10.1038/s41576-019-0171-x

Beroukhim, R., Mermel, CH., Porter, D., Wei, G., Raychaudhuri, S., Donovan, J., Barretina, J., Boehm, JS., Dobson, J., Urashima, M., Mc Henry KT, Pinchback RM, Ligon AH, Cho YJ, Haery L, Greulich H, Reich M, Winckler W, Lawrence MS, Weir BA, Tanaka KE, Chiang DY, Bass AJ, Loo A, Hoffman C, Prensner J, Liefeld T, Gao Q, Yecies D, Signoretti S, Maher E, Kaye FJ, Sasaki H, Tepper JE, Fletcher JA, Tabernero J, Baselga J, Tsao MS, Demichelis F, Rubin MA, Janne PA, Daly MJ, Nucera C, Levine RL, Ebert BL, Gabriel S, Rustgi AK, Antonescu CR, Ladanyi M, Letai A, Garraway LA, Loda M, Beer DG, True LD, Okamoto A, Pomeroy SL, Singer S, Golub TR, Lander ES, Getz G, Sellers, WR., & Meyerson, M. (2010). “The landscape of somatic copy-number alteration across human cancers”. *Nature*, *463*(7283), 899–905. https://doi.org/10.1038/nature08822

Bertoli, C., Skotheim, J. M., & de Bruin, R. A. (2013). “Control of cell cycle transcription during G1 and S phases”. *Nature reviews. Molecular cell biology*, *14*(8), 518–528. https://doi.org/10.1038/nrm3629

Berset, C., Griac, P., Tempel, R., La Rue, J., Wittenberg, C., & Lanker, S. (2002). “Transferable domain in the G(1) cyclin Cln2 sufficient to switch degradation of Sic1 from the E3 ubiquitin ligase SCF(Cdc4) to SCF(Grr1)”. *Molecular and cellular biology*, *22*(13), 4463–4476. https://doi.org/10.1128/MCB.22.13.4463-4476.2002

Bhavsar-Jog, Y. P., & Bi, E. (2017). “Mechanics and regulation of cytokinesis in budding yeast”. *Seminars in cell & developmental biology*, *66*, 107–118. https://doi.org/10.1016/j.semcdb.2016.12.010

Biggins, S., Severin, F. F., Bhalla, N., Sassoon, I., Hyman, A. A., & Murray, A. W. (1999). “The conserved protein kinase Ipl1 regulates microtubule binding to kinetochores in budding yeast”. *Genes & development*, *13*(5), 532–544. https://doi.org/10.1101/gad.13.5.532

Biggins, S., & Murray, A. W. (2001). “The budding yeast protein kinase Ipl1/Aurora allows the absence of tension to activate the spindle checkpoint”. *Genes & development*, *15*(23), 3118–3129. https://doi.org/10.1101/gad.934801

Biggins S. (2013). “The composition, functions, and regulation of the budding yeast kinetochore”. *Genetics*, *194*(4), 817–846. https://doi.org/10.1534/genetics.112.145276

Black, B. E., Jansen, L. E., Foltz, D. R., & Cleveland, D. W. (2010). “Centromere identity, function, and epigenetic propagation across cell divisions”. *Cold Spring Harbor symposia on quantitative biology*, *75*, 403–418. https://doi.org/10.1101/sqb.2010.75.038

Blanco-Ameijeiras, J., Lozano-Fernández, P., & Martí, E. (2022). “Centrosome maturation - in tune with the cell cycle”. *Journal of cell science*, *135*(2), jcs259395. https://doi.org/10.1242/jcs.259395

Blow, J. J., & Tanaka, T. U. (2005). “The chromosome cycle: coordinating replication and segregation. Second in the cycles review series”. *EMBO reports*, *6*(11), 1028–1034. https://doi.org/10.1038/sj.embor.7400557

Boeckmann, L., Takahashi, Y., Au, W. C., Mishra, P. K., Choy, J. S., Dawson, A. R., Szeto, M. Y., Waybright, T. J., Heger, C., McAndrew, C., Goldsmith, P. K., Veenstra, T. D., Baker, R. E., & Basrai, M. A. (2013). “Phosphorylation of centromeric histone H3 variant regulates chromosome segregation in Saccharomyces cerevisiae”. *Molecular biology of the cell*, *24*(12), 2034–2044. https://doi.org/10.1091/mbc.E12-12-0893

Böhm, M., Killinger, K., Dudziak, A., Pant, P., Jänen, K., Hohoff, S., Mechtler, K., Örd, M., Loog, M., Sanchez-Garcia, E., & Westermann, S. (2021). “Cdc4 phospho-degrons allow differential regulation of Ame1^{CENP-U} protein stability across the cell cycle”. *eLife*, *10*, e67390. https://doi.org/10.7554/eLife.67390

Bonner, M. K., Haase, J., Swinderman, J., Halas, H., Miller Jenkins, L. M., & Kelly, A. E. (2019). “Enrichment of Aurora B kinase at the inner kinetochore controls outer kinetochore assembly”. *The Journal of cell biology*, *218*(10), 3237–3257. https://doi.org/10.1083/jcb.201901004

Bock, L. J., Pagliuca, C., Kobayashi, N., Grove, R. A., Oku, Y., Shrestha, K., Alfieri, C., Golfieri, C., Oldani, A., Dal Maschio, M., Bermejo, R., Hazbun, T. R., Tanaka, T. U., & De Wulf, P. (2012). “Cnn1 inhibits the interactions between the KMN

complexes of the yeast kinetochore". *Nature cell biology*, *14*(6), 614–624. https://doi.org/10.1038/ncb2495

Boettcher, B., & Barral, Y. (2013). "The cell biology of open and closed mitosis". *Nucleus (Austin, Tex.)*, *4*(3), 160–165. https://doi.org/10.4161/nucl.24676

Boisvert, F. M., van Koningsbruggen, S., Navascués, J., & Lamond, A. I. (2007). "The multifunctional nucleolus". *Nature reviews. Molecular cell biology*, *8*(7), 574–585. https://doi.org/10.1038/nrm2184

Bonner, M. K., Haase, J., Swinderman, J., Halas, H., Miller Jenkins, L. M., & Kelly, A. E. (2019). "Enrichment of Aurora B kinase at the inner kinetochore controls outer kinetochore assembly". *The Journal of cell biology*, *218*(10), 3237–3257. https://doi.org/10.1083/jcb.201901004

Brewer, C. M., Holloway, S. H., Stone, D. H., Carothers, A. D., & FitzPatrick, D. R. (2002). "Survival in trisomy 13 and trisomy 18 cases ascertained from population based registers". *Journal of medical genetics*, *39*(9), e54. https://doi.org/10.1136/jmg.39.9.e54

Bunz, F., Dutriaux, A., Lengauer, C., Waldman, T., Zhou, S., Brown, J. P., Sedivy, J. M., Kinzler, K. W., & Vogelstein, B. (1998). "Requirement for p53 and p21 to sustain G2 arrest after DNA damage". *Science (New York, N.Y.)*, *282*(5393), 1497–1501. https://doi.org/10.1126/science.282.5393.1497

Burma, S., Chen, B. P., Murphy, M., Kurimasa, A., & Chen, D. J. (2001). "ATM phosphorylates histone H2AX in response to DNA double-strand breaks". *The Journal of biological chemistry*, *276*(45), 42462–42467. https://doi.org/10.1074/jbc.C100466200

Burrack, L. S., & Berman, J. (2012). "Flexibility of centromere and kinetochore structures". *Trends in genetics : TIG*, *28*(5), 204–212. https://doi.org/10.1016/j.tig.2012.02.003

Camahort, R., Li, B., Florens, L., Swanson, S. K., Washburn, M. P., & Gerton, J. L. (2007). "Scm3 is essential to recruit the histone h3 variant cse4 to centromeres and to maintain a functional kinetochore". *Molecular cell*, *26*(6), 853–865. https://doi.org/10.1016/j.molcel.2007.05.013

Campbell, C. S., & Desai, A. (2013). "Tension sensing by Aurora B kinase is independent of survivin-based centromere localization". *Nature*, *497*(7447), 118–121. https://doi.org/10.1038/nature12057

Carmena, M., Wheelock, M., Funabiki, H., & Earnshaw, W. C. (2012). "The chromosomal passenger complex (CPC): from easy rider to the godfather of mitosis". *Nature reviews. Molecular cell biology*, *13*(12), 789–803. https://doi.org/10.1038/nrm3474

Carter, S. L., Eklund, A. C., Kohane, I. S., Harris, L. N., & Szallasi, Z. (2006). “A signature of chromosomal instability inferred from gene expression profiles predicts clinical outcome in multiple human cancers”. *Nature genetics*, *38*(9), 1043–1048. https://doi.org/10.1038/ng1861

Chao, W. C., Kulkarni, K., Zhang, Z., Kong, E. H., & Barford, D. (2012). “Structure of the mitotic checkpoint complex”. *Nature*, *484*(7393), 208–213. https://doi.org/10.1038/nature10896

Cheeseman, I. M., Enquist-Newman, M., Müller-Reichert, T., Drubin, D. G., & Barnes, G. (2001). “Mitotic spindle integrity and kinetochore function linked by the Duo1p/Dam1p complex”. *The Journal of cell biology*, *152*(1), 197–212. https://doi.org/10.1083/jcb.152.1.197

Cheeseman, I. M., Anderson, S., Jwa, M., Green, E. M., Kang, J.s, Yates, J. R., 3rd, Chan, C. S., Drubin, D. G., & Barnes, G. (2002). “Phospho-regulation of kinetochore-microtubule attachments by the Aurora kinase Ipl1p”. *Cell*, *111*(2), 163–172. https://doi.org/10.1016/s0092-8674(02)00973-x

Cheeseman, I. M., Chappie, J. S., Wilson-Kubalek, E. M., & Desai, A. (2006). “The conserved KMN network constitutes the core microtubule-binding site of the kinetochore”. *Cell*, *127*(5), 983–997. https://doi.org/10.1016/j.cell.2006.09.039

Chen, G., Bradford, W. D., Seidel, C. W., & Li, R. (2012). “Hsp90 stress potentiates rapid cellular adaptation through induction of aneuploidy”. *Nature*, *482*(7384), 246–250. https://doi.org/10.1038/nature10795

Chen, Y., Riley, D. J., Chen, P. L., & Lee, W. H. (1997). “HEC, a novel nuclear protein rich in leucine heptad repeats specifically involved in mitosis”. *Molecular and cellular biology*, *17*(10), 6049–6056. https://doi.org/10.1128/MCB.17.10.6049

Ciferri, C., Musacchio, A., & Petrovic, A. (2007). “The Ndc80 complex: hub of kinetochore activity”. *FEBS letters*, *581*(15), 2862–2869. https://doi.org/10.1016/j.febslet.2007.05.012

Clarke L. (1998). “Centromeres: proteins, protein complexes, and repeated domains at centromeres of simple eukaryotes”. *Current opinion in genetics & development*, *8*(2), 212–218. https://doi.org/10.1016/s0959-437x(98)80143-3

Clarke, M. N., Marsoner, T., Adell, M. A. Y., Ravichandran, M. C., & Campbell, C. S. (2022). “Adaptation to high rates of chromosomal instability and aneuploidy through multiple pathways in budding yeast”. *The EMBO journal*, e111500. Advance online publication. https://doi.org/10.15252/embj.2022111500

Clarke, L., & Carbon, J. (1980). “Isolation of a yeast centromere and construction of functional small circular chromosomes”. *Nature*, *287*(5782), 504–509.

https://doi.org/10.1038/287504a0

Cohen, R. L., Espelin, C. W., De Wulf, P., Sorger, P. K., Harrison, S. C., & Simons, K. T. (2008). “Structural and functional dissection of Mif2p, a conserved DNA-binding kinetochore protein”. *Molecular biology of the cell*, *19*(10), 4480–4491. https://doi.org/10.1091/mbc.e08-03-0297

Colin, D. J., Hain, K. O., Allan, L. A., & Clarke, P. R. (2015). “Cellular responses to a prolonged delay in mitosis are determined by a DNA damage response controlled by Bcl-2 family proteins”. *Open biology*, *5*(3), 140156. https://doi.org/10.1098/rsob.140156

Connelly, C., & Hieter, P. (1996). “Budding yeast SKP1 encodes an evolutionarily conserved kinetochore protein required for cell cycle progression”. *Cell*, *86*(2), 275–285. https://doi.org/10.1016/s0092-8674(00)80099-9

Costanzo, M., VanderSluis, B., Koch, E. N., Baryshnikova, A., Pons, C., Tan, G., Wang, W., Usaj, M., Hanchard, J., Lee, S. D., Pelechano, V., Styles, E. B., Billmann, M., van Leeuwen, J., van Dyk, N., Lin, Z. Y., Kuzmin, E., Nelson, J., Piotrowski, J. S., Srikumar, T., Bahr S, Chen Y, Deshpande R, Kurat CF, Li SC, Li Z, Usaj MM, Okada H, Pascoe N, San Luis BJ, Sharifpoor S, Shuteriqi E, Simpkins SW, Snider J, Suresh HG, Tan Y, Zhu H, Malod- Dognin N, Janjic V, Przulj N, Troyanskaya OG, Stagljar I, Xia T, Ohya Y, Gingras AC, Raught B, Boutros M, Steinmetz LM, Moore CL, Rosebrock AP, Caudy AA, Myers CL, & Boone, C. (2016). “A global genetic interaction network maps a wiring diagram of cellular function”. *Science (New York, N.Y.)*, *353*(6306), aaf1420. https://doi.org/10.1126/science.aaf1420

Cuddihy, A. R., & O'Connell, M. J. (2003). “Cell-cycle responses to DNA damage in G2”. *International review of cytology*, *222*, 99–140. https://doi.org/10.1016/s0074-7696(02)22013-6

Daum, J. R., Wren, J. D., Daniel, J. J., Sivakumar, S., McAvoy, J. N., Potapova, T. A., & Gorbsky, G. J. (2009). “Ska3 is required for spindle checkpoint silencing and the maintenance of chromosome cohesion in mitosis”. *Current biology : CB*, *19*(17), 1467–1472. https://doi.org/10.1016/j.cub.2009.07.017

Davoli, T., Xu, A. W., Mengwasser, K. E., Sack, L. M., Yoon, J. C., Park, P. J., & Elledge, S. J. (2013). “Cumulative haploinsufficiency and triplosensitivity drive aneuploidy patterns and shape the cancer genome”. *Cell*, *155*(4), 948–962. https://doi.org/10.1016/j.cell.2013.10.011

Davoli, T., Uno, H., Wooten, E. C., & Elledge, S. J. (2017). “Tumor aneuploidy correlates with markers of immune evasion and with reduced response to immunotherapy”. *Science (New York, N.Y.)*, *355*(6322), eaaf8399. https://doi.org/10.1126/science.aaf8399

DeAntoni, A., Sala, V., & Musacchio, A. (2005). “Explaining the oligomerization properties of the spindle assembly checkpoint protein Mad2”. *Philosophical*

transactions of the Royal Society of London. Series B, Biological sciences, *360*(1455), 637–448. https://doi.org/10.1098/rstb.2004.1618

DeLuca, J. G., Gall, W. E., Ciferri, C., Cimini, D., Musacchio, A., & Salmon, E. D. (2006). “Kinetochore microtubule dynamics and attachment stability are regulated by Hec1”. *Cell*, *127*(5), 969–982. https://doi.org/10.1016/j.cell.2006.09.047

DeLuca, K. F., Lens, S. M., & DeLuca, J. G. (2011). “Temporal changes in Hec1 phosphorylation control kinetochore-microtubule attachment stability during mitosis”. *Journal of cell science*, *124*(Pt 4), 622–634. https://doi.org/10.1242/jcs.072629

DeWit, E., & Nora, E. P. (2023). “New insights into genome folding by loop extrusion from inducible degron technologies”. *Nature reviews. Genetics*, *24*(2), 73–85. https://doi.org/10.1038/s41576-022-00530-4

Dimitrova, Y. N., Jenni, S., Valverde, R., Khin, Y., & Harrison, S. C. (2016). “Structure of the MIND Complex Defines a Regulatory Focus for Yeast Kinetochore Assembly”. *Cell*, *167*(4), 1014–1027.e12. https://doi.org/10.1016/j.cell.2016.10.011

Dobles, M., Liberal, V., Scott, M. L., Benezra, R., & Sorger, P. K. (2000). “Chromosome missegregation and apoptosis in mice lacking the mitotic checkpoint protein Mad2”. *Cell*, *101*(6), 635–645. https://doi.org/10.1016/s0092-8674(00)80875-2

Dodgson, S. E., Santaguida, S., Kim, S., Sheltzer, J., & Amon, A. (2016). “The pleiotropic deubiquitinase Ubp3 confers aneuploidy tolerance”. *Genes & development*, *30*(20), 2259–2271. https://doi.org/10.1101/gad.287474.116

Drury, L. S., Perkins, G., & Diffley, J. F. (1997). “The Cdc4/34/53 pathway targets Cdc6p for proteolysis in budding yeast”. *The EMBO journal*, *16*(19), 5966–5976. https://doi.org/10.1093/emboj/16.19.5966

Duesberg, P., Rausch, C., Rasnick, D., & Hehlmann, R. (1998). “Genetic instability of cancer cells is proportional to their degree of aneuploidy”. *Proceedings of the National Academy of Sciences of the United States of America*, *95*(23), 13692–13697. https://doi.org/10.1073/pnas.95.23.13692

Du, R., Huang, C., Liu, K., Li, X., & Dong, Z. (2021). “Targeting AURKA in Cancer: molecular mechanisms and opportunities for Cancer therapy”. *Molecular cancer*, *20*(1), 15. https://doi.org/10.1186/s12943-020-01305-3

Dunleavy, E. M., Roche, D., Tagami, H., Lacoste, N., Ray-Gallet, D., Nakamura, Y., Daigo, Y., Nakatani, Y., & Almouzni-Pettinotti, G. (2009). “HJURP is a cell-cycle-dependent maintenance and deposition factor of CENP-A at centromeres”. *Cell*, *137*(3), 485–497. https://doi.org/10.1016/j.cell.2009.02.040

Earnshaw, W. C., & Rothfield, N. (1985). “Identification of a family of human centromere proteins using autoimmune sera from patients with scleroderma”.

Chromosoma, *91*(3-4), 313–321. https://doi.org/10.1007/BF00328227

Enquist-Newman, M., Cheeseman, I. M., Van Goor, D., Drubin, D. G., Meluh, P. B., & Barnes, G. (2001). “Dad1p, third component of the Duo1p/Dam1p complex involved in kinetochore function and mitotic spindle integrity”. *Molecular biology of the cell*, *12*(9), 2601–2613. https://doi.org/10.1091/mbc.12.9.2601

Fang, G., Yu, H., & Kirschner, M. W. (1998). “Direct binding of CDC20 protein family members activates the anaphase-promoting complex in mitosis and G1”. *Molecular cell*, *2*(2), 163–171. https://doi.org/10.1016/s1097-2765(00)80126-4

Feldman, R. M., Correll, C. C., Kaplan, K. B., & Deshaies, R. J. (1997). “A complex of Cdc4p, Skp1p, and Cdc53p/cullin catalyzes ubiquitination of the phosphorylated CDK inhibitor Sic1p”. *Cell*, *91*(2), 221–230. https://doi.org/10.1016/s0092-8674(00)80404-3

Fernius, J., & Hardwick, K. G. (2007). “Bub1 kinase targets Sgo1 to ensure efficient chromosome biorientation in budding yeast mitosis”. *PLoS genetics*, *3*(11), e213. https://doi.org/10.1371/journal.pgen.0030213

Fischböck-Halwachs, J., Singh, S., Potocnjak, M., Hagemann, G., Solis-Mezarino, V., Woike, S., Ghodgaonkar-Steger, M., Weissmann, F., Gallego, L. D., Rojas, J., Andreani, J., Köhler, A., & Herzog, F. (2019). “The COMA complex interacts with Cse4 and positions Sli15/Ipl1 at the budding yeast inner kinetochore”. *eLife*, *8*, e42879. https://doi.org/10.7554/eLife.42879

Fletcher, J. I., Haber, M., Henderson, M. J., & Norris, M. D. (2010). “ABC transporters in cancer: more than just drug efflux pumps”. *Nature reviews. Cancer*, *10*(2), 147–156. https://doi.org/10.1038/nrc2789

Foltz, D. R., Jansen, L. E., Bailey, A. O., Yates, J. R., 3rd, Bassett, E. A., Wood, S., Black, B. E., & Cleveland, D. W. (2009). “Centromere-specific assembly of CENP-a nucleosomes is mediated by HJURP”. *Cell*, *137*(3), 472–484. https://doi.org/10.1016/j.cell.2009.02.039

Fudenberg, G., Imakaev, M., Lu, C., Goloborodko, A., Abdennur, N., & Mirny, L. A. (2016). “Formation of Chromosomal Domains by Loop Extrusion”. *Cell reports*, *15*(9), 2038–2049. https://doi.org/10.1016/j.celrep.2016.04.085

Gaitanos, T. N., Santamaria, A., Jeyaprakash, A. A., Wang, B., Conti, E., & Nigg, E. A. (2009). “Stable kinetochore-microtubule interactions depend on the Ska complex and its new component Ska3/C13Orf3”. *The EMBO journal*, *28*(10), 1442–1452. https://doi.org/10.1038/emboj.2009.96

Garbrecht, J., Laos, T., Holzer, E., Dillinger, M., & Dammermann, A. (2021). “An acentriolar centrosome at the C. elegans ciliary base”. *Current biology : CB*, *31*(11), 2418–2428.e8. https://doi.org/10.1016/j.cub.2021.03.023

Gasca, J., Flores, M. L., Giráldez, S., Ruiz-Borrego, M., Tortolero, M., Romero, F., Japón, M. A., & Sáez, C. (2016). “Loss of FBXW7 and accumulation of MCL1 and PLK1 promote paclitaxel resistance in breast cancer”. *Oncotarget*, *7*(33), 52751–52765. https://doi.org/10.18632/oncotarget.10481

Gheghiani, L., Wang, L., Zhang, Y., Moore, X. T. R., Zhang, J., Smith, S. C., Tian, Y., Wang, L., Turner, K., Jackson-Cook, C. K., Mukhopadhyay, N. D., & Fu, Z. (2021). “PLK1 Induces Chromosomal Instability and Overrides Cell-Cycle Checkpoints to Drive Tumorigenesis”. *Cancer research*, *81*(5), 1293–1307. https://doi.org/10.1158/0008-5472.CAN-20-1377

Giam, M., & Rancati, G. (2015). “Aneuploidy and chromosomal instability in cancer: a jackpot to chaos”. *Cell division*, *10*, 3. https://doi.org/10.1186/s13008-015-0009-7

Gillett, E. S., Espelin, C. W., & Sorger, P. K. (2004). “Spindle checkpoint proteins and chromosome-microtubule attachment in budding yeast”. *The Journal of cell biology*, *164*(4), 535–546. https://doi.org/10.1083/jcb.200308100

Gire, V., & Dulic, V. (2015). “Senescence from G2 arrest, revisited”. *Cell cycle (Georgetown, Tex.)*, *14*(3), 297–304. https://doi.org/10.1080/15384101.2014.1000134

Glotzer M. (2005). “The molecular requirements for cytokinesis”. *Science (New York, N.Y.)*, *307*(5716), 1735–1739. https://doi.org/10.1126/science.1096896

Goh, P. Y., & Surana, U. (1999). “Cdc4, a protein required for the onset of S phase, serves an essential function during G(2)/M transition in Saccharomyces cerevisiae”. *Molecular and cellular biology*, *19*(8), 5512–5522. https://doi.org/10.1128/MCB.19.8.5512

Gombos, L., Neuner, A., Berynskyy, M., Fava, L. L., Wade, R. C., Sachse, C., & Schiebel, E. (2013). “GTP regulates the microtubule nucleation activity of γ-tubulin”. *Nature cell biology*, *15*(11), 1317–1327. https://doi.org/10.1038/ncb2863

Gonen, S., Akiyoshi, B., Iadanza, M. G., Shi, D., Duggan, N., Biggins, S., & Gonen, T. (2012). “The structure of purified kinetochores reveals multiple microtubule-attachment sites”. *Nature structural & molecular biology*, *19*(9), 925–929. https://doi.org/10.1038/nsmb.2358

Gordon, D. J., Resio, B., & Pellman, D. (2012). “Causes and consequences of aneuploidy in cancer”. *Nature reviews. Genetics*, *13*(3), 189–203. https://doi.org/10.1038/nrg3123

Greenland, K. B., Ding, H., Costanzo, M., Boone, C., & Davis, T. N. (2010). “Identification of Saccharomyces cerevisiae spindle pole body remodeling factors”. *PloS one*, *5*(11), e15426. https://doi.org/10.1371/journal.pone.0015426

Gregan, J., Polakova, S., Zhang, L., Tolić-Nørrelykke, I. M., & Cimini, D. (2011).

"Merotelic kinetochore attachment: causes and effects". *Trends in cell biology*, *21*(6), 374–381. https://doi.org/10.1016/j.tcb.2011.01.003

Gropp, A., Winking, H., Herbst, E. W., & Claussen, C. P. (1983). "Murine trisomy: developmental profiles of the embryo, and isolation of trisomic cellular systems". *The Journal of experimental zoology*, *228*(2), 253–269. https://doi.org/10.1002/jez.1402280210

Gruber, S., Haering, C. H., & Nasmyth, K. (2003). "Chromosomal cohesin forms a ring". *Cell*, *112*(6), 765–777. https://doi.org/10.1016/s0092-8674(03)00162-4

Haase, M. A. B., Ólafsson, G., Flores, R. L., Boakye-Ansah, E., Zelter, A., Dickinson, M. S., Lazar-Stefanita, L., Truong, D. M., Asbury, C. L., Davis, T. N., & Boeke, J. D. (2023). "DASH/Dam1 complex mutants stabilize ploidy in histone-humanized yeast by weakening kinetochore-microtubule attachments". *The EMBO journal*, e112600. Advance online publication. https://doi.org/10.15252/embj.2022112600

Hadders, M. A., & Lens, S. M. A. (2022). "Changing places: Chromosomal Passenger Complex relocation in early anaphase". *Trends in cell biology*, *32*(2), 165–176. https://doi.org/10.1016/j.tcb.2021.09.008

Hardwick, K. G., Weiss, E., Luca, F. C., Winey, M., & Murray, A. W. (1996). "Activation of the budding yeast spindle assembly checkpoint without mitotic spindle disruption". *Science (New York, N.Y.)*, *273*(5277), 953–956. https://doi.org/10.1126/science.273.5277.953

Hardwick, K. G., Li, R., Mistrot, C., Chen, R. H., Dann, P., Rudner, A., & Murray, A. W. (1999). "Lesions in many different spindle components activate the spindle checkpoint in the budding yeast Saccharomyces cerevisiae". *Genetics*, *152*(2), 509–518. https://doi.org/10.1093/genetics/152.2.509

Hassold, T., & Hunt, P. (2001). "To err (meiotically) is human: the genesis of human aneuploidy". *Nature reviews. Genetics*, *2*(4), 280–291. https://doi.org/10.1038/35066065

Hayden, J. H., Bowser, S. S., & Rieder, C. L. (1990). "Kinetochores capture astral microtubules during chromosome attachment to the mitotic spindle: direct visualization in live newt lung cells". *The Journal of cell biology*, *111*(3), 1039–1045. https://doi.org/10.1083/jcb.111.3.1039

Henikoff, S., & Furuyama, T. (2010). "Epigenetic inheritance of centromeres". *Cold Spring Harbor symposia on quantitative biology*, *75*, 51–60. https://doi.org/10.1101/sqb.2010.75.001

Hinshaw, S. M., & Harrison, S. C. (2013). "An Iml3-Chl4 heterodimer links the core centromere to factors required for accurate chromosome segregation". *Cell reports*, *5*(1), 29–36. https://doi.org/10.1016/j.celrep.2013.08.036

Hinshaw, S. M., Dates, A. N., & Harrison, S. C. (2019). “The structure of the yeast Ctf3 complex”. *eLife*, *8*, e48215. https://doi.org/10.7554/eLife.48215

Höckner, S., Neumann-Arnold, L., & Seufert, W. (2016). “Dual control by Cdk1 phosphorylation of the budding yeast APC/C ubiquitin ligase activator Cdh1”. *Molecular biology of the cell*, *27*(14), 2198–2212. https://doi.org/10.1091/mbc.E15-11-0787

Hofmann, C., Cheeseman, I. M., Goode, B. L., McDonald, K. L., Barnes, G., & Drubin, D. G. (1998). “Saccharomyces cerevisiae Duo1p and Dam1p, novel proteins involved in mitotic spindle function”. *The Journal of cell biology*, *143*(4), 1029–1040. https://doi.org/10.1083/jcb.143.4.1029

Hornung, P., Troc, P., Malvezzi, F., Maier, M., Demianova, Z., Zimniak, T., Litos, G., Lampert, F., Schleiffer, A., Brunner, M., Mechtler, K., Herzog, F., Marlovits, T. C., & Westermann, S. (2014). “A cooperative mechanism drives budding yeast kinetochore assembly downstream of CENP-A”. *The Journal of cell biology*, *206*(4), 509–524. https://doi.org/10.1083/jcb.201403081

Howell, B. J., Hoffman, D. B., Fang, G., Murray, A. W., & Salmon, E. D. (2000). “Visualization of Mad2 dynamics at kinetochores, along spindle fibers, and at spindle poles in living cells”. *The Journal of cell biology*, *150*(6), 1233–1250. https://doi.org/10.1083/jcb.150.6.1233

Hoyt, M. A., Totis, L., & Roberts, B. T. (1991). “S. cerevisiae genes required for cell cycle arrest in response to loss of microtubule function”. *Cell*, *66*(3), 507–517. https://doi.org/10.1016/0092-8674(81)90014-3

Hu, J., Cao, J., Topatana, W., Juengpanich, S., Li, S., Zhang, B., Shen, J., Cai, L., Cai, X., & Chen, M. (2021). “Targeting mutant p53 for cancer therapy: direct and indirect strategies”. *Journal of hematology & oncology*, *14*(1), 157. https://doi.org/10.1186/s13045-021-01169-0

Hwang, L. H., Lau, L. F., Smith, D. L., Mistrot, C. A., Hardwick, K. G., Hwang, E. S., Amon, A., & Murray, A. W. (1998). “Budding yeast Cdc20: a target of the spindle checkpoint”. *Science (New York, N.Y.)*, *279*(5353), 1041–1044. https://doi.org/10.1126/science.279.5353.1041

Indjeian, V. B., Stern, B. M., & Murray, A. W. (2005). “The centromeric protein Sgo1 is required to sense lack of tension on mitotic chromosomes”. *Science (New York, N.Y.)*, *307*(5706), 130–133. https://doi.org/10.1126/science.1101366

Indjeian, V. B., & Murray, A. W. (2007). “Budding yeast mitotic chromosomes have an intrinsic bias to biorient on the spindle”. *Current biology : CB*, *17*(21), 1837–1846. https://doi.org/10.1016/j.cub.2007.09.056

Janke, C., Ortíz, J., Tanaka, T. U., Lechner, J., & Schiebel, E. (2002). “Four new subunits of the Dam1-Duo1 complex reveal novel functions in sister kinetochore

biorientation". *The EMBO journal*, *21*(1-2), 181–193. https://doi.org/10.1093/emboj/21.1.181

Jaspersen, S. L., & Winey, M. (2004). "The budding yeast spindle pole body: structure, duplication, and function". *Annual review of cell and developmental biology*, *20*, 1–28. https://doi.org/10.1146/annurev.cellbio.20.022003.114106

Jazwinski S. M. (2005). "Rtg2 protein: at the nexus of yeast longevity and aging". *FEMS yeast research*, *5*(12), 1253–1259. https://doi.org/10.1016/j.femsyr.2005.07.001

Jenni, S., & Harrison, S. C. (2018). "Structure of the DASH/Dam1 complex shows its role at the yeast kinetochore-microtubule interface". *Science (New York, N.Y.)*, *360*(6388), 552–558. https://doi.org/10.1126/science.aar6436

Jeyaprakash, A. A., Klein, U. R., Lindner, D., Ebert, J., Nigg, E. A., & Conti, E. (2007). "Structure of a Survivin-Borealin-INCENP core complex reveals how chromosomal passengers travel together". *Cell*, *131*(2), 271–285. https://doi.org/10.1016/j.cell.2007.07.045

Jeyaprakash, A. A., Santamaria, A., Jayachandran, U., Chan, Y. W., Benda, C., Nigg, E. A., & Conti, E. (2012). "Structural and functional organization of the Ska complex, a key component of the kinetochore-microtubule interface". *Molecular cell*, *46*(3), 274–286. https://doi.org/10.1016/j.molcel.2012.03.005

Jin, Q. W., Fuchs, J., & Loidl, J. (2000). "Centromere clustering is a major determinant of yeast interphase nuclear organization". *Journal of cell science*, *113 (Pt 11)*, 1903–1912. https://doi.org/10.1242/jcs.113.11.1903

Jin, F., & Wang, Y. (2013). "The signaling network that silences the spindle assembly checkpoint upon the establishment of chromosome bipolar attachment". *Proceedings of the National Academy of Sciences of the United States of America*, *110*(52), 21036–21041. https://doi.org/10.1073/pnas.1307595111

Joglekar, A. P., Bloom, K., & Salmon, E. D. (2009). "In vivo protein architecture of the eukaryotic kinetochore with nanometer scale accuracy". *Current biology : CB*, *19*(8), 694–699. https://doi.org/10.1016/j.cub.2009.02.056

Jones, M. H., Bachant, J. B., Castillo, A. R., Giddings, T. H., Jr, & Winey, M. (1999). "Yeast Dam1p is required to maintain spindle integrity during mitosis and interacts with the Mps1p kinase". *Molecular biology of the cell*, *10*(7), 2377–2391. https://doi.org/10.1091/mbc.10.7.2377

Jones, M. H., He, X., Giddings, T. H., & Winey, M. (2001). "Yeast Dam1p has a role at the kinetochore in assembly of the mitotic spindle". *Proceedings of the National Academy of Sciences of the United States of America*, *98*(24), 13675–13680. https://doi.org/10.1073/pnas.241417098

Jones, M. H., Huneycutt, B. J., Pearson, C. G., Zhang, C., Morgan, G., Shokat, K., Bloom, K., & Winey, M. (2005). “Chemical genetics reveals a role for Mps1 kinase in kinetochore attachment during mitosis”. *Current biology : CB*, *15*(2), 160–165. https://doi.org/10.1016/j.cub.2005.01.010

Kaiser, P., Sia, R. A., Bardes, E. G., Lew, D. J., & Reed, S. I. (1998). “Cdc34 and the F-box protein Met30 are required for degradation of the Cdk-inhibitory kinase Swe1”. *Genes & development*, *12*(16), 2587–2597. https://doi.org/10.1101/gad.12.16.2587

Kalantzaki, M., Kitamura, E., Zhang, T., Mino, A., Novák, B., & Tanaka, T. U. (2015). “Kinetochore-microtubule error correction is driven by differentially regulated interaction modes”. *Nature cell biology*, *17*(4), 530. https://doi.org/10.1038/ncb3153

Kalitsis, P., Earle, E., Fowler, K. J., & Choo, K. H. (2000). “Bub3 gene disruption in mice reveals essential mitotic spindle checkpoint function during early embryogenesis”. *Genes & development*, *14*(18), 2277–2282. https://doi.org/10.1101/gad.827500

Kang, J., Chen, Y., Zhao, Y., & Yu, H. (2007). “Autophosphorylation-dependent activation of human Mps1 is required for the spindle checkpoint”. *Proceedings of the National Academy of Sciences of the United States of America*, *104*(51), 20232–20237. https://doi.org/10.1073/pnas.0710519105

Kaplan, K. B., Hyman, A. A., & Sorger, P. K. (1997). “Regulating the yeast kinetochore by ubiquitin-dependent degradation and Skp1p-mediated phosphorylation”. *Cell*, *91*(4), 491–500. https://doi.org/10.1016/s0092-8674(00)80435-3

Kemmler, S., Stach, M., Knapp, M., Ortiz, J., Pfannstiel, J., Ruppert, T., & Lechner, J. (2009). “Mimicking Ndc80 phosphorylation triggers spindle assembly checkpoint signaling”. *The EMBO journal*, *28*(8), 1099–1110. https://doi.org/10.1038/emboj.2009.62

Kim, S. H., Lin, D. P., Matsumoto, S., Kitazono, A., & Matsumoto, T. (1998). “Fission yeast Slp1: an effector of the Mad2-dependent spindle checkpoint”. *Science (New York, N.Y.)*, *279*(5353), 1045–1047. https://doi.org/10.1126/science.279.5353.1045

Kim, S., & Yu, H. (2011). “Mutual regulation between the spindle checkpoint and APC/C”. *Seminars in cell & developmental biology*, *22*(6), 551–558. https://doi.org/10.1016/j.semcdb.2011.03.008

Kinner, A., Wu, W., Staudt, C., & Iliakis, G. (2008). “Gamma-H2AX in recognition and signaling of DNA double-strand breaks in the context of chromatin”. *Nucleic acids research*, *36*(17), 5678–5694. https://doi.org/10.1093/nar/gkn550

Kitagawa, M., & Lee, S. H. (2015). “The chromosomal passenger complex (CPC) as a key orchestrator of orderly mitotic exit and cytokinesis”. *Frontiers in cell and developmental biology*, *3*, 14. https://doi.org/10.3389/fcell.2015.00014

Kitagawa, R., & Rose, A. M. (1999). “Components of the spindle-assembly checkpoint are essential in Caenorhabditis elegans”. *Nature cell biology*, *1*(8), 514–521. https://doi.org/10.1038/70309

Kitajima, T. S., Hauf, S., Ohsugi, M., Yamamoto, T., & Watanabe, Y. (2005). “Human Bub1 defines the persistent cohesion site along the mitotic chromosome by affecting Shugoshin localization”. *Current biology : CB*, *15*(4), 353–359. https://doi.org/10.1016/j.cub.2004.12.044

Kitajima, T. S., Sakuno, T., Ishiguro, K., Iemura, S., Natsume, T., Kawashima, S. A., & Watanabe, Y. (2006). “Shugoshin collaborates with protein phosphatase 2A to protect cohesin”. *Nature*, *441*(7089), 46–52. https://doi.org/10.1038/nature04663

Kitamura, E., Tanaka, K., Kitamura, Y., & Tanaka, T. U. (2007). “Kinetochore microtubule interaction during S phase in Saccharomyces cerevisiae”. *Genes & development*, *21*(24), 3319–3330. https://doi.org/10.1101/gad.449407

Kline-Smith, S. L., & Walczak, C. E. (2002). “The microtubule-destabilizing kinesin XKCM1 regulates microtubule dynamic instability in cells”. *Molecular biology of the cell*, *13*(8), 2718–2731. https://doi.org/10.1091/mbc.e01-12-0143

Knop, M., Pereira, G., & Schiebel, E. (1999). “Microtubule organization by the budding yeast spindle pole body”. *Biology of the cell*, *91*(4-5), 291–304.

Kollman, J. M., Zelter, A., Muller, E. G., Fox, B., Rice, L. M., Davis, T. N., & Agard, D. A. (2008). “The structure of the gamma-tubulin small complex: implications of its architecture and flexibility for microtubule nucleation”. *Molecular biology of the cell*, *19*(1), 207–215. https://doi.org/10.1091/mbc.e07-09-0879

Kollman, J. M., Polka, J. K., Zelter, A., Davis, T. N., & Agard, D. A. (2010). “Microtubule nucleating gamma-TuSC assembles structures with 13-fold microtubule-like symmetry”. *Nature*, *466*(7308), 879–882. https://doi.org/10.1038/nature09207

Kothiwal, D., Gopinath, S., & Laloraya, S. (2021). “Cohesin dysfunction results in cell wall defects in budding yeast”. *Genetics*, *217*(1), 1–16. https://doi.org/10.1093/genetics/iyaa023

Kuilman, T., Michaloglou, C., Mooi, W. J., & Peeper, D. S. (2010). “The essence of senescence”. *Genes & development*, *24*(22), 2463–2479. https://doi.org/10.1101/gad.1971610

Kurimchak, A. M., Herrera-Montávez, C., Montserrat-Sangrà, S., Araiza-Olivera, D., Hu, J., Neumann-Domer, R., Kuruvilla, M., Bellacosa, A., Testa, J. R., Jin, J., & Duncan, J. S. (2022). “The drug efflux pump MDR1 promotes intrinsic and acquired resistance to PROTACs in cancer cells”. *Science signaling*, *15*(749), eabn2707. https://doi.org/10.1126/scisignal.abn2707

Lampson, M. A., & Cheeseman, I. M. (2011). “Sensing centromere tension: Aurora B and the regulation of kinetochore function”. *Trends in cell biology*, *21*(3), 133–140. https://doi.org/10.1016/j.tcb.2010.10.007

Lang, J., Barber, A., & Biggins, S. (2018). “An assay for de novo kinetochore assembly reveals a key role for the CENP-T pathway in budding yeast”. *eLife*, *7*, e37819. https://doi.org/10.7554/eLife.37819

Lara-Gonzalez, P., Pines, J., & Desai, A. (2021). “Spindle assembly checkpoint activation and silencing at kinetochores”. *Seminars in cell & developmental biology*, *117*, 86–98. https://doi.org/10.1016/j.semcdb.2021.06.009

Lau, D. T., & Murray, A. W. (2012). “Mad2 and Mad3 cooperate to arrest budding yeast in mitosis”. *Current biology : CB*, *22*(3), 180–190. https://doi.org/10.1016/j.cub.2011.12.029

Lee, J., Ogushi, S., Saitou, M., & Hirano, T. (2011). “Condensins I and II are essential for construction of bivalent chromosomes in mouse oocytes”. *Molecular biology of the cell*, *22*(18), 3465–3477. https://doi.org/10.1091/mbc.E11-05-0423

Li, Y., Gorbea, C., Mahaffey, D., Rechsteiner, M., & Benezra, R. (1997). “MAD2 associates with the cyclosome/anaphase-promoting complex and inhibits its activity”. *Proceedings of the National Academy of Sciences of the United States of America*, *94*(23), 12431–12436. https://doi.org/10.1073/pnas.94.23.12431

Li, Y., Bachant, J., Alcasabas, A. A., Wang, Y., Qin, J., & Elledge, S. J. (2002). “The mitotic spindle is required for loading of the DASH complex onto the kinetochore”. *Genes & development*, *16*(2), 183–197. https://doi.org/10.1101/gad.959402

Li, R., & Murray, A. W. (1991). “Feedback control of mitosis in budding yeast”. *Cell*, *66*(3), 519–531. https://doi.org/10.1016/0092-8674(81)90015-5

Li, X., & Nicklas, R. B. (1995). “Mitotic forces control a cell-cycle checkpoint”. *Nature*, *373*(6515), 630–632. https://doi.org/10.1038/373630a0

Liu, D., & Lampson, M. A. (2009). “Regulation of kinetochore-microtubule attachments by Aurora B kinase”. *Biochemical Society transactions*, *37*(Pt 5), 976–980. https://doi.org/10.1042/BST0370976

London, N., Ceto, S., Ranish, J. A., & Biggins, S. (2012). “Phosphoregulation of Spc105 by Mps1 and PP1 regulates Bub1 localization to kinetochores”. *Current biology : CB*, *22*(10), 900–906. https://doi.org/10.1016/j.cub.2012.03.052

Luo, X., Fang, G., Coldiron, M., Lin, Y., Yu, H., Kirschner, M. W., & Wagner, G. (2000). “Structure of the Mad2 spindle assembly checkpoint protein and its interaction with Cdc20”. *Nature structural biology*, *7*(3), 224–229. https://doi.org/10.1038/73338

Luo, X., Tang, Z., Rizo, J., & Yu, H. (2002). “The Mad2 spindle checkpoint protein undergoes similar major conformational changes upon binding to either Mad1 or Cdc20”. *Molecular cell*, *9*(1), 59–71. https://doi.org/10.1016/s1097-2765(01)00435-x

Maciejowski, J., Drechsler, H., Grundner-Culemann, K., Ballister, E. R., Rodriguez-Rodriguez, J. A., Rodriguez-Bravo, V., Jones, M. J. K., Foley, E., Lampson, M. A., Daub, H., McAinsh, A. D., & Jallepalli, P. V. (2017). “Mps1 Regulates Kinetochore-Microtubule Attachment Stability via the Ska Complex to Ensure Error-Free Chromosome Segregation”. *Developmental cell*, *41*(2), 143–156.e6. https://doi.org/10.1016/j.devcel.2017.03.025

Maiato, H., Rieder, C. L., & Khodjakov, A. (2004). “Kinetochore-driven formation of kinetochore fibers contributes to spindle assembly during animal mitosis”. *The Journal of cell biology*, *167*(5), 831–840. https://doi.org/10.1083/jcb.200407090

Maiato, H., Gomes, A. M., Sousa, F., & Barisic, M. (2017). “Mechanisms of Chromosome Congression during Mitosis”. *Biology*, *6*(1), 13. https://doi.org/10.3390/biology6010013

Malvezzi, F., Litos, G., Schleiffer, A., Heuck, A., Mechtler, K., Clausen, T., & Westermann, S. (2013). “A structural basis for kinetochore recruitment of the Ndc80 complex via two distinct centromere receptors”. *The EMBO journal*, *32*(3), 409–423. https://doi.org/10.1038/emboj.2012.356

Mapelli, M., Massimiliano, L., Santaguida, S., & Musacchio, A. (2007). “The Mad2 conformational dimer: structure and implications for the spindle assembly checkpoint”. *Cell*, *131*(4), 730–743. https://doi.org/10.1016/j.cell.2007.08.049

Mantovani, F., Collavin, L., & Del Sal, G. (2019). “Mutant p53 as a guardian of the cancer cell”. *Cell death and differentiation*, *26*(2), 199–212. https://doi.org/10.1038/s41418-018-0246-9

Marco, E., Dorn, J. F., Hsu, P. H., Jaqaman, K., Sorger, P. K., & Danuser, G. (2013). “S. cerevisiae chromosomes biorient via gradual resolution of syntely between S phase and anaphase”. *Cell*, *154*(5), 1127–1139. https://doi.org/10.1016/j.cell.2013.08.008

Marsoner, T., Yedavalli, P., Masnovo, C., Fink, S., Schmitzer, K., & Campbell, C. S. (2022). “Aurora B activity is promoted by cooperation between discrete localization sites in budding yeast”. *Molecular biology of the cell*, *33*(9), ar85. https://doi.org/10.1091/mbc.E21-11-0590

Marsoner, T. (2022) “Mechanistic characterization of Aurora B regulation pathways during chromosome biorientation”. *University of Vienna*. https://ubdata.univie.ac.at/AC16743320 [Accessed 20.02.2023]

Martínez-García, B., Dyson, S., Segura, J., Ayats, A., Cutts, E. E., Gutierrez-

Escribano, P., Aragón, L., & Roca, J. (2023). “Condensin pinches a short negatively supercoiled DNA loop during each round of ATP usage”. *The EMBO journal*, *42*(3), e111913. https://doi.org/10.15252/embj.2022111913

Maskell, D. P., Hu, X. W., & Singleton, M. R. (2010). “Molecular architecture and assembly of the yeast kinetochore MIND complex”. *The Journal of cell biology*, *190*(5), 823–834. https://doi.org/10.1083/jcb.201002059

Mathias, N., Johnson, S. L., Winey, M., Adams, A. E., Goetsch, L., Pringle, J. R., Byers, B., & Goebl, M. G. (1996). “Cdc53p acts in concert with Cdc4p and Cdc34p to control the G1-to-S-phase transition and identifies a conserved family of proteins”. *Molecular and cellular biology*, *16*(12), 6634–6643. https://doi.org/10.1128/MCB.16.12.6634

Mattison, C. P., Old, W. M., Steiner, E., Huneycutt, B. J., Resing, K. A., Ahn, N. G., & Winey, M. (2007). “Mps1 activation loop autophosphorylation enhances kinase activity”. *The Journal of biological chemistry*, *282*(42), 30553–30561. https://doi.org/10.1074/jbc.M707063200

McGranahan, N., Burrell, R. A., Endesfelder, D., Novelli, M. R., & Swanton, C. (2012). “Cancer chromosomal instability: therapeutic and diagnostic challenges”. *EMBO reports*, *13*(6), 528–538. https://doi.org/10.1038/embor.2012.61

Meluh, P. B., Yang, P., Glowczewski, L., Koshland, D., & Smith, M. M. (1998). “Cse4p is a component of the core centromere of Saccharomyces cerevisiae”. *Cell*, *94*(5), 607–613. https://doi.org/10.1016/s0092-8674(00)81602-5

Menendez, D., Shatz, M., & Resnick, M. A. (2013). “Interactions between the tumor suppressor p53 and immune responses”. *Current opinion in oncology*, *25*(1), 85–92. https://doi.org/10.1097/CCO.0b013e32835b6386

Merdes, A., & De Mey, J. (1990). “The mechanism of kinetochore-spindle attachment and polewards movement analyzed in PtK2 cells at the prophase-prometaphase transition”. *European journal of cell biology*, *53*(2), 313–325.

Meyer, A. E., Furumo, Q., Stelloh, C., Minella, A. C., & Rao, S. (2020). “Loss of Fbxw7 triggers mammary tumorigenesis associated with E2F/c-Myc activation and Trp53 mutation”. *Neoplasia (New York, N.Y.)*, *22*(11), 644–658. https://doi.org/10.1016/j.neo.2020.07.001

Meyer, R. E., Brown, J., Beck, L., & Dawson, D. S. (2018). “Mps1 promotes chromosome meiotic chromosome biorientation through Dam1”. *Molecular biology of the cell*, *29*(4), 479–489. https://doi.org/10.1091/mbc.E17-08-0503

Miller, S. A., Johnson, M. L., & Stukenberg, P. T. (2008). “Kinetochore attachments require an interaction between unstructured tails on microtubules and Ndc80(Hec1)”. *Current biology : CB*, *18*(22), 1785–1791. https://doi.org/10.1016/j.cub.2008.11.007

Mirchenko, L., & Uhlmann, F. (2010). “Sli15(INCENP) dephosphorylation prevents mitotic checkpoint reengagement due to loss of tension at anaphase onset”. *Current biology : CB*, *20*(15), 1396–1401. https://doi.org/10.1016/j.cub.2010.06.023

Murray A. W. (2011). “A brief history of error”. *Nature cell biology*, *13*(10), 1178–1182. https://doi.org/10.1038/ncb2348

Musacchio A. (2011). “Spindle assembly checkpoint: the third decade”. *Philosophical transactions of the Royal Society of London. Series B, Biological sciences*, *366*(1584), 3595–3604. https://doi.org/10.1098/rstb.2011.0072

Musacchio, A., & Desai, A. (2017). “A Molecular View of Kinetochore Assembly and Function”. *Biology*, *6*(1), 5. https://doi.org/10.3390/biology6010005

Nakajima, Y., Tyers, R. G., Wong, C. C., Yates, J. R., 3rd, Drubin, D. G., & Barnes, G. (2009). “Nbl1p: a Borealin/Dasra/CSC-1-like protein essential for Aurora/Ipl1 complex function and integrity in Saccharomyces cerevisiae”. *Molecular biology of the cell*, *20*(6), 1772–1784. https://doi.org/10.1091/mbc.e08-10-1011

Nash, P., Tang, X., Orlicky, S., Chen, Q., Gertler, F. B., Mendenhall, M. D., Sicheri, F., Pawson, T., & Tyers, M. (2001). “Multisite phosphorylation of a CDK inhibitor sets a threshold for the onset of DNA replication”. *Nature*, *414*(6863), 514–521. https://doi.org/10.1038/35107009

Navarro, A. P., & Cheeseman, I. M. (2021). “Kinetochore assembly throughout the cell cycle”. *Seminars in cell & developmental biology*, *117*, 62–74. https://doi.org/10.1016/j.semcdb.2021.03.008

Ng, C. T., Deng, L., Chen, C., Lim, H. H., Shi, J., Surana, U., & Gan, L. (2019). “Electron cryotomography analysis of Dam1C/DASH at the kinetochore-spindle interface in situ”. *The Journal of cell biology*, *218*(2), 455–473. https://doi.org/10.1083/jcb.201809088

Nicholson, J. M., & Cimini, D. (2013). “Cancer karyotypes: survival of the fittest”. *Frontiers in oncology*, *3*, 148. https://doi.org/10.3389/fonc.2013.00148

Nicklas R. B. (1967). “Chromosome micromanipulation. II. Induced reorientation and the experimental control of segregation in meiosis”. *Chromosoma*, *21*(1), 17–50. https://doi.org/10.1007/BF00330545

Nicklas R. B. (1997). “How cells get the right chromosomes”. *Science (New York, N.Y.)*, *275*(5300), 632–637. https://doi.org/10.1126/science.275.5300.632

Nicklas, R. B., & Koch, C. A. (1969). “Chromosome micromanipulation. 3. Spindle fiber tension and the reorientation of maloriented chromosomes”. *The Journal of cell biology*, *43*(1), 40–50. https://doi.org/10.1083/jcb.43.1.40

Nishide, K., & Hirano, T. (2014). “Overlapping and non-overlapping functions of

condensins I and II in neural stem cell divisions". *PLoS genetics*, *10*(12), e1004847. https://doi.org/10.1371/journal.pgen.1004847

Oliveira, R. A., & Nasmyth, K. (2010). "Getting through anaphase: splitting the sisters and beyond". *Biochemical Society transactions*, *38*(6), 1639–1644. https://doi.org/10.1042/BST0381639

Orlicky, S., Tang, X., Neduva, V., Elowe, N., Brown, E. D., Sicheri, F., & Tyers, M. (2010). "An allosteric inhibitor of substrate recognition by the SCF(Cdc4) ubiquitin ligase". *Nature biotechnology*, *28*(7), 733–737. https://doi.org/10.1038/nbt.1646

Oromendia, A. B., Dodgson, S. E., & Amon, A. (2012). "Aneuploidy causes proteotoxic stress in yeast". *Genes & development*, *26*(24), 2696–2708. https://doi.org/10.1101/gad.207407.112

Palmer, D. K., O'Day, K., Wener, M. H., Andrews, B. S., & Margolis, R. L. (1987). "A 17-kD centromere protein (CENP-A) copurifies with nucleosome core particles and with histones". *The Journal of cell biology*, *104*(4), 805–815. https://doi.org/10.1083/jcb.104.4.805

Pangilinan, F., & Spencer, F. (1996). "Abnormal kinetochore structure activates the spindle assembly checkpoint in budding yeast". *Molecular biology of the cell*, *7*(8), 1195–1208. https://doi.org/10.1091/mbc.7.8.1195

Passerini, V., & Storchová, Z. (2016). "Too much to handle - how gaining chromosomes destabilizes the genome". *Cell cycle (Georgetown, Tex.)*, *15*(21), 2867–2874. https://doi.org/10.1080/15384101.2016.1231285

Patton, E. E., Willems, A. R., Sa, D., Kuras, L., Thomas, D., Craig, K. L., & Tyers, M. (1998). "Cdc53 is a scaffold protein for multiple Cdc34/Skp1/F-box proteincomplexes that regulate cell division and methionine biosynthesis in yeast". *Genes & development*, *12*(5), 692–705. https://doi.org/10.1101/gad.12.5.692

Pavani, M., Bonaiuti, P., Chiroli, E., Gross, F., Natali, F., Macaluso, F., Póti, Á., Pasqualato, S., Farkas, Z., Pompei, S., Cosentino Lagomarsino, M., Rancati, G., Szüts, D., & Ciliberto, A. (2021). "Epistasis, aneuploidy, and functional mutations underlie evolution of resistance to induced microtubule depolymerization". *The EMBO journal*, *40*(22), e108225. https://doi.org/10.15252/embj.2021108225

Peters, J. M., Tedeschi, A., & Schmitz, J. (2008). "The cohesin complex and its roles in chromosome biology". *Genes & development*, *22*(22), 3089–3114. https://doi.org/10.1101/gad.1724308

Peters, J. M., & Nishiyama, T. (2012). "Sister chromatid cohesion". *Cold Spring Harbor perspectives in biology*, *4*(11), a011130. https://doi.org/10.1101/cshperspect.a011130

Pettersen, E. F., Goddard, T. D., Huang, C. C., Meng, E. C., Couch, G. S., Croll, T.

I., Morris, J. H., & Ferrin, T. E. (2021). “UCSF ChimeraX: Structure visualization for researchers, educators, and developers”. *Protein science : a publication of the Protein Society*, *30*(1), 70–82. https://doi.org/10.1002/pro.3943

Pereira, G., & Schiebel, E. (2003). “Separase regulates INCENP-Aurora B anaphase spindle function through Cdc14”. *Science (New York, N.Y.)*, *302*(5653), 2120–2124. https://doi.org/10.1126/science.1091936

Pfau, S. J., & Amon, A. (2012). “Chromosomal instability and aneuploidy in cancer: from yeast to man”. *EMBO reports*, *13*(6), 515–527. https://doi.org/10.1038/embor.2012.65

Pinsky, B. A., Kung, C., Shokat, K. M., & Biggins, S. (2006). “The Ipl1-Aurora protein kinase activates the spindle checkpoint by creating unattached kinetochores”. *Nature cell biology*, *8*(1), 78–83. https://doi.org/10.1038/ncb1341

Pinsky, B. A., Nelson, C. R., & Biggins, S. (2009). “Protein phosphatase 1 regulates exit from the spindle checkpoint in budding yeast”. *Current biology : CB*, *19*(14), 1182–1187. https://doi.org/10.1016/j.cub.2009.06.043

Raaijmakers, J. A., Tanenbaum, M. E., Maia, A. F., & Medema, R. H. (2009). “RAMA1 is a novel kinetochore protein involved in kinetochore-microtubule attachment”. *Journal of cell science*, *122*(Pt 14), 2436–2445. https://doi.org/10.1242/jcs.051912

Rancati, G., Pavelka, N., Fleharty, B., Noll, A., Trimble, R., Walton, K., Perera, A., Staehling-Hampton, K., Seidel, C. W., & Li, R. (2008). “Aneuploidy underlies rapid adaptive evolution of yeast cells deprived of a conserved cytokinesis motor”. *Cell*, *135*(5), 879–893. https://doi.org/10.1016/j.cell.2008.09.039

Ravichandran, M. C., Fink, S., Clarke, M. N., Hofer, F. C., & Campbell, C. S. (2018). “Genetic interactions between specific chromosome copy number alterations dictate complex aneuploidy patterns”. *Genes & development*, *32*(23-24), 1485–1498. https://doi.org/10.1101/gad.319400.118

Ravichandran, M.C. (2020) “Genetic interactions between specific chromosome copy number alterations dictate complex aneuploidy patterns” *University of Vienna*. https://ubdata.univie.ac.at/AC15594127 [Accessed 20.02.2023]

Rayment, I. (2023), *Ivan Rayment: faculty: biochemistry: UW-Madison*, Available at: https://biochem.wisc.edu/faculty/rayment, [Accessed February 10, 2023], last updated February, 2023

Replogle, J. M., Zhou, W., Amaro, A. E., McFarland, J. M., Villalobos-Ortiz, M., Ryan, J., Letai, A., Yilmaz, O., Sheltzer, J., Lippard, S. J., Ben-David, U., & Amon, A. (2020). “Aneuploidy increases resistance to chemotherapeutics by antagonizing cell division”. *Proceedings of the National Academy of Sciences of the United States of America*, *117*(48), 30566–30576. https://doi.org/10.1073/pnas.2009506117

Rieder, C. L., & Alexander, S. P. (1990). “Kinetochores are transported poleward along a single astral microtubule during chromosome attachment to the spindle in newt lung cells”. *The Journal of cell biology*, *110*(1), 81–95. https://doi.org/10.1083/jcb.110.1.81

Rieder, C. L., & Palazzo, R. E. (1992). “Colcemid and the mitotic cycle”. *Journal of cell science*, *102 (Pt 3)*, 387–392. https://doi.org/10.1242/jcs.102.3.387

Rieder C. L. (2011). “Mitosis in vertebrates: the G2/M and M/A transitions and their associated checkpoints”. *Chromosome research : an international journal on the molecular, supramolecular and evolutionary aspects of chromosome biology*, *19*(3), 291–306. https://doi.org/10.1007/s10577-010-9178-z

Rosenberg, J. S., Cross, F. R., & Funabiki, H. (2011). “KNL1/Spc105 recruits PP1 to silence the spindle assembly checkpoint”. *Current biology : CB*, *21*(11), 942–947. https://doi.org/10.1016/j.cub.2011.04.011

Rüthnick, D., & Schiebel, E. (2016). “Duplication of the Yeast Spindle Pole Body Once per Cell Cycle”. *Molecular and cellular biology*, *36*(9), 1324–1331. https://doi.org/10.1128/MCB.00048-16

Rutledge, S. D., Douglas, T. A., Nicholson, J. M., Vila-Casadesús, M., Kantzler, C. L., Wangsa, D., Barroso-Vilares, M., Kale, S. D., Logarinho, E., & Cimini, D. (2016). “Selective advantage of trisomic human cells cultured in non-standard conditions”. *Scientific reports*, *6*, 22828. https://doi.org/10.1038/srep22828

Ryu, H. Y., Wilson, N. R., Mehta, S., Hwang, S. S., & Hochstrasser, M. (2016). “Loss of the SUMO protease Ulp2 triggers a specific multichromosome aneuploidy”. *Genes & development*, *30*(16), 1881–1894. https://doi.org/10.1101/gad.282194.116

Ryu, J. K., Rah, S. H., Janissen, R., Kerssemakers, J. W. J., Bonato, A., Michieletto, D., & Dekker, C. (2022). “Condensin extrudes DNA loops in steps up to hundreds of base pairs that are generated by ATP binding events”. *Nucleic acids research*, *50*(2), 820–832. https://doi.org/10.1093/nar/gkab1268

Santaguida, S., & Musacchio, A. (2009). “The life and miracles of kinetochores”. *The EMBO journal*, *28*(17), 2511–2531. https://doi.org/10.1038/emboj.2009.173

Sansregret, L., Patterson, J. O., Dewhurst, S., López-García, C., Koch, A., McGranahan, N., Chao, W. C. H., Barry, D. J., Rowan, A., Instrell, R., Horswell, S., Way, M., Howell, M., Singleton, M. R., Medema, R. H., Nurse, P., Petronczki, M., & Swanton, C. (2017). “APC/C Dysfunction Limits Excessive Cancer Chromosomal Instability”. *Cancer discovery*, *7*(2), 218–233. https://doi.org/10.1158/2159-8290.CD-16-0645

Sansregret, L., Vanhaesebroeck, B., & Swanton, C. (2018). “Determinants and clinical implications of chromosomal instability in cancer”. *Nature reviews. Clinical*

oncology, *15*(3), 139–150. https://doi.org/10.1038/nrclinonc.2017.198

Sarangapani, K. K., Akiyoshi, B., Duggan, N. M., Biggins, S., & Asbury, C. L. (2013). "Phosphoregulation promotes release of kinetochores from dynamic microtubules via multiple mechanisms". *Proceedings of the National Academy of Sciences of the United States of America*, *110*(18), 7282–7287. https://doi.org/10.1073/pnas.1220700110

Sauer, G., Körner, R., Hanisch, A., Ries, A., Nigg, E. A., & Silljé, H. H. (2005). "Proteome analysis of the human mitotic spindle". *Molecular & cellular proteomics : MCP*, *4*(1), 35–43. https://doi.org/10.1074/mcp.M400158-MCP200

Schellhaus, A. K., De Magistris, P., & Antonin, W. (2016). "Nuclear Reformation at the End of Mitosis". *Journal of molecular biology*, *428*(10 Pt A), 1962–1985. https://doi.org/10.1016/j.jmb.2015.09.016

Schleiffer, A., Maier, M., Litos, G., Lampert, F., Hornung, P., Mechtler, K., & Westermann, S. (2012). "CENP-T proteins are conserved centromere receptors of the Ndc80 complex". *Nature cell biology*, *14*(6), 604–613. https://doi.org/10.1038/ncb2493

Schwob, E., Böhm, T., Mendenhall, M. D., & Nasmyth, K. (1994). "The B-type cyclin kinase inhibitor p40SIC1 controls the G1 to S transition in S. cerevisiae". *Cell*, *79*(2), 233–244. https://doi.org/10.1016/0092-8674(94)90193-7

Shang, C., Hazbun, T. R., Cheeseman, I. M., Aranda, J., Fields, S., Drubin, D. G., & Barnes, G. (2003). "Kinetochore protein interactions and their regulation by the Aurora kinase Ipl1p". *Molecular biology of the cell*, *14*(8), 3342–3355. https://doi.org/10.1091/mbc.e02-11-0765

Sheltzer, J. M., Blank, H. M., Pfau, S. J., Tange, Y., George, B. M., Humpton, T. J., Brito, I. L., Hiraoka, Y., Niwa, O., & Amon, A. (2011). "Aneuploidy drives genomic instability in yeast". *Science (New York, N.Y.)*, *333*(6045), 1026–1030. https://doi.org/10.1126/science.1206412

Sheltzer, J. M., Torres, E. M., Dunham, M. J., & Amon, A. (2012). "Transcriptional consequences of aneuploidy". *Proceedings of the National Academy of Sciences of the United States of America*, *109*(31), 12644–12649. https://doi.org/10.1073/pnas.1209227109

Shimogawa, M. M., Graczyk, B., Gardner, M. K., Francis, S. E., White, E. A., Ess, M., Molk, J. N., Ruse, C., Niessen, S., Yates, J. R., 3rd, Muller, E. G., Bloom, K., Odde, D. J., & Davis, T. N. (2006). "Mps1 phosphorylation of Dam1 couples kinetochores to microtubule plus ends at metaphase". *Current biology : CB*, *16*(15), 1489–1501. https://doi.org/10.1016/j.cub.2006.06.063

Shimogawa, M. M., Wargacki, M. M., Muller, E. G., & Davis, T. N. (2010). "Laterally

attached kinetochores recruit the checkpoint protein Bub1, but satisfy the spindle checkpoint". *Cell cycle (Georgetown, Tex.)*, *9*(17), 3619–3628. https://doi.org/10.4161/cc.9.17.12907

Shintomi, K., & Hirano, T. (2011). "The relative ratio of condensin I to II determines chromosome shapes". *Genes & development*, *25*(14), 1464–1469. https://doi.org/10.1101/gad.2060311

Shukla, A., Nguyen, T. H. M., Moka, S. B., Ellis, J. J., Grady, J. P., Oey, H., Cristino, A. S., Khanna, K. K., Kroese, D. P., Krause, L., Dray, E., Fink, J. L., & Duijf, P. H. G. (2020). "Chromosome arm aneuploidies shape tumour evolution and drug response". *Nature communications*, *11*(1), 449. https://doi.org/10.1038/s41467-020-14286-0

Sironi, L., Mapelli, M., Knapp, S., De Antoni, A., Jeang, K. T., & Musacchio, A. (2002). "Crystal structure of the tetrameric Mad1-Mad2 core complex: implications of a 'safety belt' binding mechanism for the spindle checkpoint". *The EMBO journal*, *21*(10), 2496–2506. https://doi.org/10.1093/emboj/21.10.2496

Sivakumar, S., Daum, J. R., Tipton, A. R., Rankin, S., & Gorbsky, G. J. (2014). "The spindle and kinetochore-associated (Ska) complex enhances binding of the anaphase-promoting complex/cyclosome (APC/C) to chromosomes and promotes mitotic exit". *Molecular biology of the cell*, *25*(5), 594–605. https://doi.org/10.1091/mbc.E13-07-0421

Sivakumar, S., Janczyk, P. Ł., Qu, Q., Brautigam, C. A., Stukenberg, P. T., Yu, H., & Gorbsky, G. J. (2016). "The human SKA complex drives the metaphase-anaphase cell cycle transition by recruiting protein phosphatase 1 to kinetochores". *eLife*, *5*, e12902. https://doi.org/10.7554/eLife.12902

Skibbens R. V. (2019). "Condensins and cohesins - one of these things is not like the other!". *Journal of cell science*, *132*(3), jcs220491. https://doi.org/10.1242/jcs.220491

Smardová, J., Smarda, J., & Koptíková, J. (2005). "Functional analysis of p53 tumor suppressor in yeast". *Differentiation; research in biological diversity*, *73*(6), 261–277. https://doi.org/10.1111/j.1432-0436.2005.00028.x

Smoyer, C. J., & Jaspersen, S. L. (2014). "Breaking down the wall: the nuclear envelope during mitosis". *Current opinion in cell biology*, *26*, 1–9. https://doi.org/10.1016/j.ceb.2013.08.002

Sorger, P. K., Doheny, K. F., Hieter, P., Kopski, K. M., Huffaker, T. C., & Hyman, A. A. (1995). "Two genes required for the binding of an essential Saccharomyces cerevisiae kinetochore complex to DNA". *Proceedings of the National Academy of Sciences of the United States of America*, *92*(26), 12026–12030. https://doi.org/10.1073/pnas.92.26.12026

Stellfox, M. E., Bailey, A. O., & Foltz, D. R. (2013). "Putting CENP-A in its place". *Cellular and molecular life sciences : CMLS*, *70*(3), 387–406.

https://doi.org/10.1007/s00018-012-1048-8

Stoler, S., Keith, K. C., Curnick, K. E., & Fitzgerald-Hayes, M. (1995). “A mutation in CSE4, an essential gene encoding a novel chromatin-associated protein in yeast, causes chromosome nondisjunction and cell cycle arrest at mitosis”. *Genes & development*, *9*(5), 573–586. https://doi.org/10.1101/gad.9.5.573

Storchová, Z., Becker, J. S., Talarek, N., Kögelsberger, S., & Pellman, D. (2011). “Bub1, Sgo1, and Mps1 mediate a distinct pathway for chromosome biorientation in budding yeast”. *Molecular biology of the cell*, *22*(9), 1473–1485. https://doi.org/10.1091/mbc.E10-08-0673

Storchova Z. (2018). “Evolution of aneuploidy: overcoming the original CIN”. *Genes & development*, *32*(23-24), 1459–1460. https://doi.org/10.1101/gad.321810.118

Straight, P. D., Giddings, T. H., Jr, & Winey, M. (2000). “Mps1p regulates meiotic spindle pole body duplication in addition to having novel roles during sporulation”. *Molecular biology of the cell*, *11*(10), 3525–3537. https://doi.org/10.1091/mbc.11.10.3525

Tanaka, K., Mukae, N., Dewar, H., van Breugel, M., James, E. K., Prescott, A. R., Antony, C., & Tanaka, T. U. (2005). “Molecular mechanisms of kinetochore capture by spindle microtubules”. *Nature*, *434*(7036), 987–994. https://doi.org/10.1038/nature03483

Tanaka, T. U., Rachidi, N., Janke, C., Pereira, G., Galova, M., Schiebel, E., Stark, M. J., & Nasmyth, K. (2002). “Evidence that the Ipl1-Sli15 (Aurora kinase-INCENP) complex promotes chromosome bi-orientation by altering kinetochore-spindle pole connections”. *Cell*, *108*(3), 317–329. https://doi.org/10.1016/s0092-8674(02)00633-5

Tanaka T. U. (2010). “Kinetochore-microtubule interactions: steps towards biorientation”. *The EMBO journal*, *29*(24), 4070–4082. https://doi.org/10.1038/emboj.2010.294

Taylor, A. M., Shih, J., Ha, G., Gao, G. F., Zhang, X., Berger, A. C., Schumacher, S. E., Wang, C., Hu, H., Liu, J., Lazar, A. J., Cancer Genome Atlas Research Network, Cherniack, A. D., Beroukhim, R., & Meyerson, M. (2018). “Genomic and Functional Approaches to Understanding Cancer Aneuploidy”. *Cancer cell*, *33*(4), 676–689.e3. https://doi.org/10.1016/j.ccell.2018.03.007

Theis, M., Slabicki, M., Junqueira, M., Paszkowski-Rogacz, M., Sontheimer, J., Kittler, R., Heninger, A. K., Glatter, T., Kruusmaa, K., Poser, I., Hyman, A. A., Pisabarro, M. T., Gstaiger, M., Aebersold, R., Shevchenko, A., & Buchholz, F. (2009). “Comparative profiling identifies C13orf3 as a component of the Ska complex required for mammalian cell division”. *The EMBO journal*, *28*(10), 1453–1465. https://doi.org/10.1038/emboj.2009.114

Torres, E. M., Sokolsky, T., Tucker, C. M., Chan, L. Y., Boselli, M., Dunham, M. J., &

Amon, A. (2007). “Effects of aneuploidy on cellular physiology and cell division in haploid yeast”. *Science (New York, N.Y.)*, *317*(5840), 916–924. https://doi.org/10.1126/science.1142210

Torres, E. M., Dephoure, N., Panneerselvam, A., Tucker, C. M., Whittaker, C. A., Gygi, S. P., Dunham, M. J., & Amon, A. (2010). “Identification of aneuploidy-tolerating mutations”. *Cell*, *143*(1), 71–83. https://doi.org/10.1016/j.cell.2010.08.038

Tsukahara, T., Tanno, Y., & Watanabe, Y. (2010). “Phosphorylation of the CPC by Cdk1 promotes chromosome biorientation”. *Nature*, *467*(7316), 719–723. https://doi.org/10.1038/nature09390

Umbreit, N. T., Miller, M. P., Tien, J. F., Ortolá, J. C., Gui, L., Lee, K. K., Biggins, S., Asbury, C. L., & Davis, T. N. (2014). “Kinetochores require oligomerization of Dam1 complex to maintain microtubule attachments against tension and promote biorientation”. *Nature communications*, *5*, 4951. https://doi.org/10.1038/ncomms5951

Vader, G., Kauw, J. J., Medema, R. H., & Lens, S. M. (2006). “Survivin mediates targeting of the chromosomal passenger complex to the centromere and midbody”. *EMBO reports*, *7*(1), 85–92. https://doi.org/10.1038/sj.embor.7400562

van der Horst, A., & Lens, S. M. (2014). “Cell division: control of the chromosomal passenger complex in time and space”. *Chromosoma*, *123*(1-2), 25–42. https://doi.org/10.1007/s00412-013-0437-6

Vanoosthuyse, V., Prykhozhij, S., & Hardwick, K. G. (2007). “Shugoshin 2 regulates localization of the chromosomal passenger proteins in fission yeast mitosis”. *Molecular biology of the cell*, *18*(5), 1657–1669. https://doi.org/10.1091/mbc.e06-10-0890

Vanoosthuyse, V., & Hardwick, K. G. (2009). “Overcoming inhibition in the spindle checkpoint”. *Genes & development*, *23*(24), 2799–2805. https://doi.org/10.1101/gad.1882109

Vasquez-Limeta, A., & Loncarek, J. (2021). “Human centrosome organization and function in interphase and mitosis”. *Seminars in cell & developmental biology*, *117*, 30–41. https://doi.org/10.1016/j.semcdb.2021.03.020

Walczak, C. E., Mitchison, T. J., & Desai, A. (1996). “XKCM1: a Xenopus kinesin-related protein that regulates microtubule dynamics during mitotic spindle assembly”. *Cell*, *84*(1), 37–47. https://doi.org/10.1016/s0092-8674(00)80991-5

Wang, Q., Moyret-Lalle, C., Couzon, F., Surbiguet-Clippe, C., Saurin, J. C., Lorca, T., Navarro, C., & Puisieux, A. (2003). “Alterations of anaphase-promoting complex genes in human colon cancer cells”. *Oncogene*, *22*(10), 1486–1490. https://doi.org/10.1038/sj.onc.1206224

Warren, C. D., Brady, D. M., Johnston, R. C., Hanna, J. S., Hardwick, K. G., &

Spencer, F. A. (2002). “Distinct chromosome segregation roles for spindle checkpoint proteins”. *Molecular biology of the cell*, *13*(9), 3029–3041. https://doi.org/10.1091/mbc.e02-04-0203

Weaver, B. A., & Cleveland, D. W. (2006). “Does aneuploidy cause cancer?”. *Current opinion in cell biology*, *18*(6), 658–667. https://doi.org/10.1016/j.ceb.2006.10.002

Wei, R. R., Sorger, P. K., & Harrison, S. C. (2005). “Molecular organization of the Ndc80 complex, an essential kinetochore component”. *Proceedings of the National Academy of Sciences of the United States of America*, *102*(15), 5363–5367. https://doi.org/10.1073/pnas.0501168102

Weiss, E., & Winey, M. (1996). “The Saccharomyces cerevisiae spindle pole body duplication gene MPS1 is part of a mitotic checkpoint”. *The Journal of cell biology*, *132*(1-2), 111–123. https://doi.org/10.1083/jcb.132.1.111

Welburn, J. P., Grishchuk, E. L., Backer, C. B., Wilson-Kubalek, E. M., Yates, J. R., 3rd, & Cheeseman, I. M. (2009). “The human kinetochore Ska1 complex facilitates microtubule depolymerization-coupled motility”. *Developmental cell*, *16*(3), 374–385. https://doi.org/10.1016/j.devcel.2009.01.011

Welburn, J. P., Vleugel, M., Liu, D., Yates, J. R., 3rd, Lampson, M. A., Fukagawa, T., & Cheeseman, I. M. (2010). “Aurora B phosphorylates spatially distinct targets to differentially regulate the kinetochore-microtubule interface”. *Molecular cell*, *38*(3), 383–392. https://doi.org/10.1016/j.molcel.2010.02.034

Wenzel, E. S., & Singh, A. T. K. (2018). “Cell-cycle Checkpoints and Aneuploidy on the Path to Cancer”. *In vivo (Athens, Greece)*, *32*(1), 1–5. https://doi.org/10.21873/invivo.11197

Westermann, S., & Schleiffer, A. (2013). “Family matters: structural and functional conservation of centromere-associated proteins from yeast to humans”. *Trends in cell biology*, *23*(6), 260–269. https://doi.org/10.1016/j.tcb.2013.01.010

Wigge, P. A., Jensen, O. N., Holmes, S., Souès, S., Mann, M., & Kilmartin, J. V. (1998). “Analysis of the Saccharomyces spindle pole by matrix-assisted laser desorption/ionization (MALDI) mass spectrometry”. *The Journal of cell biology*, *141*(4), 967–977. https://doi.org/10.1083/jcb.141.4.967

Winey, M., Goetsch, L., Baum, P., & Byers, B. (1991). “MPS1 and MPS2: novel yeast genes defining distinct steps of spindle pole body duplication”. *The Journal of cell biology*, *114*(4), 745–754. https://doi.org/10.1083/jcb.114.4.745

Winey, M., Mamay, C. L., O'Toole, E. T., Mastronarde, D. N., Giddings, T. H., Jr, McDonald, K. L., & McIntosh, J. R. (1995). “Three-dimensional ultrastructural analysis of the Saccharomyces cerevisiae mitotic spindle”. *The Journal of cell biology*, *129*(6), 1601–1615. https://doi.org/10.1083/jcb.129.6.1601

Winey, M., & Bloom, K. (2012). “Mitotic spindle form and function”. *Genetics*, *190*(4), 1197–1224. https://doi.org/10.1534/genetics.111.128710

Xiao, H., Wang, F., Wisniewski, J., Shaytan, A. K., Ghirlando, R., FitzGerald, P. C., Huang, Y., Wei, D., Li, S., Landsman, D., Panchenko, A. R., & Wu, C. (2017). “Molecular basis of CENP-C association with the CENP-A nucleosome at yeast centromeres”. *Genes & development*, *31*(19), 1958–1972. https://doi.org/10.1101/gad.304782.117

Xu, Q., Zhu, S., Wang, W., Zhang, X., Old, W., Ahn, N., & Liu, X. (2009). “Regulation of kinetochore recruitment of two essential mitotic spindle checkpoint proteins by Mps1 phosphorylation”. *Molecular biology of the cell*, *20*(1), 10–20. https://doi.org/10.1091/mbc.e08-03-0324

Yamamoto, S., & Iwakuma, T. (2018). “Regulators of Oncogenic Mutant TP53 Gain of Function”. *Cancers*, *11*(1), 4. https://doi.org/10.3390/cancers11010004

Yamagishi, Y., Yang, C. H., Tanno, Y., & Watanabe, Y. (2012). “MPS1/Mph1 phosphorylates the kinetochore protein KNL1/Spc7 to recruit SAC components”. *Nature cell biology*, *14*(7), 746–752. https://doi.org/10.1038/ncb2515

Yeh, C. H., Bellon, M., & Nicot, C. (2018). “FBXW7: a critical tumor suppressor of human cancers”. *Molecular cancer*, *17*(1), 115. https://doi.org/10.1186/s12943-018-0857-2

Yochem, J., & Byers, B. (1987). “Structural comparison of the yeast cell division cycle gene CDC4 and a related pseudogene”. *Journal of molecular biology*, *195*(2), 233–245. https://doi.org/10.1016/0022-2836(87)90646-2

Yona, A. H., Manor, Y. S., Herbst, R. H., Romano, G. H., Mitchell, A., Kupiec, M., Pilpel, Y., & Dahan, O. (2012). “Chromosomal duplication is a transient evolutionary solution to stress”. *Proceedings of the National Academy of Sciences of the United States of America*, *109*(51), 21010–21015. https://doi.org/10.1073/pnas.1211150109

Yu S. (2022). “Overexpression of SKA Complex Is Associated With Poor Prognosis in Gliomas”. *Frontiers in neurology*, *12*, 755681. https://doi.org/10.3389/fneur.2021.755681

Zhang, M., Zhuang, G., Sun, X., Shen, Y., Wang, W., Li, Q., & Di, W. (2017). “TP53 mutation-mediated genomic instability induces the evolution of chemoresistance and recurrence in epithelial ovarian cancer”. *Diagnostic pathology*, *12*(1), 16. https://doi.org/10.1186/s13000-017-0605-8

Zich, J., & Hardwick, K. G. (2010). “Getting down to the phosphorylated 'nuts and bolts' of spindle checkpoint signaling”. *Trends in biochemical sciences*, *35*(1), 18–27. https://doi.org/10.1016/j.tibs.2009.09.002